Enhancement of pathogen-specific immunity following co-administration of whole inactivated respiratory vaccines

Shannon Christa David, B. Sc.

A thesis submitted for the fulfilment of the
Degree of Doctor of Philosophy

School of Biological Sciences
The University of Adelaide
Adelaide, South Australia, Australia

August 2018

TABLE OF CONTENTS

LIST OF FIGURES & TABLES

ABBREVIATIONS

γ	Gamma
γ-Flu/γ-Flu-OVA	Gamma-irradiated Influenza A Vaccine
γ-PN/γ-PN(ΔPsaA)	Gamma-irradiated *Streptococcus pneumoniae* Vaccine
µg	Microgram/s
µl	Microlitre/s
µM	Micromolar
γδ T	Gamma-delta T-Cells
A/PC	A/PortChalmers/1/73 [H3N2] influenza
A/PR8	A/PuertoRico/8/34 [H1N1] influenza
Alum	Aluminium Hydroxide Adjuvant
APCs	Antigen Presenting Cells
CbpA	Choline Binding Protein A
CPS	Capsular Polysaccharide
CTL	Cytotoxic $CD8^+$ T Lymphocyte
D_{10}	Decimal Reduction Dose
DC	Dendritic Cell
DI	Dry Ice
dsDNA	Double-stranded Deoxyribonucleic Acid
HA	Haemagglutinin
HP	Highly Pathogenic
HPAI	Highly Pathogenic Avian Influenza
IAV	Influenza A Virus
IFN-γ	Interferon Gamma
IFN-I	Type I Interferon (α/β)
Ig	Immunoglobulin
IIV3/4	Inactivated Influenza Vaccine (trivalent/quadrivalent)
IL-	Interleukin
IN	Intranasally
IP	Intraperitoneally
IPD	Invasive Pneumococcal Disease
IV	Intravenously
kGy	Kilogray
LAIV	Live Attenuated Influenza Vaccine
LP	Low Pathogenic
LPS	Lipopolysaccharide
LytA	Autolysin
M1/2	Matrix Protein 1/2

MEC	Middle Ear Colonisation
mg	Milligram/s
MHC-I/II	Major Histocompatibility Complex Class I/II
ml	Millilitre/s
mLN	Mediastinal Lymph Node
Mn	Manganese
NA	Neuraminidase
nm	Nanometre/s
NP	Nucleocapsid Protein
NPP	Nucleocapsid Protein Peptide
NS1/2	Non-structural Protein 1/2
OVA	Ovalbumin
PA	Acidic Polymerase Protein
PAMP	Pathogen Associated Molecular Pattern
PB1/2	Basic Polymerase Protein 1/2
PCV13	Pneumococcal Conjugate Vaccine (13-valent)
pDC	Plasmacytoid Dendritic Cell
PdT	Non-toxic pneumolysin derivative
Ply	Pneumolysin
PPV23	Pneumococcal Polysaccharide Vaccine (23-valent)
PRR	Pattern Recognition Receptor
PsaA	Pneumococcal Surface Adhesin A
RIV	Recombinant Influenza Vaccine
RT	Room Temperature
RV	Rotavirus
SA	Sialic Acid
SAL	Sterility Assurance Level
SEM	Standard Error of the Mean
ssRNA	Single-stranded Ribonucleic Acid
TB	*Mycobacterium tuberculosis*
T_H	$CD4^+$ T Helper Cell
T_H17	IL-17-producing $CD4^+$ T Helper Cell
TLR	Toll-Like Receptor
TNF-α	Tumour Necrosis Factor α
T_{REG}	Regulatory $CD4^+$ T Cell
T_{RM}	Tissue Resident Memory
WCV	Whole Cell Vaccine

DECLARATION

I certify that this work contains no material which has been accepted for the award of any other degree or diploma in my name, in any university or other tertiary institution and, to the best of my knowledge and belief, contains no material previously published or written by another person, except where due reference has been made in the text. In addition, I certify that no part of this work will, in the future, be used in a submission in my name, for any other degree or diploma in any university or other tertiary institution without the prior approval of the University of Adelaide and where applicable, any partner institution responsible for the joint-award of this degree.

I acknowledge that copyright of published works contained within this thesis resides with the copyright holder(s) of those works.

I also give permission for the digital version of my thesis to be made available on the web, via the University's digital research repository, the Library Search and also through web search engines, unless permission has been granted by the University to restrict access for a period of time.

I acknowledge the support I have received for my research through the provision of an Australian Government Research Training Program Scholarship.

_ _____

Shannon David

03/08/2018

Date

ACKNOWLEDGEMENTS

First and foremost, I would like to thank my principle supervisor, Dr. Mohammed Alsharifi. I can't put into words how much I appreciate all the support and guidance you have given me over the years. I'm especially grateful for the optimism and encouragement you provided whenever I was feeling doubtful and overwhelmed. Your passion for your scientific endeavours has inspired me from the very beginning, and will continue to do so for years to come.

I am also deeply grateful to my co-supervisors Professor James Paton and Professor Shaun McColl, for the wealth of insight and expertise you both provided. Thank you especially to James for all your advice about experimental design, and for always finding time for last minute meetings. To Shaun, your constant support and advice about every immunology aspect of this project have been invaluable. I am incredibly appreciative to have had both of you involved in my PhD.

A very special thank you to Professor Tim Hirst for your ongoing encouragement and insightful ideas. I am very grateful for all the time you found in your busy schedule to talk through data with me and offer advice. Thank you also to Gamma Vaccines for the kind support and sponsorship during this project.

To Eve, Zoe, Arthur, and King; thank you so much for all the support, friendship, happiness, and laughter you have given me. And for all the snacks. I'm so lucky to have you all in my life. Thank you also to past members of the Alsharifi Lab, especially Rachelle, Nikki, Josy and Sha, for welcoming me and showing how to be a scientist. My utmost gratitude to Rachelle in particular; the kindness and encouragement you gave me is truly valued, and thank you so much for teaching me and letting me follow you around.

To all past and present members of the Paton Lab and Wilson Lab, especially Claudia, Richard, Vik, Lauren, Austen, and Cathy. Thank you for being my second lab family. I am so grateful for how willing you all are to help me with new techniques, and for the advice you have all given me over the years. A special mention to Austen for teaching me everything about pneumo in my first year. To all members of the McColl lab, thank you for being so wonderful and letting me join you for morning tea. Every one of you has helped me out at some point, so thank you. A special mention to Jaz, Todd, and Tim for your help with all aspects of my T-cell experiments. I couldn't have done any of it without

you guys. Thank you to Jaz also for all the tea and hugs whenever I needed them. A special thanks to Iain for your insight and advice on new experiments, and thank you to members of the Beard Lab, the McDevitt Lab, and the Kidd Lab for help with various techniques and advice, and for lending reagents.

Importantly, a big thankyou to my parents, and my brother James. Thank you for your never-ending support and understanding during the difficult and stressful times, not just during my PhD, but throughout my life. I am so lucky to have people as wonderful, caring, and loving as you in my life.

Finally, thank you to Michael. I will always be grateful for the support and love you gave me in the years leading up to and during this PhD. For all the encouragement, the drives together for late night mouse checks, and the lifts home when I was exhausted. For making me happy. You helped me more than you can ever know.

PATENTS, PUBLICATIONS, & PRESENTATIONS ARISING FROM THIS THESIS

PATENTS		
Publication No.	**Title**	**Inventors**
20180117136	Streptococcal Vaccine	Rachelle Babb, Mohammed Alsharifi, Austen Yannis Chen, **Shannon Christa David**, Timothy Raymond Hirst, Abiodun David Ogunniyi, James Cleland Paton

PUBLICATIONS	
Thesis Chapter	**Title & Publication Status**
Chapter 2	**David S.C.,** Lau J., Singleton E.V., Babb R., Davies J., Hirst T.R., McColl S.R., Paton J.C., Alsharifi M. The effect of gamma-irradiation conditions on the immunogenicity of whole-inactivated Influenza A virus vaccine (2017), *Vaccine,* **35**(7): 1071-1079.
Chapter 1 /Chapter 2	Alsharifi M. and **David S.C.** Virus Inactivation Using a High Dose of Gamma-Irradiation: A Possible Approach for Safer Vaccines Against Highly Infectious Agents (2017), *Journal of Vaccines and Vaccination,* **8**(3).
Chapter 4	Mucosal co-administration of whole inactivated influenza A and pneumococcal vaccines augments IAV-specific immunity **Manuscript under review**

CONFERENCE PRESENTATIONS		
Type	**Title**	**Conference**
Oral Presentation	Bi-directional Adjuvant Activity of Co-administered Pneumococcal and Influenza A Vaccines	International Symposium on Pneumococci and Pneumococcal Diseases (ISPPD-18), Melbourne VIC, April 2018
Oral Presentation & Poster Presentation	Enhancement of Influenza-specific Immunity following Intranasal Co-administration of Whole Inactivated Influenza and Pneumococcal Vaccines.	Australasian Virology Society (AVS) Meeting, Adelaide SA, Dec. 2017
Oral Presentation	The Effect of Gamma-irradiation Conditions on the Immunogenicity of Whole-Inactivated Influenza A Virus Vaccine.	Adelaide Immunology Meeting (AIR-16), Adelaide SA, Nov. 2016
Poster Presentation	Gamma-irradiated Influenza A Virus Vaccine: Irradiation Conditions and Impact on Vaccine Efficacy	International Congress of Immunology meeting (ICI), Melbourne VIC, Aug. 2016

ABSTRACT

Influenza A virus (IAV) and *Streptococcus pneumoniae* are two of the most prominent respiratory pathogens affecting humans worldwide. While IAV and *S. pneumoniae* cause considerable morbidity and mortality individually, their synergistic pathogenicity poses the greatest threat to human health. Co-infection is associated with dramatically increased disease severity, particularly during IAV pandemics. The 1918 pandemic remains the most lethal on record, with an estimated 50 million deaths. However, a large portion of fatalities have since been attributed to secondary bacterial infection, with *S. pneumoniae* being heavily implicated. Given the ongoing risk of a future pandemic with highly pathogenic avian IAV, protective strategies against both IAV and *S. pneumoniae* represent an urgent and unmet need. Current vaccines against each of the individual pathogens are restricted to the induction of strain- and serotype-specific responses. Thus, our group has been developing novel vaccines that confer broad-spectrum protection after mucosal administration.

These vaccines consist of whole IAV and whole un-encapsulated pneumococci that have been sterilised using gamma (γ)-irradiation, to generate γ-Flu and γ-PN. Irradiation effectively sterilises each pathogen by damaging the genomic material, whilst pathogen structure and antigenic proteins are maintained. This study describes the enhancement of safety and immunogenicity of both vaccines to facilitate future clinical advancement. Treatment of γ-Flu with a high radiation dose of 50 kGy was shown to have minimal impact on vaccine efficacy whilst exceeding a Sterility Assurance Level of 10^{-6}. Establishing the efficacy of 50 kGy-treated preparations will aid in the inclusion of highly pathogenic strains in future vaccine formulations, such as avian H5N1 or H7N9. Such strains must be irradiated with a very high dose for sterilisation, and generation of γ-Flu based on 50 kGy-treated avian strains would be immensely beneficial in the event of a future pandemic. Utilisation of high radiation dose may also aid in the transfer of this inactivation approach to other highly pathogenic agents for vaccine purposes, particularly when $CD8^+$ T-cell responses are needed. The safety profile of our γ-PN vaccine was also heightened in the current study. A growth attenuating mutation was introduced (generating γ-PN(ΔPsaA)), which is an additional safety parameter to facilitate future clinical use of our vaccine. Interestingly, the supplementation of media with manganese required to restore normal growth *in vitro* was found to have immunomodulatory effects.

Specifically, manganese supplementation was associated with enhanced TLR2 signalling by both live and irradiated samples of the pneumococcal vaccine. This phenomenon was unique to the further attenuated strain and is expected to enhance the magnitude of immune responses induced *in vivo*. In addition, antibody responses induced by γ-PN(ΔPsaA) were found to react against a wider range of pneumococcal antigens compared to those induced by the original γ-PN.

While the adjuvant activity of γ-Flu to co-administered γ-PN has been reported previously, the subsequent combination of the two optimised vaccines revealed direct interaction of γ-Flu and γ-PN(ΔPsaA) in suspension, suggesting bi-directional adjuvant activities. Mixing the two vaccines resulted in enhanced uptake of γ-Flu virions by epithelial cells and macrophages *in vitro*, and co-vaccination with γ-Flu + γ-PN(ΔPsaA) was associated with significant enhancement of IAV-specific Tissue Resident Memory cell populations in the lung. Furthermore, co-vaccination enhanced the protection in mice against lethal challenge with both drifted and heterosubtypic IAV strains. My data indicate that our novel approach of mixing whole inactivated viral and bacterial vaccine components could enhance pathogen-specific immunity, and may revolutionise vaccine design to combat infectious diseases.

CHAPTER 1

Introduction

1.1 Influenza A Virus

Influenza A virus (IAV) is a highly infectious respiratory pathogen, and a recurring global health challenge. IAV strains constantly circulate through multiple animal hosts including humans, birds, horses, and pigs [1]. This diverse host range is associated with a high risk of infection with multiple subtypes, and subsequent reassortment of genome segments can produce new and novel strains. Despite vaccines being available since the 1940s, influenza viruses continue to circulate through the human population to cause seasonal epidemics and sporadic pandemics. Seasonal epidemics are estimated to affect 5 – 10% of adults and 20 – 30% of children worldwide [2]. Clinically, IAV infection is characterized by sudden onset of high fever, cough, headache, fatigue, and inflammation of the upper respiratory tract. Severe disease from seasonal IAV is more likely in the elderly, young children, immunocompromised, diabetics, and those with chronic pulmonary or cardiac conditions [3]. It can involve haemorrhagic bronchitis, secondary bacterial pneumonia, respiratory failure, and death [4, 3].

1.1.1 Classification and Structure of Influenza Viruses

Influenza virions are roughly spherical, although somewhat pleomorphic, ranging from 80 – 120 nm in diameter [5]. They are of the family *Orthomyxoviridae*, and are enveloped viruses containing negative-sense single stranded RNA genomes. The genome of influenza is also segmented, with each virus particle containing eight individual gene segments [6] that code for at least one protein each [7]. Influenza viruses have previously been divided up into three separate virus types: Influenza A, B, and C. The three have distinct differences in the core nucleocapsid (NP) and matrix (M) proteins, and they differ in host range and pathogenicity. Type B and C influenza viruses are isolated almost exclusively from humans (although influenza B viruses have been isolated from seals [8], and influenza C viruses isolated from pigs and dogs [9]), with influenza C virus causing mild infection only. Influenza D virus has also been recently classified as a new member of the *Orthomyxoviridae* family. This virus type has been isolated from both swine and cattle in multiple countries [10-12], with cattle forming the primary reservoir [13, 14]. Influenza D has roughly 50% similarity to influenza C, though it is not currently known to cause disease symptoms in humans [15]. Influenza A viruses cause the most significant risk to human health, with epidemics causing morbidity and mortality every year.

Influenza A viruses (IAV) are further subdivided by antigenic characterization of the major surface glycoproteins haemagglutinin (HA) and neuraminidase (NA). HA binds to sialylated host cell receptors and mediates membrane fusion, whereas NA removes sialyl residues from the membrane of infected cells to enable budding and release of newly synthesized virus particles [16]. Eighteen HA and eleven NA subtypes are currently known [17], with numerous influenza A strains having been isolated. Within a given subtype, current nomenclature for naming individual strains is as follows: the type of virus is first designated (A, B, C, or D), then the host of origin, place of isolation, isolation number, and year of isolation. For influenza A specifically, the HA (H1-H18) and NA (N1-11) subtype is also specified in parentheses, e.g. A/Swine/Iowa/15/30 (H1N1). By convention, when the host of origin is human, it is omitted from the name, e.g. A/Puerto Rico/8/34 (H1N1) [18].

In addition to HA and NA, the IAV genome encodes for 14 additional proteins [19], though not every influenza virus expresses all of them [20]. The matrix protein M1, the ion channel protein M2, and the M2-related protein M42 are all encoded by the matrix M genome segment (see **Figure 1.1**). M2 is highly conserved among influenza viruses of different subtypes, and forms tetramers that function as ion-channels to facilitate acidification of the endosome for viral-host membrane fusion. These channels also neutralise the pH in the Golgi network during virus replication to prevent premature HA conformational changes prior to budding. The non-structural genome segment NS encodes the host antiviral response agonist NS1, and the nuclear export protein NS2 (also known as NEP). Together with M1, NS2 mediates export of viral RNA from the host nucleus to the cytoplasm. Though NS1 is not included in the virion, it is abundantly expressed in IAV infected cells [21].

Nucleoprotein (NP), and components of the viral polymerase (PA, PB1, and PB2) are each encoded by their respective genome segments. Alternative forms of PA with terminal truncations have been recently identified, termed PA-N155 and PA-N182. Two new proteins, PA-X (represses cellular gene expression [22]), and N40 (unknown function [23]), are also encoded by the PA and PB1 segments respectively. NP, PA, PB1, and PB2 are present within the core of the IAV particle as ribonucleoprotein complexes (RNPs). Each RNP contains one RNA genome segment, a heterotrimeric viral polymerase (consisting of PA, PB1 and PB2), and multiple copies of viral NP. Influenza

RNPs play important roles during infection, mediating viral RNA replication and transcription, and directing intracellular transport and packaging of viral gene segments into new progeny particles [24].

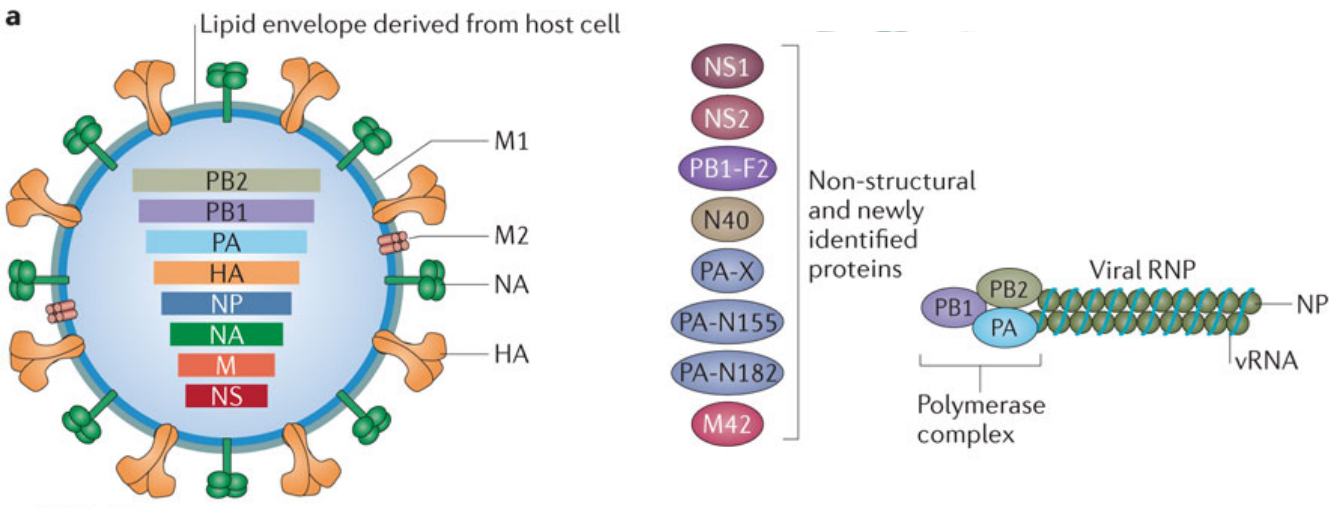

Figure 1.1. Structure of IAV. IAV contains 8 segments of single-stranded negative sense RNA, encoding 16 different proteins. Structural proteins HA and NA, and components of the viral RNP (NP, PA, PB1, and PB2) are each encoded by their respective genome segments. A second ORF in the PB1 segment encodes pro-apoptotic protein PB1-F2. The genome segment M encodes matrix protein M1, ion channel M2, and M2-related protein M42. The non-structural (NS) genome segment encodes the antiviral response agonist NS1 and the nuclear export protein NS2. Adapted from Shi et al. (2014) [20].

1.1.2 Immune Responses to IAV Infection

1.1.2.1 Innate Immunity

Respiratory epithelial cells are the main target for IAV infection [25], though other cell types including macrophages and dendritic cells (DCs) may also be infected [26, 27]. Virus particles enter the host through nasal or oral cavities, and are first impeded by the mucous layer that coats the respiratory epithelium [28], and a mucociliary escalator that continuously removes microbes and cellular debris [29]. If successful at bypassing these physical defences, IAV can attach to respiratory epithelial cells via binding of HA to sialic acid linked receptors on the host cell surface. The virus is then internalised by clathrin-dependent or clathrin-independent endocytosis [30-32], and viral membrane fusion in the endosome allows release of viral RNPs into the cytosol [24]. During the replication cycle of IAV, infection-associated signals, e.g. viral RNA are recognized as foreign by various pattern recognition receptors (PRRs), and subsequent signalling leads to induction and secretion of type I interferons (IFN-I) and pro-inflammatory mediators such as tumour necrosis factor (TNF)-α, interleukin-1β (IL-1β), IL-6, KC, and MCP-1 (see **Figure 1.2)**.

Retinoic acid-inducible gene I (RIG-I) is a crucial PRR for viral detection and IFN-I production in infected epithelial cells, conventional DCs and alveolar macrophages [33]. RIG-I specifically detects 5'-triphosphate viral ssRNA within the cytosol that is generated after viral replication [34-37]. Upon recognition of this ligand, the helicase domain of RIG-I binds ATP, and this facilitates conformational changes that enable caspase-recruitment domains on RIG-I to bind the mitochondrial antiviral signalling protein (MAVS) [38-40]. MAVS signalling then results in the expression of nuclear factor-κB (NF-κB) for production of pro-inflammatory cytokines, and IFN-I production via IFN-regulatory factor 3 (IRF3) [28]. There are hundreds of interferon-stimulated genes (ISGs) that are subsequently stimulated by IFN-I production that collectively induce an antiviral state within the infected cell and neighbouring cells. In addition to RIG-I, the NOD-like receptor family pyrin domain-containing 3 (NLRP3) protein is another class of PRR able to detect IAV within an infected cell [41]. NLRPs actually form multiprotein inflammasome complexes that detect cellular damage associated with membrane damage, cell stress, or infection [42]. IAV-associated signals for inflammasome activation include viral ssRNA in the cytosol [43], proton flux through

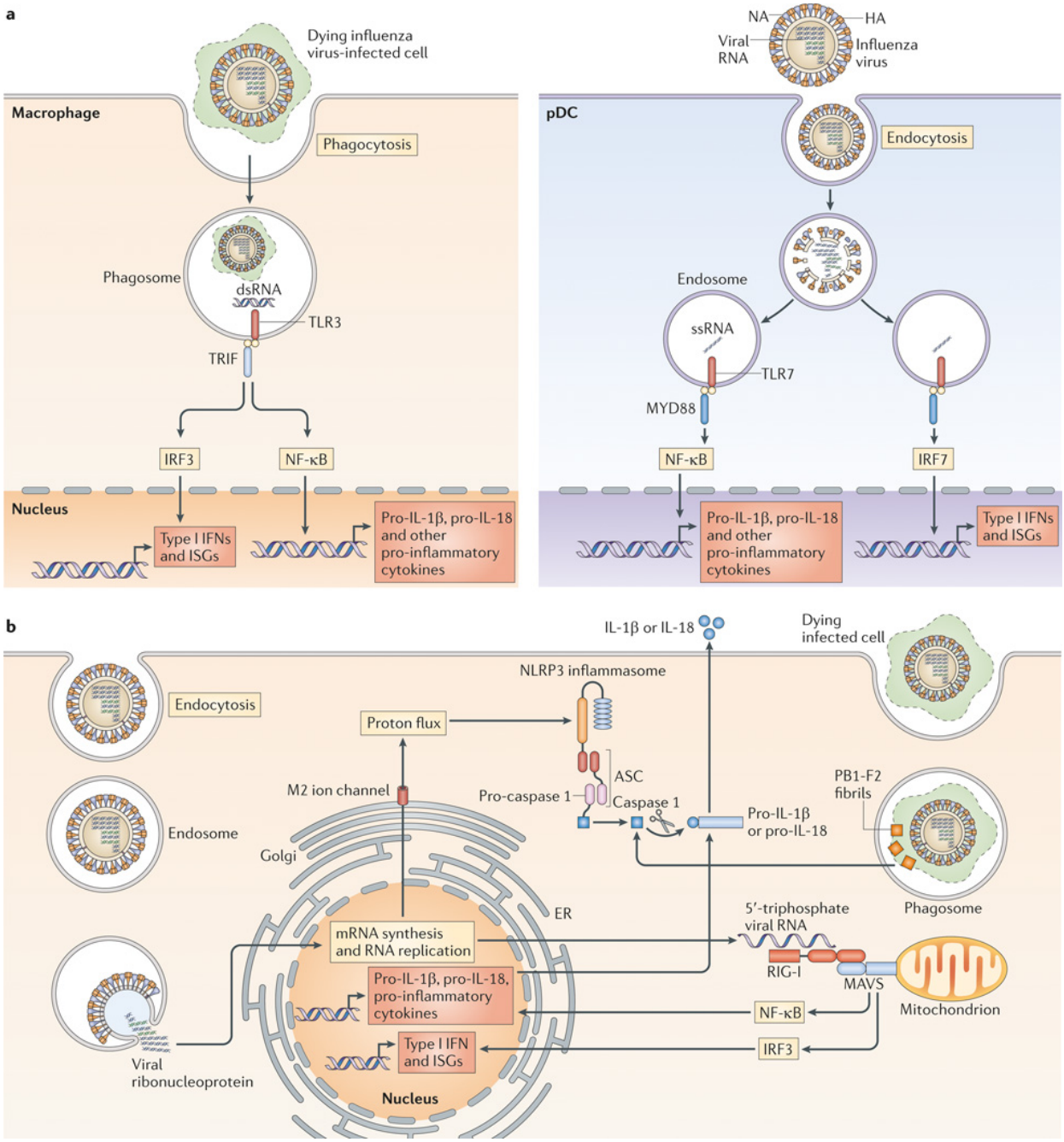

Figure 1.2. Innate Sensing of IAV Infection. IAV infection is detected by multiple PRRs that recognised unique signals associated with viral infection. (A) TLR3 and TLR7 recognise dsRNA and ssRNA respectively within a phagocytic endosome following uptake of either dying virally infected cells, or virions. (B) Viral RNA in the cytosol of infected cells is detected by RIG-I, or cell infection signals lead to activation of the NLRP3 inflammasome. Activation of these innate immune sensors results in activation of transcription factors NF-κB and IRF3 or IRF7 for production of pro-inflammatory cytokines, IFN-I, and ISGs [28].

the IAV-encoded M2 ion channel in the *trans*-Golgi network [44, 45], and high-molecular-weight aggregates of viral proteins PB1-F2 in lysosomes after the uptake of dying infected cells [46].

Whilst RIG-I and NLRP3 detect internal or cytosolic signals (cell intrinsic recognition system), Toll-like receptors (TLRs) comprise part of the cell extrinsic recognition system. TLRs are conserved type I transmembrane receptors that form a critical link between innate and adaptive immunity. These receptors can respond to a number of components of viruses, bacteria, fungi and parasites collectively known as microbial pathogen associated molecular patterns (PAMPs) [47, 48]. In the context of IAV, TLR3 recognises dsRNA of apoptotic infected cells that have been phagocytosed [49], and TLR7 detects ssRNA from endocytosed virions following endosome acidification by sentinel cells, particularly plasmacytoid dendritic cells (pDCs) [50, 51]. Similar to RIG-I signalling, TLR activation results in production of pro-inflammatory cytokines via NF-κB induction, and activation of transcription factors IRF3 or IRF7, for TLR3 and TLR7 respectively, to stimulate IFN-I and ISGs.

Genetic studies in mice have demonstrated the role of several ISGs in limiting influenza virus infection and spread – including IFN-inducible transmembrane (IFITM) proteins and protein kinase R (PKR). IFITM proteins limit the spread of many viruses, including IAV [52], by blocking virus-host cell membrane fusion to prevent viral release following attachment and endocytosis. IFITM3 is particularly important, as IFITM3-deficient mice are highly susceptible to influenza infection despite the presence of other IFITM proteins [53, 54]. Notably, IFITM3-deficient mice develop severe oedema and leakage of blood into the pleural cavity during influenza infection [54], suggesting IFITM3 not only mediates viral resistance, but may play a role in limiting host damage. PKR binds to dsRNA to inhibit translation of proteins. This results in reduction in both cellular and viral protein production, which effectively reduces viral replication within the host cell [28]. PKR also ensures robust IFN production by stabilising mRNA for IFN-α and IFN-β [55].

Collectively, pro-inflammatory cytokines produced following innate immune recognition induce a local inflammatory state within the tissue. This leads to activation of alveolar macrophages, which phagocytose apoptotic infected cells to limit virus spread [56].

Chemokines will rapidly recruit additional immune cells to the respiratory tract, including neutrophils, monocytes, and natural killer (NK) cells. Engagement of specific stimulatory NK receptors by ligands expressed on virally infected cells results in signal transduction cascades to induce NK function. This leads to cytolysis of the infected cell by (1) exocytosis of cytoplasmic granules containing perforin and granzyme, (2) Fas ligand-mediated induction of apoptosis, or (3) antibody-dependent cellular cytotoxicity [57-59]. NK cells also produce chemotactic and activating cytokines, including IFN-γ and TNF-α [60]. NK cells primarily mediate viral clearance during the innate response [61], whilst recruited monocytes, neutrophils, and alveolar macrophages assist in clearance of infected apoptotic and dead cells [62]. If the virus is able to establish infection despite these innate defences, adaptive immunity will be required for effective clearance and resolution of infection.

1.1.2.2 Adaptive Immunity

The adaptive immune system consists of humoral and cellular immunity mediated by virus-specific antibodies and T-cells, respectively. Dendritic cells (DCs) constantly monitor the airway lumen via dendrites that extend between the tight junctions of adjacent respiratory epithelial cells. DCs can be directly infected with virus or detect antibody-neutralised influenza virions and apoptotic bodies of influenza-infected cells. Upon detection and internalisation of a virus particle, the DC migrates to the draining lymph node via the lymphatic system. Viral peptides are then processed and presented via major histocompatibility complex (MHC) class I and class II, to activate antigen-specific $CD8^+$ and $CD4^+$ T-cells respectively [63]. Type I IFNs from the innate response can stimulate DCs and result in enhanced antigen presentation to T-cells, thus linking the innate and adaptive arms of immunity.

One of the most important cell subsets for combating a viral infection is cytotoxic $CD8^+$ T lymphocytes (CTLs). These antigen-specific effectors recognise and eliminate infected host cells to prevent viral spread and production of viral progeny. Lytic activity of CTLs is mediated by release of perforin and granzymes; perforin forms pores in the membrane of the target cell, and granzymes then enter the cell to induce apoptosis. CTLs can also induce apoptosis via Fas/FasL and TNF-related apoptosis-inducing ligand (TRAIL)/death receptor 5 interactions [64]. They also produce cytokines that stimulate MHC expression to enhance antigen presentation [65]. Human CTLs induced by

influenza virus are mainly directed against the internal NP, M1 and PA proteins [66-70]. These proteins are highly conserved across different subtypes of IAV, and therefore CTL responses display a high degree of cross-reactivity.

Some $CD4^+$ T-cells have also been shown to display cytotoxic activity to infected cells [71], however the most important function of this T-cell subset is as T helper (T_H) cells. Different subsets of T_H cells are distinguished based on their cytokine expression profiles. T_H2 cells mainly produce IL-4 and IL-13 and are considered to predominantly promote B-cell responses [72, 73], whereas T_H1 cells produce IFN-γ and IL-2 and are involved mainly in cellular immunity. In addition, regulatory T-cells (T_{REG}) and T-helper 17 (T_H17) cells are additional subsets that regulate the cellular immune response to influenza virus infection. Production of IL-1β via activation of the NLRP3 inflammasome is involved in induction of T_H17 cells [74] and expansion of antigen-specific $CD4^+$ T-cell populations [75], again linking innate and adaptive immune systems.

During the early adaptive phase of the immune response to IAV in naïve animals (days 5 – 7), T-cell responses mediate a rapid decline in viral titre by eliminating virally infected cells [76]. B-cells also produce an array of antigen-specific immunoglobulins to neutralise free virions. IAV-specific immunoglobulin M (IgM) is produced and secreted early after primary infection, followed later by class-switched IgA and IgG [76, 77]. IAV-specific antibodies target HA and NA surface proteins. HA-specific antibodies predominately bind the trimeric globular head of the HA protein and inhibit viral attachment and entry. As this region of HA is highly variable, these antibody responses are considered strain-specific. In contrast to the globular head, the stem region of HA is highly conserved, but also physically masked from the immune system. Antibodies against stem epitopes are induced during infection, and are able to broadly bind and neutralise HA molecules from different IAV strain [78, 79]. Unfortunately, titres of stem-specific antibodies in a host are usually very low. Bound antibodies can also facilitate phagocytosis of neutralised virus by Fc receptor expressing cells. Antibodies may also bind to viral proteins expressed on the surface of infected host cells, and mediate killing by NK cells via antibody-dependent cell cytotoxicity (ADCC) [80].

Antibodies generated against NA also have protective potential, though will not neutralise free virions to prevent cell entry. Rather, NA-specific antibodies inhibit the

enzymatic activity to limit viral spread. NA usually cleaves the sialic acid residues on the cell surface to facilitate release of newly formed viral particles [73], and inhibition of this process minimises the release of progeny virus. Additionally, NA-specific antibodies can facilitate ADCC by NK cells [81].

1.1.3 Prevention & Treatment of Influenza Infection

The primary measure against influenza A and B virus infections is vaccination using inactivated or live attenuated vaccines. Currently, only inactivated influenza vaccines (IIV) are licensed in Australia and are available as either trivalent or quadrivalent formulations containing a H1N1 influenza A virus, a H3N2 influenza A virus, and one or two influenza B viruses. Specifically, the 2017 vaccine formulation was comprised of A/Michigan/45/2015 (H1N1)pdm09*-like virus, A/Hong Kong/4801/2014 (H3N2)-like virus, B/Brisbane/60/2008-like virus, and an additional influenza B strain: B/Phuket/3073/2013-like virus for the quadrivalent formulation [82].

To manufacture the IIV, the selected influenza strains are grown in embryonated chicken eggs, then purified by zonal centrifugation. The viruses are then chemically inactivated by propiolactone and disrupted/split by sodium taurodeoxycholate. A single dose of the trivalent vaccine for adults contains the equivalent of 45 µg HA (15 µg HA for each of the 3 antigenic components). Because the influenza viruses are grown in chicken eggs, the resulting vaccine contains trace amounts of egg protein – however this amount is less that 1 µg of ovalbumin per vaccine dose [83]. An alternative to whole virus cultivation is the use of a continuous cell line and recombinant virus vector to express influenza proteins. These recombinant influenza vaccines (RIV, brand name: Flublok®) use a continuous insect cell line (*expres*SF+®) with a baculovirus vector that expresses the HA proteins of interest. This particular virus grows well in insect cells, and the HA proteins expressed are extracted with Triton X-100 and further purified by column chromatography. Recombinant vaccine formulations such as this contain 3× the antigen content of IIV formulations, with 45 µg HA for each of the included strains [84]. The manufacturing process is also quicker as it is not dependent on an egg supply, and is not limited by the selection of vaccine viruses that have been adapted for high titre growth in eggs. Both the IIV and HA-based recombinant vaccine induce neutralising antibody responses against each of the strains included in the annual formulation, but these are

rarely cross-protective, and no T-cell responses are induced due to lack of antigen presentation by MHC-I.

The second class of influenza vaccine is the live attenuated influenza vaccine (LAIV, brand name: FluMist®, available in the United States, Canada, and Europe [85], but not Australia [83]). The intranasally administered LAIV is composed of reassortant viruses containing the HA and NA surface proteins from wild-type circulating strains on an attenuated temperature-sensitive virus backbone (A/Ann Arbor/6/1960) [86]. This backbone strain was serially passaged in primary chicken kidney tissue culture at successively lower temperatures, and replicates effectively at 25°C but not higher temperatures [87]. This temperature sensitivity severely restricts viral replication in the warmer lower respiratory tract of the host [88-90]. LAIV may cause mild symptoms (rhinorrhoea, nasal congestion, fever or sore throat) due to the cooler uppermost regions of the respiratory tract being mildly permissive to replication of the attenuated strain [88, 91]. However, these are transient and minor in comparison to true influenza infection.

The replication of the live attenuated strain allows expression of influenza proteins in their native form, and consequently mucosal IgA, serum IgG responses, and cell-mediated immune responses are stimulated that mimic those induced by wild-type virus [92]. LAIV-induced immunity is significantly more cross-protective than responses elicited by chemically inactivated vaccine preparations [93, 94]. However, the effectiveness of the LAIV has not been consistently demonstrated since the 2009 IAV pandemic [95], and is currently not recommended for use in the United States during the 2017-2018 influenza season [96]. LAIV should also not be administered to immunosuppressed persons, nor to children under 2 years of age.

In addition to vaccination, antiviral drugs may be administered prophylactically [97-101], or therapeutically to minimize pathology and aid viral clearance by limiting virus replication [102]. Matrix 2 ion channel blockers (Amantadine and Rimantadine) are effective against IAV, but resistant viral strains develop rapidly and have been recognized in approximately one-third of treated patients. Neuraminidase inhibitors, Zanamivir and Oseltamivir, are effective against both influenza A and B viruses in limiting virus spread from infected cells. The HA stem region of IAV is also considered to be a promising

target for development of new antivirals, as this would prevent conformation change of HA and inhibit release of the virus once in the host-cell endosome [103].

1.1.4 Antigenic Variation

As described above, current inactivated vaccines induce strain-specific neutralising antibody responses, with limited cross-reactivity against non-vaccine strains [104, 105]. In addition, influenza has a very high mutation rate, and gradual accumulation of mutations allows the virus to escape immunity at both individual and population levels, leading to reduced vaccine efficacy. In fact, both live and inactivated influenza vaccine formulations are redesigned every year to include new emerging strains that are predicted to be most prevalent in the coming influenza season. This incurs major costs due to constant reformulation, manufacture and re-administration to the public. In addition, despite the effort by World Health Organisation (WHO) influenza centres that rigorously analyse clinical isolates to predict dominant strains, novel strains may emerge during the time needed for vaccine manufacture and distribution (roughly 6 months) [105, 106]. Evidence also suggests that immunity following IIV administration begins to wane quickly, potentially after just 3-4 months [107-111].

The mechanism of constant antigenic variation is termed antigenic drift, which is mediated by the highly error prone RNA-dependent RNA-polymerase of IAV [7]. Point mutations during genome replication are not corrected, as influenza viruses have no proof-reading ability, and the overall mutation rate is estimated at 1×10^{-3} nucleotide substitutions per site per year [112, 113]. Point mutations that alter amino acids in the HA and NA surface glycoproteins are relatively well tolerated, and can actually confer selective advantages by allowing immune evasion. Over the course of a year, these mutations accumulate and result in new drift variants, allowing seasonal outbreaks. Additionally, as vaccine-induced antibody responses target HA, they exert additional selective pressure on circulating influenza viruses to drive antigenic drift [65]. Viral epitopes recognised by CTLs are also under selective pressure, though mutations to these internal and conserved proteins are far less tolerated in comparison to HA and NA. For example, an arginine-to-glycine substitution at position 384 of the viral nucleoprotein has been associated with escape from CTLs, however it is detrimental to viral fitness [114]. Additional co-mutations were required to restore NP functionality and viral fitness to then allow benefit of the original mutation via CTL escape [115].

As IAV has a segmented genome, major and sudden changes in the combination of HA or NA glycoproteins can also occur, and is termed antigenic shift. Infection of a single host cell with multiple IAV strains (e.g. a human strain and an avian strain) allows for reassortment of gene segments during virion packaging. This can result in the release of viral particles with new HA and NA combinations, against which pre-existing immunity is minimal or entirely absent. Alternatively, a circulating human strain may acquire a HA gene from an avian or swine virus, resulting in a new strain that is both novel to the human population, and well adapted for transmission and replication in human hosts [116]. These novel viruses are capable of causing large regional or global pandemics [2]. In fact, the emergence of a novel subtype by antigenic shift was the cause of both 1957 and 1968 influenza pandemics.

As sixteen HA and nine NA subtypes are known to exist in wild birds, they form a major source of subtype combinations novel to the human population [117, 17, 118]. There is mounting evidence that bats also form a reservoir for influenza and have a role in emergence of strains novel to humans, with two new influenza-like subtypes having recently been described (H17N10 and H18N11) [119]. It is important to note that these HA and NA-like molecules do not appear to have canonical influenza HA and NA activity. H17 for example does not attach to human or avian sialic acid receptors [120-122], and N10 and N11 have no sialidase activity *in vitro* [123, 124]. Still, these viruses have been detected in seemingly healthy bats, and their role in influenza ecology and potential for genomic reassortment with canonical influenza viruses are currently undetermined [119, 118].

1.1.5 Influenza A Pandemics

Spanish Influenza (1918)

The first documented worldwide outbreak of influenza occurred in 1918, and is known as the 'Spanish Flu'. Roughly one-third of the world's population was infected, and it remains the most lethal influenza pandemic on record with an estimated 50 million deaths [125]. Infected individuals often died very rapidly after onset of symptoms, with massive acute pulmonary haemorrhage, pulmonary oedema (fluid accumulation in the tissue and air spaces of the lungs), and respiratory failure [126]. A substantially high percentage of cases also developed severe bacterial pneumonic complications as a result of primary influenza infection [3], as no antibiotic treatment options were available in 1918 [126].

This contributed dramatically to the total number of pandemic-related fatalities. Molecular characterisation of the 1918 influenza surface proteins from frozen human samples revealed the virus was a H1N1-subtype [127, 126]. The 1918 pandemic was also particularly uncharacteristic of influenza, with almost half of all deaths being young adults between 20 – 40 years of age [128, 125].

Asian Influenza (1957)

The H2N2 subtype of influenza A emerged in China in 1957, and air and sea travel aided the spread of this novel virus subtype around the world. The new virus had high sialidase/neuraminidase activity, and this activity was more stable than that of earlier strains [129]. Majority of deaths occurred in the elderly or the very young, as is typical of influenza during non-pandemic periods. Later analysis of H2N2 influenza indicated that there was a possible avian source for the HA, NA, and PB1 genes, whilst the remaining genes were from viruses already circulating through the human population. H2N2 strains proceeded to circulate worldwide until they were displaced by the novel H3N2 pandemic strain in 1968 [130].

Hong Kong Influenza (1968)

Acquisition of a novel HA and PB1 (likely from an avian reservoir) allowed emergence of the novel H3N2 strain, first in China and soon after, Hong Kong. The virus was then detected in the USA and Australia a few months later. Interestingly, the virus appeared to have circulated in Europe for 12 months before causing severe disease. Since the Hong Kong virus differed from its predecessor by its HA antigen only, researchers speculated that the variable impact in different regions of the world was mediated by differences in prior N2 immunity [131-133]. Direct support for this theory was provided by Eickhoff and Meiklejohn, who showed that vaccination of Air Force cadets with a H2N2 adjuvant vaccine reduced subsequent influenza virus infection from verified H3N2 by 54% [134]. Despite the amelioration of H3N2 virus infection by NA immunity alone, the H3N2 subtype continues to circulate as one of the two major influenza A viruses in humans today [129].

Avian Influenza

Increasing emergence of human infections with avian influenza A subtypes H5N6, H7N9, H9N2, and the highly pathogenic avian influenza (HPAI) H5N1 represent major health

concerns. These novel subtypes, particularly H5N1 and H7N9, have the potential to cause a devastating worldwide pandemic [135]. WHO has reported human cases of infection with these subtypes across 16 different countries. 860 individual cases of avian H5N1 infection have been reported and laboratory-confirmed since 2003, with an average mortality rate of 53% [136], which is unprecedented in the history of influenza. In terms of disease progression, the H5N1 avian strains that are currently circulating cause primary viral pneumonia with features characteristic of acute respiratory distress syndrome, which usually progresses to pulmonary failure [137]. Infections with HPAI virus are also more prone to cause immunopathology, as these viruses can infect blood-derived and alveolar macrophages [138, 139], leading to production of large amounts of pro-inflammatory cytokines [140].

Presently, H5N1 has not acquired the ability to efficiently transmit between humans, with most human infections occurring via direct contact with infected poultry. An important factor to consider for transmission of avian strains to humans is the binding specificity of HAs from different animal hosts [20]. For example, the HA of human influenza viruses preferentially bind to sialic acid (SA) linked to terminal oligosaccharides by an α2,6 bond (SA-α2,6-Gal-terminated saccharides), whereas avian HAs preferentially recognise SA-α2,3-Gal-terminated saccharides [141, 142]. Specific amino acid mutations in the globular head of the HA proteins can lead to a change in the receptor-binding preference, and thus in host specificity. In fact, two amino acid mutations in the HA of 1918 pandemic influenza have been shown to switch binding preference from human SA-α2,6 to avian SA-α2,3 [143]. Additionally, recent studies have demonstrated that is it possible to generate H5N1 mutants with preference for the human α2,6-linked SA receptor [144]. H5N1 mutants have also been generated that are able to break the species barrier and efficiently transmit via the aerosol route between ferrets [145, 146]. One particular study showed this transmissibility was conferred after only 5 mutations [147]. Considering IAV is renowned for a high mutation rate, avian H5N1 or a similar strain may gain enough mutations to facilitate efficient human aerosol transmission, leading to a severe global pandemic [148]. In fact, there have been rare clusters of human-human transmission reported between family groups in Thailand [149, 150], Indonesia [151], Turkey [152], and Vietnam [149].

Avian H7N9 is also of particular concern, and it has emerged more recently and substantially more rapidly than H5N1. Since 2013, a total of 1564 laboratory-confirmed cases and 612 deaths have been recorded [136]. China in particular has reported substantial increase in human infections with avian H7N9 since October 2016 [153]. Again, most human infections have occurred via direct contact with infected poultry. As such, vaccination of domestic poultry in China against A(H7) viruses has recently commenced in addition to the ongoing poultry vaccination program against A(H5) viruses [136]. Interestingly, low pathogenic (LP) avian H7N9 has been shown to be capable of transmission between ferrets via aerosol droplets, albeit inefficiently [154]. A highly pathogenic (HP) H7N9 strain that emerged in late 2016 – early 2017 was recently found to have the same capability [155]. The risk of a worldwide influenza pandemic is increasing, and the rapid, continuous, and unpredictable nature of influenza mutation makes vaccine strategies and pandemic planning very difficult. Development of a safe, universal influenza vaccine for mucosal administration would be most optimal to defend against both seasonal epidemics and future pandemics.

1.2 *STREPTOCOCCUS PNEUMONIAE*

Streptococcus pneumoniae is an encapsulated, facultative anaerobic, non-sporulating Gram-positive bacterium that is usually present as a diplococcus. Also known as the pneumococcus, *S. pneumoniae* is a major respiratory pathogen that causes both invasive and non-invasive disease. Severe disease outcomes and fatality due to pneumococcal infection are more common in infants, immune-compromised individuals, and the elderly. In fact, *S. pneumoniae* is responsible for 1 – 2 million deaths worldwide each year, and kills more children than AIDS, malaria and tuberculosis combined [156]. Moreover, since the implementation of *Haemophilus influenzae* type b (Hib) conjugate vaccines and the substantial reduction on invasive Hib disease [157], *S. pneumoniae* has become the leading cause of bacterial meningitis in children <5 years of age in the United States [158]. Analysis has also revealed meningitis caused by pneumococci has substantially greater mortality and neurological consequences when compared to meningitis caused by Hib or *Neisseria meningitidis* [159, 160].

1.2.1 Pneumococcal Carriage & Epidemiology

The only known reservoir for *S. pneumoniae* is the nasopharynx of healthy human carriers. *S. pneumoniae* colonises the nasopharynx of infants within a few months of birth. At least 98 immunologically distinct pneumococcal serotypes have been identified to date based on differences in composition of the capsular polysaccharide (CPS) [161]. This capsular polysaccharide is a major virulence factor of *S. pneumoniae* and in the absence of type-specific immunity it is poorly recognised by phagocytic cells, and thus protects the pneumococcus from being engulfed [162].

Children typically encounter several serotypes early in life (either sequentially or simultaneously) [163], and it is estimated that by the age of two years, 95% of children would have been colonised by the pneumococcus [164]. Colonisation with a given serotype may persist for a month or last up to a year. Eventually, immunity is established against colonizing pneumococci, and consequently the niche is vacated and re-colonised with different serotypes. This process is reported to continue until adulthood [165, 166]. Between 20 – 50% of children and 5 – 30% of adults in developed countries are colonised with *S. pneumoniae* at any one time with no adverse symptoms [167-169]. However, colonisation rates are closer to 70% for children attending day care centres, and upwards of 90% for those living in native communities [170]. Interestingly, colonising serotypes

have been shown to differ significantly between children (<5 years of age) and adults. For example, serotypes 6B, 9V, 14, 19F, and 23F are more commonly carried by young children [171]. Studies also suggest that invasive capability and virulence are dependent on the pneumococcal capsular serotype [172, 173]. For example, serotypes 1 and 7F are more prominent in invasive disease [171]. In addition, multiple distinct genetic clones that share a common set of genes (clonotypes) can also exist within and across serotypes [174, 175].

1.2.2 Pneumococcal Pathogenesis

The asymptomatic nasopharyngeal carriage of pneumococci is typically a dynamic process. The constantly replicating pneumococcal population is kept under control by host immune defence mechanisms, however disruption of this balance (by infection with new serotypes, loss of immune-competence, etc.) can cause the bacterium to switch from commensal to pathogenic [168]. As mentioned previously, pneumococcal infection can lead to both invasive and non-invasive disease. Infection of the sinuses (sinusitis), middle ear (otitis media), and lung (pneumonia) are considered non-invasive, and are frequent but not severe. Otitis media is especially common in infants and young children [156, 171, 176]. Invasive pneumococcal diseases (IPD) refer to the isolation of *S. pneumoniae* from a normally sterile site, including the blood (septicaemia/bacteraemia) and cerebrospinal fluid (meningitis). These are associated with severe disease outcomes and high fatality rates [177]. Initially, meningitis presents as symptoms of fever, irritability, vomiting, and impaired consciousness [178]. Progression of disease leads to seizures, focal neuropathology, and coma. Those recovering from bacterial meningitis are often left with neurological sequelae, such as hearing loss, cognitive impairment and epilepsy [179].

Infection of the lung (pneumonia) by *S. pneumoniae* requires the pneumococci to migrate from the nasopharynx to the alveoli, usually by aspiration. Establishment of infection in the alveoli causes excessive inflammation, resulting in initial symptoms of cough, fever, and abnormally rapid breathing (tachypnoea). This type of infection is considered non-invasive unless septicaemia or empyema (infection of the space between membranes surrounding the lungs and chest cavity) occur concurrently [180]. Pneumococcal pneumonia is readily treatable for healthy individuals. However, for those with existing health conditions or other respiratory infections, additional complications arising from

pneumonia are common and often severe. They include inflammation of the sac surrounding the heart (pericarditis), blockage of the airways (endobronchial obstruction), collection of pus within the lungs, and/or complete lung collapse.

1.2.3 Virulence Factors

Upon entrance of the pneumococci to the nasal cavity, components of the cell wall such as phosphorylcholine (ChoP) mediate direct attachment via binding to platelet-activating factor receptor (PAFr) [181] present on the surface of lung epithelial cells [182]. *S. pneumoniae* also secretes hyaluronidase that degrades hyaluronic acid, an important component of host connective tissue. This degradation assists in the binding of pneumococcal adhesion and virulence A (PavA) and enolase (Eno) surface proteins to host fibronectin and plasminogen respectively, further assisting bacterial adherence [183-185]. Pneumococcal neuraminidase also cleaves N-acetylneuraminic acid to decrease viscosity of the mucous lining the host respiratory tract. This enzyme can also cleave terminal sialic acids (similar to IAV NA) from glycolipids, glycoproteins, and oligosaccharides to expose additional N-acetyl-glycosamine receptors [186]. Together, these factors function to promote successful adherence and colonization.

ChoP on the bacterial cell surface also serves to anchor choline binding proteins – such as pneumococcal surface protein A (PspA) [187] and choline binding protein A (CbpA) [181] – to the bacterial surface. CbpA in particular has been shown to facilitate invasion and transmigration of the bacterium from the apical to basolateral face of mammalian cells, via interaction with the polymeric immunoglobulin receptor (pIgR) [188]. This enables the bacterium to penetrate the respiratory epithelium to reach the underlying vasculature and disseminate through the host.

S. pneumoniae also possesses many factors to enable host immune evasion. The capsule for example acts as a shield against deposition of IgG to inhibit phagocytosis mediated by Fcγ receptors. It also protects against deposition of innate complement components, particularly C3b [189, 190]. The capsule can also prevent trapping of the bacteria by neutrophil extracellular traps (NETs) [191]. Specific surface proteins also interfere with the complement pathway; PspA for example has a highly negative charge to prevent C3b deposition [192], pneumococcal histidine triad protein A (PhpA) has been reported to have C3-degrading activity [193], and CbpA recruits serum factor H and C4-binding

protein to downregulate activation of the alternative and classical complement pathways respectively [194, 195].

Pneumolysin (Ply) is another crucial virulence factor, and is a pore-forming toxin released via the autolytic activity of the pneumococcal enzyme autolysin (LytA) [196]. Ply primarily binds to cholesterol within membranes of host cells and form pores, causing cytolysis and lung injury [197]. Ply has also been shown to inhibit ciliary beating in the respiratory tract to prevent bacterial clearance [198], and can reduce lymphocyte proliferation, migration, and killing of opsonised pneumococci [199, 200]. Ply was also shown to confer protection against complement-mediated clearance [201].

1.2.4 Immune Responses to *S. pneumoniae*

1.2.4.1 Innate Immunity

Similar to influenza virus, pneumococci are initially recognised by various PRRs of the innate immune system. These include TLRs (specifically TLR2, TLR4, and TLR9 [202]), the cytosolic NOD-like receptors (NLRs), and DNA sensors (see **Figure 1.3)**. PRRs TLR2 and TLR4 are expressed at the surface of host cells, and hence recognise components of extracellular pneumococci. TLR2 ligands are lipoteichoic acid and peptidoglycan [203, 204], and TLR4 ligands include lipopolysaccharide (LPS), and Ply [205]. *S. pneumoniae* may also be internalized by phagocytic cells and subsequently degraded in phagosomes. This results in bacterial peptidoglycan and nucleic acids being released, where unmethylated CpG DNA motifs will be sensed within the phagosome by TLR9 [206-209]. Together, TLR signalling stimulates production of inflammatory cytokines via stimulation of the transcription factor NF-κB, including TNF-α, IL-6, IL-8, IL-1β, and IFN-β. TNF-α and IL-1β can further activate epithelial cells to produce additional inflammatory mediators, whilst IL-8 acts to stimulate recruitment of leukocytes. IFN-β activates expression of hundreds of ISGs in an autocrine and paracrine fashion, for multiple antimicrobial functions. Signalling via TLR2 and -9 has also been suggested to enhance pneumococcal phagocytosis and intracellular killing within leukocytes [210, 211].

Bacterial DNA and peptidoglycan may also be released to the cell cytosol from the phagosome post-degradation, or via Ply-mediate membrane lysis. Here, bacterial dsDNA

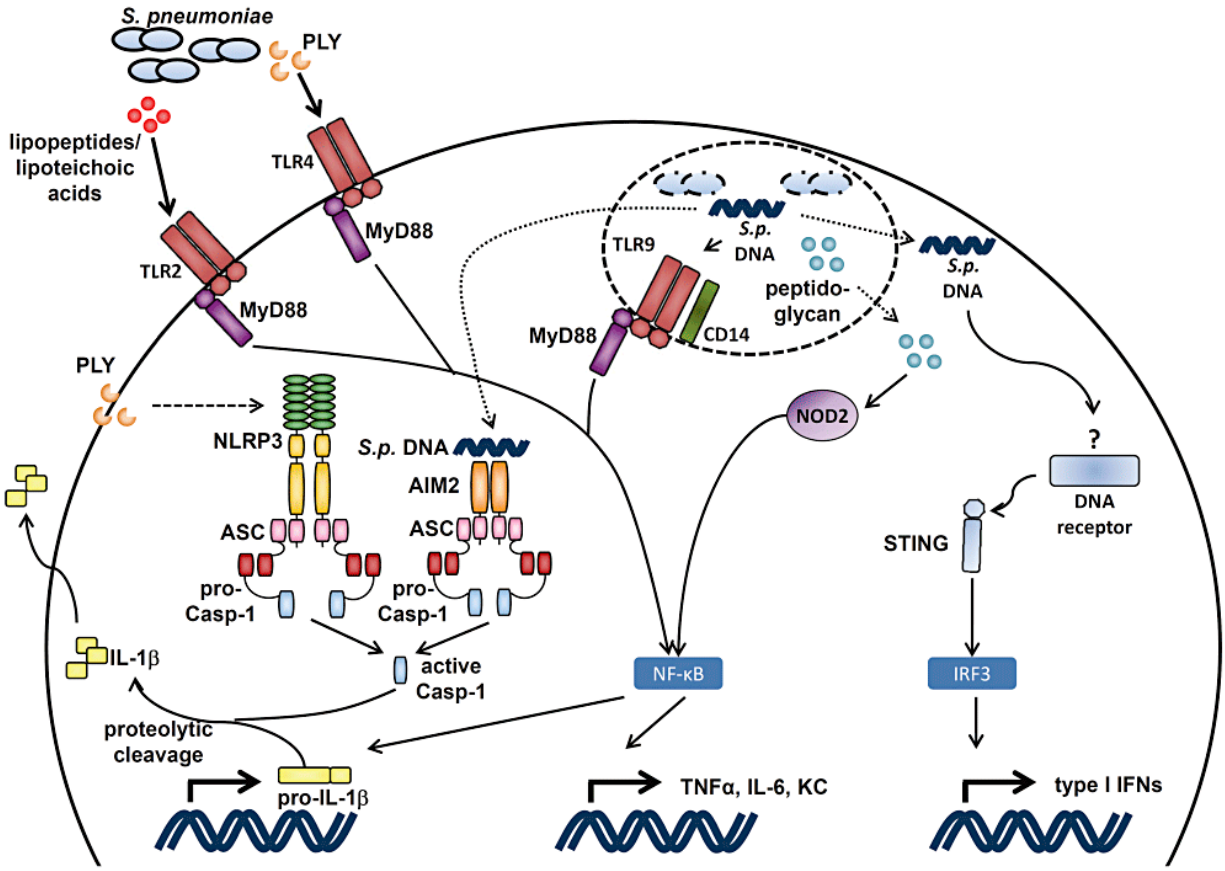

Figure 1.3. Overview of the different PRRs involved in innate recognition of *S. pneumoniae*. Cell wall components and Ply of extracellular pneumococci are recognized by TLR2 and -4 respectively. *S. pneumoniae* is also internalized by phagocytic cells and degraded in phagosomes, releasing bacterial peptidoglycan and nucleic acids. Unmethylated CpG-motifs will be detected within the phagosome by TLR9, and may also gain access to the cytosol via Ply-mediated membrane disruption. Here, pneumococcal DNA is detected by AIM2, and by an additional still not identified cytosolic PRR that leads to IRF3 activation. TLRs as well as NOD2 subsequently stimulate the production of NF-κB-dependent cytokines [209].

activates the inflammasome AIM2, and cytosolic PRR NOD2 detects peptidoglycan fragments [212]. Ply also activates the NLRP3 inflammasome to mediate production of mature IL-1β in macrophages and DCs [213]. The secondary signalling provided by NLRP3 and AIM2 inflammasomes is required for cleavage of pro-IL-1β into mature IL-1β. Sensing of *S. pneumoniae* DNA by the yet-to-be-identified cytosolic DNA sensor also activates the adaptor STING and the transcription factor IRF3, to stimulate type I IFN responses.

Other important components of the innate system for pneumococcal detection include scavenger receptors (e.g. MARCO), C-type lectins (e.g. SIGN-R1), and C-reactive protein (CRP). CRP is a soluble protein that binds to ChoP in the pneumococcal cell wall, inducing complement activation [214, 215, 190]. Activation of the complement cascade and subsequent binding of complement factors (primarily C3b) to the pneumococcal surface leads to opsonophagocytosis and the induction of inflammation. Complement activation can also lead to B-cell activation through complement receptors CD21 and CD32 [216], thereby acting as a bridge to adaptive immunity. Activation of PRRs in dendritic cells provide a necessary signal for activating T-cell responses, again linking the two arms of immunity [217].

1.2.4.2 Adaptive Immunity

Human and mouse data have demonstrated that colonization with pneumococci is actually an immunizing event that induces humoral and cellular (mainly T_H17) adaptive immune responses to *S. pneumoniae*. [218-223]. Due to the extracellular nature of pneumococci, humoral immune responses and the associated antibody production are crucial for control and clearance of infection. One study identified surface proteins PpmA, PhtD, and PsaA as major targets of colonisation-induced humoral-immunity using pneumococcal strain EF3030 [224]. All three proteins have also been identified as antibody targets in models of both murine and human pneumococcal colonisation [225, 226, 221, 222]. As these proteins are sub-capsular, antibodies directed against them can confer serotype-independent protection, and they have been demonstrated to mediate immunity to pneumococcal infections [227-229]. These antibodies are produced by B-cells via $CD4^+$ T-cell-dependent or -independent pathways. HIV-infected individuals are actually 30–100-fold more likely to suffer pneumococcal infection due to depletion of $CD4^+$ T-cells and the associated B-cell dysfunction [230, 231].

However, experiments in genetically modified mice demonstrated protection against colonisation – induced either by prior exposure to live pneumococcus or vaccination with a whole-cell vaccine – did not depend on antibody responses. Instead, protection was critically dependent on $CD4^+$ T-cells [232-234, 228]. It is worth noting that while these experiments focussed on colonisation, previous studies published by our laboratory clearly demonstrate the importance of B-cell responses induced by vaccination for protection against lethal pneumococcal sepsis [235]. Regardless, $CD4^+$ T-cell responses play a critical role in both scenarios. IL-17-producing $CD4^+$ T-cells, known as T_H17 cells, are particularly important for pneumococcal protection, and are predominately involved in host defence against many extracellular pathogens. It has been confirmed in recent years that the signature cytokine of this subset, IL-17, is essential for protection against *S. pneumoniae,* with neutralisation of IL-17 abrogating vaccine-mediated protection [236, 235]. T_H17 cells are required for early recruitment of neutrophils and macrophages during the early stages of colonisation, which mediates bacterial clearance by opsonisation-mediated mechanisms [237, 238]. T_H17-mediated neutrophil recruitment also indirectly improves lung immunity against other respiratory pathogens by boosting local phagocytic capacity, and was found to be associated with increased production of antimicrobial peptides by epithelial cells [239, 240].

1.2.5 Prevention of Pneumococcal Disease

Pneumococcal vaccines Pneumovax and Prevenar-13 (PCV13) are currently available for human use. Pneumovax is a CPS-based vaccine recommended for the elderly, immune-compromised individuals, residents of institutions, and adults in indigenous minorities [241]. Whilst effective in most of these groups, some studies have reported minimal to no decrease in disease for some Australian indigenous adult populations following Pneumovax implementation. This is likely due to low vaccine coverage and/or serotype replacement [241, 242]. Additionally, Pneumovax is ineffective in young children due to the poor immunogenicity of the T-cell independent CPS antigen. To overcome this, CPS was conjugated to a non-toxic diphtheria protein carrier, allowing T-cell dependent processing (see **Figure 1.4**) and providing immunogenicity and immune memory in young children and infants. This conjugated vaccine (PCV13) was licensed in 2010, and since its implementation, a substantial decrease in disease caused by vaccine-included serotypes has been observed [243, 244]. However, due to the complexity of manufacture,

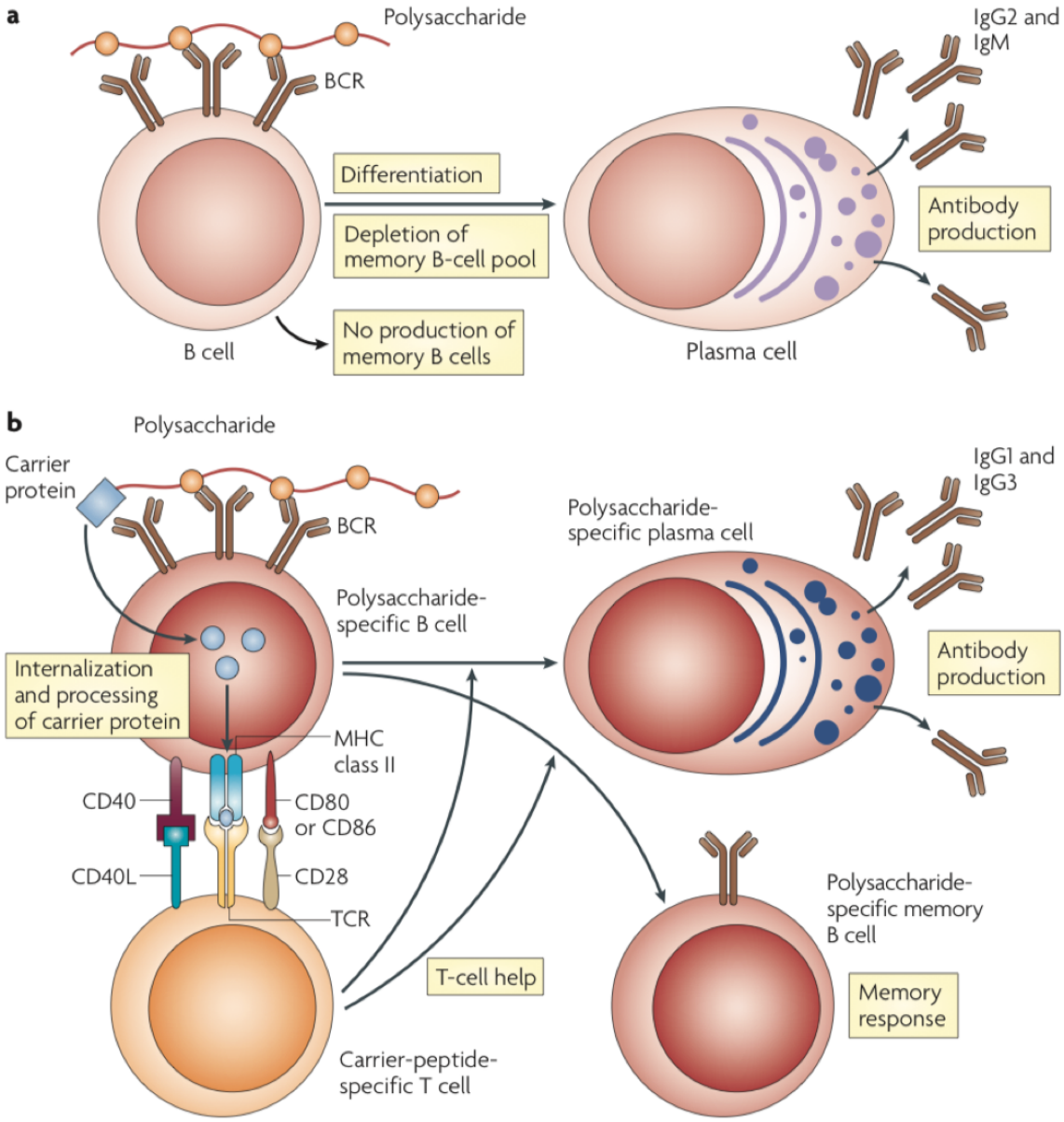

Figure 1.4. Processing of pneumococcal CPS vaccine antigens. (A) Capsular polysaccharides (CPS) stimulate B-cells by cross-linking the B-cell receptor (BCR), and driving the production of immunoglobulins. This process results in a lack of production of new memory B-cells. (B) The CPS from polysaccharide conjugate vaccines is similarly processed by the polysaccharide-specific B-cell, however peptides from the carrier protein are simultaneously presented to carrier-peptide-specific $CD4^+$ T-cells. This results in T-cell help for the production of both plasma cells and memory B-cells. CD40L, CD40 ligand; TCR, T-cell receptor [245].

PCV13 covers only 13 out of 98 identified serotypes (serotypes 1, 3, 4, 5, 6A, 6B, 7F, 9V, 14, 18C, 19A, 19F, and 23F) [246]. It also requires refrigeration, multiple injections, and does not include many of the serotypes that cause pneumococcal disease in the developing world [228].

The lack of broad serotype coverage has also resulted in substantial serotype replacement, whereby reduction in carriage of vaccine-serotypes leaves a vacant niche that is quickly occupied by non-vaccine serotypes [247, 248]. Currently, non-PCV13 serotype isolates, such as serogroup 15B/C, are becoming increasingly common [249, 250], and accounted for a staggering 84.1% of all childhood IPD cases in 2015/16 [251]. In addition, non-PCV serotypes have been recently reported as the major contributors to IPD burden in adults $\geqslant$ 65 years of age [252]. Furthermore, PCVs have not been associated with consistent reduction in the incidence of pneumococcal meningitis – one of the most severe forms of IPD – due to serotype replacement [253-255]. One US study demonstrated rates of childhood meningitis remained entirely unchanged following PCV13 introduction, with serotype distribution clearly shifting towards non-vaccine serotypes [256].

Alarmingly, serotype replacement is not a newly observed phenomenon. Serotypes 19A and 3 were included in PCV13 due to their rapid emergence as predominant causes of IPD following introduction of the preceding PCV7 vaccine (serotypes 4, 6B, 9V, 14, 18C, 19F, and 23F) [257, 248, 258, 259]. The pneumococcus also demonstrates remarkable biological fitness with an ability to exchange DNA to allow capsular switching and acquisition of antibiotic resistance [260]. Serotype 19A is a prime example of this, as this serotype was associated with penicillin and macrolide antibiotic resistance upon its emergence [261-263]. Consequently, unless serotype coverage is dramatically expanded, the clinical benefit of CPS-based pneumococcal vaccines will continually be offset by increases in both carriage and disease by non-vaccine serotypes [247, 248]. Differences in serotype distribution between IPD and acute otitis media cases, and between different countries are also being observed more frequently. Global efforts should therefore focus on accelerating the development of alternative broad-spectrum pneumococcal vaccines that address current shortcomings without compromising efficacy.

1.2.6 Co-Infection with Influenza A and *S. pneumoniae*

Influenza A and B viruses have both been shown to leave patients highly susceptible to subsequent infection (secondary infection) with opportunistic bacteria. *S. pneumoniae* is the most frequent cause of secondary bacterial pneumonia following influenza virus infection, and often leads to severe disease resulting in hospitalization and high mortality [175, 264-269]. Alternatively, existing colonisation with *S. pneumoniae* can lead to exacerbated disease when individuals are concurrently infected with influenza A (super-infection). In this scenario, bacterial pneumonia is the most common disease type to develop, leading to exacerbated influenza disease symptoms, pulmonary distress, and potential pulmonary failure.

1.2.6.1 Mechanisms Underlying Synergistic Infection

There have been several mechanisms proposed to explain how primary influenza infection sensitises the lung to secondary bacterial invaders. Epithelial and mucosal degradation due to viral replication has been reported to increase the exposure of bacterium adherence sites [270], which enhances both susceptibility to bacterial colonisation [271, 272], and nasopharyngeal carriage density [273]. Activity of viral neuraminidase is proposed to also increase exposure of pneumococcal receptors [274, 275]. The mechanical beating of cilia is also impeded [276], which, together with heightened carriage density increases the risk of transmigration of pneumococci to the lung. Enhancement of the incidence of acute otitis media has also been reported due to influenza-induced inflammation [277], suggesting migration to additional sites may also be heightened.

It has been shown that the innate cytokines produced by T-cells in response to IAV infection, e.g. IFN-I and IFN-γ, play fundamental roles in sensitising an individual to infection with pneumococci. Sun & Metzger reported that IFN-γ blocks clearance of *S. pneumoniae* by alveolar macrophages via suppression of the macrophage receptor with collagenous structure (MARCO) that is expressed on the macrophage surface. This receptor is responsible for phagocytosis of un-opsonised pneumococci [265]. IFN-I has also been reported to down-regulate neutrophil chemo-attractants such as CXCL1 and CXCL2, [278] and inhibit IL-17 production by γδ T-cells, which normally aids neutrophil recruitment from the bone marrow [279]. Moreover, the regulatory immune response that occurs following resolution of influenza diminishes the ability of the host to prevent

establishment of secondary infection. This regulatory response is necessary to limit the immuno-pathology sustained by the lung following viral clearance, however the supressed state leaves the host vulnerable to opportunistic bacteria [280, 281, 265, 282, 283]. Induction of inhibitory IL-10 for example has been proposed to inhibit the function of neutrophils, with neutralisation of this cytokine improving disease outcome [284].

Secondary pneumococcal infection has also been shown to modulate the immune response induced by primary IAV infection. In one study, mice were intranasally infected with A/PR8 (H1N1), followed by a lethal dose of pneumococci 3 days later. Co-infected mice were found to have significantly reduced titres of A/PR8-specific IgM, IgA, and IgG in lung homogenate and reduced IgG in serum, compared to mice infected with A/PR8 only. Co-infection also reduced numbers of germinal centre B-cells and T follicular helper cells (T_{FH}) in the spleen and mediastinal lymph node (mLN), which is suspected to contribute to reduced antibody production [285]. The mechanisms behind downregulation of these particular cell subsets are yet to be elucidated.

Super-infection similarly relies on synergistic mechanisms to enhance disease pathology. Exposure of human middle-ear epithelial cells to both IAV and *S. pneumoniae* for example resulted in a synergistic inflammatory response [286]. Subsequent microarray gene analysis of this system revealed that multiple inflammatory genes were upregulated by IAV infection, as was expression of TLR2. Authors postulated the enhanced TLR expression caused cells to be more responsive to concurrent stimulation by pneumococcal peptidoglycan and LTA, leading to increased inflammation [287]. In *vivo,* this could result in enhanced tissue damage and potentially mediate bacterial dissemination. Interestingly, LAIV has been demonstrated to increase pneumococcal translocation to, and persistence within the middle ear in mice. LAIV was administered either 1 or 7 days prior to or during pneumococcal colonization of the nasopharynx. Irrespective of the order of viral/bacterial inoculation, vaccination with LAIV was found to be associated with significantly increased bacterial transmigration to the middle ear, and duration of middle ear colonization (MEC). In the case of LAIV vaccination preceding pneumococcal inoculation (modelling secondary infection), the enhanced MEC was found to occur during or shortly after viral clearance from the upper respiratory tract. This result is in line with numerous other studies that demonstrate epithelial damage and poorly coordinated immune responses following IAV resolution underlie enhanced

susceptibility to bacterial infection. In the pre-colonized mice however, authors propose that low levels of viral replication immediately following vaccination with LAIV may not directly enhance density of pre-existing pneumococcal carriage, but instead could disrupt the balance that naturally exists to prevent commensal carriage progressing to invasive disease [288].

1.2.6.2 Vaccination Strategies Against Co-Infection

In general, industrialized countries recommend both influenza and pneumococcal vaccination for those at higher risk of complications, and in all adults ⩾ 65 years of age. It is recommended that the influenza vaccine is administered annually, and the pneumococcal vaccine is administered every 5 – 10 years. However, vaccine coverage does not reach recommended levels, especially for the pneumococcal vaccine [289-291]. Administering the pneumococcal vaccine at an annual influenza vaccination visit has been suggested as a strategy to improve pneumococcal vaccine uptake and population coverage [292]. This strategy could also reduce the morbidity and mortality resulting from co-infection with live influenza and *S. pneumoniae.*

Studies have reported the positive impact of vaccination against one pathogen on incidence of disease caused by the other. For example, a study evaluating the frequency of otitis media in young children reported that vaccination with the trivalent inactivated influenza vaccine reduced cases of acute otitis media by ~50% [293]. Several groups have also demonstrated dual pneumococcal and influenza vaccination is associated with greater benefits in terms of reducing hospitalization and mortality compared with either vaccine given alone, particularly in elderly populations [294-299]. A retrospective study of Japanese adults with chronic respiratory disease suggested that administration of pneumococcal and influenza vaccines resulted in significant decreases in the number of respiratory infections and hospitalizations compared with people who received the influenza vaccine alone [300].

Additionally, the immunogenicity of both vaccine components when administered simultaneously has been investigated in a number of clinical trials. A Phase III clinical trial evaluated the immunogenicity, safety, and tolerability of PCV13 co-administered with the trivalent inactivated influenza vaccine (TIV) in healthy adults. Results indicated co-administration was well tolerated, and had no negative impact on TIV-specific

antibody responses. However, co-administration was associated with lower PCV13 antibody responses [301]. Another study investigating co-administration of TIV and PCV13 showed TIV-specific responses were unaffected, whilst responses to PCV13 were again lower when compared to those induced by PCV13 administered alone [302]. However, a recent Phase III trial compared co-administration of the inactivated quadrivalent influenza vaccine (IIV4) with the 23-valent pneumococcal polysaccharide vaccine (PPV23) in adults. Immunogenicity of both IIV4 and PPV23 was similar regardless of administration schedule, with no significant reduction in antibody responses [303]. It is unknown whether differences in T-cell processing of the PPV23 and conjugated PCV13 CPS antigens account for these differences in immunogenicity between trials.

It is important to note that these investigated the effects of administering both IAV and pneumococcal vaccines at different anatomical sites. Additionally, despite success of simultaneously administered vaccines, lack of broad-spectrum protection for both influenza and *S. pneumoniae* remains a global health problem. Given the synergistic nature of infection with influenza and *S. pneumoniae*, it is justifiable that a new form of influenza vaccine should also be designed to simultaneously protect against pneumococci. Consequently, a single combination vaccine containing antigens against both of these respiratory pathogens is an appealing possibility.

1.3 Gamma Irradiation for Vaccine Purposes

Gamma(γ)-irradiation is one of the most effective means of sterilisation and has been widely used to ensure sterility of a variety of biological materials (human tissue allografts, pharmaceutical and medical items, and foods). Gamma-rays have also been used to inactivate highly pathogenic infectious agents such as Ebola, Marburg, and Lassa viruses for safe handling and biochemical analysis [304].

Gamma radiation is a form of ionising radiation consisting of high-energy photons (≥ 200 keV) [305], with very high penetrating power. Under the correct conditions, gamma-radiation is capable of inactivating pathogens whilst retaining significant antigenicity; this is a major advantage over other inactivation methods in the context of vaccine preparation [306-308]. Typically, gamma-radiation is generated via the degradation of a radioactive form of cobalt, cobalt-60 (^{60}Co), to the more stable and non-radioactive Nickel (^{60}Ni). It is also possible to use a Cesium-137 (^{137}Cs) source for gamma-ray generation, though ^{60}Co has greater availability and higher penetrating power of the resulting rays [309, 310]. Two high-energy gamma rays (1.17 MeV and 1.33 MeV) are emitted as part of the degradation process of an individual radioisotope, and these can collectively be targeted to the material of interest to neutralise contamination.

1.3.1 Mechanisms of Inactivation by Gamma Radiation

The absorption of gamma-rays results in ionisation of molecules and atoms within a given material. A gamma-ray may interact with an electron, transferring part or all of its energy and causing the electron to be ejected from its orbital path. The ejected electron is often referred to as a 'photoelectron'. Consequently, outer shell electrons drop down to lower orbitals to fill the gap left by the ejected electron, usually resulting in the atom becoming charged and unstable. Alternatively, an outer shell electron may be ejected, again leaving a gap in the outer shell and causing ionization of the atom. This process of ionisation causes deposition and subsequent dissipation of large amounts of energy, leading to disruption and cleavage of covalent bonds, and crosslinking [311, 312]. This effect is termed direct damage. Considering the simple molecular structure of DNA/RNA molecules compared to globular proteins, genomes are far more susceptible to direct damage. Sufficient 'hits' to the genome via this mechanism will render a pathogen inactive, as the genome is unable to be effectively replicated. Due to the globular nature

of most proteins, multiple breaks in the polypeptide chain are needed for complete protein denaturation. However, cleavage of the peptide bond has been reported following exposure to high radiation doses [313].

In addition to the direct damage, the ionization of atoms and molecules may lead to the generation of unstable chemical species termed free radicals. They are chemically reactive and seek stability of their outer shell by interacting or binding with surrounding molecules and atoms. Gamma-rays often interact with water molecules due to their high intracellular concentration, resulting in excitation and dissociation of oxygen and hydrogen, and formation of highly reactive free radicals such as •OH. In fact, ionising radiation damages biological contaminants primarily through radiolysis of water and the damaging action of resulting free radicals on proteins and nucleic acids [314] – this is termed indirect damage. Free radicals may cause oxidative damage to the genome, leading to chemical crosslinking of DNA/RNA, and damage to individual nucleotides. In some instances, base modification and base loss from oxidative free radical attack can be mutagenic [315]. Lesions within DNA/RNA molecules and loss of base information prevents effective replication of the pathogen's genome, rendering it inactive. Free radicals can also cause chemical modification to proteins, resulting in cleavage of polypeptide bonds, aggregation, and oxidation [316]. This enhances inactivation of certain pathogens, as internal proteins carried for genome replication can be rendered non-functional. Additionally, in higher order organisms such as parasites, DNA is typically bound to a 'core' of four histone proteins, forming the nucleosome, as well as to other DNA-associated proteins required for transcription. Crosslinking between DNA and these bound proteins, both histone and non-histone fractions, has been reported following *in vitro* irradiation and analysis by filter retention assay, and again, blocks genome replication [317].

1.3.2 Decimal Reduction Dose (D_{10}) & Sterility Assurance Level (SAL)

Sterility of a product refers to the complete absence of viable microorganisms that may pose a health risk during administration [318]. A sterility assurance level (SAL) of 10^{-6} is currently accepted for treatment of medical products intended to come into contact with compromised tissue barriers, such as surgical equipment, and indicates that the chance of having one viable microorganism in any sterilised unit is one in a million. SAL of 10^{-3} is required for products not intended for such contact [319]. An increasingly common

approach is to use a radiation dose that exceeds these critical parameters to further reduce the probability of any live bio-burden persisting [320, 321]. Calculation of the total radiation dose required to achieve a given SAL is dependent on estimation of the Decimal Reduction Dose, or D_{10} value. This value indicates the radiation dose that reduces viral or bacterial titre by 1-$\log_{10}$ (i.e. 90% reduction) [322]. Assuming log-linear inactivation, this dose can then be scaled up using the following formula to determine the total dose required for sterilization [323].

Sterilising Dose = D_{10} ($\log_{10} N - \log_{10} SAL$), where:

- D_{10} = Decimal Reduction Dose of contaminating pathogen
- N = initial titre/bioburden
- SAL = required Sterility Assurance Level

If a product is suspected of being contaminated with more than one pathogen, the D_{10} value of the most radio-resistant pathogen is to be used to calculate the final sterilizing dose [310]. Previously, a gamma-radiation dose of 25 kilogray (kGy) was thought to be sufficient to achieve a SAL of 10^{-6} irrespective of the type of contaminating pathogen [319]. In the early 1990's, this recommended dose was increased to 50 kGy, particularly for products containing high bio-burden, or when handling agents of high pathogenicity such as Ebola virus and certain Avian influenza strains [310]. However, 50 kGy may not be a universal sterilising dose, as illustrated by the release of live *Bacillus anthracis* (Anthrax) spores from a Department of Defence (DoD) laboratory in the United States. Transportation of live Anthrax had actually occurred by the DoD over a period of 10 years to 9 different countries, though viability of spores was only realized in 2015. Various batches of spores were treated by four different DoD laboratories, and were exposed to irradiation doses ranging from 38 – 54 kGy. However, given the high starting titres reported, a minimum dose of 68 kGy should have been utilised. Additionally, published studies have highlighted that spores are particularly difficult to neutralise [324], and that those damaged by irradiation may have repair mechanisms to restore viability [325, 326]. Thus, pathogen-specific and condition-specific SALs should be considered to ensure appropriate inactivation of pathogens by γ-rays.

1.3.3 Applications of Gamma Irradiation

1.3.3.1 Food Industry

Gamma-radiation is currently used to safely remove bio-contamination from foods that can cause illness, such as *Escherichia coli*, and *Salmonella* spp. Studies have also demonstrated the efficacy of irradiation for removal of viral agents, including Poliovirus [327] and Hepatitis A Virus (HepA) [328]. Gamma-radiation doses of just 2.7 kGy and 3.0 kGy for contaminated lettuce and strawberry respectively were sufficient to reduce inoculated HepA titres by ≥ 90%. Additionally, despite the perishable nature of the food samples tested, no food deterioration was observed, even following treatment with the highest dose of 10 kGy. Irradiation is also used to inactivate food-borne parasites [329], and micro-organisms that cause decomposition and spoilage of foods, thereby increasing food preservation and shelf life [330]. The Food & Drug Administration (FDA) in the United States has approved irradiation of red meats (beef and pork) and poultry, as well as seafood items, eggs, spices, fresh fruit and vegetables Low-level gamma radiation is also being used as an alternative to harsh chemical based-pesticides for crop treatment, as irradiation sterilizes insect pests such as the fruit-fly to prevent their reproduction and reduce the overall pest population [331, 310].

1.3.3.2 Medical & Pharmaceutical Industries

Sterilisation of medical and pharmaceutical products is vital to ensure safety and prevent accidental infection. The use of gamma-radiation in the medical field is progressively increasing, including sterilization of many medical devices [332], animal sera [333, 334], and plasma-derived bio-therapeutics such as albumin, immunoglobulins, and factor VIII (an essential coagulation factor) [335, 336]. Plasma derived products have previously been associated with transmission of infectious diseases such as HIV, Hepatitis viruses, and B19 parvovirus [337-339]. It has been shown that a virally spiked albumin solution could be irradiated at doses of up to 50 kGy whilst maintaining the majority of albumin's structural integrity[340]. Infectious virus was undetectable at just 30 kGy, thus gamma-radiation offers a highly effective method for sterilisation. It also has a few noteworthy advantages over other more conventional methods, such as membrane filtration, heat treatment, and ethylene-oxide (EtO) treatment. For example, gamma-rays possess high penetrating power, enabling the penetration of most external packaging to facilitate terminal sterilization [321].

1.3.3.3 Vaccine Industry

Currently, formalin and beta-propiolactone (BPL) are two of the most common inactivation methods used for viral vaccine inactivation. Formalin exposure results in stabilization and immobilisation of proteins, resulting in loss of both protein function and viral infectivity. Cross-linking of proteins inevitably causes alteration to protein structure and modifications to amino acids, which reduce antigenic integrity and vaccine immunogenicity [341]. BPL inactivation differs from formalin inactivation, as the main target is nucleic acid [342-344]. BPL reacts with the Nitrogen-7 atom of guanine [345], leading to base alteration and subsequent misreading by polymerase of the BPL-altered guanine as an adenine. Hence, for every modified guanine, a transition mutation is incorporated upon genome replication [346]. BPL exposure can also induce DNA double helix cross-linking [347]. This, in combination with numerous guanine base mutations, renders genomes non-functional and the virus becomes replication incompetent. As BPL primarily targets nucleic acid, it was thought that proteins would be left undamaged, resulting in highly immunogenic inactivated preparations. Unfortunately, this is not the case, as BPL also readily interacts with nucleophile moieties present on amino acids. A recent study investigated the effects of BPL exposure on infectivity of IAV H3N2, and reported that virus infectivity was gradually reduced as BPL concentration was increased, with infectivity being eliminated entirely at 1000 μM [348]. However, this loss of infectivity was found to be primarily due to modification of HA2 and M1 viral proteins, which inhibited fusion of the viral envelope with the host cell endosome during infection.

Gamma-irradiation on the other hand is significantly less damaging to protein than both formalin and BPL treatment, and other conventional inactivation approaches that often alter the conformation of antigenic epitopes [76]. While gamma-irradiation damages viral genomes, the structure of the virion as well as external antigenic proteins are relatively well maintained. For example, a 2010 study by Furuya *et al.* showed a three-fold reduction in haemagglutination activity of gamma-irradiated IAV preparations, indicative of slight damage to the HA surface protein. Strikingly, nine-fold reductions in haemagglutination activity were observed for both formalin-inactivated and UV-light inactivated preparations [349]. Thus, gamma-irradiated viruses are still able to be internalised by host cells due to intact surface proteins, and can effectively induce IFN-I responses and associated lymphocyte activation. [350]. Chemical modification of peptides (common with formalin and BPL treatment) also interferes with the process of

uptake and presentation by MHC-I molecules [351], inhibiting induction of effective T-cell responses [352]. Given the superiority of gamma-irradiation over chemical-based methods for antigen maintenance and processing, it has gained substantial interest as a new viral vaccine inactivation approach.

Furthermore, this technology has also been applied to inactivation of bacteria, again for vaccine purposes. A key difference between irradiation of viruses and bacteria is that irradiated bacteria are potentially able to retain metabolic activity despite being non-dividing. Due to the extensively larger genome of most bacteria, irradiation may leave sections of the genome intact, allowing genes on these segments to be expressed and the corresponding proteins to be produced and/or secreted [353]. This would allow the irradiated bacterium to provide prolonged exposure of the immune system to native antigens. Irradiated *Brucella melentenis* for example was shown to possess transcriptional and metabolic activity similar to that of live *Brucella*, and was able to persist within macrophages. Despite this, the irradiated bacteria showed no signs of residual virulence, as mice challenged with irradiated *Brucella* did not develop any signs of disease [353]. The illustration that metabolic activity alone is not sufficient for pathogenesis will be very important for future clinical application of γ-irradiated bacterial vaccines. In contrast to γ-irradiation, traditional inactivation methods such as heat or chemical agents impair replicative ability and also denature proteins and nucleic acids, abrogating both transcription and metabolic activity. Consequently, inactivated bacterial vaccines often have low immunogenicity due to insufficient immune stimulation. In support of this, Magnani *et al.* showed that heat-killed *Brucella* had impaired protective ability compared to an irradiated preparation, which induced both antigen-specific T-cells and protection against bacterial challenge [353].

Irradiation of whole *Mycobacterium tuberculosis* (TB) as a novel vaccine candidate has also been in development [354]. Gamma-irradiated TB was shown to provide significant protection in mice against challenge, and inclusion of an aluminium hydroxide-based adjuvant in the vaccine resulted in protection equivalent to that of control Bacillus Calmette-Guérin (BCG, existing vaccine strain) treated mice [355]. Irradiated TB was also shown to induce nitric oxide release for antimicrobial activity [356, 357], and T_H2 responses resembling that induced by a live TB infection [358, 354]. Whole irradiated *Salmonella typhimurium* [359] and *Brucella neotomae* [360] have also been investigated

as potential inactivated vaccine candidates. Both vaccines were able to induce elevated levels of antigen-specific antibodies, and conferred protection against challenge. Gamma-irradiated *B. neotomae* was also shown to induce antigen-specific $CD4^+$ and $CD8^+$ T-cell responses, with IFN-γ and TNF-α secretion [360].

1.3.4 Gamma Irradiated IAV Vaccine (γ-Flu)

Our group has developed an intranasally administered IAV vaccine comprised of whole gamma-irradiated influenza A virus, termed γ-Flu. A single intranasal dose of γ-Flu (A/PC, H3N2 strain) was shown to induce cross-protective immunity against heterosubtypic non-vaccine strains, including H1N1 and highly pathogenic avian H5N1 [361]. This is major step forward from current inactivated influenza vaccines, which offer strain-specific protection only. Interestingly, the same A/PC influenza preparation failed to induce heterosubtypic protection when inactivated with formalin or UV (conventional methods) as opposed to gamma-radiation [349].

The superiority of irradiated IAV is related to the retained functionality of viral surface proteins, which mediate binding to host cells and subsequent membrane fusion. In fact, γ-Flu effectively mimics a live virus infection, inducing IFN-I responses and the associated lymphocyte activation in a TLR7-indpendent manner, indicating virus internalisation by host cells [350]. This is confirmed by the ability of target cells to process and present γ-Flu antigens vial MHC-I, leading to induction of cytotoxic $CD8^+$ T-cell responses targeting internal proteins such as NP [362]. These internal proteins are highly conserved between different strains and subtypes of IAV, allowing T-cell responses induced by one strain to be broadly cross-protective. In contrast to γ-Flu, UV- and formalin-inactivated IAV preparations, as well as the licensed trivalent IIV were all shown to be unable to induce cross-reactive cytotoxic T-cell responses [349]. It has also been reported that intranasal vaccination with whole BPL-inactivated IAV was associated with very poor $CD8^+$ T cell responses, which corresponded to only partial protection in mice against heterosubtypic challenge [363]. The efficacy of γ-Flu following intranasal administration has advantages for respiratory vaccines in general, and has the potential to be of considerable benefit for mass vaccination regimes involving self-administration in the face of a future pandemic.

1.3.5 Gamma Irradiated Pneumococcal Vaccine (γ-PN)

Past studies have demonstrated that immunisation with a genetically detoxified derivative of *S. pneumoniae* protein pneumolysin (termed pneumolysoid) provides significant protection against numerous serotypes of *S. pneumoniae* [364, 365]. In addition, immunisation with combinations of virulence proteins was reported to provide synergistically enhanced protection when compared to single antigens [366-368]. Immunisation with whole-cell pneumococci is therefore expected to enhance protection even further due to inclusion of a vast majority of pneumococcal antigens. In fact, an ethanol-killed (conventional method) whole-cell pneumococcal preparation has been shown to elicit protection against nasopharyngeal carriage, though protection was dependent on using cholera toxin as an adjuvant [369].

Given the enhanced immunogenicity of γ-Flu compared to conventionally-inactivated preparations, it was postulated that gamma-irradiation could be used as an inactivation method to develop a whole-cell pneumococcal vaccine. In fact, our group has recently published that intranasal vaccination with a non-adjuvanted whole-cell gamma-inactivated *S. pneumoniae* vaccine (γ-PN) induced serotype-independent protection against lethal intranasal challenge models of pneumococcal sepsis and focal pneumonia. This protection was demonstrated to be dependent on B-cell responses and IL-17 production by innate γδT17-cells. Vaccination with γ-PN was also shown to induce elevated *S. pneumoniae*-specific IgG and IgA in serum [235]. Furthermore, current CPS and conjugate pneumococcal vaccines are effective against vaccine-included serotypes, however their continued use is leading to serotype replacement, whereby non-vaccine serotypes simply replace vaccine serotypes in the newly vacant nasopharyngeal niche. As serotype specificity is conferred by the capsular polysaccharide, our group utilized a capsule deficient derivative of *S. pneumoniae* D39 (serotype 2) to overcome this. Removal of the capsule from our vaccine strain successfully allowed exposure of key surface antigens, and consequently induction of serotype-independent protection [235].

1.4 COMBINATION VACCINES

As outlined in *Section 1.2.6.2,* concurrent administration of inactivated IAV and CPS-based pneumococcal vaccines has been investigated previously by other groups, with promising results. This strategy, termed simultaneous administration, has also been investigated for other vaccine antigens, both live and inactivated. In general, concurrently administered vaccines have been shown to produce seroconversion rates equivalent to those seen when the vaccines are administered independently [370-374]. For example, the Varicella vaccine and LAIV can be administered simultaneously with no interference of immune responses [375], as can the Yellow Fever vaccine with both Hepatitis B [376], and measles vaccines [377].

The mixing of multiple vaccine components into a single product is an alternative strategy to induce protection against multiple pathogens. Initially this was thought to be associated with higher risk of immune interference, due to multiple conflicting immune responses being induced at a single site. Despite this, a number of combination vaccines have been very successful. The first to be trialled was DTP, containing individual diphtheria, tetanus, and pertussis vaccine antigens in a single vial. This combined vaccine was first administered to infants and children in 1948 [378], and its success paved the way for the addition of other vaccine components to the DTP formulation, and the eventual replacement of specific components to minimise reactogenicity [379]. Combination vaccines bring numerous benefits from a vaccine coverage perspective, and the increasing complexity of recommended childhood and elderly vaccination schedules continues to necessitate the development of new combination formulations.

1.4.1 Licensed Combination Vaccines

Based on the formulation of diphtheria, tetanus, and acellular pertussis toxin (DTaP) [379], two pentavalent combinations have been created, containing additional vaccine antigens. The first is Pediarix, a DTaP, hepatitis B (HepB) and inactivated poliovirus (IPV) formulation, and the second is Pentacel, a DTaP-IPV plus a *H. influenzae* type b (Hib) polysaccharide formulation. An additional advance on this combination is Infanrix-hexa from GSK, containing all aforementioned antigens (DTaP-HepB-Hib/IPV) to protect against a total of 6 different infectious agents [380]. In all instances, the bacterial DTaP components are all acellular. Infanrix-hexa is adjuvanted with both aluminium hydroxide and aluminium phosphate adjuvants, which adsorb to the DTaP and the HepB

vaccine components respectively. While this combination is currently licenced in Europe [160], it is yet to gain licensure in the US due to the reported reductions in antibody titres to Hib [381].

Interestingly, this reduction in titre has been clinically reported for multiple DTaP-based combination vaccines [382-384, 245]. The mechanism by which mixing Hib with a DTaP-based vaccine affects antibody titres against the Hib component only is currently unknown. Incompatibility of Hib vaccines with aluminium adjuvant [385], or carrier-induced epitopic suppression [386, 387], have both been considered. The antibody reduction has also been studied in a preclinical rat model. Similar to clinical data, authors of this study observed no reduction in antibody response to any of the DTaP components following co-administration with Hib, though a reduction in anti-Hib responses was observed [388]. This study demonstrated that aluminium hydroxide adsorbed Hib vaccine induced 5 – 11-fold lower antibody titres compared to un-adsorbed Hib alone, which supports the theory of adjuvant incompatibility. The authors also reported that mixing of Hib with DTaP resulted in complete adsorption of Hib to aluminium hydroxide, whilst mixing Hib with a formulation containing aluminium phosphate only did not reduce Hib-specific antibody titres [388].

In contrast to antibody responses, co-administration of Hib with DTaP components resulted in higher IFN-γ secretion by spleen cells compared to separate administration of the same components [389]. This suggests that whilst antibody titres may be lowered, cell-mediated immune responses may be increased, indicating a shift in adaptive immunity and potentially enhanced protection.

Vivaxim is another licenced combination vaccine, offering protection against enteric diseases Hepatitis A virus and typhoid fever. It contains a sterile suspension of purified *Salmonella typhi* Vi capsular polysaccharide and formaldehyde inactivated Hepatitis A virus antigen, presented in a dual-chamber syringe [390]. The contents of each chamber are mixed within the syringe immediately prior to injection. Clinical trials illustrated the combination vaccine was highly immunogenic and offered rapid seroconversion. No differences in immune responses were observed between patients immunised with the two vaccine components separately or combined, indicating minimal interference between responses raised against the individual antigens. Seroconversion occurred to the

same extent against both antigens irrespective of administration type (single or combination), and co-administration had no impact on safety or reactogenicity [391, 392].

Other combination vaccines currently available include Priorix-Tetra (a live combination vaccine against measles, mumps, rubella and varicella viruses), and MenHibrix (containing CPS antigens from *Neisseria meningitidis* serogroups C and Y, and from *Haemophilus influenzae* type b, with each CPS type covalently bound to inactivated tetanus toxoid). Currently, there is no combination vaccine that is comprised of whole inactivated bacteria and whole inactivated virus.

1.4.2 Combination Strategies under Investigation

Many groups have explored novel combinations of individual antigens with the intent of collectively protecting against certain types of infectious disease. For example, *S. pneumoniae and Neisseria meningitidis* have sufficient overlap in terms of epidemiology and meningitis burden to warrant a single combination vaccine [393]. To assess suitability, one study combined the 13-valent pneumococcal conjugate vaccine and a *N. meningitidis* serogroup B vaccine (MenB) in mice, to determine any immunological interference. Antibody responses specific to MenB were not influenced by co-administration. Interestingly, pneumococcal-specific antibody titres against multiple included serotypes were significantly enhanced when MenB was co-administered. It is likely that this enhancement was mediated by the lipopolysaccharide (LPS) present in the outer membrane vesicles that comprise the MenB vaccine, as LPS has strong adjuvant activity [394]. In fact, enhanced immunity to a MenC conjugate vaccine was also seen after co-administration with MenB in healthy adults, though the difference was not statistically significant [395].

Other studies have intentionally co-administered novel vaccine components with the intent of using one as an adjuvant to boost immunogenicity of the other. A combined Norovirus (NoV) and Rotavirus (RV) vaccine was investigated that consisted of NoV-like particles and recombinant polymeric RV VP6 protein. VP6 was engineered to self-assemble into polymeric tubular structures for adjuvant activity, as this form of VP6 has heightened immunogenicity compared to the monomeric form, and readily activates APCs. Initially, the NoV and RV components were administered either individually or in

combination, and investigators observed no negative impact of co-administration on antibody or T-cell responses [396, 397]. Subsequently, the adjuvant effect of polymeric VP6 on NoV-specific responses was investigated. Sub-optimal doses of NoV-like particles did not induce significant antibody titres, however, when intramuscularly co-administered with VP6, considerable levels of both type-specific and cross-reactive anti-NoV antibodies were elicited. High levels of IL-4 produced by $CD4^+$ T_H2 cells in response to VP6 was thought to promote proliferation and differentiation of NoV-antigen primed B lymphocytes, leading to enhanced antibody titres. In addition, the ready uptake of polymerised VP6 by macrophages and DCs was proposed to induce cell maturation and production of pro-inflammatory cytokines IL-6 and TNF-α. Hence, VP6 may create a favourable milieu for adequate antigen presentation of co-delivered antigens [398].

1.4.3 Co-administration of γ-Flu and γ-PN

Our group is currently investigating a novel vaccine strategy based on combining whole-inactivated IAV (γ-Flu) and whole-inactivated *S. pneumoniae* (γ-PN) in a single vaccine formulation. The combining of whole viral and bacterial vaccine components has never been investigated to our knowledge, and the success of our approach thus far has the potential to reshape the combination vaccine field. Our group has previously demonstrated that potent IFN-I responses and lymphocyte activation are induced by γ-Flu vaccination [350], which allow it to act as an effective adjuvant for low immunogenicity vaccines, such as gamma-irradiated SFV vaccine [399]. Unlike irradiation of influenza, SFV irradiation nullifies its ability to induce IFN-I and IFN-mediated responses, leading to insufficient stimulation of B-lymphocytes [400-402]. When co-administered with γ-Flu however, significant enhancement of SFV-specific antibody titres and neutralising ability were observed.

Given this, intranasal co-administration of γ-Flu and γ-PN vaccines has since been investigated by our group, with the intent of enhancing pneumococcal-specific responses. According to the traditional dogma of T_H1 and T_H2-type immune responses, whole virus and whole bacteria induce competing arms of immunity, and thus co-vaccination was expected to impair immune responses to each antigen type. However, it was found that γ-Flu significantly enhanced γ-PN specific responses when the two vaccines were intranasally co-administered. In contrast to vaccination with γ-PN alone, co-

immunization boosted populations of pneumococcal-specific T_H17 and T_H1 cells in the lung, and reduced lung and nasopharyngeal CFU titres after pneumococcal challenge. It also promoted development of lung $CD4^+$ tissue-resident memory (T_{RM}) cells and enhanced *S. pneumoniae*-specific antibody responses. Additionally, co-administration did not compromise IAV-specific immunity, with both γ-Flu-vaccinated and co-vaccinated groups showing 100% protection against lethal influenza challenge [403]. Furthermore, only the combination vaccine was able to confer significant protection against a lethal super-infection challenge model in mice (EF3030 colonisation followed by intranasally administered A/PR8). This work clearly demonstrated the ability of γ-Flu to behave as an effective adjuvant to a whole-cell bacterial vaccine, specifically by priming the lung microenvironment to favour induction of highly effective immune responses against the co-administered antigen. Furthermore, the serotype- and strain-independent protection offered by γ-PN and γ-Flu respectively heralds the possibility for our novel combination vaccine to offer a simplified universal vaccine strategy to protect against diverse strains and serotypes of IAV and *S. pneumoniae*.

1.5 RESEARCH PROJECT

1.5.1 Rationale for Project

IAV continues to be a global health and vaccination challenge. Currently available vaccines are sub-optimal, as inactivated formulations induce strain-specific immunity only, and require annual reformulation. The method of inactivation for these vaccines interferes with induction of cross-reactive T-cell responses targeting conserved viral proteins, which would be far more effective against both circulating and emerging strains. Live attenuated IAV vaccines are available in some regions, however reports of limited efficacy and adverse side effects mean it is not recommended for use in certain groups such as the immune-compromised [404]. The use of LAIV during a pandemic scenario is also thought to be associated with high risk of viral recombination [405].

Past work by our group has established the efficacy of whole gamma-irradiated influenza A vaccine (γ-Flu) as a novel inactivated vaccine capable of inducing robust cross-protective immunity in mice. This vaccine would therefore be suitable to use in all populations, and would not require annual reformulation. As gamma-irradiation is a promising approach to design a universal flu vaccine (and other next generation vaccines), inactivation conditions and the impact on virus structure and vaccine efficacy will be investigated in this study. Importantly, the suitability of high radiation doses such as 50 kGy for IAV vaccine inactivation will be determined, as this could allow inclusion of highly pathogenic strains in future γ-Flu formulations.

S. pneumoniae is another respiratory pathogen of interest, as despite the availability of pneumococcal vaccines, invasive pneumococcal diseases remain prevalent and severe. Similar to IAV, current pneumococcal vaccines have major shortcomings. These include limited serotype coverage (current vaccines cover only 23 serotypes out of a total 98), and serotype replacement, whereby non-vaccine serotypes simply recolonise the host by occupying the vacated nasopharyngeal niche after vaccination. Whilst disease due to vaccine-included serotypes is substantially reduced, these non-vaccine serotypes subsequently emerge as major causes of invasive disease. This phenomenon compromises the positive impact of vaccination on global disease burden. To combat these issues, a novel pneumococcal vaccine has been recently developed in our lab based on gamma-irradiation of whole un-encapsulated *S. pneumoniae* (γ-PN), that is capable of

providing serotype-independent protection in mice. Serotype-independent responses were achieved by removal of the capsule from our vaccine strain, to allow exposure of conserved sub-capsular antigens. This unencapsualted strain (termed Rx1) was also altered by removal of the *lytA* gene to facilitate growth to high titre *in vitro*, and replacement of the *ply* gene with a non-toxic PdT derivative (generating Rx1(ΔLytA, PdT)). One particular study observed that IL-17A responses induced by a whole-cell vaccine were attributable in some part to Ply, since responses were significantly reduced when using a Ply-negative whole cell antigen [237]. Thus, Ply was replaced rather than being removed from our vaccine strain to maintain Ply-specific immunity. This attenuated strain is then inactivated by γ-irradiation to generate γ-PN. To aid in licensing and to further improve the safety profile of this potential vaccine candidate, an additional mutation to reduce bacterial virulence prior to irradiation will be beneficial. Such a mutation would be required to effectively attenuate the vaccine strain, without altering expression of key surface properties to preserve immune-stimulation and antigenic targets. An auxotrophic mutation that affects *in vivo* growth whilst being dispensable under select laboratory conditions was considered, and the solute binding component of the manganese import pathway, *psaA,* was selected for deletion. The impact of this growth-attenuating mutation on γ-PN vaccine immunogenicity and protective efficacy will be determined during this study.

In addition to causing severe morbidity and mortality on their own, IAV and *S. pneumoniae* exhibit lethal synergism. A large portion of yearly influenza related fatalities are actually due to subsequent bacterial pneumonia, as the host is left highly susceptible upon resolution of primary viral infection. Despite this, strategies to avoid both sequential and simultaneous infections with IAV and *S. pneumoniae* remain unsuccessful. As such, a single combined vaccine containing both γ-Flu and γ-PN has been the source of recent investigation. Studies by Babb *et al*. have clearly demonstrated that co-administration of these whole-inactivated vaccines results in significant enhancement of pneumococcal-specific responses, in comparison to administration of γ-PN alone.

Intriguingly, killed whole-cell bacteria has been observed to have some adjuvant effect on co-administered antigens in other studies. Szostak *et al.* utilised a controlled lysis system to generate non-living bacterial ‘ghosts’, which were devoid of all cytoplasmic contents whilst bacterial morphology, envelope and cell surface structures were

effectively maintained. By utilising the whole intact bacterium, innate immune-stimulatory agonists (e.g. LPS, lipoteichoic acids, flagellin etc.) are included, and act as potent activators of a broad range of cell types via TLR signalling [406]. This induces production of pro-inflammatory cytokines [407, 408], which augment expression of co-stimulatory and adhesion molecules on both immune and non-immune cell types. Adjuvant activity of the bacterial ghosts was investigated via co-administration with purified HIV-l protein reverse transcriptase (RT). Elevated RT-specific humoral responses were observed following co-administration via both subcutaneous and intraperitoneal routes. In fact, co-administration with bacterial ghosts resulted in higher RT-specific titres than both Freund's complete adjuvant and aluminium hydroxide (Alum) when administered IP [409]. Foreign bacterial and viral antigens have also been loaded inside the cytoplasmic lumen of these bacterial ghosts, or expressed on the surface and in the periplasmic space [410, 411]. It has been observed that bacterial ghosts induce potent protective responses at mucosal surfaces against such 'ghost delivered' foreign antigens, and bias the immune response toward the Th1 type [412, 413], which is typically indicative of $CD8^+$ T-cell activation [414].

To our knowledge, bacterial ghosts have not been co-administered with whole virus, and the observations above indicate that such an approach could be very beneficial for viral-specific immune responses. In fact, given that γ-Flu provides adjuvant activity to co-administered γ-PN, the reverse phenomenon would result in a co-vaccination approach that enables bi-directional adjuvant activity. Furthermore, our killed pneumococcal cells contain intracellular components in addition to the maintained surface structures and morphology. Unlike bacterial ghosts, our pneumococcal vaccine would also be capable of stimulating TLR9 via bacterial CpG-DNA, e.g. upon uptake and degradation in the endosome of phagocytic cells [415, 209]. Thus, following optimisation of safety and further characterisation of both γ-Flu and γ-PN vaccines alone, the impact of mucosal co-vaccination on IAV-specific immune responses will be thoroughly investigated using both *in vivo* and *in vitro* models.

Overall, both IAV and *S. pneumoniae* continue to pose profound threats to global human health. A successful combination vaccine could save millions of lives every year by minimising disease due to both IAV and *S. pneumoniae* alone. The novel approach outlined here will ensure protection is conferred by vaccination regardless of which IAV

strains and pneumococcal serotypes circulate, and/or emerge as major causes of severe disease. The co-administration of γ-Flu + γ-PN would also effectively protect against secondary and super-infection with both IAV and *S. pneumoniae* to minimise severe morbidity and mortality during seasonal outbreaks and future influenza pandemics.

1.5.2 Hypotheses & Aims

Hypothesis 1: Irradiation conditions can influence the efficacy of the γ-Flu vaccine.

Hypothesis 2: Co-administration of γ-Flu and γ-PN will enhance IAV-specific immunity.

Aim 1. To investigate the effect of irradiation conditions on γ-Flu immunogenicity.

Aim 1.1. To investigate the effect of irradiation temperature on IAV protein and virion structural integrity.

Aim 1.2. To investigate the effect of high irradiation dose on γ-Flu immunogenicity *in vivo* and *in vitro.*

Aim 1.3. To investigate the effect of high irradiation dose on γ-Flu protective efficacy, using mouse models of lethal influenza infection.

Aim 2. To enhance safety and immunogenicity of γ-PN.

Aim 2.1. To introduce an auxotrophic mutation to our existing Rx1(ΔLytA, PdT) vaccine strain, to generate Rx1(ΔLytA, PdT, ΔPsaA).

Aim 2.2. To inactivate Rx1(ΔLytA, PdT, ΔPsaA) using γ-irradiation, generating γ-PN(ΔPsaA).

Aim 2.3. To characterise the impact of the growth attenuating mutation on γ-PN(ΔPsaA) immunogenicity and protective efficacy using mouse models of lethal pneumococcal infection.

Aim 3. To study the protective immunity induced following co-administration of γ-Flu and γ-PN(ΔPsaA).

Aim 3.1. To determine the impact of co-administration on influenza-specific immune responses and protection.

Aim 3.2. To determine the mechanism(s) of interaction between γ-Flu and γ-PN(ΔPsaA) vaccines when co-administered.

CHAPTER 2

The effect of gamma-irradiation conditions on the immunogenicity of whole-inactivated influenza A virus vaccine

2.1. INTRODUCTION

Emergence of Avian influenza strains H5N1, H5N6, H7N9, and H9N2 represent major health concerns due to their potential to cause the next worldwide viral pandemic [135]. Since 2003, the World Health Organization (WHO) has reported 860 cases of human infection with the highly pathogenic avian influenza (HPAI) strain H5N1, with an average mortality rate of 53% [136]. Avian H7N9 is also of particular concern, and it has emerged more recently and substantially more rapidly than H5N1. Since 2013, a total of 1564 laboratory-confirmed cases and 612 deaths have been recorded [136]. China in particular has reported substantial increase in human infections with avian H7N9 since October 2016 [153]. Most human infections with these avian strains occur via contact with infected poultry, and consequently vaccination of domestic poultry against A(H7) viruses has recently commenced in addition to the ongoing poultry vaccination program against avian A(H5) viruses [136]. However, rare clusters of human-human transmission of avian influenza viruses have been reported between family groups in Thailand [149, 150], Indonesia [151], Turkey [152], and Vietnam [149]. Through increased human infection, these strains may gain mutations to facilitate sustained aerosol transmission between humans. Notably, a mere five mutations in a laboratory H5N1 strain allowed efficient aerosol transmission between ferrets [145, 148]. Interestingly, low pathogenic (LP) avian H7N9 has been shown to be capable of transmission between ferrets via aerosol droplets, albeit inefficiently [154] A highly pathogenic (HP) H7N9 strain that emerged in late 2016 – early 2017 was recently found to have the same capability [155].

Serological surveys reported zero or very low levels of existing immunity within the human population against avian H7N9 [416-418]. Additionally, currently available inactivated vaccines solely induce antibody responses against vaccine-included influenza strains. Protective efficacy against potentially pandemic H7N9 and H5N1 avian strains is therefore minimal. Consequently, new approaches are needed for development of broadly-protective next-generation influenza vaccines. We have previously reported the use of gamma-irradiated whole influenza A virus (γ-Flu) as a vaccine candidate capable of inducing cross-protective immunity against both emerging seasonal and pandemic influenza strains [361]. We demonstrated the superiority of γ-Flu against UV- and formalin-inactivated preparations for conferral of protection against both homotypic and heterosubtypic challenge strains [349]. In fact, conventional inactivation methods often alter the conformation of antigenic epitopes, compromising immunogenicity and vaccine

efficacy [76]. Chemical modification also interferes with antigen uptake and presentation of peptides by MHC-I molecules, thereby inhibiting induction of class I restricted T cell responses. In contrast, γ-irradiation conditions can be manipulated such that the viral genome is sufficiently damaged to render the virus replication incompetent, but virus structure and internal and external antigens are relatively unaffected [320, 331, 310]. Our irradiated influenza virus can therefore bind to and be internalised by host cells for processing and presentation of internal viral peptides via MHC-I, similar to a live infection [349, 350].

To ensure sterility of irradiated influenza materials, the concept of Sterility Assurance Level (SAL) has been adopted and a value of 10^{-3} or 10^{-6} (one in a thousand or million chance of live micro-organisms remaining in any one unit after treatment) has been arbitrarily determined and widely accepted [319]. To estimate the irradiation dose required to achieve a chosen SAL, a mathematical concept based on the decimal reduction value (D_{10} value) has been used. The D_{10} value refers to the irradiation dose required to inactivate 90 per cent of the microbial population (i.e. a dose causing a one log reduction). Theoretically, it is possible to calculate the radiation dose required to achieve the desired SAL if the D_{10} value and the initial virus titre have been determined, using the mathematical formula "SAL = D_{10} value × N". Here, N represents the number of $\log_{10}$ reductions in bioburden required to achieve a theoretical titre of 10^{-3} or 10^{-6} as required. The Australian Department of Agriculture recently considered an irradiation dose of 50 kGy as mandatory for sterilisation of highly pathogenic agents of biosecurity concern [310]. Considering the potential risk of a future influenza pandemic involving a HPAI strain, inclusion of such pathogenic strains may be warranted in future γ-Flu preparations. This would allow immediate protection offered by antibody responses in addition to cross-reactive T cell immunity. In this case, vaccine irradiation dose may be increased to 50 kGy or above to meet the safety requirement. However, increasing irradiation dose may affect protein integrity and thus vaccine efficacy. For example, Feng *et al.* demonstrated using SDS-PAGE that the abundance of Murine Norovirus 1 (MNV-1) capsid protein VP1 decreased as radiation dose was progressively increased [419]. In addition, whilst the damaging effects of γ-irradiation are primarily dose-dependent, the extent of structural damage is also influenced by other factors such as irradiation temperature [420, 421]. Importantly, protein antigenicity is reported to be better maintained when virus samples are irradiated on dry-ice [306]. In the current study, we

investigated the effect of both irradiation dose and irradiation temperature on the immunogenicity of γ-Flu.

2.1. MATERIALS AND METHODS

2.2.1. Ethics statement

This study was conducted in strict accordance with Australian Code of Practice for Care and Use of Animals for Scientific Purposes (7th edition [2004], 8th edition [2013]) and South Australian Animal Welfare Act 1985. Experimental protocol approved by Animal Ethics Committee at The University of Adelaide (S-2013/014 & S-2016/036).

2.2.2. Cells & Viruses

Influenza A virus [A/Puerto Rico/8/34 (H1N1) (A/PR8)] was grown in allantoic cavity of 10-day-old embryonated chicken eggs. Eggs were injected with 10^3 $TCID_{50}$ A/PR8, incubated for 48 h at 37°C, and chilled at 4°C overnight. Allantoic fluid was harvested, pooled and stored at -80°C. Virus stock was titrated in Madin-Darby Canine Kidney (MDCK) cells using $TCID_{50}$ assay as previously described [422], and estimated as 1.5×10^6 $TCID_{50}$/ml. Virus stock was concentrated using chick erythrocytes (cRBCs) essentially as previously described [423]. Briefly, allantoic fluid was incubated with cRBCs for 45 min at 4°C to allow haemagglutinin to bind erythrocytes, then centrifuged for 10 min at 300 g (at 4°C), and allantoic supernatant was removed. Pellets were resuspended in normal saline and incubated for 1 h at 37°C to release virus from cRBCs, prior to centrifugation to separate erythrocytes from virus-containing supernatant. Concentrated A/PR8 stock titre was estimated as 2×10^8 $TCID_{50}$/ml.

2.2.3. Vaccine preparations

A/PR8 stocks were inactivated by exposure to γ-radiation from ^{60}Co irradiation facility at the Australian Nuclear Science and Technology Organisation (ANSTO), either on dry-ice or at room temperature. Sterility was confirmed by passages as recommended by WHO [424]. In brief, 10-day-old embryonated eggs were inoculated with 100 µl of inactivated preparation and incubated for 2 days at 37°C. The allantoic fluid of individual eggs was then harvested and used to infect new 10-day-old embryonated eggs. This process was repeated 3 times and lack of detectable hemagglutination by HA assay in allantoic fluid from 3 passages indicated complete loss of virus infectivity.

2.2.4. Haemagglutination Assay (HA Assay)

Serial dilutions of gamma-irradiated A/PR8 (γ-A/PR8) and control non-irradiated preparations were performed in PBS using a 96-well round bottom plate (100 µl/well). PBS containing 0.8% cRBCs was added to each well and incubated at 4°C, and haemagglutination patterns were analysed 24 h later.

2.3.5. Transmission Electron Microscopy (TEM)

γ-A/PR8 samples were loaded into 3mm formvar-amorphous carbon-coated copper grids and left for 2 min to settle. Excess solution was removed by blotting, and samples stained with 2% Uranyl Acetate for 2 min. Samples were blotted, then left to dry at RT for 10 min before visualisation with the FEI Tecnai G2 Spirit Transmission Electron Microscope (Adelaide Microscopy, University of Adelaide).

2.2.6. SDS-PAGE

Irradiated and non-irradiated control samples were heat-treated at 85°C for 20 min. Viral proteins were separated by electrophoresis on Pre-Cast NuPAGE Novex 4-12% Bis-Tris gels (Thermo Fisher), then stained with Coomassie Brilliant Blue. Novex Sharp Pre-Stained Protein Standards (Thermo Fisher) were used for molecular weight comparison.

2.2.7. Mice & Treatment

Six-week-old female wild-type BALB/c mice (H-2^d) were supplied by Laboratory Animal Services, University of Adelaide. Mice were anaesthetized intraperitoneally (IP) with 10 µl/gram body weight ketamine anaesthetic (1% xylazine, 10% ketamine in sterile H_20), and vaccinated intranasally (IN) with one or two doses 14 days apart of γ-A/PR8 in a volume of 32 µl ($TCID_{50}$ equivalent/mouse for different vaccine doses specified in the Results section). Control animals were mock-vaccinated with PBS. This immunisation route paired with anaesthesia was chosen to allow the vaccine inoculum to enter the lung, to induce immune responses specifically at the site of infection. This administration approach has been previously validated to allow inoculum to enter the lungs, using a challenge model of *S. pneumoniae* [224]. On Day 21 post-vaccination, animals were anaesthetised as above, and challenged IN with A/PR8 (1.6×10^2 $TCID_{50}$/mouse). Mice were monitored for 3 weeks for clinical symptoms and weight loss. Animals were culled if they lost 20% of their starting body weight.

2.2.8. Measurement of influenza-specific antibody responses

Blood samples were collected from all mice via submandibular bleeding on Day 20 post-vaccination, and serum levels of A/PR8-specific IgG were determined by ELISA as described previously [399]. Absorbance measured at 450/620 nm using a Biotrack II plate reader, and end point titres expressed as the reciprocal of the last dilution where the OD value was greater than or equal to the cut-off value. The cut-off value was calculated as the mean + (3 × S.D.) of OD values of samples from control mice at a 1:100 dilution.

2.2.9. In vitro Neutralisation Assay

96-well tissue-culture plates were seeded with 6×10^4 MDCK cells/well. A/PR8 was activated by treatment with 2 µg/ml TPCK-trypsin (Sigma-Aldrich) for 30 min at 37°C. Heat-inactivated sera were serially diluted, mixed with A/PR8 (diluted in allantoic fluid with 4 µg/ml TPCK-trypsin) in 1:1 ratio, and incubated for 1 h at 37°C. Mixtures were added to MDCK monolayers at multiplicity of infection (MOI) of 0.1 and incubated for 2 h at 37°C with 5% CO_2. Then, inoculum was removed, monolayers washed with PBS and incubated for an additional 22 h in serum-free media. Monolayers were then washed, fixed and permeabilised with acetone/methanol (1:1 ratio) at 4° C and incubated with polyclonal murine anti-A/PR8 sera (generated as previously described [425]) for 1h at 4°C. Then, secondary antibody Alexa-Fluor® 488 goat anti-mouse IgG (H+L) (Life Technologies) was added for 1 h at 4°C. Nuclei were stained with DAPI (1 µg/ml) for 30 min at room temperature. Images were acquired using a Nikon TiE inverted fluorescence microscope and analysed using NIS elements software (Tokyo, Japan).

2.2.10. Cytotoxic T lymphocyte (CTL) Assay

Mice were primed by intravenous injection of live or γ-A/PR8. 6 days later, target splenocytes from naïve mice were labelled with 5,6-carboxyfluorescein diacetate succinimidyl ester (CFSE) (0.125 mM) or CellTrace™ Far-Red DDAO-SE (2 µM, Thermo Fisher Molecular-Probes). The CFSE-labelled population was pulsed with Influenza A nucleoprotein peptide (GL Biochem (Shanghai) Ltd, sequence: TYQRTRALV, K^d, 10^{-3}M in PBS), whereas the CellTrace Red population was left untreated). Target cells were mixed at 1:1 ratio (CFSE:CellTrace Red) and adoptively transferred into primed mice using intravenous injection (10^7 cells/mouse total). 24 h later, mice were sacrificed, and spleens were harvested and processed to single-cell suspensions prior to analysis using flow cytometry (LSRII, BD Biosciences). Data

analysed using FlowJo (Treestar Incorporated). Percentage lysis was calculated as follows: % lysis = [1 – (% primed pulsed targets/ % primed non-pulsed targets)/(% unprimed pulsed targets/ % unprimed non-pulsed targets)] × 100.

2.2.11. Statistical Analysis

Quantitative results are expressed as mean ± SEM, to indicate the closeness of the data to the population means rather than variability within small sample size. Unpaired Student's *t*-test was used for comparison of data from two separate groups, One-way ANOVA was used for comparison of data from 3 or more groups with a single variable, and two-way ANOVA was used to analyse data sets with multiple variables. Statistical analysis was performed using GraphPad Prism 6, version 6.0d (GraphPad Software, La Jolla, CA, USA). *P* values < 0.05 (95% confidence) were considered statistically significant.

2.3. RESULTS

2.3.1. The effect of irradiation conditions on HA titres and virion morphology

A/PR8 virus samples were exposed to 25 or 50 kGy of γ-radiation, either at room temperature (RT) or on dry-ice (DI). Haemagglutination assay was used to determine the effect of irradiation conditions on HAU titres. **Figure 2.1A** shows RT irradiation resulted in loss of 90% and 99% of initial HAU titres after irradiation at 25 and 50 kGy respectively. In contrast, only a 50% loss in HAU was detected after irradiation on DI, regardless of irradiation dose. Considering that HAU titre is dependent on binding of viral HA to cRBCs, loss in HAU titre after irradiation at RT may be associated with some structural damage. Therefore, TEM was used to visualise overall structure of irradiated viruses (**Fig. 2.1B**). Samples irradiated on DI show a more intact virus structure compared to preparations irradiated at RT. It should be noted that DI samples were resolved at 220,000× magnification, whilst clear resolution for RT samples could only be visualised at a lesser magnification of 135,000×. Additionally, we detected dark aggregates in RT-irradiated images, indicating potential formation of protein aggregates or split viral particles.

We also used SDS-PAGE to compare integrity of viral proteins in irradiated samples and non–irradiated controls. All major viral proteins were visible in control non-irradiated

samples (**Fig. 2.1C**). The three influenza polymerase proteins resolved as two bands, with PB1 and PB2 migrating together to form a less defined band. Bands consistent with molecular weights for NP and M1 were visible for all samples. Importantly, uncleaved (HA0) and cleaved (HA1, HA2) forms of HA were present in control samples and DI irradiated samples. In contrast, HA0 and HA1 bands appeared faint in RT irradiated samples, consistent with reduced HAU titres. Furthermore, lanes related to RT samples showed an increase in smearing of proteins as opposed to formation of discrete bands, indicative of increased protein damage. Considering the significant reduction in HA titre and the observed effect on virion structure and protein integrity, RT-irradiated samples were considered non-optimal as vaccine preparations and excluded from further testing.

2.3.2. Estimating D_{10} value and SAL

Sterility of 25 and 50 kGy-irradiated materials was confirmed using 3 passages in 10-day-old embryonated eggs. Additionally, to test whether these doses met the internationally accepted SAL, aliquots of cRBC-concentrated live virus were subjected to different irradiation doses on DI and tested for reduction in virus titre using $TCID_{50}$ assay. We detected a log-linear relationship between the increased irradiation dose and the associated reduction in virus titre (**Fig. 2.2**). Based on this linear inactivation curve ($R^2 = 0.9511$) following exposure to irradiation doses of up to 8 kGy, we estimated a D_{10} value of 2.04 kGy. Due to irradiation of frozen samples on dry ice, we anticipated a relatively high D_{10} value. To calculate the SAL, we then considered the linear inactivation curve, the D_{10} value, the initial titre of 2×10^8 $TCID_{50}$/mL, and the need for 11 or 14 $\log_{10}$ titre reductions to achieve a SAL of 10^{-3} or 10^{-6}, respectively. Therefore, the SAL for our vaccine could be calculated based on the formula "SAL = D_{10} value × 11", which would give a total value of 22.4 kGy for a SAL value of 10^{-3}. Alternatively, SAL could also be calculated based on the formula "SAL = D_{10} value × 14", which would give a total value of 28.6 kGy for a SAL value of 10^{-6}. This indicates that materials exposed to 25 or 50 kGy both meet the internationally accepted SAL for γ -irradiated pathogens. In fact, 50 kGy represents a much higher dose than is required to achieve sterility, representing approximately 24 $\log_{10}$ reductions in virus titre. Importantly, we confirmed the complete inactivation of our preparations in accordance with the WHO recommended method of two passages in 10-day-old embryonated eggs [424]. In fact, we performed 3 passages in total, with no detectable HA in allantoic fluid.

2.3.3. The effect of irradiation dose on induction of protective immunity

To study the effect of irradiation dose on vaccine efficacy, mice were vaccinated with 25 or 50 kGy γ-A/PR8 irradiated on DI, or PBS for mock-control mice. Serum samples were taken on Day 20 post-vaccination and analysed for A/PR8-specific IgG titres using ELISA. **Figure 2.3A** shows both vaccine preparations induced elevated A/PR8-specific IgG titres in serum following mucosal vaccination compared to controls, and titres for 25 and 50 kGy γ-A/PR8 vaccinated groups were comparable. Additionally, vaccinated and control animals were challenged IN with lethal A/PR8 on Day 21 post-vaccination, and monitored for clinical symptoms and weight loss. **Figure 2.3B** shows γ-A/PR8 irradiated with either 25 or 50 kGy induced 100% protection against lethal IN challenge, and vaccinated mice showed no weight loss compared to controls. Our data indicate that both vaccine preparations (25 and 50 kGy) are highly immunogenic and show comparable protective efficacies when using a vaccine dose of 6.4×10^6 $TCID_{50}$ equivalent/mouse.

2.3.4. The effect of vaccination dose on vaccine efficacy

Our data and previously published studies [426, 420, 427-431] clearly indicate that structural damage caused by γ-rays could be controlled using freezing irradiation conditions. Nonetheless, increased exposure to γ-rays despite the use of DI may be associated with reduced vaccine efficacy, albeit to a limited extent. To test this, mice were vaccinated with a single intranasal dose of γ-A/PR8, using either one-half or one-eighth of the dose previously used in **Figure 2.3**. Protective efficacy was then monitored following challenge with live A/PR8. **Figure 2.4A** shows that vaccination with reduced doses of 25 or 50 kGy γ-A/PR8 still resulted in 100% survival. However, we observed some weight loss (~10%) in animals vaccinated with one-eighth dose of 50 kGy γ-A/PR8 prior to full recovery. No weight loss was observed for the other vaccinated groups. We also analysed antibody responses; whilst all reduced doses induced seroconversion following intranasal vaccination, we detected a 50% reduction in IgG titres in serum from mice vaccinated with 50 kGy γ-A/PR8 compared to mice vaccinated with the same dose of 25 kGy γ-A/PR8. However, this reduction did not reach statistical significance (**Fig. 2.4B**). This indicates that while 50 kGy γ-A/PR8 appears to be immunogenic and confers high protective efficacy, exposure to 50 kGy may be associated with some damage to viral proteins. As such, this may have affected antibody responses and the ability of γ-A/PR8 to induce protection without weight loss when using a reduced antigen dose.

To further investigate the effect of high radiation dose on γ-A/PR8, we employed a two-dose vaccination strategy using a dramatically reduced vaccine dose of 5×10^4 $TCID_{50}$ equivalent/mouse, approximately one-hundredth of the dose used in **Fig. 2.3**. A single vaccination with this reduced vaccine dose was not sufficient to induce protective immunity against lethal challenge, regardless of irradiation dose (**Fig. 2.5A**). Consequently, mice were vaccinated with two doses of 5×10^4 $TCID_{50}$ equivalent, two weeks apart, followed by a lethal A/PR8 challenge 3 weeks later. When considering the two-dose strategy, vaccination with 25 kGy γ-A/PR8 resulted in significant protection (50% survival) following homotypic challenge. In contrast, two-dose vaccination with 50 kGy γ-A/PR8 was not associated with any protection. Interestingly, analysis of antibody titres in serum harvested 24 h pre-2nd vaccination and 24 h pre-challenge showed both 25 and 50 kGy γ-A/PR8 induced comparable A/PR8-specific IgG titres (**Fig. 2.5B**). Additionally, *in vivo* CTL assay was performed to determine whether the observed difference in protection was due to T-cell mediated mechanisms rather than antibody responses. As shown in **Figure 2.5C**, 50 kGy γ-A/PR8 induced slightly less potent CTL responses against nucleoprotein peptide (NPP) pulsed target cells compared to both 25 kGy γ-A/PR8 and live virus control groups, however this trend was not statistically significant.

2.3.5. Neutralising antibody responses induced by γ-A/PR8

Antibody levels detected using ELISA in immune sera from mice vaccinated with 25 and 50 kGy γ-A/PR8 did not differ significantly, despite observed differences in protective efficacies in **Figure 2.5**. Therefore, we investigated whether high radiation dose affected the quality of humoral responses rather than the total quantity. Serum samples from mice vaccinated with 6.4×10^6 $TCID_{50}$ equivalent/mouse and 2 doses of 5×10^4 $TCID_{50}$ equivalent/mouse of γ-A/PR8 were tested using an *in vitro* neutralisation assay to quantify neutralising antibody responses. MDCK cells were infected with immune- and control-sera-treated A/PR8 at MOI of 0.1. PBS-treated A/PR8 was used as a virus only control. Fluorescent staining of infected monolayers showed incubation of A/PR8 with sera from control mice (mock-sera) did not affect the ability of A/PR8 to infect MDCK cells, as infectivity for both mock-sera treated virus and the virus-only control were comparable (**Fig. 2.6**).

Importantly, A/PR8 treatment with immune sera from mice vaccinated with 6.4×10^6 $TCID_{50}$ of 25 and 50 kGy γ-A/PR8 showed complete abrogation of virus infectivity (100% neutralisation), indicating that both vaccines induced strong neutralising antibody responses (**Fig. 2.6A**). Different serum dilutions (1:20, 1:40 and 1:80) were also tested, and no difference in virus neutralisation was detected. Conversely, when testing serum samples from mice vaccinated with 5×10^4 $TCID_{50}$ γ-A/PR8, we detected differences in virus neutralisation between serum samples from mice vaccinated with 25 versus 50 kGy γ-A/PR8. Importantly, serum from both 25 and 50 kGy γ-A/PR8 vaccinated groups induced significant virus neutralisation when compared to control samples (**Fig. 2.6B**). However, neutralisation ability between samples from vaccinated groups was also significantly different, as sera from the 25 kGy γ-A/PR8 vaccinated group appeared to be ~2.3-fold more effective at neutralising A/PR8 (determined by difference between means of normalized FITC fluorescence) when compared to sera from 50 kGy γ-A/PR8 vaccinated mice (**Fig. 2.6B**).

2.4. DISCUSSION

Rapid emergence of HPAI strains highlights the urgent need to develop safe vaccines capable of providing protection against circulating as well as emerging pandemic influenza A viruses. We reported previously that vaccination with γ-Flu confers protection against lethal homotypic and heterosubtypic influenza A challenges, including HPAI strain H5N1 [432, 361]. Considering the increasing risk of a worldwide influenza pandemic, inclusion of HPAI virus strains may be desirable in future clinical developments of γ-Flu. To comply with safety regulations regarding irradiation of highly pathogenic agents, 50 kGy may be required for vaccine inactivation. Therefore, we estimated the irradiation dose required to achieve a SAL of 10^{-3} or 10^{-6}, and investigated the effect of high irradiation dose and temperature conditions on γ-Flu efficacy.

Viruses are primarily inactivated by the direct effects of γ-rays, whereby deposition and transfer of energy by an incident gamma-ray causes rupture of covalent bonds within genetic material [426, 433-435]. Exposure to γ-rays is also associated with indirect effects, which result from chemical damage by free radicals generated by the interaction of γ-rays with water and oxygen molecules [435]. Due to differences in the physical and chemical properties of polynucleotides and polypeptides, the genetic material of

pathogens is much more sensitive to direct damage than proteins [336]. It has been reported previously that freezing target materials at ultra-low temperatures during irradiation reduces the formation of free radicals. This consequently minimizes indirect damage to proteins, and allows genome damage by direct effects to dominate [420, 428]. For example, γ-irradiation of frozen plasma samples has been effective in sterilizing contaminating HIV virus with minimal impact on functionality of coagulation factors [335]. Furthermore, irradiation of freeze-dried materials was associated with maintained protein biological activity even after exposure to 45 kGy [336]. Interestingly, Feng *et al.* [419] used SDS-PAGE to demonstrate a decrease in abundance of Murine Norovirus-1 capsid protein VP1 as irradiation dose increased. We showed a similar trend for γ-A/PR8 samples irradiated at room temperature, as we detected increased protein smearing (as opposed to formation of discrete bands) with higher irradiation doses (**Fig. 2.1C**). In contrast, materials irradiated on dry-ice showed discrete protein bands, particularly those corresponding to key proteins NA, HA1, and NP (45, 55, and 56kDa respectively) that were maintained following exposure to both 25 and 50 kGy. Our data indicate that we could better maintain both protein integrity and viral morphology by irradiating frozen materials in contrast to irradiation at room temperature. HA surface protein functionality was also better maintained following irradiation on dry-ice (**Fig. 2.1A**). Room temperature-irradiated samples also failed to induce A/PR8-specific serum antibody responses and sufficient homotypic protection (data not shown). Thus, we concluded that irradiation at room temperature is not suitable for influenza vaccine development.

To ensure our dry-ice irradiated preparations satisfied requirements for internationally accepted standards [436-438, 310], we established the killing curve of A/PR8 using vaccine samples irradiated at different doses. Our data show a clear log-linear relationship between increased irradiation doses and the associated reduction in virus titre. This mathematical relationship was used to calculate a D_{10} value of 2.04 kGy and a SAL value of 22.4 – 28.6 kGy. Therefore, 25 kGy sufficiently complies with guidelines of the International Atomic Energy Agency (IAEA) and International Standards Organisation (ISO). It is important to note that guidelines related to SAL should be accompanied by approved sterility tests, which we performed based on WHO recommendations. While SAL for our preparation is achieved using 25 kGy, 50 kGy may still be desirable to inactivate HPAI preparations. Interestingly, 50 kGy is reported as the lowest dose capable of inactivating Venezuelan equine encephalitis virus (VEEV) [439], and an exposure to

50 kGy on dry-ice was reported to reduce γ-VEEV antigenicity and epitope integrity [440]. In contrast, our data show vaccination with either 25 or 50 kGy dry-ice γ-A/PR8 resulted in significantly elevated A/PR8-specific IgG titres and 100% protection against lethal intranasal challenge (**Fig. 2.3**). Similar treatment of HPAI vaccine preparations is therefore viable. In fact, such preparations could be treated with 50 kGy and stockpiled for future pandemic preparedness.

Despite high efficacy of 50 kGy γ-A/PR8 observed in **Figure 2.3**, we further investigated whether exposure to high irradiation dose affected vaccine immunogenicity, and whether increased vaccination dose could overcome such effects. To address these possibilities, we used reduced γ-A/PR8 vaccine doses. Remarkably, these doses still conferred 100% protection against lethal challenge. We did notice that animals vaccinated with 8×10^5 $TCID_{50}$ equivalent/mouse (one-eighth dose) of 50 kGy γ-A/PR8 lost some weight prior to full recovery, in contrast to animals vaccinated with the same dose of 25 kGy γ-A/PR8 (**Fig. 2.4A**). This minor difference in vaccine efficacy was confirmed using a severely reduced vaccine dose (5×10^4 $TCID_{50}$ equivalent/mouse) administered using a two-dose vaccination strategy. Whilst 25 and 50 kGy γ-A/PR8 induced comparable levels of A/PR8-specific IgG in this low-dose setting, we detected a significant difference in A/PR8 neutralisation by immune sera *in vitro* (**Fig. 2.6B**). This likely contributed to the difference in protective efficacy observed using our low dose vaccination strategy. Interestingly, a study investigating γ-irradiation of allergens showed irradiation with 15 kGy abolished binding of IgE from allergic individuals to allergen proteins, whilst treatment with lower radiation doses permitted strong binding [441]. The higher irradiation dose potentially damaged allergen epitopes, consequently affecting total antibody binding. Similarly, antibodies induced here by 50 kGy-treated virus samples may recognise slightly damaged epitopes rather than native ones, hence recognition and neutralisation of live A/PR8 epitopes is slightly reduced. Importantly, our data indicate that using higher vaccination doses could overcome the reduced efficacy of 50 kGy γ-A/PR8, as equal and highly effective virus neutralisation by 25 and 50 kGy γ-A/PR8 was observed when using increased vaccine doses (**Fig. 2.6A**). Additionally, both 25 and 50 kGy γ-A/PR8 preparations induced CTL responses against internal influenza nucleoprotein peptide that resembled CTL activity induced by live virus.

Overall, our data show no detectable difference in performance between 25 and 50 kGy γ-A/PR8 when using standard vaccination doses. Reduction in 50 kGy γ-A/PR8 efficacy was only apparent when using intentionally low antigen dose, which is not relevant to a clinical setting nor for future γ-Flu development. This study has also demonstrated the suitability of using freezing conditions for γ-irradiation of influenza A virus to produce inactivated vaccines that elicit strong protective immunity. Data presented here supports the use of 50 kGy for developing future γ-Flu formulations that may include HPAI virus strains.

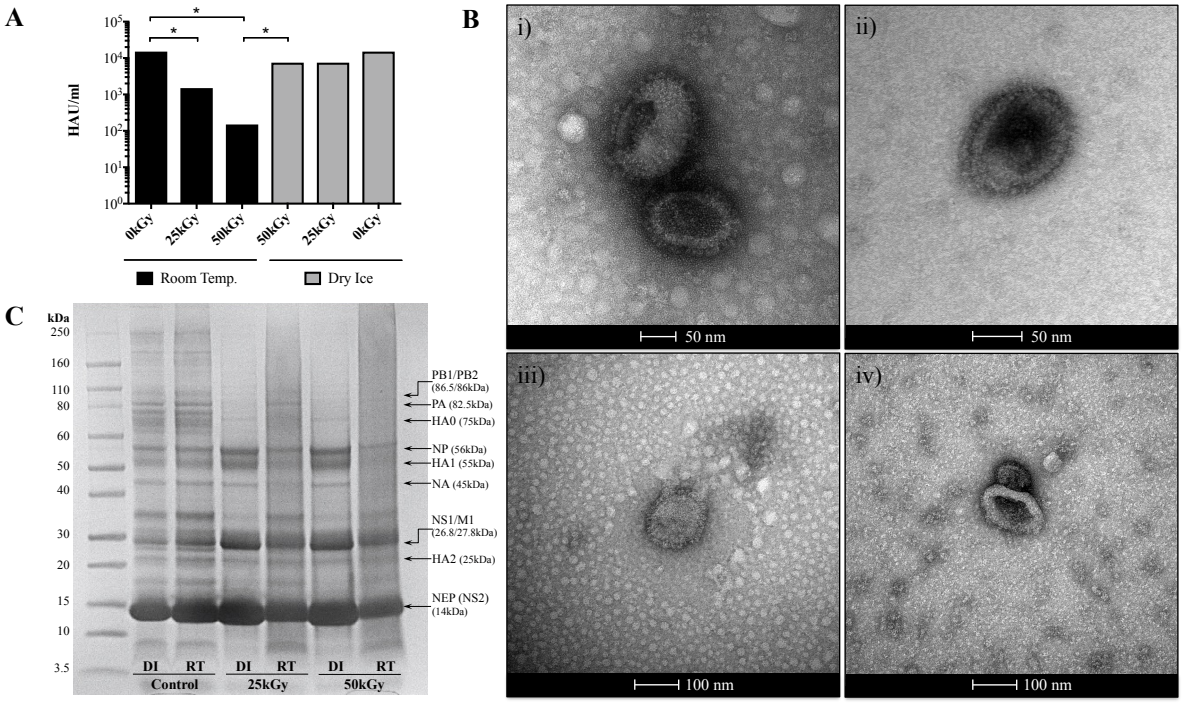

Figure 2.1. The effect of irradiation dose and temperature on the structure of influenza A virus. A/PR8 samples were exposed to 25 or 50 kGy of γ-irradiation either on dry-ice (DI) or at room temperature (RT). Untreated (0 kGy) samples were used as controls. (A) Virus titre was estimated using haemagglutination assay, and expressed as HAU/ml. Each column indicates the mean value of quadruplicates ± SEM. Groups compared by Mann-Whitney tests (*, $P < 0.05$). (B) Transmission Electron Microscopy (TEM) was used to visualise virion morphology changes following irradiation on dry-ice using (i) 25 kGy or (ii) 50 kGy, or at RT using (iii) 25 kGy or (iv) 50 kGy. Virus preparations were negatively stained with 2% uranyl acetate and visualised using the FEI Tecnai G2 Spirit Transmission Electron Microscope. (C) SDS-PAGE of heat-lysed influenza preparations, both DI and RT irradiated samples, and non-irradiated controls. Influenza proteins are annotated according to their known MW from UniProtKB database *(Influenza A virus (strain A/Puerto Rico/8/1934 H1N1)*), and according to those identified by Shaw *et al.* [21].

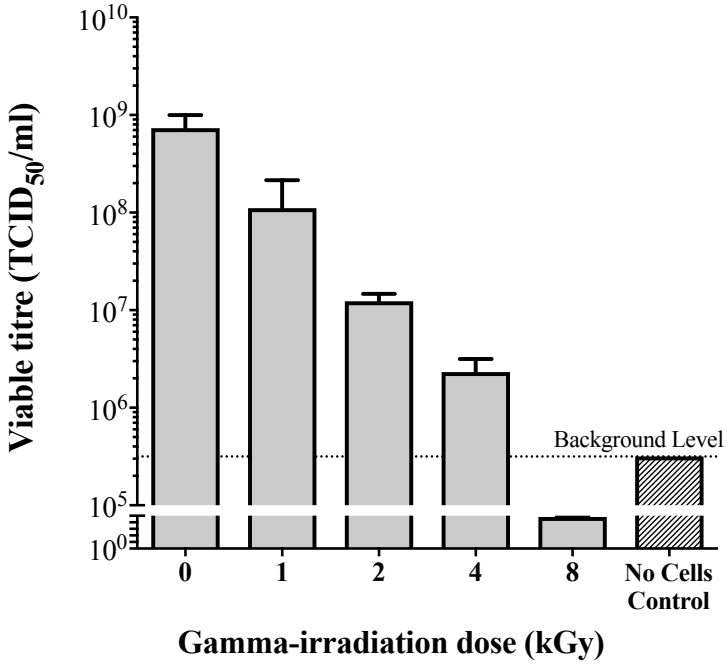

Figure 2.2. Inactivation curve of A/PR8 following exposure to different doses of γ-rays. Samples of A/PR8 virus were exposed to increasing doses of γ-irradiation on dry-ice, and remaining virus infectivity was determined by $TCID_{50}$ assay using MDCK cells. Data presented as mean titre ± SEM. Background level (dotted line) was measured by the binding of cRBCs to A/PR8 virus after incubation for 5 days in the absence of MDCK cells.

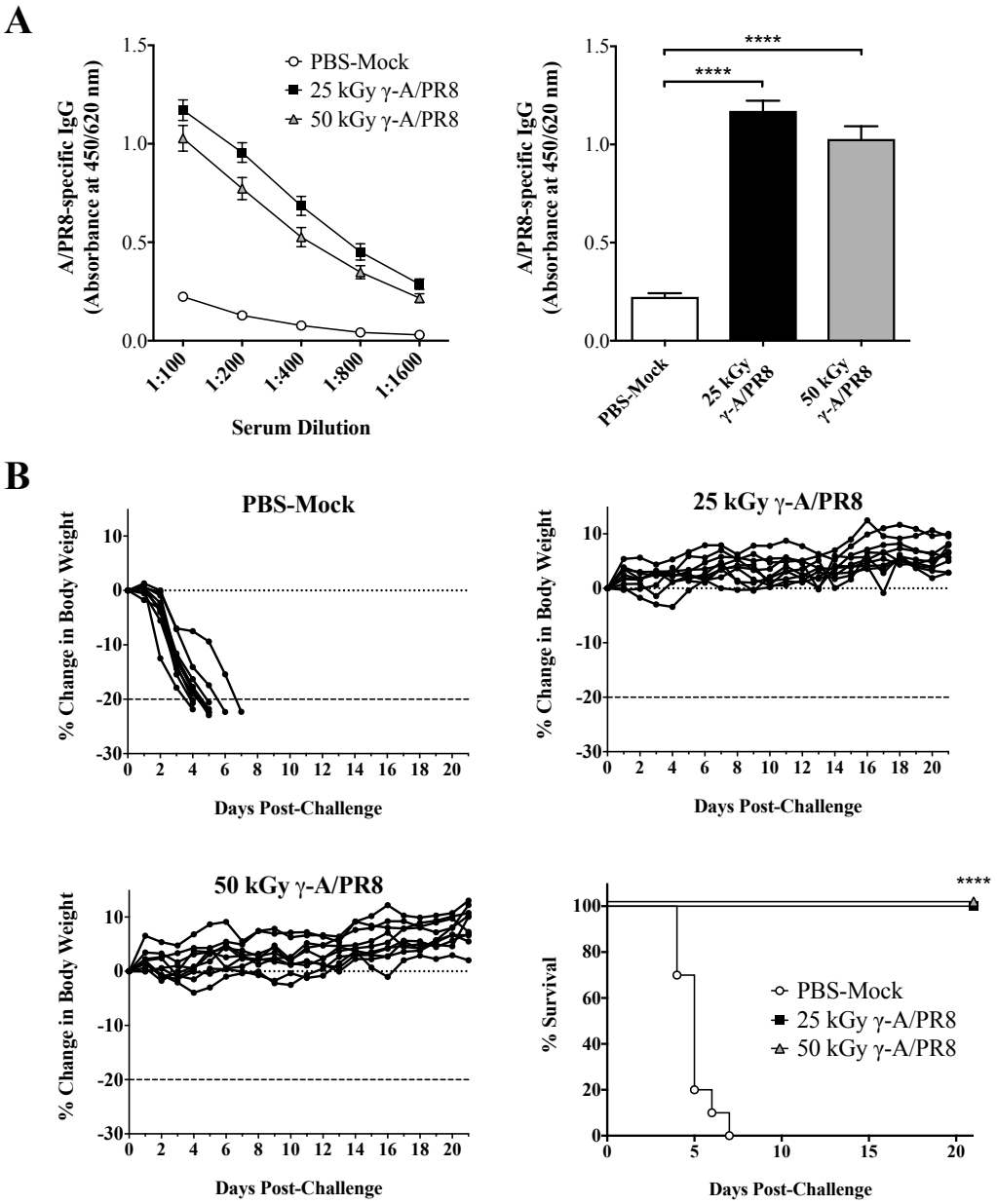

Figure 2.3. Vaccination with 25 kGy and 50 kGy γ-A/PR8 induces homotypic protection. Balb/c mice were vaccinated IN with γ-A/PR8 irradiated with 25 or 50 kGy on dry-ice (6.4×10^6 $TCID_{50}$ equivalent/mouse). Control mice received a PBS-mock vaccine. (A) Serum was harvested on Day 20 post-vaccination and analysed for A/PR8-specific IgG by ELISA. Data presented as mean absorbance at 450/620 nm. 1:100 dilution analysed by One-Way ANOVA (****, $P < 0.0001$). (B) Mice challenged IN with lethal A/PR8 (1.6×10^2 $TCID_{50}$/mouse) on day 21 post-vaccination. Data presented as weight loss of vaccinated and control mice, and survival percentages. Data compiled from two independent experiments (n = 10). Survival data analysed by Fisher's Exact test in comparison to PBS-mock control group (****, $P < 0.0001$).

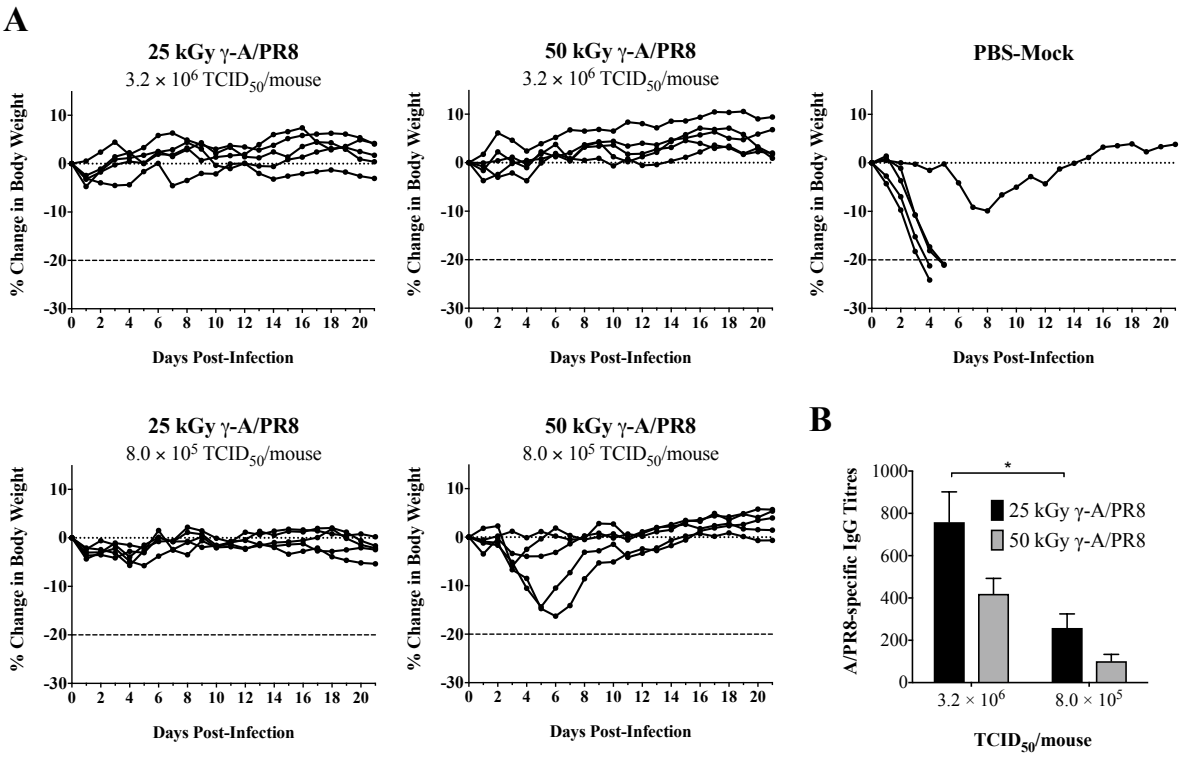

Figure 2.4. Efficacy of the γ-A/PR8 vaccine. Balb/c mice were vaccinated IN with either 3.2×10^6 or 8.0×10^5 $TCID_{50}$ equivalent/mouse of γ-A/PR8 irradiated with 25 or 50 kGy on dry-ice. Control mice received a PBS-mock vaccine. (A) Weight loss of vaccinated and control mice following IN challenge with lethal A/PR8 (n = 5). (B) Serum samples were harvested from all mice on day 20 post-vaccination, and analysed for A/PR8-specific IgG by ELISA. Absorbance readings at 450/620 nm of control sera were used to calculate relative IgG titres. Data presented as mean ± SEM (n = 5), and analysed by One-Way ANOVA (*, $P < 0.05$).

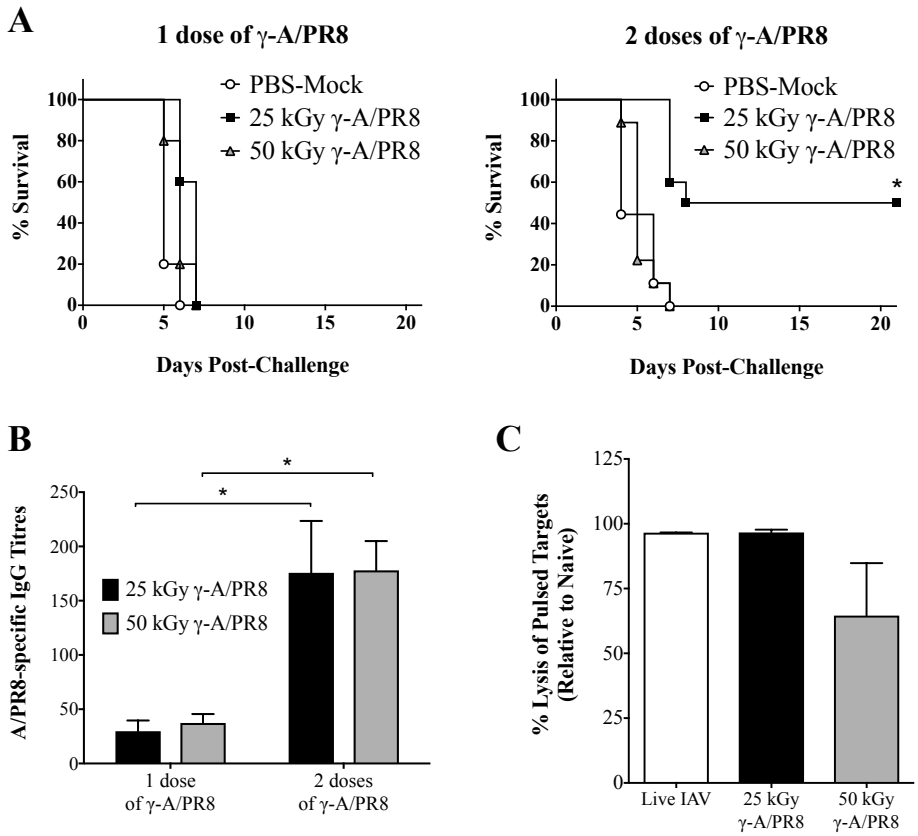

Figure 2.5. Enhanced protective efficacy of 25 kGy γ-A/PR8 when using low vaccine dose. (A) Balb/c mice were vaccinated IN with a single dose of γ-A/PR8 irradiated at 25 or 50 kGy on dry-ice (5×10^4 $TCID_{50}$ equivalent/mouse), or two doses administered two weeks apart. Three weeks later, mice were challenged IN with lethal A/PR8. Data is representative of two independent experiments. Data presented as survival rate (n = 10), and analysed by Fisher's exact test (*, $P < 0.05$ compared to control group). (B) Serum was harvested 24 h pre-challenge, and tested for A/PR8-specific IgG using ELISA. Absorbance readings at 450/620 nm of naïve sera used to calculate relative IgG titres. Data presented as mean ± SEM, analysed by One-Way ANOVA (*, $P < 0.05$). (C) CTL-mediated killing of NPP pulsed target splenocytes 24 h after adoptive transfer into mice primed with live influenza, or 25 or 50 kGy γ-A/PR8 (dry-ice irradiated). Percentage killing determined in relation to un-primed control mice. Data presented as mean ± SEM, no significance determined by One-Way ANOVA.

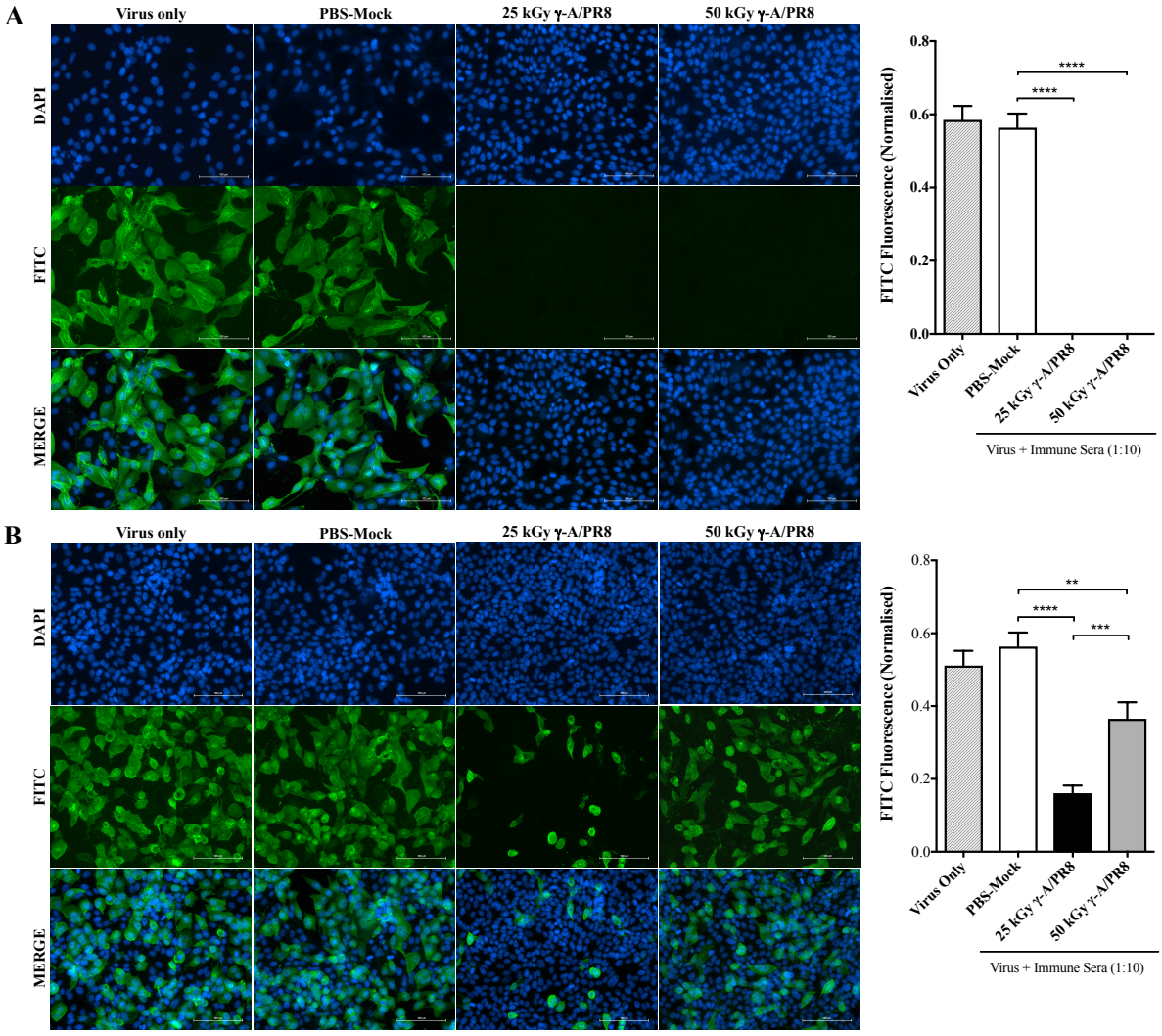

Figure 2.6. Neutralising antibody responses induced by 25 and 50 kGy γ-A/PR8. Mice were vaccinated IN with (A) 6.4×10^6 $TCID_{50}$, or (B) two doses of 5×10^4 $TCID_{50}$ equivalent of γ-A/PR8 irradiated on dry-ice. Serum was harvested on day 20 post-vaccination, and neutralisation efficacy against live A/PR8 determined by *in vitro* neutralisation assay. Representative images of infection after treatment of IAV with sera from control or vaccinated mice at 1:10 dilution, with DAPI (blue) detecting cell nuclei, and FITC (green) detecting A/PR8 virus. FITC fluorescence also quantified with NIS elements software, and normalised using corresponding quantified DAPI fluorescence. Data presented as mean ± SEM (n = 8), analysed by One-Way ANOVA (**, $P < 0.01$, ***, $P < 0.001$, ****, $P < 0.0001$).

CHAPTER 3

Enhancement of safety and immunogenicity of the γ-PN vaccine

3.1. INTRODUCTION

Streptococcus pneumoniae (the pneumococcus) remains one of the leading causes of bacterial pneumonia worldwide [176], and has recently become the leading cause of bacterial meningitis in children < 5 years of age in the United States [442]. *S. pneumoniae* is commonly found as a commensal bacterium of the human nasopharynx. However asymptomatic colonisation can progress to invasive disease depending on factors such as host immune-competence and simultaneous infection with other pathogens. Diseases caused by the pneumococcus can range from mild infections including otitis media and sinusitis, to very severe outcomes of pneumonia, septicaemia, and meningitis. Increasing prevalence of antibiotic resistant pneumococcal strains also limits therapeutic treatment options for pneumococcal disease [443].

Prevention of pneumococcal infection poses a persistent challenge. Existing capsular polysaccharide (CPS)-based vaccines provide strictly serotype-dependent protection, and cover a limited range of pneumococcal serotypes. Moreover, their ongoing use has consistently resulted in serotype replacement [444-446]. This phenomenon occurs when reduction in carriage of vaccine-serotypes leaves a vacant niche that is quickly occupied by non-vaccine serotypes [247, 444]. Non-PCV13 serotype isolates such as serogroup 15B/C, are becoming increasingly common [249, 250], and accounted for a staggering 84.1% of all childhood IPD cases in 2015/16 [251]. A 2017 study also found non-PCV serotypes are now the major contributors to IPD burden in adults ≥ 65 years of age [252]. Furthermore, studies have concluded that PCVs have not consistently reduced the incidence of pneumococcal meningitis – one of the most severe forms of IPD – due to serotype replacement [256, 253-255].

Furthermore, emergence of non-encapsulated *S. pneumoniae* (NESp, or non-typeable) isolates has recently been reported. These are primarily isolated from patients with non-invasive pneumococcal disease, though NESp invasive disease isolates have been observed [447]. These NESp strains express unique surface proteins that enhance colonization and virulence, despite lacking capsular polysaccharide, and they typically carry multiple antibiotic resistance genes [448]. Importantly, existing CPS-based

vaccines do not offer any protection against disease caused by non-encapsulated strains, or strains belonging to non-included CPS serotypes.

We have previously published our approach to circumvent these vaccine shortcomings, with a whole-cell non-encapsulated *S. pneumoniae* preparation. The pneumococci within this vaccine are inactivated using gamma-irradiation, generating γ-PN, which completely abolishes pneumococcal viability whilst leaving antigenic structures intact. Importantly, removal of capsule from this vaccine strain allows exposure of highly conserved surface antigens for induction of broad cross-protective immune responses. In fact, non-adjuvanted intranasal vaccination with this novel vaccine was shown to confer significant protection against multiple vaccine and non-vaccine serotypes in mice. γ-PN-mediated protection was found to be dependent on antibody responses to non-capsular antigens [235]. Interestingly, a recent publication by Wilson *et al.* demonstrated that naturally acquired immunity to pneumococci in humans is similarly dependent on antibodies against pneumococcal protein antigens, rather than anti-capsular responses [449].

To enable the progression of our novel γ-PN vaccine through clinical development, further enhancement of the safety profile is required. Generation of an auxotrophic mutant of the existing non-encapsulated vaccine strain would fulfil this requirement. It is well documented that survival and virulence of *S. pneumoniae* in different niches within a host is dependent on acquisition of various nutrients, including sugars and metal ions [450-453]. To ensure sufficient uptake and maintenance of metal ion homeostasis, *S. pneumoniae* possesses import and export systems specific to different ions, including iron (Fe^{2+}), zinc (Zn^{2+}) and manganese (Mn^{2+}) [454-456, 451]. Of particular interest is the *psaBCA* operon, which encodes the ABC-type manganese importer. Whilst mutation of components required for iron, copper, and zinc import are reported to have variable effects on pneumococcal virulence [457], mutation of *psaA* alone was found to dramatically attenuate virulence in multiple disease models *in vivo*, including otitis media, respiratory infection, and systemic invasion models [458-461]. PsaA mutants are also attenuated *in vitro,* and have a complete requirement for manganese supplementation for growth [459, 462]. Sufficient supplementation can restore normal growth kinetics in ΔPsaA strains [463-465]; this is crucial to allow production of highly concentrated

preparations for vaccine purposes. Thus, *psaA* was selected as a target for this study. Additionally, studies have indicated that manganese levels can alter the expression of certain surface proteins, particularly antigenic choline-binding proteins such as PcpA [460, 466, 467]. Thus, effects of the growth-attenuating mutation and the required manganese supplementation on pneumococcal morphology, antigenic targets, and vaccine immunogenicity were thoroughly investigated.

3.2. Materials and Methods

3.2.1. Ethics statement

Animal experimentation was carried out in strict accordance with the Australian Code of Practice for the Care and Use of Animals for Scientific Purposes (7th edition [2004] and 8th edition [2013]) and the South Australian Animal Welfare Act 1985. Experimental protocols were approved by the Animal Ethics Committee at The University of Adelaide (Approval numbers **S-2013-053** and **S-2016-183**).

3.2.2. Bacterial strains and construction of Rx1(ΔLytA, PdT, ΔPsaA) vaccine strain

Streptococcus pneumoniae strains were statically grown in Todd–Hewitt broth supplemented with 0.5% yeast extract (THY) at 37°C in 5% CO_2 unless otherwise stated. The *S. pneumoniae* strain Rx1 used in this study is a capsule-deficient derivative of D39 (serotype 2). The isogenic mutant derivative Rx1(ΔLytA, PdT) was generated as previously described [235]. Additional genetic manipulation was performed on strain Rx1(ΔLytA, PdT) to delete the pneumococcal surface antigen A (*psaA*) gene in-frame, in a similar manner as described in [468]. All PCR primers used are listed in **Table 3.1**. First, a tagged *psaA* deletion mutant was generated by transformation of Rx1(ΔLytA, PdT) with a cassette comprised of an erythromycin resistance gene (Ery^R) fused to *psaA* 5' and 3' flanking regions. The 5' flanking region of *psaA* was obtained using the primers PsaAuF and PsaAuR-J214, whilst the 3' flanking region was obtained using primers LM8-J215 and PsaAdR. The Ery^R gene was amplified using primers J214 and J215. The cassette was assembled by overlap extension PCR with primers PsaAuF and PsaAdR, and used to transform Rx1(ΔLytA, PdT). All transformation steps and subsequent growth steps with the resultant Rx1(ΔLytA, PdT, ΔPsaA::Ery^R) strain used THY supplemented

with 400 μM $MnCl_2$ to overcome the growth defect of PsaA-null mutants. A PCR product that fused the *psaA* 5' and 3' flanking regions was then generated via amplification of the 5' *psaA* flanking region with primers PsaAuF and PsaAuRtuF, and the 3' region with primers LM8tdR and PsaAdR. These flanks were joined via overlap extension PCR with primers PsaAuF and PsaAdR, and the resulting PCR product used to replace the Ery^R cassette in Rx1(ΔLytA, PdT, ΔPsaA::Ery^R), thus deleting *psaA* in-frame. Successful transformants were screened for loss of erythromycin resistance by replica plating onto blood agar plates containing $MnCl_2$, or $MnCl_2$ + Erythromycin. The flanking regions of putative mutants were PCR amplified, and in frame deletions confirmed by sequencing. The final Rx1(ΔLytA, PdT, ΔPsaA) strain was additionally validated using PCR, Sanger Sequencing, and Western Blot.

3.2.3. Western Blotting

For confirmation of mutants, western blotting was performed essentially as described [464]. The encapsulated strain D39, the parent Rx1 strain, and the vaccine strains Rx1(ΔLytA, PdT) and Rx1(ΔLytA, PdT, ΔPsaA) were grown to mid-log phase in THY (supplemented with additional Mn as specified in figure legends). Cultures were washed in PBS, and concentrated ~50× by centrifugation prior to lysis in PBS. Samples were lysed by sonication (25 cycles: 30 sec on, 30 sec off), then boiled in 1× LUG buffer for 5 mins at 95°C prior to SDS-PAGE (using NuPAGE Novex 4 – 12% Bis-Tris gels with 1% MES running buffer). After transfer of proteins to nitrocellulose membranes using the iBlot System, membranes were probed with either anti-Ply (1:10,000 dilution), anti-LytA (1:10,000), or anti-PsaA (1:2000) murine polyclonal antisera. Primary Abs were detected with an IRDye 800CW goat anti-mouse IgG (LI-COR) at 1:50,000, and visualised using the Odyssey imaging system.

3.2.4. Growth Curves

Rx1(ΔLytA, PdT) and Rx1(ΔLytA, PdT, ΔPsaA) vaccine strains were inoculated from blood agar plates into THY broth or THY supplemented with 400 μM $MnCl_2$ (THY + Mn) to a starting OD_{600} of 0.02. Cultures were incubated at 37°C + 5% CO_2, and aliquots taken every 30-60 min for 10 h to determine increase in OD_{600}.

3.2.5. Scanning Electron Microscopy

Vaccine strains were inoculated from blood agar plates into ~100 ml pre-warmed plain THY or THY + Mn for a starting OD_{600} of 0.02. Cultures were incubated at 37°C + 5% CO_2, and 25 ml samples were removed from each culture at OD_{600} = 0.2, 0.4, and 0.65. 25 ml samples were spun at 4,000 rpm for 10 min at 4°C, then washed three times in PBS. Pellets resuspended in 250 µl PBS + 13% glycerol (100× concentration from original volume). 15 µl neat sample then diluted in 2 ml sterile PBS and attached to Nucleopore Track-Etch polycarbonate membrane filter (Whatman) for SEM preparation. Briefly, samples fixed in EM fixative (4% paraformaldehyde, 1.25% glutaraldehyde, 4% sucrose in PBS, pH 7.2), then stained with 2% Osmium tetroxide (OsO_4) prior to progressive dehydration as previously described (Alternate Protocol 6 and Basic Protocol 3 from [469]). Membranes were left to air dry, then coated by gold sputter. Imaging conducted using Quanta 450 Scanning Electron Microscope at Adelaide Microscopy, University of Adelaide.

3.2.6. Generation of γ-irradiated vaccines

Vaccine strains Rx1(ΔLytA, PdT) and Rx1(ΔLytA, PdT, ΔPsaA) were grown in either THY or THY + Mn (as specified in results) at 37°C + 5% CO_2 to OD_{600} = 0.65. Cells were pelleted by centrifugation at 8,000 rpm for 10 min at 4°C, washed three times in PBS, and resuspended in PBS + 13% glycerol at a density of ~10^{10} CFU/ml (approximately 100× concentration from original volume). 200 µl aliquots of vaccine samples were inactivated by exposure to gamma (γ)-irradiation at the Australian Nuclear Science and Technology Organization (ANSTO, Lucas Heights, NSW). Samples were kept frozen on dry-ice during irradiation and transportation. Remaining viable titres were then determined by CFU counts on blood agar plates. All vaccine preparations intended for administration to animals were treated with 16 kGy, and sterility confirmed by plating of neat samples.

3.2.7. Bicinchoninic acid (BCA) protein assay

To determine total protein content in all vaccine preparations, a Pierce BCA Protein Assay Kit (Thermo Scientific) was used according to the manufacturer's specifications [470]. Aliquots of each vaccine suspension were diluted 1:10 in PBS, and added to tubes

containing 40 mg glass beads (acid-washed, ≤ 106 μm, Sigma, G4649-10G) for sonication at 4°C (25 cycles of 30 seconds on, 30 seconds off). Whole cell lysates then added to 200 μl of working reagent (50 parts BCA kit reagent A to 1 part reagent B) in a 96-well microtiter plate. After gentle mixing, plates incubated at 37°C for 30 min. Plate cooled to room temperature, and absorbance measured on a microplate reader at 562 nm (with Softmax Pro software, Millennium Science). Protein content in vaccine samples was calculated using a standard curve of bovine serum albumin (BSA) in PBS.

3.2.8. TLR4 and TLR2 Stimulation

Human embryonic kidney cells (HEK-293) cells stably transfected with human TLR4a gene (293/TLR4a, Cat. #293-htlr4a) or human TLR2 and CD14 genes (293/hTLR2-CD14, Cat. #293-htlr2cd14) were obtained from InvivoGen. Cells were grown in DMEM + HEPES supplemented with 10% (v/v) foetal calf serum (FCS), 1% L-glutamine, 1% penicillin/streptomycin, 100 μg/ml normocin (InvivoGen, Cat. #ant-nr-1), and 10 μg/ml blasticidin (InvivoGen, Cat. #ant-bl-1). Cells were maintained as per manufacturer's instructions. For stimulation, cells were seeded in a 24-well tissue culture plate at 3×10^5 cells/well in 0.5 ml growth medium, and incubated for ~24 h until cells reached confluency. Growth medium was gently removed, and replaced with 0.3 ml of assay medium (growth medium with 1% FCS only) containing whole cell antigens at 10 μg/ml. Each antigen was tested in quadruplicate. Plain assay medium was used to determine background IL-8 production. After 24 h stimulation, culture supernatants were removed, and IL-8 levels were determined by ELISA using a human IL-8/CXCL8 DuoSet ELISA kit (Cat. #DY208-05), according to the manufacturer's instructions.

3.2.9. Mice & Treatment

Female outbred Swiss mice (4–6 weeks old) were supplied by Laboratory Animal Services at the University of Adelaide, South Australia. Mice were first anaesthetised intraperitoneally (IP) with sodium pentobarbitone (60 mg/ml stock, Ilium) at a dose of 66 μg/g body weight. The anaesthetised mice were then intranasally (IN) vaccinated by gently applying 30 μl of inactivated vaccine preparation (diluted in PBS as required, 21.25 μg total protein/dose, approx. 10^8 CFU equivalent/dose) to the nostrils. This immunisation route paired with anaesthesia was chosen to allow the vaccine inoculum to

enter the lung, as outlined in *Section 2.2.7.* Control mice received PBS-mock vaccinations. Mice were immunised IN twice at 2-week intervals. 1 week post-2nd vaccination, serum samples were collected from all mice by submandibular bleeding, and saliva was harvested after intraperitoneal injection of pilocarpine (2 mg/ml, 250 µl per mouse) to stimulate saliva production. For challenge experiments, mice were challenged IN 2 weeks after the 2nd vaccination with lethal D39 or P9. Mice were anaesthetised as above, and 25 µl of live pneumococci in PBS gently administered to the nostrils (10^7 CFU/mouse for both D39 and P9 challenges). Mice were monitored daily for 3 weeks post-challenge for development of clinical symptoms, and humanely euthanized once mice became moribund.

3.2.10. Measurement of antibody responses

Sera and saliva samples from vaccinated and control mice were assayed by ELISA to determine *S. pneumoniae*-specific antibody responses, as described previously [471]. Live whole-cell Rx1(ΔLytA, PdT) was used as coating antigen, at 5 × 10^6 CFU/well in bicarbonate/carbonate coating buffer (100 mM, 3.03 g Na_2CO_3, 6.0 g $NaHCO_3$ per 1 L miliQ, pH 9.6). Alkaline phosphatase (AP) conjugated goat anti-mouse IgA (Zymed, 1:1000) and horseradish peroxidase (HRP) conjugated goat anti-mouse IgG (Thermo Fisher, 1:10,000) were used to detect IgA and total IgG respectively. Absorbance readings of sera and saliva samples from PBS-Mock vaccinated mice at 1:160 dilution were used to calculate the cut-off value for all antibody titres. The cut-off was calculated by adding the mean absorbance value to 3 × standard deviation (SD). End point titres for samples were then expressed as the reciprocal of the dilution where the OD value equalled the cut-off value.

3.2.11. Western Blot analysis of antigen profiles

Irradiated vaccine samples were sonicated, and protein content measured as described in *Section 3.2.7.* Lysates were boiled in 1× LUG buffer for 5 mins at 95°C, and 20 µg total protein was loaded per well for SDS-PAGE. After transfer to nitrocellulose membranes, samples were probed with pooled immune sera from vaccinated Swiss mice at 1:500 dilution. Primary murine antibody was then detected with IRDye 800CW goat anti-mouse IgG and visualised as described in Section 3.2.3.

3.2.12. Statistical Analysis

Quantitative results were expressed as mean ± SEM to indicate the closeness of the data to the population means rather than variability within small sample size. Unpaired Student's *t*-test was used for comparison of data from two separate groups, One-way ANOVA was used for comparison of data from 3 or more groups with a single variable, and two-way ANOVA was used to analyse data sets with multiple variables. For survival data, the Mann-Whitney U-test was used to analyse statistical differences. All analyses were performed using GraphPad Prism 6, version 6.0d (GraphPad Software, La Jolla, CA, USA). *P* values < 0.05 (95% confidence) were considered statistically significant.

Table 3.1. Primers used for *psaA* in-frame deletion

Primer Name	Sequence (5' → 3')
PsaAuF (forward)	TCATTATTCTACGCGGGATGTCACTCATGG
PsaAuR-J214 (reverse)	TTGTTCATGTAATCACTCCTTCCAATTTATTAGGGCTTTGCCC
LM8-J215 (forward)	CGGGAGGAAATAATTCTATGAGAGAAGGCGACAGCTACTACAG
PsaAdR (reverse)	CAGTGGCAGCAGTAAGCATCATTTTGACC
J214 (forward)	GAAGGAGTGATTACATGAACAA
J215 (reverse)	CTCATAGAATTATTTCCTCCCG
PsaAuRtuF (reverse)	TAGTAGCTGTCGCCTTCTTTACCCAATTTATTAGGGCTTTGC
LM8tdR (forward)	GCAAAGCCCTAATAAATTGGGTAAAGAAGGCGACAGCTACTA

3.3. RESULTS

3.3.1. Confirmation of mutant strains and protective efficacy

The vaccine strain Rx1(ΔLytA, PdT) was previously generated by replacing the *ply* gene with a non-toxic derivative (PdT) and deleting the *lytA* gene [235]. This strain was further modified in the present study by in-frame deletion of *psaA*, to generate Rx1(ΔLytA, PdT, ΔPsaA). The progression of gene manipulation for both Rx1(ΔLytA, PdT) and Rx1(ΔLytA, PdT, ΔPsaA) is shown in **Figure 3.1A**. PCR analysis shows that Rx1(ΔLytA, PdT) lacks the full-length gene for *lytA*, and the further attenuated Rx1(ΔLytA, PdT, ΔPsaA) lacks full-length genes for both *lytA* and *psaA*. In each case, the truncated version of *lytA* or *psaA* was detected instead, indicating successful removal of the entire coding region, with only the flanking regions remaining. *Ply/pdt* was present in all strains as expected. Sequencing also confirmed successful in-frame deletion of *psaA* in the modified vaccine strain. A total of 865 nucleotides were deleted from the transcription start site through to 56 nucleotides upstream of the stop codon.

Expression of PdT and lack of both LytA and PsaA proteins in Rx1(ΔLytA, PdT, ΔPsaA) was then confirmed by Western Blot (**Fig. 3.1B**). Ply-, LytA-, and PsaA-specific murine antibodies detected expression of all three proteins in both D39 and Rx1 parent strains. PsaA was also detected in Rx1(ΔLytA, PdT) but not Rx1(ΔLytA, PdT, ΔPsaA) as expected. Purified proteins in Lane 1 of the blot ran at slightly higher molecular weights than native protein due to presence of His6-tags.

The functional impact of the PsaA deletion on cell growth is illustrated in **Figure 3.1C**. Rx1(ΔLytA, PdT, ΔPsaA) showed dramatically delayed growth kinetics, with no obvious log-phase of growth during the entire monitoring period when THY growth media was not supplemented with additional manganese (THY). In comparison, Rx1(ΔLytA, PdT) entered a clear log-phase, and reached stationary phase after roughly 7.5 h. However, when growth media was supplemented with manganese (THY + Mn), both vaccine strains displayed near identical growth curves, indicating wild-type kinetics could be restored in the ΔPsaA strain by appropriate Mn supplementation. Interestingly, Rx1(ΔLytA, PdT) showed slightly better growth in the supplemented media as opposed to plain THY, despite having no manganese-uptake defects.

Once the attenuating mutation was confirmed, it was crucial to establish that the modified vaccine strain Rx1(ΔLytA, PdT, ΔPsaA) was still capable of conferring protection against lethal pneumococcal challenge. Thus, this strain was grown in THY + Mn to OD_{600} = 0.65, then processed as per *Section 3.2.6* and sterilised by exposure to gamma-irradiation (16 kGy). Swiss mice received two IN vaccinations with the either irradiated vaccine (termed γ-PN(ΔPsaA)), or PBS as a mock-vaccine control. All mice were then challenged IN with lethal D39, and monitored for survival. **Figure 3.2** clearly shows the modified vaccine was able to induce significant protection against this lethal challenge in comparison to controls. Furthermore, the survival rate (~50%) of vaccinated animals matches that previously observed by Babb *et al*. when testing the original Rx1(ΔLytA, PdT) irradiated vaccine (γ-PN) against D39 challenge [235].

3.3.2. Morphology of manganese-supplemented vaccine strains

Previous studies have suggested that manganese stress is associated with alteration of pneumococcal cell division and morphology. One study in particular reported manganese over-supplementation caused elongation of cells, whilst manganese limitation imposed by zinc toxicity led to dramatically shortened cells [472]. Given that a Mn-import deficient strain has been utilised here, paired with high concentrations of extracellular manganese for growth, it was important to ensure this had no negative effects on morphology of vaccine strains. Additionally, chaining of cells via dysregulated cell division could lead to aggregation of pneumococci within vaccine suspensions.

To assess changes to morphology, the original Rx1(ΔLytA, PdT) strain was grown in THY or THY + Mn media, and samples taken at OD_{600} = 0.2, 0.4, and 0.65 for imaging by scanning electron microscopy (SEM). Direct comparison of this strain in the presence and absence of manganese ensured that any observed changes were solely due to Mn supplementation, as opposed to ΔPsaA growth-related changes. The Rx1(ΔLytA, PdT, ΔPsaA) strain was also grown in THY + Mn, and samples were taken at the same OD_{600} values. Comparison of both strains grown in Mn-supplemented media would allow the determination of morphology changes due to the ΔPsaA mutation alone. Note Rx1(ΔLytA, PdT, ΔPsaA) grown in plain THY was not used for morphology comparison due to excess stress and altered kinetics when cultured in this media type. **Figure 3.3A**

illustrates that neither manganese levels nor the ΔPsaA mutation had any observable effect on cell morphology, cell length, or chain formation. Additionally, dynamic light scattering (DLS) was used to quantify the mean diameter of pneumococcal aggregates within each vaccine preparation. **Figure 3.3B** shows the peak diameter for all tested vaccine preparations was approximately 1μm, indicating the majority of the suspension was comprised of diplococci, rather than aggregates or long cell chains.

3.3.3 Inactivation of vaccine strains by gamma-irradiation

For comparison of inactivation of vaccines grown with or without manganese, Rx1(ΔLytA, PdT) and the newly generated Rx1(ΔLytA, PdT, ΔPsaA) were both grown in THY or THY + Mn to OD = 0.65. Once at this density, all cultures were extensively washed and processed for irradiation. Aliquots were exposed to gamma-radiation whilst frozen on dry-ice, and inactivation curves were generated using CFU counts of treated samples. Control samples remained frozen but were not exposed to irradiation (0 kGy), and were used to estimate the initial viable titre. **Figure 3.4A** shows both vaccine strains were inactivated in a sigmoidal fashion irrespective of manganese supplementation, with an initial area of resistance at low irradiation doses, followed by log-linear inactivation. Additionally, manganese supplementation appeared to have no effect on the sterilisation of Rx1(ΔLytA, PdT), with the two curves being almost identical and returning very similar D_{10} values (0.82 kGy and 0.75 kGy for Rx1(ΔLytA, PdT) grown in THY and THY + Mn, respectively). Interestingly, Rx1(ΔLytA, PdT, ΔPsaA) grown in the absence of additional Mn seemed to have increased sensitivity to irradiation, with a calculated D_{10} value of just 0.37 kGy. Conversely, the D_{10} value of the same ΔPsaA strain grown in Mn supplemented THY was 0.80 kGy, which closely matches values for both Rx1(ΔLytA, PdT) preparations.

Subsequently, potential reasons for this difference in slope between inactivation curves for the modified strain were investigated. First, Rx1(ΔLytA, PdT, ΔPsaA) was grown in THY + Mn to OD_{600} = 0.65, then diluted to different starting titres in PBS + 13% glycerol prior to gamma-irradiation. **Figure 3.4B** shows that differences in start titre had no dramatic impact on the slope of the inactivation curves, with all three preparations giving D_{10} values of approximately 1.0 kGy. Next, Rx1(ΔLytA, PdT) was grown in plain THY,

then supplemented with increasing manganese concentrations *after* growth, but prior to irradiation. This was to assess the potential impact of external manganese on irradiation resistance. Again, no impact was detected, with all inactivation curves overlapping (**Fig. 3.4C**). Thus, it is likely that the absence of internal manganese during growth of the ΔPsaA strain in THY only (stressed condition) resulted in increased sensitivity to gamma-irradiation.

Additionally, all four vaccine preparations in **Figure 3.4A** were sterile following exposure to 12 kGy of gamma-irradiation, which matches the dose used previously by Babb *et al.* for pneumococcal vaccine inactivation [235, 403]. However, a sterilising dose of 16 kGy was chosen for all irradiated vaccines used here to further enhance safety. This increased dose was not anticipated to influence vaccine efficacy, as neither strain showed any increase in damage or alteration to cell morphology when exposed to irradiation doses as high as 25 kGy (**Fig. 3.5**).

3.3.4. Comparable antibody responses induced by γ-PN and γ-PN(ΔPsaA)

Given that pneumococcal morphology and aggregation were not affected by the ΔPsaA mutation nor the required manganese supplementation, it was next investigated whether vaccine-induced humoral responses were altered. For this *in vivo* investigation,16 kGy-treated samples of all vaccine preparations were used. Note that the 16 kGy-treated vaccines are termed γ-PN and γ-PN(ΔPsaA) for irradiated Rx1(ΔLytA, PdT) and Rx1(ΔLytA, PdT, ΔPsaA), respectively.

Two IN vaccinations were administered to Swiss mice using equivalent protein content per dose of each vaccine preparation (γ-PN or γ-PN(ΔPsaA) grown ± Mn). Serum and saliva samples were harvested a week after the second vaccination dose, and antibody responses to whole-cell pneumococcal antigen were determined by ELISA. In all cases, titres were calculated relative to sera and saliva samples from PBS-mock vaccinated mice. As shown by **Figure 3.6**, total IgG and IgA titres in serum were very similar for all four vaccine preparations, with no statistically significant differences. Mn-supplementation did appear to marginally elevate salivary IgA titres for the γ-PN(ΔPsaA) vaccine, though this did not reach statistical significance by One-way ANOVA.

To further characterise the antibody responses induced by each vaccine preparation, the reactivity of harvested immune sera against whole-cell vaccine lysates was determined using Western Blot. This allowed comparison of the profile of pneumococcal antigens in each vaccine that were being processed for humoral immune responses *in vivo*. Remarkably, the γ-PN(ΔPsaA) vaccine grown in Mn-supplemented THY (γ-PN(ΔPsaA) + Mn) induced antibodies that reacted against a substantially wider range of pneumococcal antigens than antibodies induced by the original γ-PN preparation (**Fig. 3.7**). The ΔPsaA mutation itself appeared to be contributing towards this enhanced reactivity of vaccine-induced responses. When comparing the original γ-PN and the modified γ-PN(ΔPsaA) both grown in un-supplemented THY, antibodies induced against the modified ΔPsaA strain showed a more diverse range of reactivity to pneumococcal proteins. A similar trend for enhanced reactivity was seen when comparing the original γ-PN and the modified γ-PN(ΔPsaA) both grown in THY + Mn. Thus, data indicates the removal of PsaA from our pneumococcal vaccine strain is associated with increased immunogenicity as well as heightened safety.

Manganese supplementation also appeared to have a minor effect on antibody reactivity to pneumococcal antigens. Specifically, we detected a slight alteration to the banding pattern of proteins bound by antibodies raised against γ-PN compared to those raised again γ-PN + Mn. Similarly, comparison of the banding profile for antibodies raised against γ-PN(ΔPsaA) compared to γ-PN(ΔPsaA) + Mn showed a slight change in dominant antigens. Furthermore, Mn-supplementation of both γ-PN and γ-PN(ΔPsaA) appears to have suppressed expression of an antigenic protein ~250kDa present in the whole-cell lysates themselves. The lysate of γ-PN(ΔPsaA) grown in plain THY also showed some bands with less intensity compared to the other three lysates when probed with a single immune sera type; this is likely due to increased stress during growth of the modified strain in non-supplemented media.

Overall, titres of both IgG and IgA were very similar across the four individual vaccines, but stark differences in antibody reactivity between the original and modified strain were detected. Thus, the original formulation (γ-PN grown in plain THY) and the modified γ-

PN(ΔPsaA) (grown in THY + Mn for sufficient antigen concentration) were selected for further comparative studies. Inclusion of the original formulation was intended to allow comparison of responses observed here to those seen in previously published studies by Babb *et al.* [235]. These two vaccine preparations were administered either IN or IP to assess whether similarity in antibody titre was maintained across multiple immunisation routes. Again, titres of IgA and IgG in sera, and of sIgA in saliva were comparable between the two pneumococcal vaccines for both routes tested (**Fig. 3.8**). Each vaccine given IP also induced significantly elevated IgG in sera compared to the same preparations administered IN, as expected. sIgA was markedly less when both vaccines were given IP as opposed to IN, though this drop did not reach statistical significance.

3.3.5. Confirmation of protective efficacy against lethal heterologous challenge

Thus far, the modified pneumococcal vaccine was found to induce comparable antibody titres to the original vaccine (**Fig. 3.6** and **Fig. 3.8**), but with an enhanced spectrum of antigen reactivity (**Fig. 3.**7). Protection against homologous pneumococcal challenge was also maintained (**Fig. 3.2**)**.** Next, a direct comparison of protection mediated by γ-PN and γ-PN(ΔPsaA) against a highly virulent heterologous serotype was sought. Swiss mice were therefore vaccinated IN with the same antigen dose of either vaccine, and challenged two weeks later with lethal P9 (heterologous serotype 6A). Survival data presented in **Figure 3.9** illustrates that γ-PN(ΔPsaA) vaccinated mice were significantly protected against the lethal challenge compared to control mice, confirming that the modified vaccine retained the ability to induce serotype-independent protection. In fact, γ-PN(ΔPsaA) performed significantly better than the original γ-PN in this model of severe pneumococcal infection.

3.3.6. Innate immune signalling is modulated by growth in manganese-supplemented media

Given that γ-PN and γ-PN(ΔPsaA) induced different degrees of protection, it was of interested to determine whether innate immune signalling was augmented by the modified vaccine. Thus, samples of γ-PN and γ-PN(ΔPsaA) were used to stimulate cultures of HEK-293 cells stably expressing human TLR4 or TLR2. IL-8 production by these cells was determined by ELISA, which is used as a measure for the degree of TLR

signalling induced by each preparation. Samples of each vaccine preparation grown with and without manganese were included, as well as live samples of each strain for controls. **Figure 3.10A** shows consistent TLR4 signalling across all tested vaccine formulations, with the ΔPsaA mutation and the presence of manganese during growth having no significant effects. Importantly, no loss of TLR4 signalling was observed for any of the vaccine preparations after irradiation at 16 kGy, indicating robust maintenance of immune stimulating molecules. However, TLR2 signalling did appear to be influenced by both the ΔPsaA mutation, and Mn presence during growth of the vaccines. **Figure 3.10B** shows that Mn supplementation during growth of the modified γ-PN(ΔPsaA) was able to significantly enhance the ability of the pneumococci to stimulate TLR2 *in vitro.* This enhancement was not observed for the original γ-PN strain when grown in the same Mn-containing media. Importantly, this trend was observed for both live and irradiated versions of the vaccine, again confirming the maintenance of ligands important for innate immune signalling after gamma-irradiation. Additionally, enhanced TLR2 signalling detected for both live and irradiated γ-PN(ΔPsaA) confirms that potential increases in replication of the Mn-grown pneumococci during incubation with HEK cells is not the cause for the enhanced signalling.

3.4. DISCUSSION

S. pneumoniae remains a global health concern, with the limited serotype coverage of current vaccines leading to continual serotype replacement. Existing vaccines also offer no coverage against newly emerging serotypes and non-encapsulated isolates. These limitations have led to a search for novel pneumococcal vaccines offering broad-spectrum protection. Our lab has previously published a novel approach to meet this need, with a whole-cell gamma-irradiated *S. pneumoniae* preparation (γ-PN). This was shown to be highly effective in conferring protection against both vaccine and non-vaccine serotypes without requirement for adjuvant [235].

The γ-PN vaccine strain is based on an un-encapsulated D39 derivative, termed Rx1, which was genetically modified to achieve further attenuation, generating Rx1(ΔLytA, PdT). Specifically, native Ply was replaced by a non-toxic derivative, PdT, and LytA was

deleted to enable growth of high cell densities *in vitro* by preventing stationary phase autolysis. The three amino acid substitutions within PdT abrogate the toxicity of native Ply whilst retaining antigen structure and immunogenicity [473]. Here, we have improved the suitability of this novel vaccine candidate for clinical development by further enhancing the safety profile via deletion of the *psaA* gene. A higher irradiation dose was also used in this study to further enhance vaccine safety.

PsaA functions as the solute-binding component of the ABC-type manganese import system [455]. Manganese (Mn^{2+}) serves as a cofactor for a variety of bacterial proteins involved in glycolysis, nucleic acid degradation, signal transduction, and oxidative stress defence [474]. Numerous studies examining *psaA* mutants have illustrated the absolute requirement of manganese supplementation for normal growth *in vitro* [463, 459]. This is also illustrated in **Fig. 3.1C**, were Rx1(ΔLytA, PdT, ΔPsaA) displayed minimal increases in cell density when cultured in un-supplemented THY media. The manganese concentration in un-supplemented THY is approximately 0.25 μM [475], and whilst this concentration allowed minimal ΔPsaA growth, the manganese concentration within internal body sites such as blood serum is estimated at just 20 nM [476, 477]. Thus, in the unlikely event that any Rx1(ΔLytA, PdT, ΔPsaA) pneumococci survive the irradiation process, they will be unable to replicate in these sterile sites following vaccine administration. *In vivo* models have also demonstrated a dramatic loss of virulence due to *psaA* mutation [458], with mutants being unable to colonise the lungs, disseminate into blood, or grow in an otitis media model [459]. Taken together, this mutation represents an added safety feature to the previously reported gamma-irradiated pneumococcal vaccine (γ-PN).

Importantly, the growth defect of the *psaA* mutant could be negated by appropriate Mn supplementation *in vitro* to facilitate manufacture of highly concentrated vaccine preparations. Growth kinetics that closely matched those of the original Rx1(ΔLytA, PdT) were achieved simply by culturing the modified Rx1(ΔLytA, PdT, ΔPsaA) in manganese-supplemented THY media (THY +Mn). The concentration of Mn employed here was intentionally high to facilitate high titre growth. However, modulating external Mn has been shown previously to affect cell morphology. For example, Martin *et al.*

[472] demonstrated the enzyme PhpP of *S. pneumoniae* can become hyper-activated due to over-metalation by excess Mn. This resulted in reduced phosphorylation status and caused defects in cell division, leading to elongated and highly chained pneumococci. In contrast, Mn limitation induced by zinc toxicity was found to cause inhibition of PhpP activity, leading to shortened cell morphology [472]. Importantly, no obvious effect on cell morphology, length, or chain formation was observed due to Mn supplementation of either vaccine strain (**Fig. 3.3**). In fact, Martin *et al.* employed mutation of the constitutively expressed manganese exporter, MntE [456, 478], to cause accumulation of excess intracellular Mn, leading to the aforementioned morphology changes. Whilst Mn may be accumulating in the pneumococci used here during growth in THY + Mn, it is unlikely to reach a toxic level as the MntE exporter remains entirely functional in both vaccine strains.

Following confirmation of morphology, vaccine strains were inactivated by gamma-irradiation, and all preparations deemed sterile at doses of 12 kGy and above. However, due to the nature of sterilization, there always exists a small but calculable probability that a pathogen will survive treatment; this is denoted as the Sterility Assurance Level, or SAL [319]. Additionally, for clinical application, the pneumococcal vaccine may be treated with radiation doses substantially higher than 12 kGy to meet a SAL of 10^{-6} (one in a million chance of a cell remaining viable after treatment). To calculate this potential SAL dose, inactivation curves for each of the vaccine preparations were determined. The shape of inactivation curves for all preparations were sigmoidal, with an initial short region of radiation resistance, followed by log-linear inactivation. This linear region was used to estimate D_{10} values (indicating the dose required for a single $\log_{10}$ titre reduction) for all preparations. Interestingly, the calculated D_{10} value was considerably lower for γ-PN(ΔPsaA) grown in un-supplemented THY when compared to the other three formulations (**Fig. 3.4A**). My data indicate that a lower starting titre was not the reason for this increase in radio-sensitivity (**Fig. 3.4B**), nor were differences in external manganese concentration (**Fig. 3.4C**). Hence, differences in intracellular Mn may be the essential factor underlying the variation in radio-sensitivity. Daly *et al*. demonstrated that accumulation of intracellular Mn(II) is critical to radiation resistance in *Deinococcus radiodurans*, where it acts in detoxification of reactive oxygen species (ROS), and is a

cofactor for the Mn-dependent superoxide dismutase (Mn-SOD) [479]. It was also proposed in follow-up studies that the accumulation of manganese facilitates formation of Mn(II)-metabolite complexes within *D. radiodurans* that protect essential enzymes from oxidative damage [480-483]. Furthermore, both ΔPsaA and ΔPsaD pneumococcal strains have been shown to be highly sensitive to oxidative stress in comparison to wild-type counterparts, and have lowered ability to neutralise reactive oxygen species (ROS) [462]. Lack of this crucial co-factor within the Mn-starved ΔPsaA strain is therefore likely to contribute to the enhanced sensitivity to radiation damage. In further support of this, Ogunniyi *et al*. demonstrated by ICPMS that a *psaA* deletion mutant of D39 accumulated less than a third of the intracellular manganese of wild-type cells when grown in un-supplemented media [465].

In terms of D_{10} values, γ-PN grown in both THY and THY + Mn, and γ-PN(ΔPsaA) grown in THY + Mn all returned values of approximately 0.8 kGy. To then accurately calculate the total dose required to achieve a SAL of 10^{-6}, the initial region of radiation resistance and the subsequent log-linear region of the inactivation curves were both considered. Based on data presented in **Figure 3.4A**, the dose required to overcome the short resistance region was estimated to be 3 kGy. Assuming a starting titre of 10^{10} CFU/ml, a total of 16 $\log_{10}$ reductions would be required to achieve a theoretical titre of 10^{-6}. The D_{10} value of 0.8 kGy is therefore multiplied by 16, giving 12.8 kGy. This is paired with the additional 3 kGy to overcome initial resistance, giving a total sterilising dose of 15.8 kGy. Consequently, 16 kGy irradiated pneumococcal vaccines were used for all subsequent immunogenicity experiments. The D_{10} value and resulting SAL for the γ-PN(ΔPsaA) vaccine grown in plain THY were substantially lower than this. However, 16 kGy was still used to allow accurate comparison with the other vaccine preparations. Furthermore, doses up to 25 kGy were observed to have no negative impact on pneumococcal integrity (**Fig. 3.5**).

Another potential effect of supplementing vaccine strains with high manganese was the alteration of expression profiles for important antigenic proteins. For example, high manganese leads to suppression of genes under control of *psaR*, the transcriptional regulator of the *psaBCA* operon [467]. These include the extracellular serine protease

PrtA, and choline binding protein PcpA [460, 484, 485, 465], both of which are protective immunogens [466, 486]. It was therefore important to determine that vaccine immunogenicity was not negatively affected by manganese supplementation. Swiss mice were vaccinated with four different vaccine formulations (γ-PN or γ-PN(ΔPsaA) grown ± Mn), and the potency of antibody responses in serum and saliva were determined against whole cell pneumococcal antigen. Note that the antigen used for coating of ELISA plates was the original PN strain grown in plain THY, hence all surface antigens were theoretically available for binding (no suppression of proteins by PsaR, nor loss of PsaA expression). My data shows no detectable changes in the overall titres of IgG and IgA in sera and saliva between the four vaccine preparations (**Fig. 3.6**). This indicates that antigenic proteins against which humoral responses are induced are not decreased by alteration of manganese levels, nor by loss of PsaA expression. In fact, data presented in **Figure 3.7** indicates that the ΔPsaA mutation actually enhances reactivity of vaccine-induced antibodies to pneumococcal antigens. Whilst these antigens were actually present in lysates of all four vaccine preparations, genetic modification of the vaccine may have up- or down-regulated certain proteins, thus shifting the profile of dominant antigens. Alternatively, there may be some differences in the recognition of γ-PN(ΔPsaA) by the immune system may differ, e.g. due to modulated innate signalling and/or different cytokine profiles.

In addition to diversified antibody reactivity, the modified version of the vaccine retained the ability to induce serotype-independent protection against lethal pneumococcal challenges (**Fig 3.2** and **Fig. 3.9**). In fact, γ-PN(ΔPsaA) offered significantly better protection than the original γ-PN against challenge with the heterologous serotype 6A (P9 strain). This may be due to the increased range of antigens that γ-PN(ΔPsaA)-induced antibodies are able to recognize, leading to an enhancement of opsonophagocytosis, complement deposition, and pneumococcal clearance. It is worth noting that γ-PN has been shown to be highly protective against both vaccine and non-vaccine serotypes in prior studies [235, 403]. The challenge dose utilised here was substantially increased compared to that used previously to maximise any detectable differences in vaccine performance. Additionally, the change in mouse strain from C57BL/6 to Swiss mice is likely to be a contributing factor to the observed disparities in protection rates. This

mouse model was selected to provide a better representation of potential vaccine performance in a highly variable human population.

The increase in survival of γ-PN(ΔPsaA) vaccinated mice was of particular interest, and may be partially explained by differences in innate immune responses induced by each vaccine formulation. Prior study revealed that γ-PN-mediated protection is largely dependent on innate-like pulmonary γδT_{17} responses [235]. Unlike αβ T-cells, γδ T-cells can recognise a broad range of stress antigens independently of classical MHC molecules [487, 488], and production of IL-17A and other inflammatory cytokines by these cells rapidly orchestrates rapid neutrophil responses that are vital for mucosal defence [489]. Interestingly, both murine and bovine γδ cells are able to directly respond to TLR2 ligands, leading to increased proliferation and cytokine production in a TCR-independent manner. Cross-talk of TCR- and TLR2 signalling is also reported to further enhance effector function of human γδ T-cells [490-492], and indirect stimulatory effects of IFN-γ on murine γδ T-cells via TLR2-ligand activated DCs have been previously described [493]. Given that γ-PN(ΔPsaA) was able to induce elevated TLR2 signalling *in vitro* (**Fig. 3.10**), it is likely that γδ T-cell responses would be enhanced *in vivo.* This could contribute substantially to the heightened protection observed against challenge with non-vaccine serotypes. Modulated innate signalling may also explain the increased reactivity of humoral immune responses. Innate signalling and innate-like cell subsets induced *in vivo* by each vaccine will be the focus of thorough investigation in future studies. This aspect of vaccine-induced immunity could not be investigated further in the current study due to time constraints.

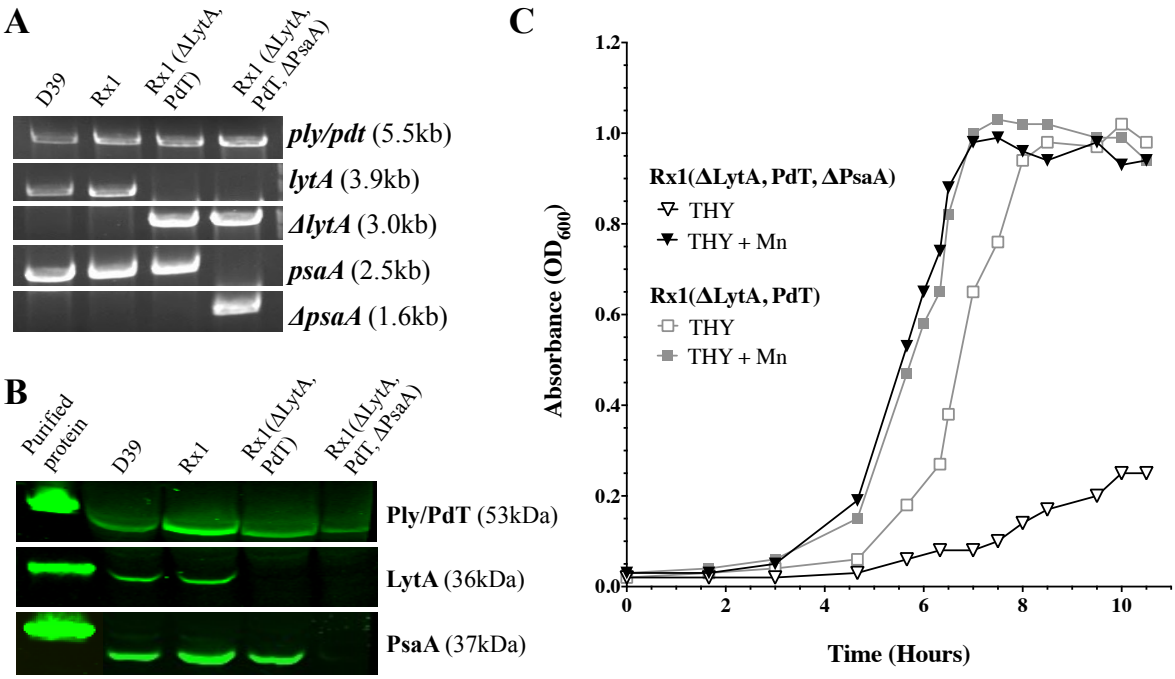

Figure 3.1. Genetic manipulation of pneumococcal vaccine strain Rx1(ΔLytA, PdT, ΔPsaA) successfully attenuates growth. (A) Progression of genetic manipulation of the vaccine strains Rx1(ΔLytA, PdT) and Rx1(ΔLytA, PdT, ΔPsaA) shown by PCR. (B) Western Blot showing lack of LytA and PsaA protein expression in attenuated strains. (C) *In vitro* growth curves for Rx1(ΔLytA, PdT) (squares) and Rx1(ΔLytA, PdT, ΔPsaA) (triangles) cultures in plain THY media or THY supplemented with 400 μM $MnCl_2$ (THY + Mn).

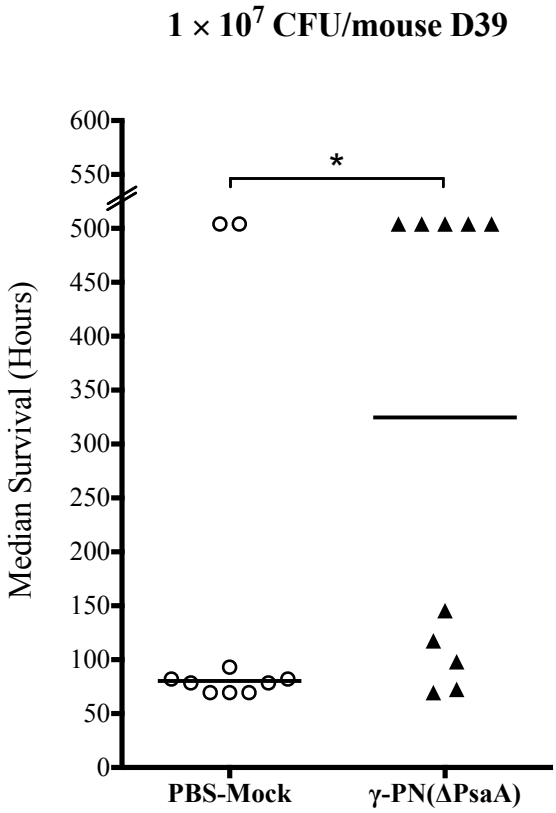

Figure 3.2. Protection against lethal D39 challenge conferred by IN vaccination with γ-PN(ΔPsaA). Swiss mice were IN vaccinated twice, two weeks apart with 21.25 μg total protein/dose/mouse (~10^8 CFU equivalent/mouse) of γ-PN(ΔPsaA). Control mice received PBS-mock vaccinations. Two weeks post-2nd vaccination, mice challenged IN with 10^7 CFU/mouse of D39 (vaccine serotype 2). All mice were monitored daily for 3 weeks for development of clinical symptoms and overall survival. Data are presented as median survival time (n = 10), analysed by Mann-Whitney test (*, $P < 0.05$).

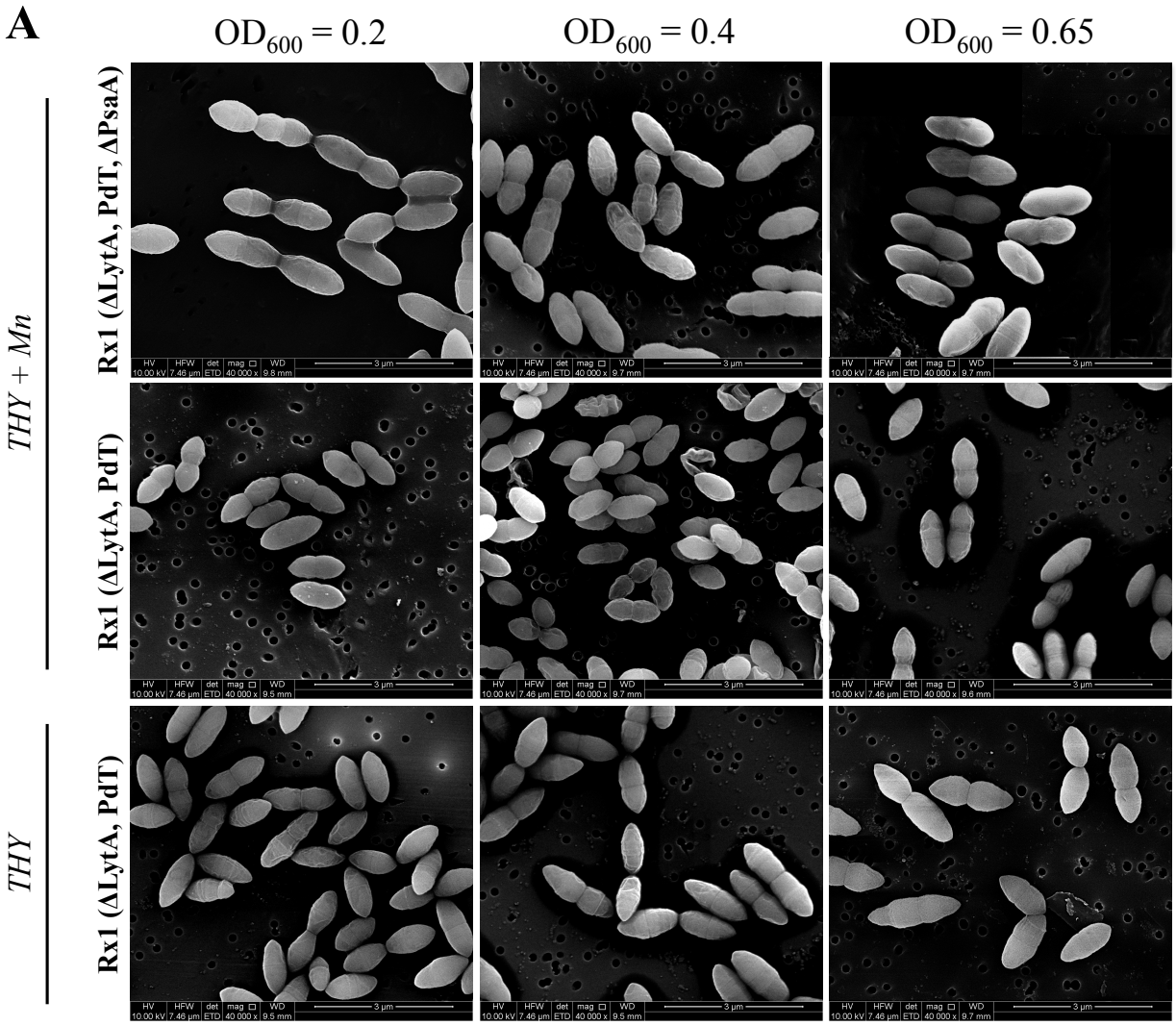
A
OD600 = 0.2
OD600 = 0.4
OD600 = 0.65
THY + Mn
THY
Rx1 (ΔLytA, PdT, ΔPsaA)
Rx1 (ΔLytA, PdT)
Rx1 (ΔLytA, PdT)

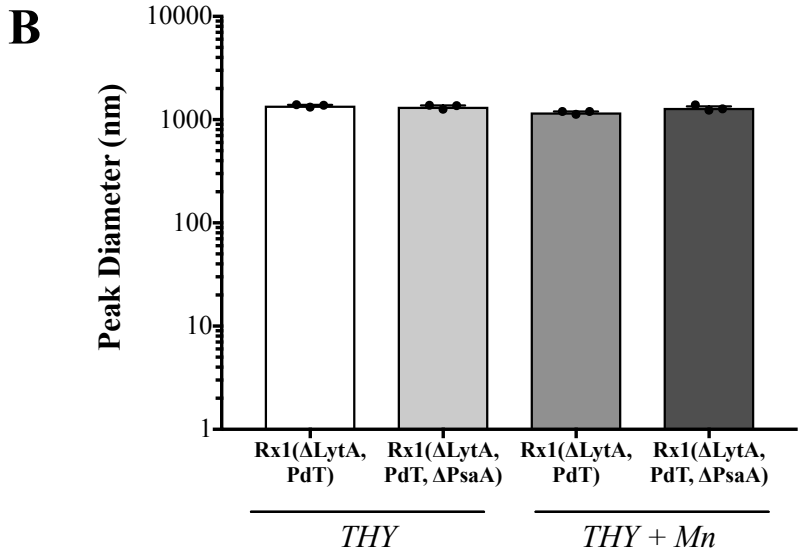
B
Peak Diameter (nm)
10000
1000
100
10
1
Rx1(ΔLytA, PdT)
Rx1(ΔLytA, PdT, ΔPsaA)
Rx1(ΔLytA, PdT)
Rx1(ΔLytA, PdT, ΔPsaA)
THY
THY + Mn

Figure 3.3. Manganese supplementation of pneumococcal vaccine strains does not alter cell morphology or aggregation. (A) Representative scanning electron microscopy images of Rx1(ΔLytA, PdT) and Rx1(ΔLytA, PdT, ΔPsaA) vaccine strains. Both strains were grown to OD_{600} = 0.2, 0.4, and 0.65 in THY or THY supplemented with 400 μM $MnCl_2$ (THY + Mn). Samples were stained with 2% Osmium tetroxide (OsO_4) prior to progressive dehydration and imaging with the Quanta 450 Scanning Electron Microscope. 40,000× magnification was used for all images, scale bar = 3 μm. (B) Rx1(ΔLytA, PdT) and Rx1(ΔLytA, PdT, ΔPsaA) vaccine strains were each grown to OD_{600} = 0.65 in THY and THY + Mn. Dynamic light scattering (DLS) was then used to assess the peak diameter of pneumococcal cells within solution following a single freeze-thaw cycle. Samples were read in triplicate, data indicates mean diameter ± SEM.

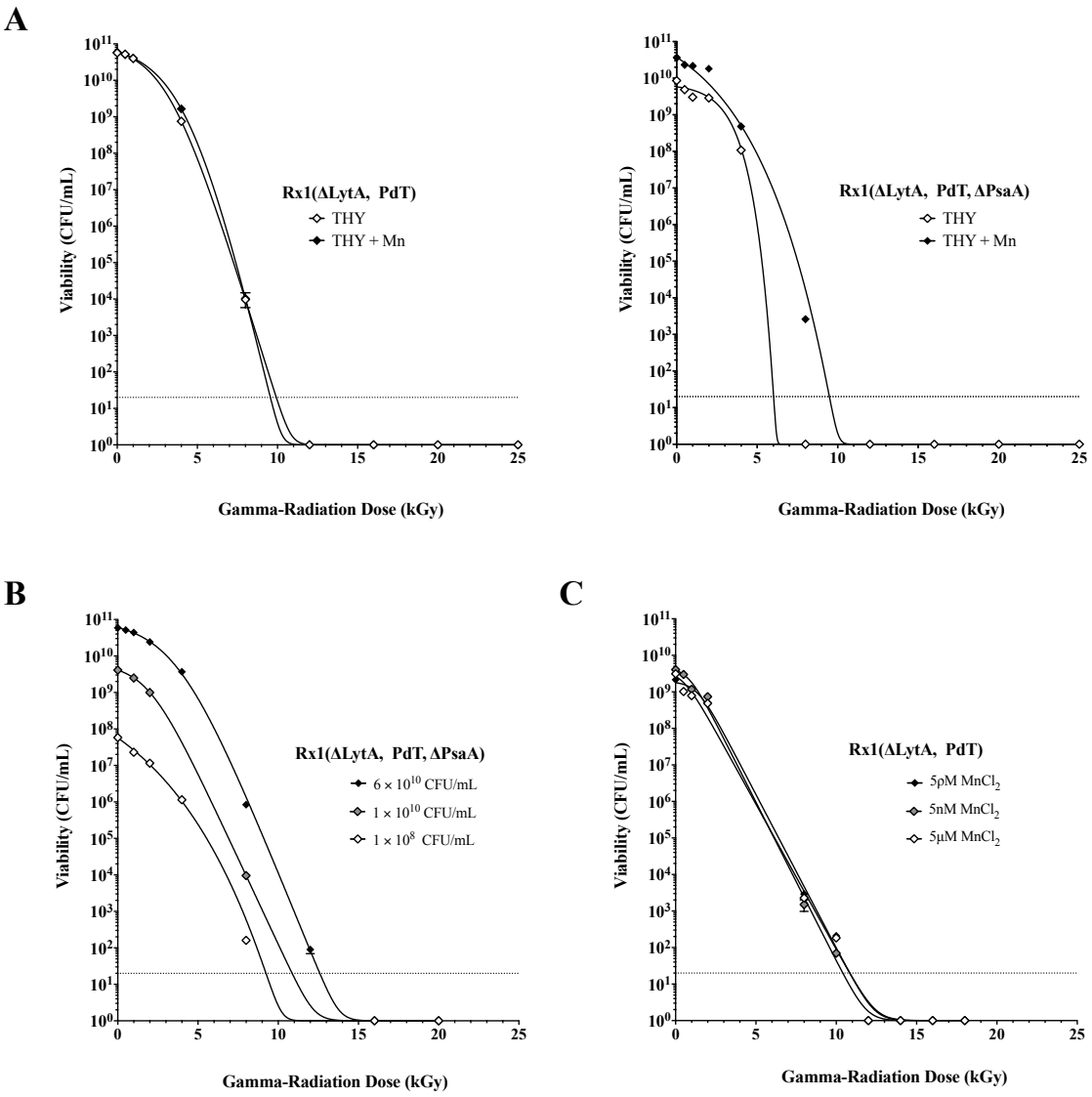

Figure 3.4. Irradiation of Rx1(ΔLytA, PdT) and Rx1(ΔLytA, PdT, ΔPsaA) vaccine strains. (A) Strain were grown to OD_{600} = 0.65 in THY or THY + Mn, then exposed to increasing doses of gamma irradiation whilst frozen on dry ice. (B) Strain Rx1(ΔLytA, PdT, ΔPsaA) was grown to OD_{600} = 0.65 in THY + Mn, then diluted to 6×10^{10}, 1×10^{10}, or 1×10^{8} CFU/ml prior to irradiation. (C) Strain Rx1(ΔLytA, PdT) was grown to OD_{600} = 0.65 in plain THY, and aliquots supplemented with external $MnCl_2$ after growth to a final concentration of 5ρM, 5ηM, or 5μM prior to irradiation. CFU counts used to determine starting titre in non-irradiated (0 kGy) controls, and remaining viable titre in irradiated samples, presented as mean ± SEM (n = 3). The asymmetric sigmoidal (5PL) non-linear regression model was used to generate curves of best fit, $R^2 \geq 0.70$ in all cases.

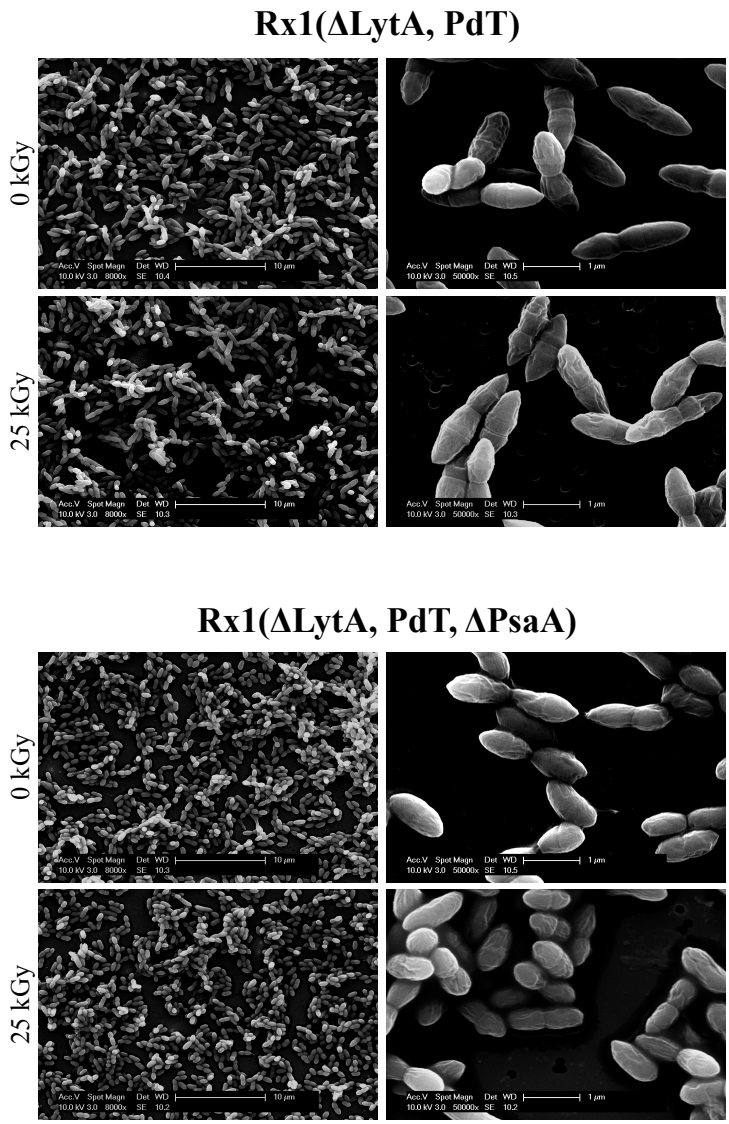

Figure 3.5. Morphology of live and irradiated Rx1(ΔLytA, PdT) and Rx1(ΔLytA, PdT, ΔPsaA). Representative scanning electron microscopy images of pneumococcal vaccine samples, either frozen and untreated (0 kGy, live controls), or inactivated with 25 kGy of gamma-irradiation whilst frozen on dry-ice. Samples were stained with 2% Osmium tetroxide (OsO_4) prior to progressive dehydration and imaging with the Quanta 450 Scanning Electron Microscope. All samples were viewed at 8000× magnification (scale bar = 10 μm) and 50,000× magnification (scale bar = 1 μm).

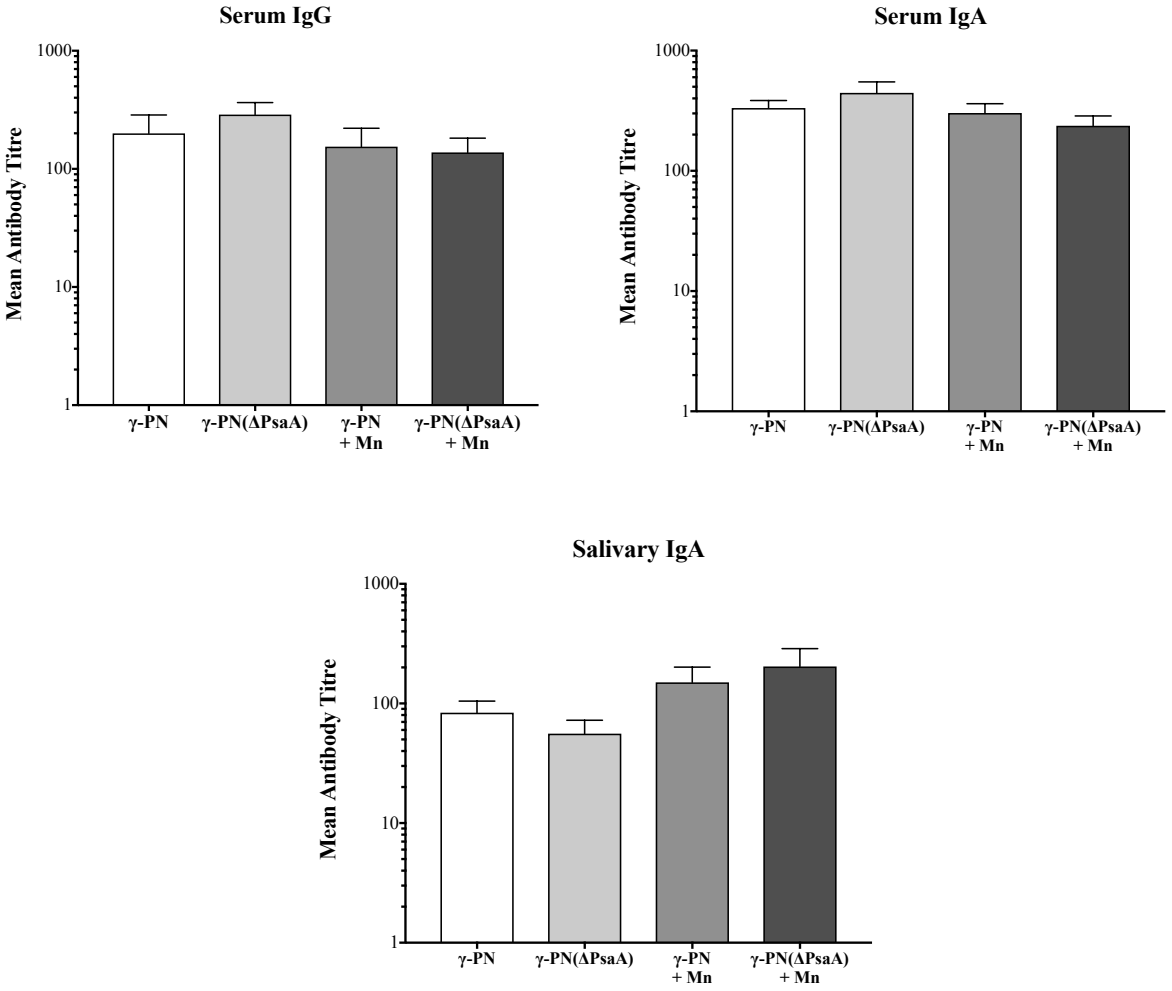

Figure 3.6. Comparable antibody responses induced by intranasal vaccination with γ-PN and γ-PN(ΔPsaA). Swiss mice were IN vaccinated twice two weeks apart with 21.25 μg total protein/dose (~10^8 CFU equivalent) of γ-PN or γ-PN(ΔPsaA) grown in THY or THY + Mn. Control mice received PBS-mock vaccinations. Serum and saliva samples were harvested on day 7 post-2nd-vaccination, and analysed for *S. pneumoniae*-specific total IgA and IgG by ELISA. Absorbance readings of samples from control mice were used to calculate relative titres. Data are presented as mean ± SEM (n = 5), and analysed by One-way ANOVA (no significant differences determined).

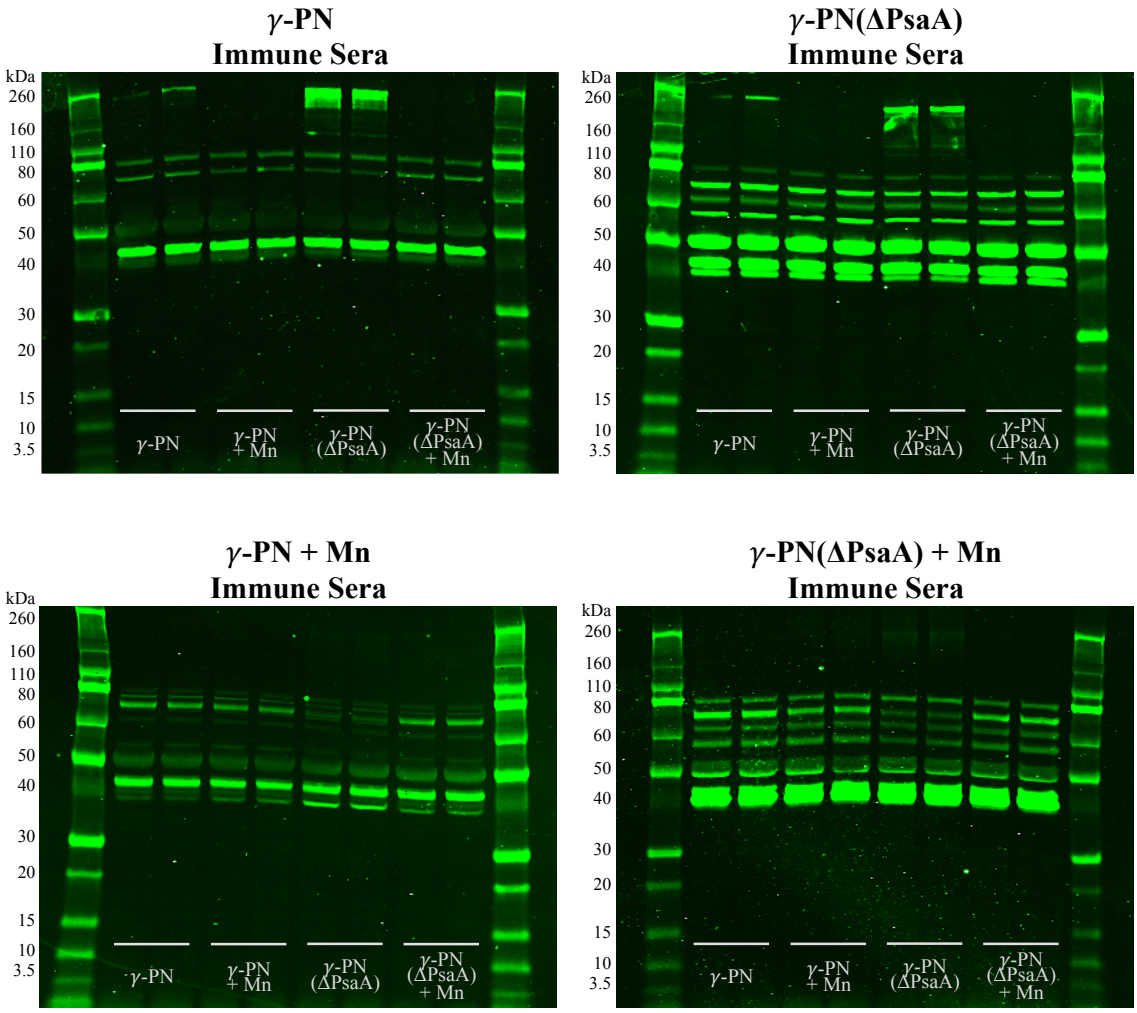

Figure 3.7. Increased reactivity of immune sera from γ-PN(ΔPsaA)-vaccinated mice against whole cell vaccine lysates. γ-PN and γ-PN(ΔPsaA) vaccines (grown in THY and THY + Mn) lysed by sonication, and 20 µg total protein loaded per well in duplicate for SDS-PAGE. Separated proteins were transferred to nitrocellulose membranes and probed with immune sera from Swiss mice vaccinated with one of the four vaccine preparations, as indicated. Bound IgG was detected using IRDye 800CW goat anti-mouse, and fluorescence was visualised using the Odyssey imaging system. Novex Sharp Pre-Stained Protein Standard was run on all gels for size comparison.

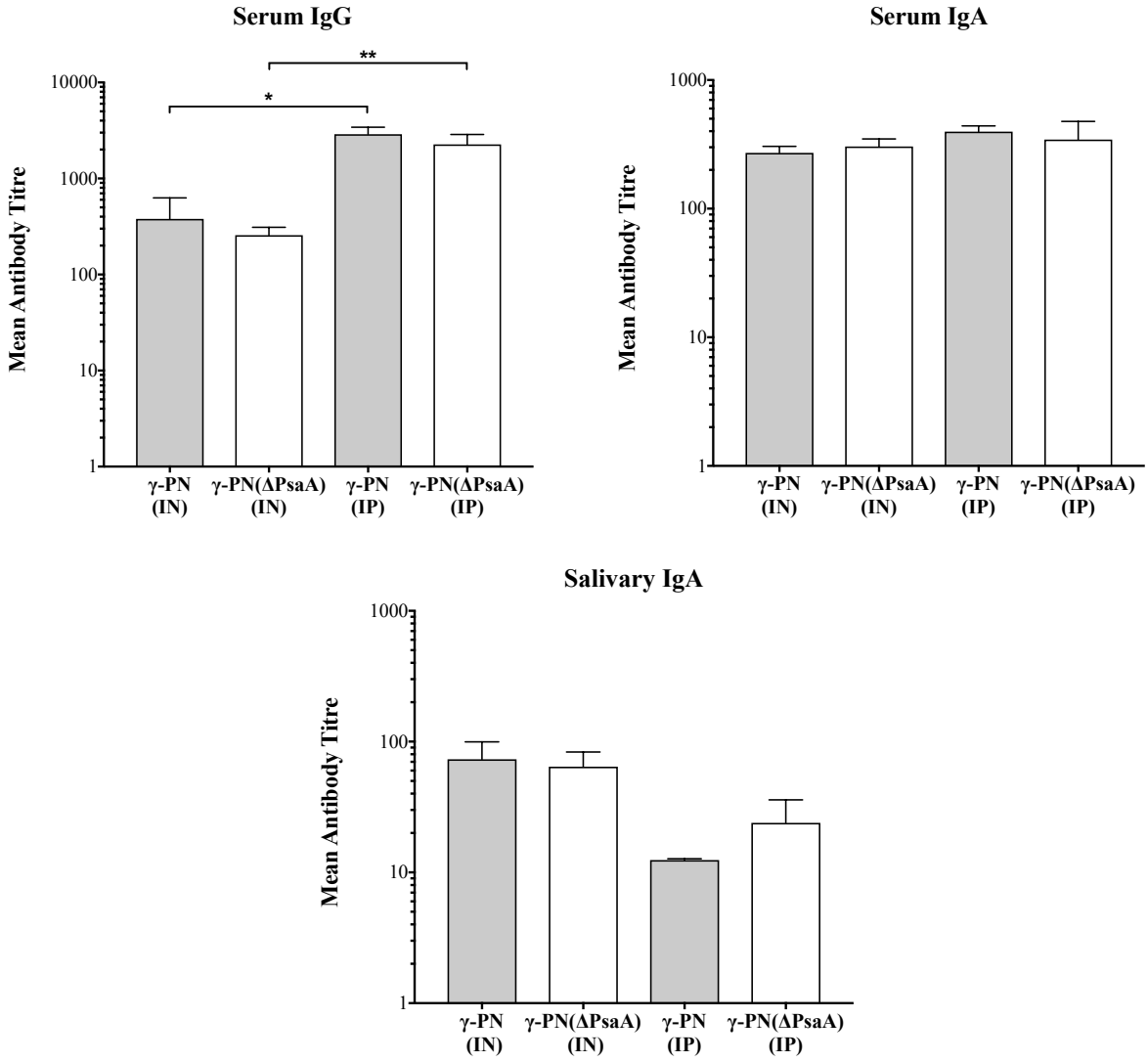

Figure 3.8. Comparable antibody titres are induced by γ-PN and γ-PN(ΔPsaA) independently of inoculation route. Swiss mice were IN vaccinated twice two weeks apart with 21.25 μg total protein/dose (~10^8 CFU equivalent) of γ-PN (grown in THY) or γ-PN(ΔPsaA) (grown in THY + Mn). This antigen dose was suspended in a volume of 30 μl for IN vaccinations, and a volume of 100 μl for IP vaccinations. Control mice received PBS-mock vaccinations. Serum and saliva samples were harvested on day 7 post-2^{nd}-vaccination, and analysed for *S. pneumoniae*-specific IgG and IgA using ELISA. Absorbance readings of samples from control mice were used to calculate relative titres. Data are representative of two independent experiments. Data are presented as mean ± SEM (n = 5), and analysed by One-way ANOVA (*, $P < 0.05$, **, $P < 0.01$).

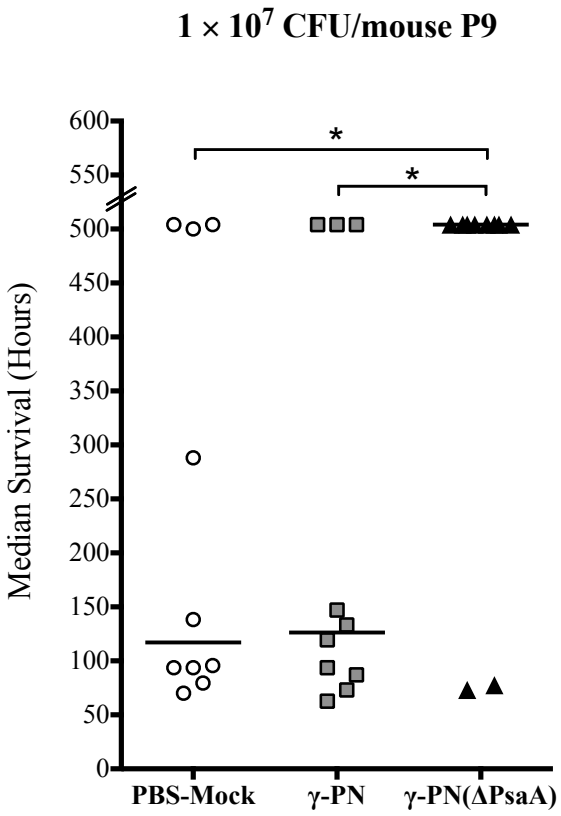

Figure 3.9. Protection against lethal P9 challenge conferred by IN vaccination with γ-PN(ΔPsaA). Swiss mice were IN vaccinated twice two weeks apart with 21.25 μg total protein/dose/mouse (~10^8 CFU equivalent/mouse) of γ-PN (grown in plain THY) or γ-PN(ΔPsaA) (grown in THY + Mn). Control mice received PBS-mock vaccinations. Two weeks post-2nd vaccination, mice challenged IN with 10^7 CFU/mouse of P9 (non-vaccine serotype 6A). All mice monitored for 3 weeks for clinical symptoms and overall survival. Data presented as median survival time (n = 10), analysed by Mann-Whitney test (*, $P < 0.05$).

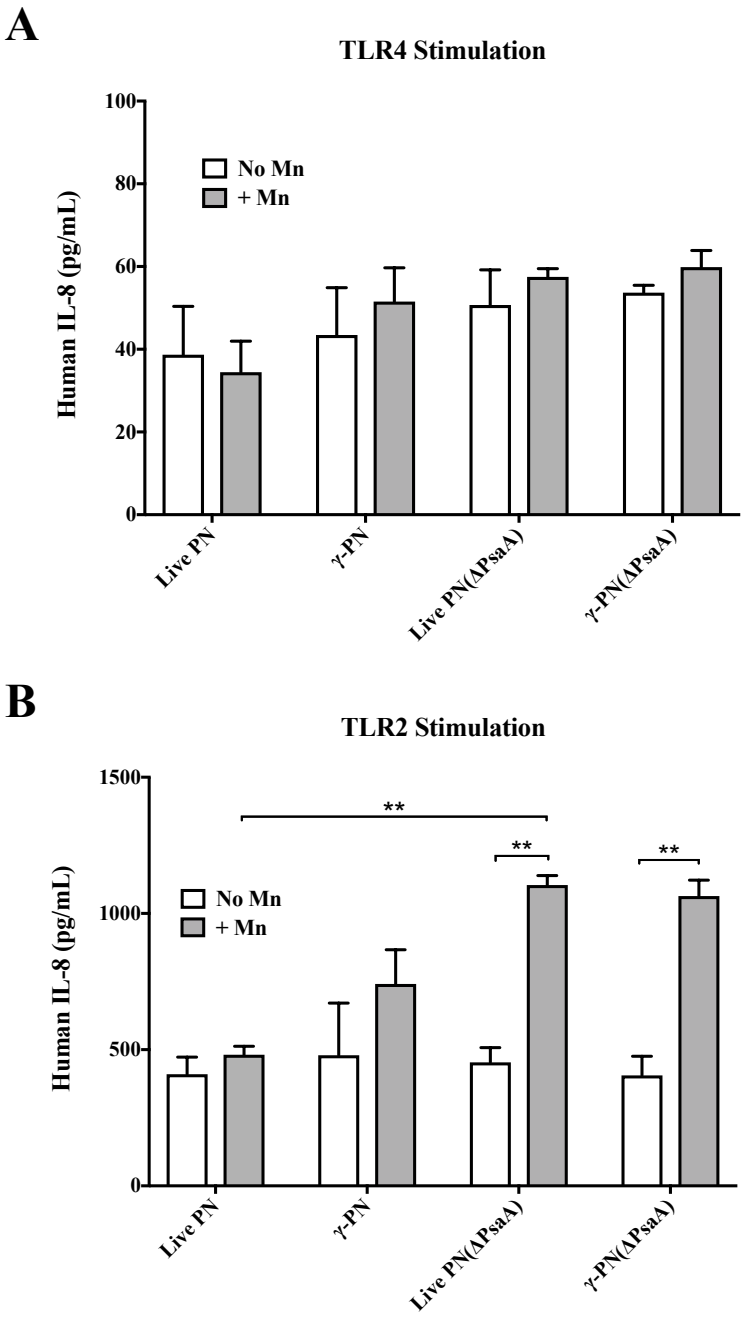

Figure 3.10. γ-PN(ΔPsaA) grown in Mn-supplemented THY is associated with enhanced TLR2 signalling *in vitro*. Live and 16 kGy-irradiated samples of PN and PN(ΔPsaA) vaccines (grown in THY or THY + Mn), were added to HEK-293 cells stably expressing (A) human TLR4, or (B) human TLR2. All antigens were added to cells at 10 μg/ml. Human IL-8 (pg/ml) in culture SN after incubation with antigens was determined by ELISA. Data is representative of three independent experiments. Data presented as mean IL-8 pg/ml ± SEM (n = 4), and analysed by Two-way ANOVA (**, $P < 0.01$).

CHAPTER 4

Co-administration of γ-Flu and γ-PN(ΔPsaA) vaccines augments IAV-specific immunity

4.1. INTRODUCTION

The upper respiratory tract is continuously exposed to a vast array of potentially pathogenic viruses and bacteria. The synergy between respiratory pathogens influenza A virus (IAV) and *Streptococcus pneumoniae* (the pneumococcus) is well documented in this setting [175, 494-496]. This particular combination of infections leads to exacerbated disease symptoms and high mortality, and is particularly prevalent during IAV pandemics [175, 264-269]. For example, the vast majority of lung culture samples taken during the 1918 Spanish Flu were positive for secondary bacteria, with *S. pneumoniae* being the most common bacterium isolated. As a result, *S. pneumoniae* is estimated to have contributed to over 50% of recorded deaths over the course of the pandemic [497]. Similar findings were reported with the more recent 2009 H1N1 pandemic, with 30% of fatal cases being attributed to combined IAV and *S. pneumoniae* infection [498].

Despite vaccines being available for both IAV and *S. pneumoniae,* co-infection with both pathogens continues to be associated with high morbidity and mortality. To address this, studies have investigated the possibility of simultaneously administering existing IAV and pneumococcal vaccines. Whilst successful at reducing disease incidence (particularly in the elderly population [294, 295, 300, 296-299]), this strategy does not offer broad-spectrum protection. In fact, irrespective of co-infection, existing IAV and pneumococcal vaccines have a limited degree of coverage against each individual pathogen. Inactivated IAV vaccines only induce strain-specific neutralizing antibody responses, and their efficacy against emerging seasonal and pandemic strains is limited. Live attenuated IAV vaccines can induce cross-protective T-cell responses, however reversion to wild-type and possible recombination with circulating annual strains represent major safety concerns. Their use is also restricted to immunocompetent healthy individuals [499], who are usually at the lowest risk of severe IAV disease and secondary complications. Similarly, *S. pneumoniae* vaccines are limited, as they currently cover only 23 of 98 immunologically distinct pneumococcal serotypes. Again, protection against emerging serotypes is limited, and the ongoing use of current vaccines drives serotype replacement.

A combination of broad-spectrum vaccines against both respiratory pathogens is an appealing possibility to overcome existing coverage issues and minimise the risk of co-

infection. We have previously published an approach to meet this need, with novel vaccines comprised of whole-inactivated IAV and whole-inactivated pneumococci. Mucosal co-administration of these vaccines provides significant protection against single challenges with IAV and pneumococci, as well as against lethal co-infection [403]. Additionally, co-administration of these vaccines resulted in superior induction of pneumococcal-specific responses in mice when compared to administration of whole-inactivated pneumococci alone, suggesting adjuvant activity of the IAV vaccine [403]. In the current study, we investigated whether the inactivated pneumococcal vaccine could similarly enhance IAV-specific responses. Data illustrates enhancement of IAV-specific T-cell immunity and protection against challenge following co-administration of our whole inactivated vaccines, indicating that our novel co-vaccination approach enables bi-directional adjuvant activity. Furthermore, data suggests this enhancement appears to be associated with to direct interaction between the whole IAV and pneumococcal vaccine components, which augments antigen uptake and immune stimulation.

4.2. Materials and Methods

4.2.1. Ethics statement

This study was conducted in strict accordance with Australian Code of Practice for Care and Use of Animals for Scientific Purposes (7th edition [2004], 8th edition [2013]) and South Australian Animal Welfare Act 1985. Experimental protocols approved by Animal Ethics Committee at The University of Adelaide (S/2016/183 & S/2018/013).

4.2.2. Bacterial and viral vaccine stocks

Influenza A viruses [A/Puerto Rico/8/34 (H1N1) (A/PR8)] and A/PR8-OVA were grown in the allantoic cavity of 10-day-old embryonated chicken eggs. A/PR8-OVA is engineered to express the ovalbumin peptide SIINFEKL (original stock was a gift from Professor Stephen Turner, Monash University). Eggs were injected with 10^3 $TCID_{50}$ of virus, incubated for 48 h at 37°C, and chilled at 4°C overnight. Allantoic fluid was harvested, pooled and stored at -80°C. Virus stocks were then concentrated using chicken red blood cells (cRBCs), as previously described [423]. Briefly, allantoic fluid was incubated with cRBCs for 45 min at 4°C to allow binding of viral HA to erythrocytes,

then centrifuged for 10 min at 300 g (at 4°C), and allantoic supernatant was removed. Pellets were resuspended in 0.85% saline, incubated for 1 h at 37°C to release virus from cRBCs, then centrifuged to separate erythrocytes from virus-containing supernatant. Concentrated stocks were titrated in Madin-Darby Canine Kidney (MDCK) cells using $TCID_{50}$ assay [422] and virus titres were estimated to be 2×10^8 $TCID_{50}$/mL for A/PR8, and 6×10^6 $TCID_{50}$/mL for A/PR8-OVA.

The *S. pneumoniae* vaccine strain Rx1(ΔLytA, PdT, ΔPsaA) was generated as per *Section 3.2.2*, and grown in THY + 400 μM $MnCl_2$ at 37°C + 5% CO_2 to OD_{600} = 0.65. Cells were pelleted by centrifugation at 8,000 rpm for 10 min at 4°C, then washed three times in PBS and resuspended in PBS + 13.33% glycerol at a density of ~10^{10} CFU/mL in 200 μl aliquots.

4.2.3. Generation of whole inactivated vaccines

Concentrated A/PR8, A/PR8-OVA and Rx1(ΔLytA, PdT, ΔPsaA) stocks were inactivated by exposure to 50 kGy, 25 kGy, and 16 kGy respectively of gamma(γ)-radiation from ^{60}Co irradiation facility at the Australian Nuclear Science and Technology Organisation (ANSTO). All samples were kept frozen on dry-ice during irradiation and transportation. Sterility of irradiated A/PR8 (γ-Flu) and irradiated A/PR8-OVA (γ-Flu-OVA) was confirmed by passages in embryonated chicken eggs as recommended by WHO [424]. In brief, 10-day-old embryonated eggs were inoculated with 100 μl of inactivated virus preparation and incubated for 2 days at 37°C. The allantoic fluid (AF) of individual eggs was then harvested and used to infect new 10-day-old embryonated eggs. This process was repeated 3 times and lack of detectable hemagglutination in AF from all 3 passages indicated complete loss of viral infectivity. To determine haemagglutination, harvested AF was serially diluted in PBS using a 96-well round-bottom plate and 0.8% cRBCs in PBS were added. Plates were incubated at 4°C and haemagglutination patterns analysed 24 h later. Sterility of irradiated Rx1(ΔLytA, PdT, ΔPsaA) (γ-PN(ΔPsaA)) was determined by lack of detectable CFU after plating of neat samples on blood agar plates.

4.2.4. Mice & vaccinations

For challenge experiments, 6 – 7 week old female wild-type BALB/c mice were supplied by Laboratory Animal Services, University of Adelaide. Mice were first anaesthetized intraperitoneally (IP) with 10 µl/gram body weight ketamine anaesthetic (1% xylazine, 10% ketamine in sterile H_20). Anaesthetized mice were then vaccinated intranasally (IN) with either γ-Flu only (6.4×10^6 $TCID_{50}$ equivalent/mouse in 32 µl), or γ-Flu + γ-PN(ΔPsaA) (6.4×10^6 $TCID_{50}$ equivalent + 10^8 CFU equivalent γ-PN(ΔPsaA) in 32 µl). This immunisation route paired with anaesthesia was chosen to allow the vaccine inoculum to enter the lung, as outlined in *Section 2.2.7.* Control animals received γ-PN(ΔPsaA) (10^8 CFU equivalent in 32 µl), or plain PBS (mock-vaccine). Where necessary, inactivated vaccine components were mixed and incubated on ice for ~15 min prior to immunisation. Serum was collected from all mice via submandibular bleeding on day 20 post-vaccination. On day 21 post-vaccination, animals were anaesthetised, and challenged IN with either A/PR8 (homotypic H1N1, 1.6×10^2 $TCID_{50}$/mouse), A/California/07/09 (drifted pdmH1N1, 1.3×10^5 $TCID_{50}$/mouse) or A/PortChalmers/1/73 (heterosubtypic H3N2, 5.4×10^5 $TCID_{50}$/mouse). Challenged mice were monitored for 3 weeks for development of clinical symptoms (including weight loss), and animals were humanely euthanised if they lost 20% of their starting body weight.

For analysis of influenza-specific T-cell responses, OT-I mice (a H-$2K^b$ restricted anti-OVA TCR transgenic line under a C57BL/6 background) were used for T lymphocyte isolation. Splenocytes were harvested from naive OT-I mice, and naive OT-I T-cells were subsequently isolated using the EasySep™ Mouse Naive CD8+ T-cell isolation kit (Stem Cell Technologies), as per the manufacturer's instructions. Naive OT-I T-cell purity was determined by flow cytometry ($CD8^+Va2^+CD44^-CD62L^+$). Purity of at least 90% was required for all transfers. 7 week old female C57BL/6 mice were purchased from the Animal Resource Centre (ARC, Western Australia), and a total of 1×10^4 naive OT-I T-cells were transferred per mouse. All cells were injected via the tail vein in 200 µl of PBS.

24 h post OT-I transfer, C57BL/6 mice were anaesthetized as above, then vaccinated IN with either γ-Flu-OVA only (3×10^5 $TCID_{50}$ equivalent/mouse in 50 µl), or γ-Flu-OVA

+ γ-PN(ΔPsaA) (3×10^5 $TCID_{50}$ equivalent + 10^8 CFU equivalent γ-PN(ΔPsaA) in 50 µl). Inactivated vaccine components were mixed and incubated on ice for ~15 min prior to immunisation. Control animals received PBS only. Blood samples were collected from all mice via submandibular bleeding on days 7 and 14 post-vaccination. Mice were then euthanised on day 21 post-vaccination by CO_2 inhalation, and blood, lungs, spleen, and mediastinal lymph node (mLN) were harvested for analysis by flow cytometry.

4.2.5. Measurement of influenza-specific antibody responses

Serum samples harvested from BALB/c mice were assessed for A/PR8-specific IgA and IgG (including subclasses IgG1, IgG2a, IgG2b, and IgG3) by ELISA as described previously [399]. Goat anti-mouse IgA (alkaline phosphatase (AP) conjugated, 1:1000 dilution, Zymed) and goat anti-mouse IgG (horse radish peroxidase (HRP) conjugated, 1:10,000 dilution, Thermo Fisher) were used as secondary antibodies to detect IgA and total IgG, respectively. IgG subclasses were detected using HRP conjugated rabbit anti-mouse IgG1 (1:1000 dilution, Zymed #61-0120), rabbit anti-mouse IgG2a (1:1000, Zymed #61-0220), rabbit anti-mouse IgG2b (1:1000, Invitrogen #610320), and goat anti-mouse IgG3 (1:4000 dilution, Southern Biotech #1100-05). Absorbance measured at 405nm for AP-conjugated antibody, and 450/620nm for HRP-conjugated antibodies using a Biotrack II plate reader. End point titres for all samples are expressed as the reciprocal of the last dilution where the OD value was equal to or more than the cut-off value. The cut-off was calculated by adding 3-fold standard deviation (SD) to the mean (i.e. mean + 3 × SD) of the OD values of samples from PBS-mock control mice.

4.2.6. In vitro neutralisation assay

96-well tissue-culture plates were seeded with 6×10^4 MDCK cells/well. Live A/PR8 or A/Cal virus was diluted in allantoic fluid, and activated by treatment with 4 µg/ml TPCK-trypsin (Sigma-Aldrich) for 30 min at 37°C. Serum samples from vaccinated and control BALB/c mice were pooled for each vaccine group, and heat-inactivated (HI) for 30 min at 56°C. HI sera was then serially diluted in PBS, mixed with activated IAV in a 1:1 ratio, and incubated for 1 h at 37°C to allow binding. IAV + sera mixtures were then added to MDCK monolayers at a multiplicity of infection (MOI) of 0.1, and incubated for 2 h at 37°C + 5% CO_2. Monolayers were then washed with PBS to remove unbound

virus, and incubated for an additional 22 h in serum-free media. Monolayers then fixed for 15 min in ice-cold acetone/methanol (mixed in 1:1 ratio), and stained using polyclonal murine anti-A/PR8 or -A/Cal sera at 1:200 dilution (generated as previously described [425]) for 1 h at 4°C. Secondary antibody Alexa-Fluor488-conjugated goat anti-mouse IgG (H+L) (1:200 dilution, Life Technologies) was then added for 1 h at 4°C, and nuclei stained with DAPI (1 µg/ml in miliQ) for 30 min at room temperature. Fluorescence imaging was performed using a Nikon TiE inverted fluorescence microscope, and images analysed using NIS elements software (Tokyo, Japan).

4.2.7. Preparation of cell suspensions for flow cytometry

C57BL/6 mice were euthanised by CO_2 asphyxiation, and 0.5 ml of blood was immediately collected into 10 ml PBS via cardiac puncture. Mice were then perfused with 10 ml cold PBS through the right ventricle. Lungs were finely macerated in 1 ml pre-warmed digestion medium (DMEM (Gibco) supplemented with 5% FCS, 10 mM HEPES, 2.5 mM $CaCl_2$, 0.2 U/ml penicillin/gentamycin, 1 mg/ml collagenase IA (Sigma-Aldrich), and 30 U/ml DNase (Sigma-Aldrich)) and incubated at 37°C for 1 h, with mixing every 20 min. Single cell suspensions were filtered through 70 µm filters (BD). Spleen and mLN were harvested, and single cell suspensions prepared by mechanical disruption through a 70 µm filter. All tissue samples were incubated in red cell lysis buffer (155 mM NH_4Cl and 170 mM Tris-HCl (pH 7.65) combined in 9:1 ratio, and pH adjusted to 7.2) for 5 min at 37°C. Samples were thoroughly washed in PBS and kept on ice. Cell counts were determined using a haemocytometer and Trypan blue exclusion.

4.2.8. Cell staining and flow cytometric analysis

Single cell suspensions were pelleted in 96-well U-bottom trays (400 rcf, 2 min) at 2 × 10^6 cells/well. Cells were resuspended in Near Infrared fixable dye (1:1000 dilution in PBS, BD) for 15 min at RT in the dark. All subsequent incubations were performed at 4°C. Cells were washed twice in FACS buffer (PBS + 1% BSA + 0.04% Sodium Azide), and blocked with murine γ-globulin (200 µg/ml in FACs buffer) for 10 min. Cells were stained with primary antibodies detailed in **Table 4.1** for 20 – 30 min. For intracellular cytokine staining, cells were first stimulated for 4 h with SIINFEKL peptide in restimulation medium (IMDM (Gibco) supplemented with 10% FCS, 1×

penicillin/streptomycin (Gibco), 1× Glutamax (Gibco), 54 pM β-mercaptoethanol (Sigma), 1 nM ionomycin (Life Technologies), GolgiStop (BD, 1/1500 dilution of stock) and 1 µg/ml SIINFEKL (InVivoGen)). Stimulated cells were then washed twice in PBS before viability staining and incubation with primary antibodies against surface antigens as above. Cells were then permeabilised in BD CytoFix/CytoPerm (BD) for 20 min. Cells washed in Permwash (BD) and stained with a cocktail of antibodies against intracellular cytokines as per **Table 4.1** for 20 min. Cells were then washed in Permwash (BD), followed by a PBS + 0.04% Sodium Azide wash prior to resuspension in 1% PFA. Acquisition of all samples was performed on the BD LSRFortessa X-20 flow cytometer.

4.2.8. Flow cytometry to assess interaction of vaccine components

All buffers were 0.2 µm filter sterilised prior to use. γ-PN(ΔPsaA) was diluted to 5×10^8 CFU equivalent/ml in sterile PBS. Increasing amounts of γ-Flu were added to diluted γ-PN(ΔPsaA) suspensions, ranging from $2 \times 10^5 – 5 \times 10^7$ $TCID_{50}$ equivalent/ml. As a control, γ-PN(ΔPsaA) was also mixed with increasing amounts of allantoic fluid (AF) only. Mixtures were incubated for 30 min at 37°C + 5% CO_2, then spun at 10,000 g for 3 min (to pellet pneumococci but not free virions), and pellets were washed in sterile PBS. Mixtures were then plated in a 96-well U-bottom tray at 5×10^7 CFU equivalent/well, and spun at 3,750 rpm for 10 min. Pellets were then resuspended in 50 µl polyclonal murine anti-A/PR8 sera diluted 1:200 in PBS + 1% BSA (generated as described in [425]), and incubated on ice for 45 min. Wells were then topped up to 200 µl in PBS, and cells washed 3× in PBS. Pellets then resuspended in 50 µl goat anti-mouse IgG (H+L) (AlexaFluor488 conjugated, Life Technologies) diluted 1:500 in PBS + 1% BSA. Plates were incubated on ice for 45 min, and cells were washed 3× in PBS, then resuspended in 200 µl 2% PFA for acquisition on the Accuri flow cytometer. A minimum of 10,000 events were acquired per sample.

4.2.9. Transmission Electron Microscopy

γ-Flu-OVA and γ-PN(ΔPsaA) preparations were mixed in 0.2 µm filter sterilised PBS (3×10^5 $TCID_{50}$ equivalent γ-Flu-OVA added to 10^8 CFU equivalent γ-PN(ΔPsaA)), and incubated for 30 min on ice. Mixtures were then washed twice in PBS by spinning at

10,000 g for 3 min. Pellets were resuspended in PBS and loaded into 3 mm formvar-amorphous carbon-coated copper grids and left for 2 min. Excess solution was removed by blotting with Whatman paper. Samples were stained with 2% Uranyl Acetate for 2 min, then blotted and left to dry at RT for 10 min before visualisation with FEI Tecnai G2 Spirit Transmission Electron Microscope (Adelaide Microscopy, University of Adelaide).

4.2.10. Focus forming assay

96-well tissue-culture plates were seeded with 6×10^4 MDCK cells/well. Live A/PR8 was diluted in allantoic fluid and activated by treatment with 4 μg/ml TPCK-trypsin (Sigma-Aldrich) for 30 min at 37°C. γ-PN(ΔPsaA) was serially diluted in PBS (ranging from 10^0 – 10^7 CFU equivalent/well of inactivated pneumococci), and mixed in a 1:1 ratio with activated A/PR8. After thorough mixing, suspensions incubated at 37°C for 30 min, then added to MDCK monolayers to give either 100 FFU/well of A/PR8, or A/PR8 MOI of 0.1. Cell monolayers were incubated with the virus + pneumococci mixtures for 2 h at 37°C to allow viral adhesion. Inoculum was then removed, and monolayers washed with PBS to remove unbound virus. Monolayers were incubated for an additional 22 h in serum-free media, and then washed, fixed and permeabilised with acetone/methanol, and stained for IAV infection as per *in vitro* neutralisation assay (*Section 4.2.6*).

4.2.11. Macrophage uptake assay

THP-1 cells (Sigma) were maintained in RPMI + 1% Penicillin/Streptomycin, 1% L-Glutamine, 10% FCS. Cells were seeded into 12-well plates at 5×10^5 cells/well, and differentiated into macrophage-like cells with 50 ng/ml PMA for 3 days. Media was then aspirated to remove non-adherent cells and replaced with fresh media (no PMA). Cells were rested for 36 h prior to use in assays. For assessment of antigen uptake, live and irradiated A/PR8 was diluted to 10^6 $TCID_{50}$/ml equivalent in RPMI, and mixed with 10^7 CFU/ml equivalent γ-PN(ΔPsaA) where appropriate. Suspensions were statically incubated at 37°C for 30 min, then added to washed THP-1 monolayers (1ml diluted antigen mixture per well). Monolayers were incubated with vaccine antigens for 3 h, then washed thoroughly with PBS. Cells were trypsinised for 10 min. RPMI + 10% FCS was added to neutralise trypsin, and cells were washed thoroughly in PBS prior to cell

counting and plating in 96-well trays at 40,000 cells/well. Cells were incubated with Near Infrared fixable dye (1:1000 dilution in PBS, BD), and Fc receptors were blocked with human sera (1:50 dilution in PBS + 1% BSA + 0.04% Sodium Azide). Cells were permeabilized using the BD CytoFix/CytoPerm Fixation/permeabilization Solution Kit according to the manufacturer's instructions, and stained for intracellular antigen with FITC-conjugated mouse anti-IAV nucleoprotein (ab20921, diluted 1:150 in BD PermWash) for 30 min on ice. Cells were washed, and resuspended in 1% PFA for acquisition on the BD LSRFortessa X-20 flow cytometer.

4.2.12. Statistical analysis

Quantitative results are expressed as mean ± SEM, to indicate the closeness of the data to the population means rather than variability within small sample size. Unpaired Student's *t*-test was used for comparison of data from two separate groups, One-way ANOVA used for comparison of data from 3 or more groups with a single variable, and two-way ANOVA was used to analyse data sets with multiple variables. Survival data was analysed using two-tailed Fisher's exact test. Statistical analyses were performed using GraphPad Prism 6, version 6.0d (GraphPad Software, La Jolla, CA, USA). *P* values < 0.05 (95% confidence) were considered statistically significant.

Table 4.1. Fluorophore conjugated anti-murine antibody panels.

Circulating Memory T-cell subsets *Used for Day 7, 14 & 21 blood samples, and day 21 spleen and mLN samples.*				
Antigen	**Fluorophore**	**Supplier**	**Clone**	**Final conc.**
CD8	BUV395	BD	53-6.7	0.67 μg/ml
CD44	FITC	BD	IM7	0.67 μg/ml
CD45.1	BV421	BD	A20	0.67 μg/ml
CD127	PECy7	eBioscience	A7R34	0.83 μg/ml
KLRG1	APC	eBioscience	2F1	0.83 μg/ml
CX3CR1	PE	Biolegend	SA011F11	0.67 μg/ml
CD27	BUV711	BD	LG.3A10	0.67 μg/ml

Intracellular Cytokine Staining *Used for day 21 lung samples after 4 h ex vivo stimulation with SIINFEKL.*				
Antigen	**Fluorophore**	**Supplier**	**Clone**	**Final conc.**
CD8	BUV395	BD	53-6.7	0.67 μg/ml
CD45.1	PE	BD	A20	0.67 μg/ml
CD44	BV450	BD	IM7	0.67 μg/ml
IFN-γ	PECy7	eBioscience	XMG1.2	0.67 μg/ml
Gzmβ	Alexa647	Biolegend	GB11	5 μl/reaction
TNF-α	FITC	eBioscience	MP6-XT22	3.33 μg/ml
IL-17	BUV711	Biolegend	TC11.18H10.1	1.11 μg/ml

Tissue Resident Memory cells *Used for day 21 lung samples.*				
Antigen	**Fluorophore**	**Supplier**	**Clone**	**Final conc.**
CD4	BUV395	BD	GK1.5	0.67 μg/ml
CD8	BUV737	BD	53-6.7	0.67 μg/ml
CD45.1	FITC	BD	A20	0.67 μg/ml
CD69	PECy7	BD	H1.2F3	0.67 μg/ml
CD103	PE	eBioscience	2E7	1.67 μg/ml
CD11a	Biotin	BD	HL111	2.5 μg/ml
CD44	BV450	BD	IM7	0.67 μg/ml
Biotin	Alexa647	Biolegend	-	1.67 μg/ml

Live/dead stain (eFluor780 conjugate, BD, 1:1000 dilution) used for all panels.

4.3. RESULTS

4.3.1. Homotypic protection following intranasal co-vaccination with γ-Flu and γ-PN(ΔPsaA)

Prior study has demonstrated that combining γ-Flu with a previous version of the irradiated pneumococcal vaccine (γ-PN) does not affect IAV-specific homotypic protection [403]. To ensure this is maintained when γ-Flu is mixed with the further attenuated γ-PN(ΔPsaA) (generated in Chapter 3), γ-Flu only and γ-Flu + γ-PN(ΔPsaA) co-vaccinated mice were challenged IN with the homotypic vaccine strain A/PR8. As illustrated in **Figure 4.1,** γ-Flu alone conferred complete protection against this challenge type, with 100% survival and no measurable weight loss over the entire monitoring period. Combining γ-Flu with γ-PN(ΔPsaA) did not interfere with this homotypic protection, as co-vaccinated mice also showed 100% survival with no weight loss. This is in comparison to PBS-mock vaccinated control mice, which were euthanized due to excessive weight loss (≥ 20% of starting weight) by day 6 post-challenge. Additionally, vaccination with γ-PN(ΔPsaA) alone did not offer any protection against IAV challenge. This indicates immune responses induced by γ-PN(ΔPsaA) have no cross-reactivity against live IAV. Thus, vaccination with γ-PN(ΔPsaA) alone was excluded from future challenge experiments to minimize animal usage.

4.3.2. Significantly enhanced protection against drifted and heterosubtypic IAV challenges following co-administration of γ-Flu and γ-PN(ΔPsaA)

As homotypic protection was illustrated following vaccination with γ-Flu alone and γ-Flu + γ-PN(ΔPsaA), subsequent investigation focussed on testing more diverse IAV challenge models, including drifted and heterosubtypic strains. Thus, vaccinated and control mice were challenged IN with either the pandemic H1N1 strain A/California (drifted strain), or the H3N2 strain A/PC (heterosubtypic strain). Data shown in **Figure 4.2A** illustrates vaccination with γ-Flu alone or γ-Flu + γ-PN(ΔPsaA) confers 100% protection against a drifted pdmH1N1 challenge. This is in comparison to the control group, where the majority of mice succumbed to infection by day 8 post-challenge. In contrast to the homotypic challenge however, some weight loss was also detected prior to recovery in the vaccinated groups (**Fig. 4.2B**). Both γ-Flu-vaccinated and co-

vaccinated mice lost approximately 10% of their starting weight prior to complete recovery. This is likely due to the drifted surface antigens presented by the recent pdmH1N1 clinical isolate, causing reduced neutralisation by vaccine-induced antibody responses. Interestingly, the mice vaccinated with γ-Flu + γ-PN(ΔPsaA) recovered faster, with significantly reduced total weight loss from day 6 onwards in comparison to mice vaccinated with γ-Flu alone. Co-vaccinated mice also returned to their starting weight by day 8 post-challenge, whilst γ-Flu-only vaccinated mice remained approximately 5% below their starting weight at this time point.

Heterosubtypic challenge of γ-Flu-vaccinated and co-vaccinated mice further amplified these differences in vaccine performance. It is important to note that the IAV challenge dose utilised here was intentionally higher than doses used in previous publications to maximise detectable differences. As a result, γ-Flu alone conferred only 60% protection against heterosubtypic challenge (**Fig. 4.3A**). In contrast, the co-administration of γ-Flu with γ-PN(ΔPsaA) continued to confer 100% protection, and the weight loss of co-vaccinated mice was again significantly reduced in comparison to mice vaccinated with γ-Flu alone (**Fig. 4.3B**). Co-vaccinated mice also began to recover weight a mere 4 days post-challenge, indicating the induction of robust immune responses for effective control of the severe IAV challenge.

4.3.3. The impact of co-vaccination on IAV-specific humoral responses

Different arms of immunity were subsequently investigated for potential mechanisms underlying the enhanced protection observed following γ-Flu + γ-PN(ΔPsaA) co-administration. Initially, humoral responses were analysed using serum samples harvested from γ-Flu-vaccinated and co-vaccinated mice in *Section 4.4.1* (prior to challenge with A/PR8). As shown in **Figure 4.4**, co-administration of γ-Flu with γ-PN(ΔPsaA) was associated with reduced overall titres of IAV-specific IgG and IgA. The loss of total IgG titre was specifically due to decreases in the subclasses IgG1, IgG2a, and IgG3, whilst IgG2b titres appeared to be unaffected by co-administration of γ-Flu with γ-PN(ΔPsaA) (**Fig. 4.5**). Also, mice vaccinated with γ-PN(ΔPsaA) alone showed no detectable IAV-specific antibodies above background levels. This drop in antibody titre

for co-vaccinated animals was unexpected, as homotypic protection – known to be primarily antibody mediated – was entirely maintained for γ-Flu-vaccinated and co-vaccinated groups. Thus, *in vitro* neutralisation assays were conducted to assess the functionality of vaccine-induced antibody responses. Sera samples from γ-Flu-vaccinated and co-vaccinated mice, or PBS-mock controls were incubated with a fixed titre of live A/PR8 virus prior to infection of MDCK monolayers. As shown in **Figure 4.6A,** sera from γ-Flu-vaccinated and co-vaccinated mice were equivalent in their ability to neutralise A/PR8 infection, despite the overall reduced titres in serum from co-vaccinated animals. Complete neutralisation of A/PR8 infection was observed at the lower sera dilutions (1:10), and infection began to return as immune sera was titrated out (1:160 onwards). At the 1:160 dilution, FITC fluorescence, which indicates A/PR8 infection, was quantified to enable statistical analysis. Significant reduction in FITC fluorescence was observed following treatment of live A/PR8 with sera from γ-Flu-vaccinated and co-vaccinated mice (**Fig. 4.6B**). This is in comparison to control sera from PBS-mock vaccinated mice. It is important to note that PBS-mock sera had no impact on viral infectivity, as illustrated by the representative images and quantified FITC fluorescence showing IAV infection levels comparable to the virus only control. Hence, neutralisation of infection seen with the immune sera groups was IAV-specific, rather than a non-specific consequence of incubation with murine sera. Importantly, there was no detectable difference in FITC fluorescence between the two vaccine sera groups, indicating equivalent neutralisation efficacy.

Efficacy of immune sera to mediate cross-neutralisation of live IAV was subsequently investigated. Sera harvested from vaccinated and control groups was incubated with a fixed titre of drifted pdmH1N1 prior to infection of MDCK monolayers. Interestingly, fluorescent imaging of monolayers showed that neither immune sera nor control sera had any neutralising activity against this drifted IAV strain. Representative images show equivalent levels of infection across all sera groups at all tested dilutions in comparison to the virus only control (**Fig. 4.7A**), and quantification of FITC fluorescence confirmed the absence of neutralising activity (**Fig. 4.7B**). Lack of cross-neutralisation of drifted H1N1 was expected, as constant antigenic drift is known to allow IAV to escape vaccine-induced humoral immunity [113]. Thus, the minimised clinical symptoms of co-

vaccinated mice after pdmH1N1 challenge is likely due to augmented T-cell immunity, rather than antibody responses.

4.3.4. Minimal impact of co-vaccination on circulating IAV-specific T-cell responses

$CD8^+$ T cell responses are crucial for cross-protection against influenza A infection. To explore whether co-administration altered cell-mediated immune mechanisms, the OT-I system was utilised. OT-I cells were adoptively transferred to naïve C57BL/6 mice, followed by intranasal vaccination with irradiated A/PR8-OVA (γ-Flu-OVA) alone, or γ-Flu-OVA co-administered with γ-PN(ΔPsaA). Subsequent harvesting and analysis of OT-I cells would then allow examination of IAV-specific T-cell responses despite simultaneous administration of non-IAV vaccine components. Initially, peripheral blood was harvested from vaccinated and control mice on days 7, 14 and 21 post-vaccination, as well as the spleen and mLN on Day 21. Significantly enhanced frequencies of activated OT-I cells ($CD8^+CD45.1^+CD44^{hi}$) were detected in these tissues for mice receiving γ-Flu-OVA alone and γ-Flu-OVA + γ-PN(ΔPsaA) in comparison to PBS-mock controls. This indicates robust induction of IAV-specific cell-mediated responses after a single non-adjuvanted intranasal vaccination. Furthermore, IAV-specific responses circulating in peripheral blood at days 7 and 14 post-vaccination were comparable between γ-Flu-OVA-vaccinated and co-vaccinated groups (**Fig. 4.8A**). A slight decrease in the frequency of activated OT-I cells in the blood of co-vaccinated mice was detected on day 7 in comparison to those receiving γ-Flu-OVA alone, however this did not reach statistical significance, and the difference was no longer present by day 14. The peak frequency of activated cells in peripheral blood was detected on day 7 post-vaccination, corresponding to the expansion phase of the primary T-cell response. Frequency was substantially less by day 14, and no OT-I cells at all were detected by day 21 in any group, consistent with contraction of the T-cell population.

The magnitude of IAV-specific T-cell responses were also comparable in the mLN for γ-Flu-OVA-vaccinated and co-vaccinated groups. The frequency of activated OT-I cells for both vaccine groups were significantly elevated in this tissue above PBS-mock control levels (**Fig. 4.8B**). Total cell number was also substantially increased for both vaccine groups, however the difference between γ-Flu-OVA alone and PBS-mock controls did

not quite statistical significance (P = 0.0735 by One-Way ANOVA). In the spleen, both the frequency and the total number of activated OT-I cells were again significantly elevated above controls for each vaccine group. However, co-administration of γ-Flu-OVA with γ-PN(ΔPsaA) appeared to reduce the frequency and total number of activated OT-I cells in comparison to mice receiving γ-Flu-OVA alone (**Fig. 4.8C**). Despite this, profiles for the memory T-cell subsets central memory (T_{CM}), peripheral memory (T_{PM}), and effector memory (T_{EM}) present in the spleen were comparable between both vaccine groups (**Fig. 4.9B**). Similar profiles for these T-cell subsets were also observed in the mLN at day 21, and in peripheral blood samples at days 7 and 14 (**Fig. 4.9A**). A small but significant decrease in the frequency of T_{EM} cells was detected in the blood of co-vaccinated mice at day 14 relative to those receiving γ-Flu-OVA alone. This trend was also apparent in the spleen on day 21, though did not reach statistical significance.

4.3.5. Enhanced population of IAV-specific CD8⁺ T-cells in the lungs of co-vaccinated mice

Given that circulating memory T-cell responses in blood and secondary lymphoid organs were not overly affected by co-vaccination, the elevated protection against drifted and heterosubtypic IAV challenge may be related to lung-specific responses. To address this, OT-I cells were transferred IV to mice, followed by a single intranasal vaccination 24 h later. Lungs were then harvested and processed for flow cytometry analysis on day 21 post-vaccination. In this tissue, a significant increase in the total number of activated OT-I cells was detected for co-vaccinated mice compared to those receiving γ-Flu-OVA alone (**Fig. 4.10A**). Thus, whilst circulating T-cell responses were relatively unaltered, the magnitude of response at the site of pathogen encounter was markedly greater following co-vaccination. Lung suspensions were also stimulated *ex vivo* with the OVA peptide SIINFEKL to assess functionality and cytokine production of activated OT-I cells. As shown in **Figure 4.10B,** OT-I cells from γ-Flu-OVA-vaccinated and co-vaccinated mice were equivalent in terms of their ability to produce inflammatory cytokines IL-17, Gzmβ, TNF-α, and IFN-γ in response to stimulation with cognate antigen. The co-vaccinated group tended to have slightly lower frequencies of cells producing these cytokines, however no statistical differences were detected. Furthermore, the mean fluorescence intensity (MFI) for each of these cytokines was comparable between vaccine groups (**Fig.**

4.10C). Thus, activated T-cells from γ-Flu-OVA-vaccinated and co-vaccinated mice appear functionally equivalent, with the co-administration of γ-Flu-OVA and γ-PN(ΔPsaA) resulting in a larger bulk population of OT-I cells residing in the lung.

4.3.6. Lung Tissue Resident Memory cells (T_{RM}) are enhanced by co-vaccination

In addition to the circulating memory $CD8^+$ T-cell subsets mentioned in *Section 4.3.4*, studies have identified a highly specialized subset of tissue-resident memory cells (T_{RM}), which are retained for extended periods of time in nonlymphoid tissues including the skin, gut, and lung [500-503]. As T_{RM} are permanently positioned at sites of pathogen entry, they are superior to circulating memory T-cells for provision of rapid protection against a variety of infections. Given the enhanced number of activated OT-I cells detected in the lungs of co-vaccinated mice, it was of interest to determine whether these cells also displayed a T_{RM} phenotype. Following IV transfer of OT-I cells and IN vaccination with γ-Flu-OVA or γ-Flu-OVA + γ-PN(ΔPsaA), lungs were harvested and processed for analysis of T_{RM} populations by flow cytometry. Both transferred $CD45.1^+$ OT-I cells and endogenous $CD45.1^-$ T-cells were classified based on their surface expression of established T_{RM} markers CD69 and CD103 [504]. Gating on these key markers is shown by representative plots in **Figure 4.11A.**

Remarkably, quantification of OT-I-derived T_{RM} demonstrated a significant enhancement of this cell population in the lungs of co-vaccinated mice in comparison to those vaccinated with γ-Flu-OVA alone (**Fig. 4.11B**). Note that no OT-I cells were detected at day 21 post-vaccination in the lungs of PBS-mock control mice, hence no comparison to this group was possible. Given the enhancement in the total number of OT-I cells in the lungs of co-vaccinated animals (**Fig. 4.10A**), it was expected that there would be a similar increase in total cell number for individual OT-I cell subsets. The frequency of OT-I T_{RM} cells was also significantly elevated in co-vaccinated mice, hence data indicates that on a single cell basis, $CD8^+$ T-cells are more likely to convert to a T_{RM} phenotype in the lung microenvironment of co-vaccinated animals.

Enhancement of total T_{RM} populations was also observed for endogenous $CD8^+$ and $CD4^+$ T-cells following co-vaccination. In both instances, the T_{RM} populations were

significantly larger in co-vaccinated mice compared to those seen in PBS-mock controls (**Fig. 4.11C**). Importantly, there was an obvious trend for the co-vaccinated mice to have a larger population of T_{RM} cells compared to those receiving γ-Flu-OVA alone. This difference between vaccine groups was significant for $CD4^+$ T-cells, but did not reach significance for the $CD8^+$ population ($P = 0.08$ by One-Way ANOVA), despite the obvious increase in cell number. As endogenous cells were analysed here, it was not possible to determine antigen specificity. Thus, it is likely that administration of both viral and bacterial vaccine antigens resulted in induction of multiple populations of T_{RM} cells, leading to a larger cell population overall compared to that generated after administration of a single antigen.

4.3.7. Whole inactivated IAV and pneumococcal vaccine components directly associate in suspension

Altered recognition of γ-Flu vaccine antigens when co-administered with γ-PN(ΔPsaA) was considered as a potential mechanism contributing to the augmented T-cell responses seen in the lung. Flow cytometry was therefore used to assess any direct interaction between the whole inactivated IAV and pneumococcal vaccine components when mixed prior to administration. In this assay, γ-PN(ΔPsaA) was incubated alone or with increasing amounts of γ-Flu, prior centrifugation using speeds that would pellet pneumococci but not free virions. Thus, the presence of γ-Flu virions in the pellets would indicate a direct interaction between IAV and the pneumococci, allowing co-sedimentation of the substantially smaller IAV virions during low-speed centrifugation. After extensive washing in PBS, cell pellets were treated with murine antibody raised against A/PR8, and a FITC-conjugated anti-mouse secondary antibody. Flow cytometry was used to quantify the percentage of pneumococci in each sample that were positive for IAV-specific fluorescence. As illustrated in **Figure 4.12A**, irradiated pneumococci alone (grey histogram) treated with primary and secondary antibodies had minimal background for IAV-specific fluorescence. In contrast, incubation of pneumococci with γ-Flu prior to addition of antibodies resulted in a steady increase in the amount of FITC signal detected by flow cytometry (**Fig. 4.12A** and **4.12B**). This phenomena was dose-dependent, and at the highest concentration of γ-Flu tested, almost 80% of all

pneumococci within suspension showed a shift in FITC signal, indicating binding of γ-Flu to γ-PN(ΔPsaA).

Transmission electron microscopy also supported the notion of a direct interaction between the whole inactivated vaccine components. Here, γ-Flu-OVA was utilised, and mixed with γ-PN(ΔPsaA) at the same ratio as was used in previous OT-I transfer experiments. Again, mixtures were washed extensively in PBS using speeds that pellet pneumococci but not free virions. Negative staining allowed visualisation of both IAV virions and pneumococcal cells. As shown in **Figure 4.12C,** multiple inactivated IAV virions appear to be directly bound to the surface of single inactivated pneumococci.

4.3.8. Combining live IAV or irradiated IAV with γ-PN(ΔPsaA) is associated with enhanced viral uptake by epithelial and immune cell lines

The direct interaction between γ-Flu and γ-PN(ΔPsaA) was likely to have an impact on the uptake and subsequent processing of IAV virions by host cells. To address this, the effect of γ-PN(ΔPsaA) on the ability of live IAV to infect epithelial cells *in vitro* was assessed. A fixed MOI of live A/PR8 was mixed with increasing amounts of irradiated pneumococci, then added to epithelial cell monolayers for 2 h to allow viral adherence. The inoculum was thoroughly washed, and cells were incubated for an additional 22 h to allow bound virus to replicate. Compared to cells incubated with live IAV alone, the level of IAV infection appears to be influenced by the concentration of γ-PN(ΔPsaA). Specifically, the presence of high concentrations of γ-PN(ΔPsaA) resulted in significantly enhanced viral infection compared to virus only controls (**Fig. 4.13A**). Similar to flow cytometry data in **Figure 4.12B**, the effect of adding γ-PN(ΔPsaA) to live IAV was dose-dependent. Lower concentrations of γ-PN(ΔPsaA), e.g. 10^1 and 10^2 CFU equivalent per well, appeared to decrease IAV infection slightly, though no significance was determined by One-way ANOVA. Potentially, lower γ-PN(ΔPsaA) concentrations caused multiple IAV virions to collect around a single pneumococcal cell, resulting in infection of a single mammalian cell with multiple virions due to close proximity. At higher concentrations, IAV virions are likely to be more dispersed. From 10^4 CFU/well onwards, addition of more pneumococci caused progressively more IAV infection, until the total number of

FFU/well was significantly higher than the virus only control. At this high CFU concentration, individual pneumococci are likely to be associated with a small number of virions only, and the substantially larger pneumococci may then allow the bound virions to settle more rapidly onto mammalian cells for faster binding and viral internalisation. This is supported by representative fluorescence images in **Figure 4.13B**. Here. IAV was added to cell monolayers at the same MOI of 0.1, however pre-incubation of IAV with γ-PN(ΔPsaA) resulted in considerably more dispersed infection.

Next, the influence of γ-PN(ΔPsaA) on uptake of IAV virions by an immune cell type was investigated. Macrophage-like THP-1 cells were incubated with γ-Flu only, γ-PN(ΔPsaA) only, or a mixture of the two. Macrophages were then washed to remove free antigen. γ-Flu internalisation by these phagocytic cells was quantified by intracellular staining with a FITC-conjugated anti-IAV nucleoprotein (NP) antibody, followed by flow cytometry. **Figure 4.14A** shows that macrophages incubated with γ-Flu alone and the γ-Flu + γ-PN(ΔPsaA) mixture had a positive shift in FITC fluorescence in comparison to macrophages incubated with media only (no antigen, grey histogram). Also, incubation with γ-PN(ΔPsaA) alone showed no shift whatsoever when compared to the no antigen control, indicating the detected shift in FITC fluorescence for macrophages incubated with γ-Flu or γ-Flu + γ-PN(ΔPsaA) was IAV specific. Subsequently, we tested whether γ-PN(ΔPsaA) could enhance uptake of live IAV as well as irradiated virions. Again, macrophage-like THP-1 cells were incubated with IAV alone (either live or γ-irradiated), or IAV pre-incubated with γ-PN(ΔPsaA). Again, we detected an increase in FITC fluorescence for both single and combination antigen mixtures when compared to the no antigen control. The fold increase in NP^+ cells was quantified for each antigen type, and data demonstrates that pre-incubation with γ-PN(ΔPsaA) significantly enhances the uptake of both live and irradiated IAV by macrophages (**Fig. 4.14B(i)**). Quantification of the total number of live NP^+ cells confirmed this trend (**Fig. 4.14B(ii)**).

4.4. DISCUSSION

IAV and *S. pneumoniae* are two of the world's foremost respiratory pathogens, collectively causing millions of deaths every year. IAV and *S. pneumoniae* also exhibit lethal synergism, and strategies to avoid both sequential and simultaneous infection with both of these pathogens remain unsuccessful. In fact, current inactivated IAV vaccines are limited to induction of strain-specific antibody responses, with requirement for annual reformulation and redistribution to ensure coverage of seasonal strains. The time required to generate strain specific vaccines is approximately six months [505], which is too long in the event of a sudden pandemic to protect against the first wave of infection. In addition, current *S. pneumoniae* vaccines are similarly limited with respect to overall coverage of pneumococcal serotypes. The increasing potential for a widespread avian influenza pandemic paired with ongoing emergence of antibiotic resistant *S. pneumoniae* isolates makes the need for new broad-spectrum vaccines considerably more urgent [135].

This study demonstrates the immense value of utilising both the known and novel aspects of the synergism between IAV and *S. pneumoniae*, and applying them to vaccine development. Previously, the whole gamma-irradiated IAV (γ-Flu) and pneumococcal (γ-PN) vaccines have been shown to provide strain- and serotype-independent protection respectively when administered individually [361, 362, 235]. Prior publication by our lab has also demonstrated that potent IFN-I responses and lymphocyte activation are induced by γ-Flu [350], which allow it to act as an effective adjuvant for co-administered viral vaccines [399]. Co-administration of γ-Flu with γ-PN was subsequently shown to have a similar adjuvant effect on pneumococcal-specific responses, with enhancement of γ-PN-specific antibody titres and protective IL-17 production [403]. We postulated this enhancement to be similarly mediated by IFN-I induction by the co-administered γ-Flu vaccine. Remarkably, data presented here (using the further attenuated γ-PN(ΔPsaA) generated in Chapter 3) demonstrates that γ-Flu-specific responses are also improved by mucosal co-administration. This bi-directional enhancement of responses was not at all anticipated, and data presented here could revolutionise the design of next generation combination vaccines.

We observed that co-administration of γ-Flu with γ-PN(ΔPsaA) significantly increased protection against both drifted (**Fig. 4.2**) and heterosubtypic IAV challenges (**Fig. 4.3**). In fact, γ-Flu + γ-PN(ΔPsaA) conferred 100% survival against all IAV challenge strains tested in this study. Reduced clinical weight loss was also observed for co-vaccinated mice compared to those receiving γ-Flu alone, indicating a broader reactivity of immune responses in these animals. Considering that presentation of drifted surface antigens by emerging seasonal isolates is the main mechanism by which IAV escapes vaccine-induced immunity, our co-vaccination strategy could enhance cross-reactivity of IAV-specific immunity.

Interestingly, analysis of humoral immune responses revealed that co-administration was associated with a reduction in IAV-specific IgG and IgA titres (**Fig 4.4** and **Fig. 4.5**). A similar effect on antibody titres was reported previously by Desheva *et al*. when investigating an alternative IAV + *Streptococcus* combination vaccine [506]. Their formulation contained live attenuated IAV (H7N3) mixed with recombinant polypeptides from Group B *Streptococcus* (GBS vaccine), and was administered intranasally. The authors observed significantly reduced H7N3-specific IgG titres in serum after a single dose of IAV + GBS vaccine, which is very similar to data presented here. However, data suggests the effect of co-administered bacterial antigens on IAV-specific antibodies is not dependent on the overall structure, given the same trend was observed for both protein components and whole-cell pneumococci. Following a booster vaccination, Desheva *et al.* also reported that antibody titres from mice given the IAV vaccine alone or in combination with GBS were more comparable, with titres from the combination-vaccinated mice actually being the higher of the two. This is consistent with work previously published by Babb *et al.* [403], demonstrating comparable IgG and IgA following two doses of either γ-Flu alone or γ-Flu co-administered with the original γ-PN vaccine [506].

Importantly, Desheva *et al*. demonstrated that the decrease in antibody titre after a single dose of their vaccine mixture was associated with reduced virus neutralization [506]. In contrast, despite the decrease in total antibody shown by my data, serum from γ-Flu-vaccinated and γ-Flu + γ-PN(ΔPsaA) co-vaccinated mice showed equivalent

neutralization efficacy *in vitro* (**Fig. 4.6**). This indicates that antibody quality is entirely maintained in co-vaccinated mice despite differences in the bulk quantity. Humoral responses induced by co-vaccination were also sufficient to confer complete homotypic protection *in vivo* (**Fig. 4.1**). Alteration to the ratio of IgG1/IgG2a and/or other subclasses shown in **Figure 4.5B** may reduce the competition for binding, and allow antibodies at a lower concentration but with higher affinity to effectively bind and neutralise free virions. Alternatively, IgG2b may be the primary subclass responsible for A/PR8 neutralisation. Consequently, equivalent IgG2b levels between vaccine groups would justify the similarity in viral neutralisation and *in vivo* homotypic protection. Overall, despite the reduced antibody titre, co-vaccinated mice showed 100% protection against homotypic challenge, and immune sera from these mice showed comparable neutralisation efficacy to that seen for the γ-Flu vaccinated group. In contrast, protection against drifted IAV challenge may not be associated with neutralising antibody responses. In fact, data presented in **Figure 4.7** shows no cross-neutralising activity of serum from γ-Flu-vaccinated or co-vaccinated mice against the drifted pdmH1N1 strain. Therefore, data indicates that the enhancement of protection against drifted and heterosubtypic IAV observed in co-vaccinated animals is primarily due to cell mediated immunity. Prior publication by our group has demonstrated that γ-Flu-induced cross-protection is mainly dependent on cytotoxic T-cell responses [362]. Live H7N9 challenge studies in mice have also shown cross-reactive memory T-cell responses, rather than neutralising antibodies, are responsible for reduced mortality following secondary challenge [507].

Data presented here indicates co-vaccination with γ-Flu and γ-PN(ΔPsaA) does enhance the magnitude of IAV-specific T-cell responses specifically at the site of pathogen re-encounter. The use of OT-I cells and an irradiated A/PR8-OVA vaccine preparation (γ-Flu-OVA) effectively demonstrated the population of IAV-specific T-cells in the lung to be greater in co-vaccinated mice compared to animals receiving γ-Flu-OVA alone (**Fig. 4.10B**). However, activated OT-I cells detected in the spleen of co-vaccinated mice at the same time point were substantially decreased (**Fig. 4.8C**). Thus, it is unlikely that the total activation of transferred OT-I cells is greater in either vaccine group, but the subsequent trafficking of activated cells to the lung is likely to be augmented by co-vaccination. This could be due to differences in the cytokine milieu of the lung

microenvironment after co-vaccination, or increased longevity of a mild inflammatory state within the lung after administration of multiple vaccine components. In addition, a higher frequency of activated OT-I cells isolated from the lung showed a T_{RM} phenotype in co-vaccinated mice (**Fig. 4.11B**). This may also be due to differences in the lung cytokine milieu after co-vaccination. Initial 'programming' events that occur during the priming phase in local draining lymph nodes, and upon entry into inflamed tissues greatly influence the phenotypic specialization and longevity of memory T-cell pools [508]. Local conversion of lung-resident T_{RM} is reported to require a variety of tissue-derived factors, including transforming growth factor-β (TGF-β), interleukin-15 (IL-15), tumour necrosis factor (TNF), and IL-33 [509, 500, 510, 511]. TNF is reported to be induced in the lung following intranasal *S. pneumoniae* infection [512], and low pneumococcal carriage density causes sustained elevation of nasopharyngeal TGF-β1 [513]. Thus, the presence of high densities of inactivated pneumococci at the time of γ-Flu vaccination is likely to dramatically alter the profile of cytokines within the lung. Characterising the cytokine milieu in the lung and the draining mediastinal lymph node immediately after vaccination will be an important area to address in follow-up studies. Nonetheless, co-vaccination may in fact augment memory T-cell populations by influencing both trafficking/recruitment of $CD8^+$ T-cells to the lung, and subsequent cytokine-induced differentiation to T_{RM}.

Alternatively, interactions with other lymphocytes may be the primary mechanism for the observed enhancement of IAV-specific T-cell populations in the lung. Multiple immune cells are known to interact with $CD8^+$ T-cells in the lymph nodes and the lung in a highly orchestrated manner to ensure efficient trafficking, differentiation and maintenance. For example, $CD4^+$ T-cells and the associated IFN-γ have both been shown to facilitate the entry of $CD8^+$ T-cells into tissues such as the skin, vaginal mucosa, and the lung epithelium [514-516]. After IAV infection specifically, $CD4^+$ T-cells are required for expression of trafficking molecule CXC-chemokine receptor 3 (CXCR3) by $CD8^+$ T-cells, and for CD103 expression to aid T_{RM} formation [515]. Interestingly, previously published work from our lab has demonstrated that total $CD4^+$ T-cells, and IFN-γ^+ $CD4^+$ T-cells were significantly enhanced in the lungs of γ-Flu + γ-PN co-vaccinated mice in comparison to those receiving γ-Flu alone following a pneumococcal

challenge [403]. We expect a similar enhancement in $CD4^+$ T-cell populations following co-immunisation with γ-Flu and γ-PN(ΔPsaA), and it will be immense interest to determine if this is associated with heightened expression of trafficking and adhesion molecules on circulating $CD8^+$ T-cells. IFN-γ is also known to be induced in the lungs 24 h post-*S. pneumoniae* challenge [512]. It will be important to investigate whether γ-PN(ΔPsaA) could induce IFN-γ to some degree when co-administered with γ-Flu, to further aid entry of circulating $CD8^+$ T cells into the lung tissue.

Regardless of the mechanism, increased populations of lung T_{RM} are beneficial for a multitude of reasons. $CD8^+$ memory T-cells populating the lung mucosae are critical for heterosubtypic immunity against IAV [517], and for immune defence against secondary encounters with respiratory viruses in general [518]. Upon antigen contact, activated T_{RM} cells will orchestrate circulating memory T-cell responses, drive maturation of DCs, and rapidly induce a tissue-wide antiviral state via secretion of key cytokines to minimize viral replication [519-521]. Viral load and the duration of infection is therefore minimised, as is the ensuing tissue damage due to viral replication. Furthermore, the reduction in initial viral load will limit the degree of subsequent immune activation, thus limiting immunopathology and disease symptoms [522]. Thus, the enhanced T_{RM} population in co-vaccinated mice is expected to contribute greatly to the rapid recovery and heightened survival rates observed against lethal drifted and heterosubtypic IAV challenges. A follow-up study could focus on the lung environment in γ-Flu-vaccinated and co-vaccinated mice at early time points post-challenge, to characterise the recall responses in each group and their efficacy in controlling infection.

Differential uptake of vaccine antigens may be an additional factor contributing to altered immune responses in co-vaccinated mice. My data demonstrates an enhancement in adhesion/uptake of live IAV by epithelial MDCK cells when pre-incubated with inactivated pneumococci (**Fig. 4.13**). In this setting, the substantially larger pneumococci may allow bound virions to settle more rapidly onto mammalian cells, facilitating faster binding and viral internalisation during the initial 2 h inoculation period. Pneumococcal neuraminidase has previously been shown to enhance IAV infection in MDCK and A549 cells [523]. Both NanA and NanB from *S. pneumoniae* were reported to complement the

cleavage function of viral NA to aid the release of newly synthesised virions and promote viral spread. This was observed after incubation of infected monolayers with recombinant pneumococcal neuraminidase for 48 h. However, in this study, inactivated pneumococci were present only for the first two hours of viral inoculation prior to removal of all pneumococci and free virions by extensive washing. This time frame is too short for release of progeny IAV virions (usually begins ~ 4 – 6 h after the initial infection of epithelial cells [524-526]). Thus, the brief presence of pneumococcal neuraminidase is unlikely to contribute to the enhanced viral infection observed. Rather, the inactivated pneumococci are likely to exert their effect at the initial stage of viral attachment. It is important to note that γ-PN(ΔPsaA) alone had no cytopathic effects on cell monolayers, even at the highest concentration tested (10^7 CFU equivalent/well). This is in contrast to the cytotoxicity observed by Walther *et al.* [523] when adding live *S. pneumoniae* and IAV to MDCK monolayers at low pneumococcal MOIs. Thus, the variation in IAV infection rate seen here was not caused by increased cell cytotoxicity due to addition of pneumococci.

Uptake of both live IAV and γ-Flu virions by macrophages *in vitro* was also enhanced when mixed with inactivated pneumococci (**Fig. 4.14**). Although DCs are the predominant APC participating in antigen uptake and stimulation of naive T-cells, peptide pulsed macrophages have been shown to induce proliferation and differentiation of naïve $CD8^+$ T-cells [527]. Additionally, cytokines produced by macrophages in response to antigen, including IFN-I, have been postulated to function in the activation of DCs [528]. Increased antigen uptake mediated by co-administration of γ-Flu with γ-PN(ΔPsaA) is therefore likely to increase innate immune stimulation *in vivo*, potentially enhancing naïve $CD8^+$ T-cell and DC activation. Chatziandreou *et al.* demonstrated that lymph node macrophages undergo necrosis-like death in response to UV-inactivated A/PR8 antigen, and in response to heat-killed *S. pneumoniae*. Importantly, macrophage death in the draining lymph node was associated with activation and relocation of $CD11b^+$ DCs [529]. Thus, uptake of both inactivated IAV and pneumococcal vaccine components could cause more macrophage death, leading to additional DC activation and trafficking.

Overall, the enhancement of viral uptake and augmentation of immune responses observed appear to be mediated by a direct interaction between the functionally intact, but inactivated, IAV and pneumococci vaccines. This interaction is illustrated in **Figure 4.12**. In the case of uptake by phagocytes, the direct binding of vaccine components is expected to cause uptake of the entire IAV-pneumococcal complex. This would dramatically alter the production of inflammatory cytokines by these cells, due to the presence of both viral and bacterial PAMPs and subsequent TLR signalling. Further investigation into the cytokine milieu in the lung, and the complex interplay between phagocytes and T-cells following co-administration of γ-Flu and γ-PN(ΔPsaA) *in vivo* will be the focus of future studies. Furthermore, the mechanism of direct interaction between IAV and the pneumococcus is yet to be elucidated, and will also be the focus of future investigation. In addition to IAV, animal models have shown synergistic interactions between *S. pneumoniae* and multiple other respiratory viruses, including RSV, parainfluenza viruses and human metapneumovirus [530-532]. Thorough investigation of the mechanisms permitting these interaction may shed light on disease progression during respiratory co-infections in general, and aid in development of new therapeutic options to mitigate the severity of symptoms. Crucially, the bacterial-viral interactions observed here should be applied to next-generation vaccine design to hijack the existing synergy of pathogens for superior immune stimulation and protection.

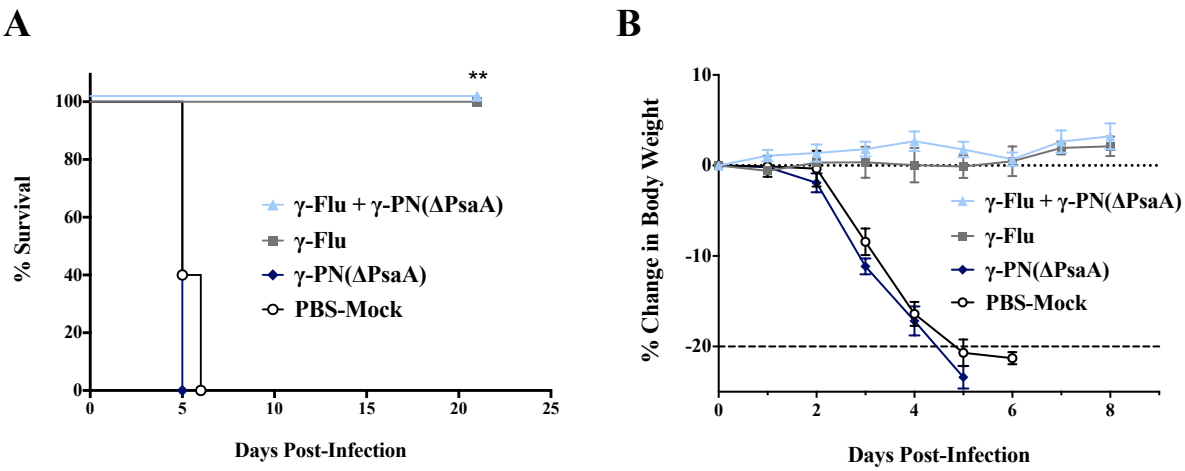

Figure 4.1. Protection against homotypic IAV challenge. Balb/c mice were vaccinated IN with γ-Flu alone or co-vaccinated with γ-Flu + γ-PN(ΔPsaA). Control mice received γ-PN(ΔPsaA) only, or were PBS-mock vaccinated. 21 days post-vaccination, all mice were challenged IN with lethal A/PR8. Mice were monitored for 3 weeks for development of clinical symptoms, and euthanized if they lost 20% of their body weight. Data presented as (A) overall survival percentages, and (B) mean weight loss ± SEM (n = 5) over the first 8 days post-challenge. Survival percentages were analysed using Fisher's Exact Test (**, $P < 0.01$, compared to PBS-Mock control group).

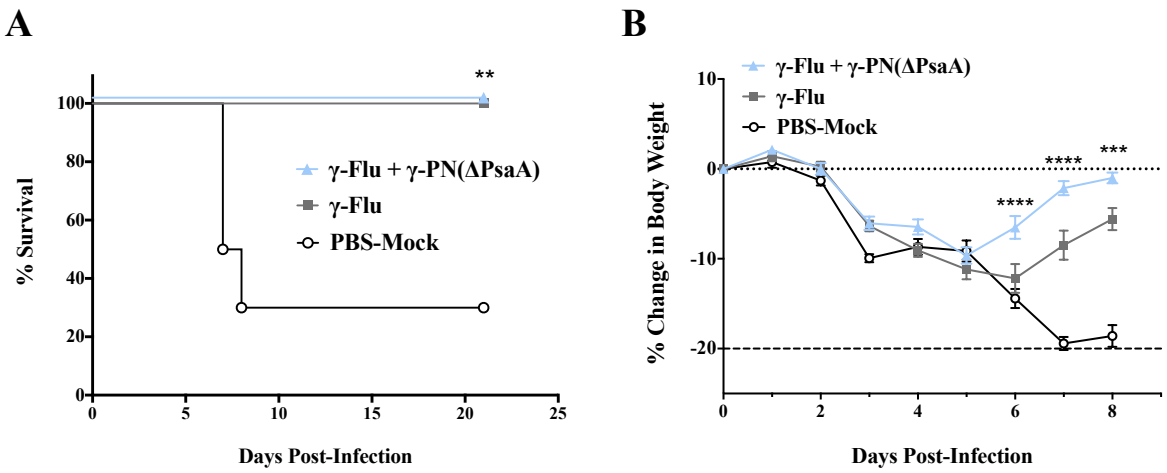

Figure 4.2. Enhanced protection against pdmH1N1 challenge following co-vaccination with γ-Flu + γ-PN(ΔPsaA). Balb/c mice were vaccinated IN with γ-Flu alone or co-vaccinated with γ-Flu + γ-PN(ΔPsaA). Control mice were PBS-Mock vaccinated. 21 days post-vaccination, mice were challenged IN with drifted pdmH1N1 (A/California/07/2009). Mice were monitored for 3 weeks for development of clinical symptoms, and euthanized if they lost 20% of their body weight. (A) Data compiled from two independent experiments. Survival percentages (n = 10), analysed by two-tailed Fisher's Exact Test compared to the PBS-Mock control group (** $P < 0.01$). (B) Weight loss of vaccinated and control mice, presented as mean ± SEM. Statistical analysis performed using Two-way ANOVA to compare γ-Flu only and co-vaccinated groups (***, $P < 0.001$, ****, $P < 0.0001$).

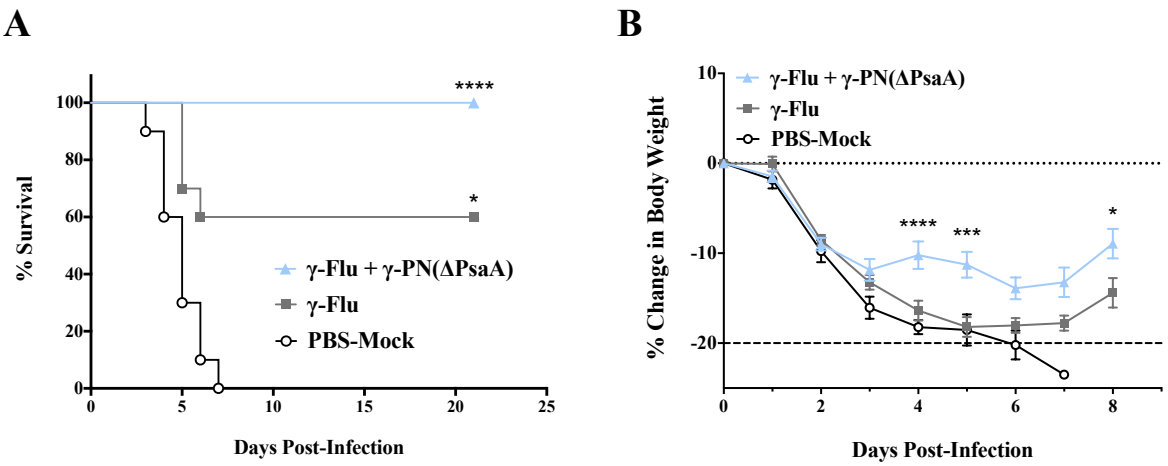

Figure 4.3. Enhanced protection against heterosubtypic IAV challenge following co-vaccination with γ-Flu + γ-PN(ΔPsaA). Balb/c mice were vaccinated IN with γ-Flu alone or co-vaccinated with γ-Flu + γ-PN(ΔPsaA). Control mice were PBS-Mock vaccinated. 21 days post-vaccination, mice were challenged IN with heterosubtypic H3N2 (A/PortChalmers/1/73). Mice were monitored for 3 weeks for development of clinical symptoms, and euthanized if they lost 20% of their body weight. (A) Data compiled from two independent experiments. Survival percentages (n = 10), analysed by two-tailed Fisher's Exact Test compared to the PBS-Mock control group (*, $P < 0.05$, ****, $P < 0.0001$). (B) Weight loss of vaccinated and control mice, presented as mean ± SEM. Statistical analysis performed using Two-way ANOVA to compare γ-Flu only and co-vaccinated groups (*, $P < 0.05$, ***, $P < 0.001$, ****, $P < 0.0001$).

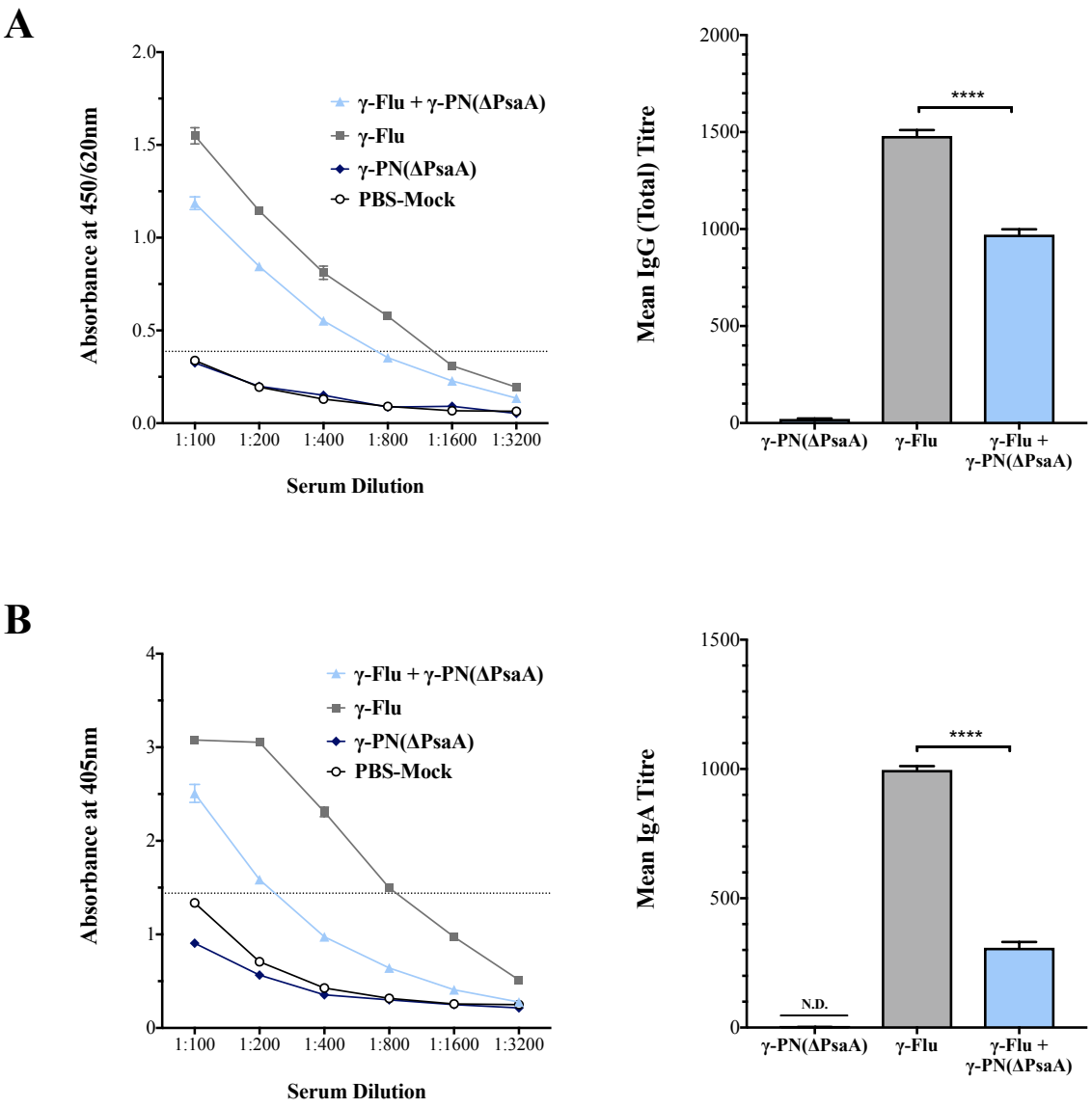

Figure 4.4. The effect of co-vaccination on A/PR8-specific antibody responses. Balb/c mice were vaccinated IN with γ-Flu alone or co-vaccinated with γ-Flu + γ-PN(ΔPsaA). Control mice received γ-PN(ΔPsaA) alone, or PBS as a mock-vaccine (n = 5 per group). 20 days post-vaccination, serum was harvested from all mice by submandibular bleed. (A) Total IgG and (B) IgA in pooled serum from vaccinated and control mice was determined by ELISA. Data presented as absorbance at 450/620nm or 405nm respectively, and as mean titre ± SEM. Titres were calculated relative to the cut-off value (dotted line), which was determined using readings of control sera from PBS-Mock mice at a 1:100 dilution. Data analysed by One-Way ANOVA (****, $P < 0.0001$). N.D. not detected.

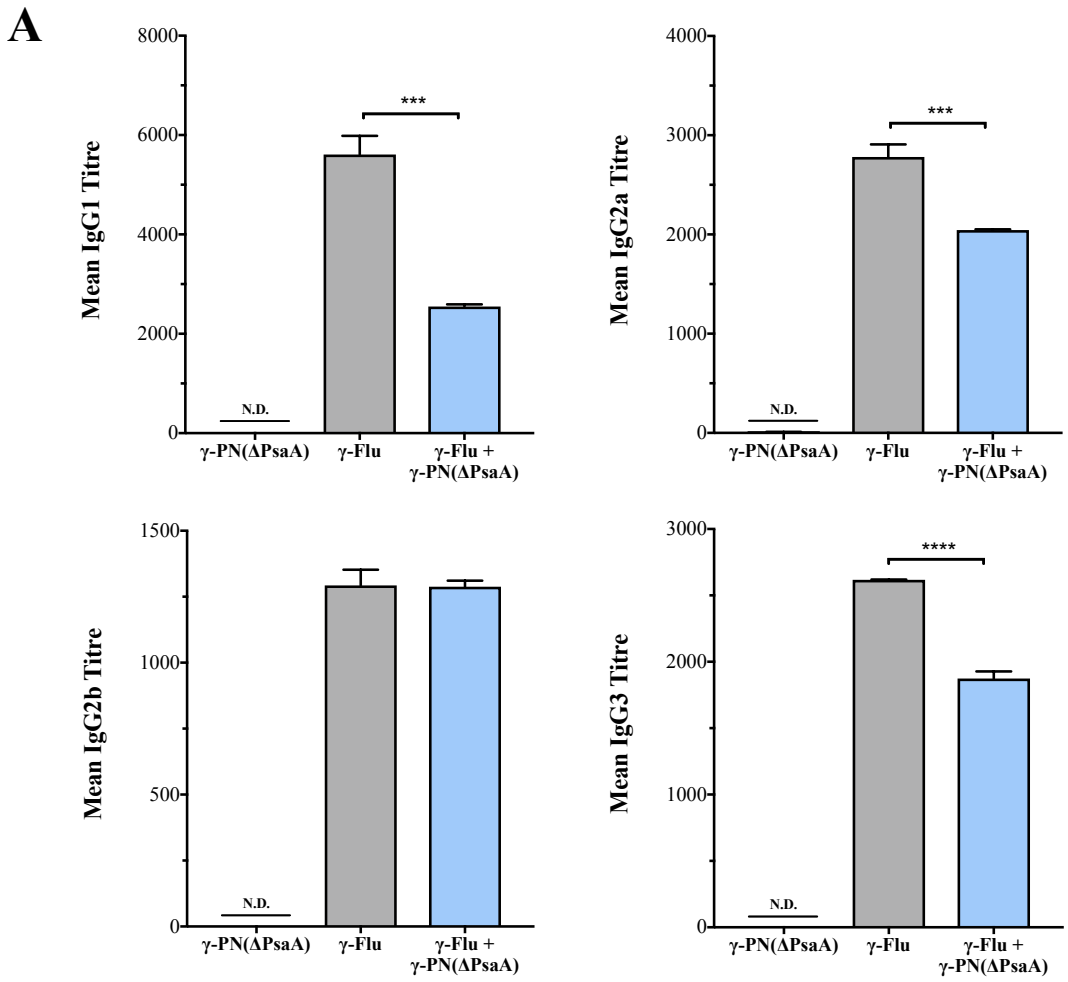
A
Mean IgG1 Titre
8000
6000
4000
2000
0
***
N.D.
γ-PN(ΔPsaA)
γ-Flu
γ-Flu +
γ-PN(ΔPsaA)
Mean IgG2a Titre
4000
3000
2000
1000
0
***
N.D.
γ-PN(ΔPsaA)
γ-Flu
γ-Flu +
γ-PN(ΔPsaA)
Mean IgG2b Titre
1500
1000
500
0
N.D.
γ-PN(ΔPsaA)
γ-Flu
γ-Flu +
γ-PN(ΔPsaA)
Mean IgG3 Titre
3000
2000
1000
0
****
N.D.
γ-PN(ΔPsaA)
γ-Flu
γ-Flu +
γ-PN(ΔPsaA)

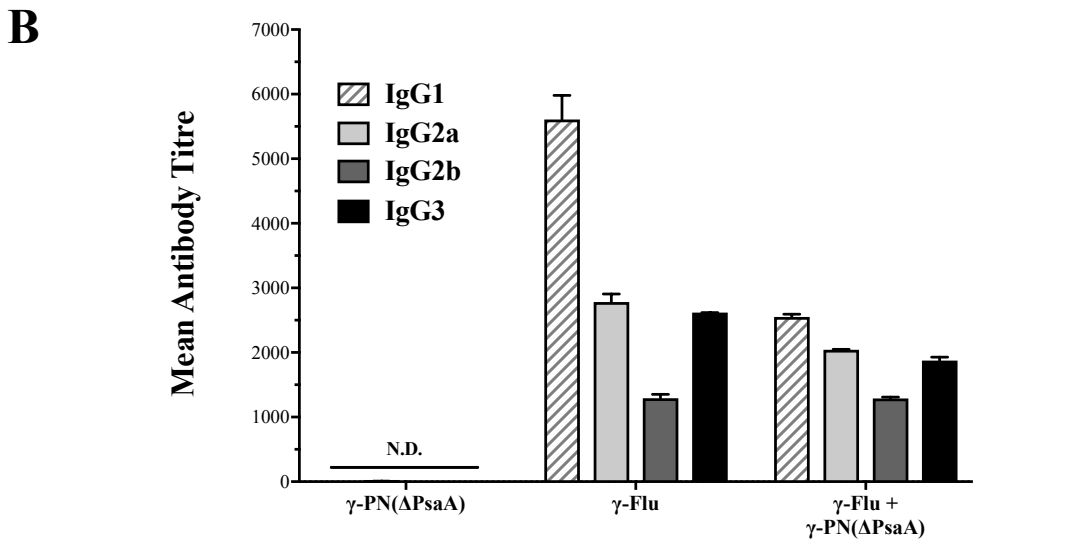
B
Mean Antibody Titre
7000
6000
5000
4000
3000
2000
1000
0
IgG1
IgG2a
IgG2b
IgG3
N.D.
γ-PN(ΔPsaA)
γ-Flu
γ-Flu +
γ-PN(ΔPsaA)

Figure 4.5. The effect of co-vaccination on A/PR8-specific IgG subclasses. Balb/c mice were vaccinated IN with γ-Flu alone or co-vaccinated with γ-Flu + γ-PN(ΔPsaA). Control mice received γ-PN(ΔPsaA) alone, or PBS as a mock-vaccine (n = 5 per group). 20 days post vaccination, serum was harvested from all mice by submandibular bleed, and titres of A/PR8-specific IgG1, IgG2a, IgG2b, and IgG3 were determined by ELISA. Data presented as (A) mean titres ± SEM, calculated relative to cut-off value, which was determined using a 1:100 dilution of control sera from PBS-Mock mice. Data analysed by One-Way ANOVA (***, $P < 0.001$, ****, $P < 0.0001$). (B) Relative profiles of IgG1, IgG2a, IgG2b, and IgG3 subclasses between vaccine groups. N.D. not detected.

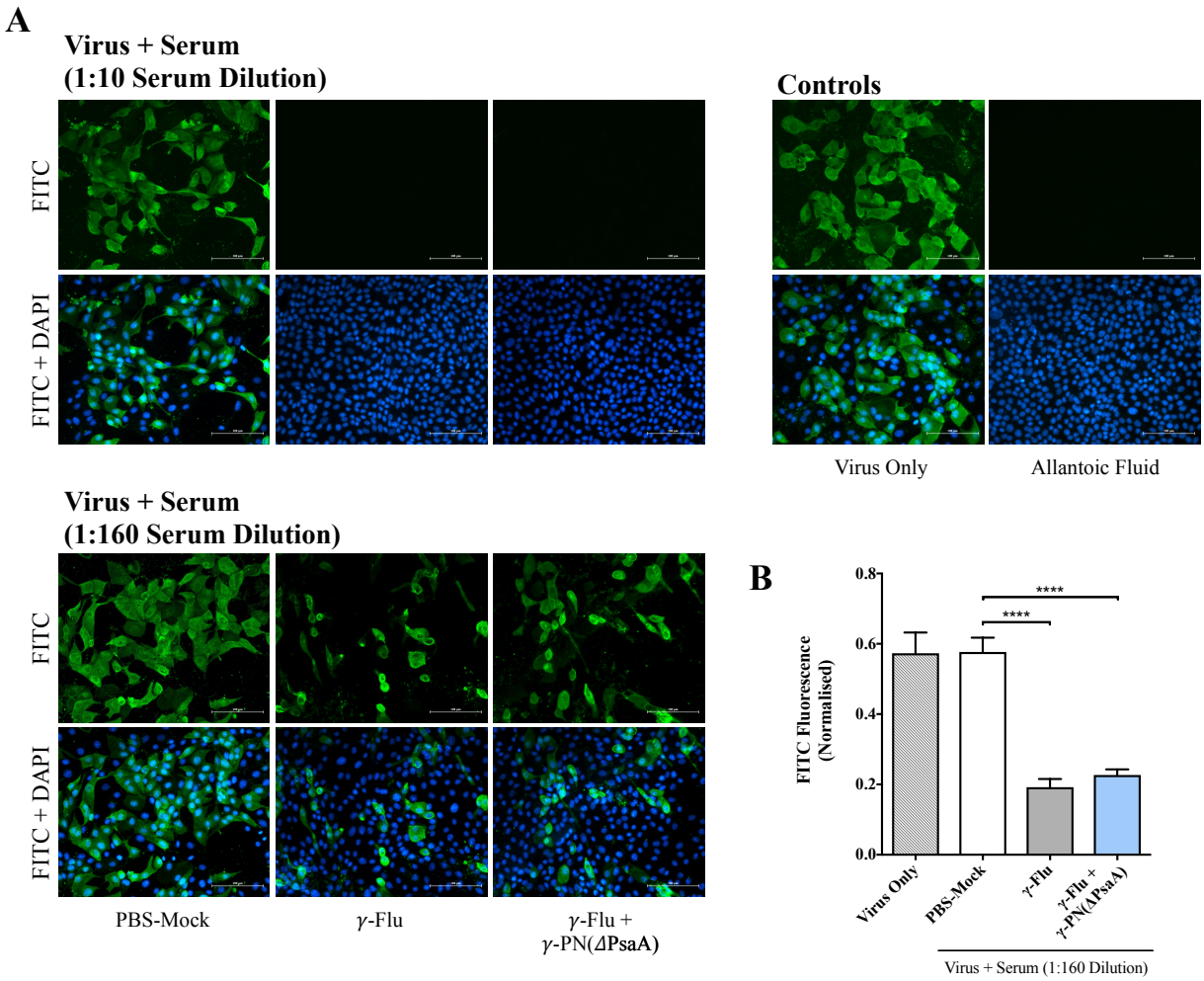

Figure 4.6. *In vitro* neutralisation of A/PR8 by sera from vaccinated and control mice. Serum samples were harvested on day 20 post-vaccination from Balb/c mice receiving γ-Flu only, γ-Flu + γ-PN(ΔPsaA), or a PBS-Mock vaccine. Serum samples were pooled for each vaccine group (n = 5 per group) and serially diluted, then incubated with live A/PR8. Virus + serum mixtures were added to MDCK cell monolayers at MOI 0.1 to assess neutralization of infection. (A) Representative images of infected MDCK cells visualised using Nikon TiE inverted fluorescence microscope, DAPI (blue) indicates cell nuclei, and FITC (green) indicates A/PR8 virus. Control wells were incubated with virus only (no sera), or allantoic fluid as a negative control. (B) FITC fluorescence was quantified for 1:160 serum dilution using NIS elements software, and normalised using corresponding quantified DAPI fluorescence. Data presented as mean ± SEM (n = 8), analysed by One-Way ANOVA (****, $P < 0.0001$).

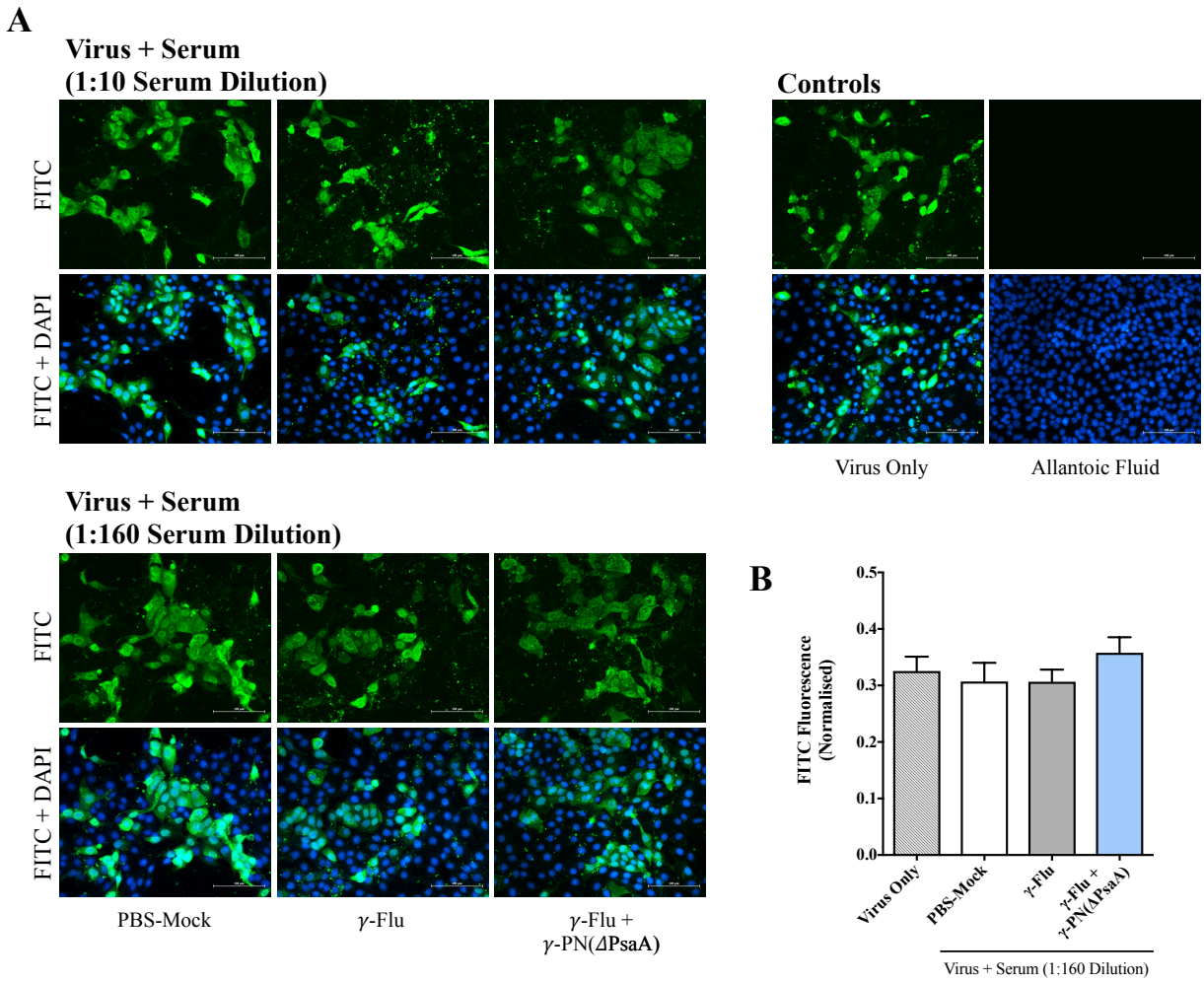

Figure 4.7. No cross-neutralisation of pdmH1N1 *in vitro* by sera from vaccinated or control mice. Serum samples were harvested on day 20 post-vaccination from Balb/c mice receiving γ-Flu only, γ-Flu + γ-PN(ΔPsaA), or a PBS-Mock vaccine (n = 5 per group). Serum samples were pooled for each vaccine group and serially diluted, then incubated with live pdmH1N1. Virus + serum mixtures were added to MDCK cell monolayers at MOI 0.1 to assess neutralization of infection. (A) Representative images of infected MDCK cells visualised using Nikon TiE inverted fluorescence microscope, DAPI (blue) indicates cell nuclei, and FITC (green) indicates A/PR8 virus. Control wells were incubated with virus only (no sera), or allantoic fluid as a negative control. (B) FITC fluorescence was quantified for 1:160 sera dilution using NIS elements software, and normalised using corresponding quantified DAPI fluorescence. Data presented as mean ± SEM (n = 8), no significance by One-Way ANOVA.

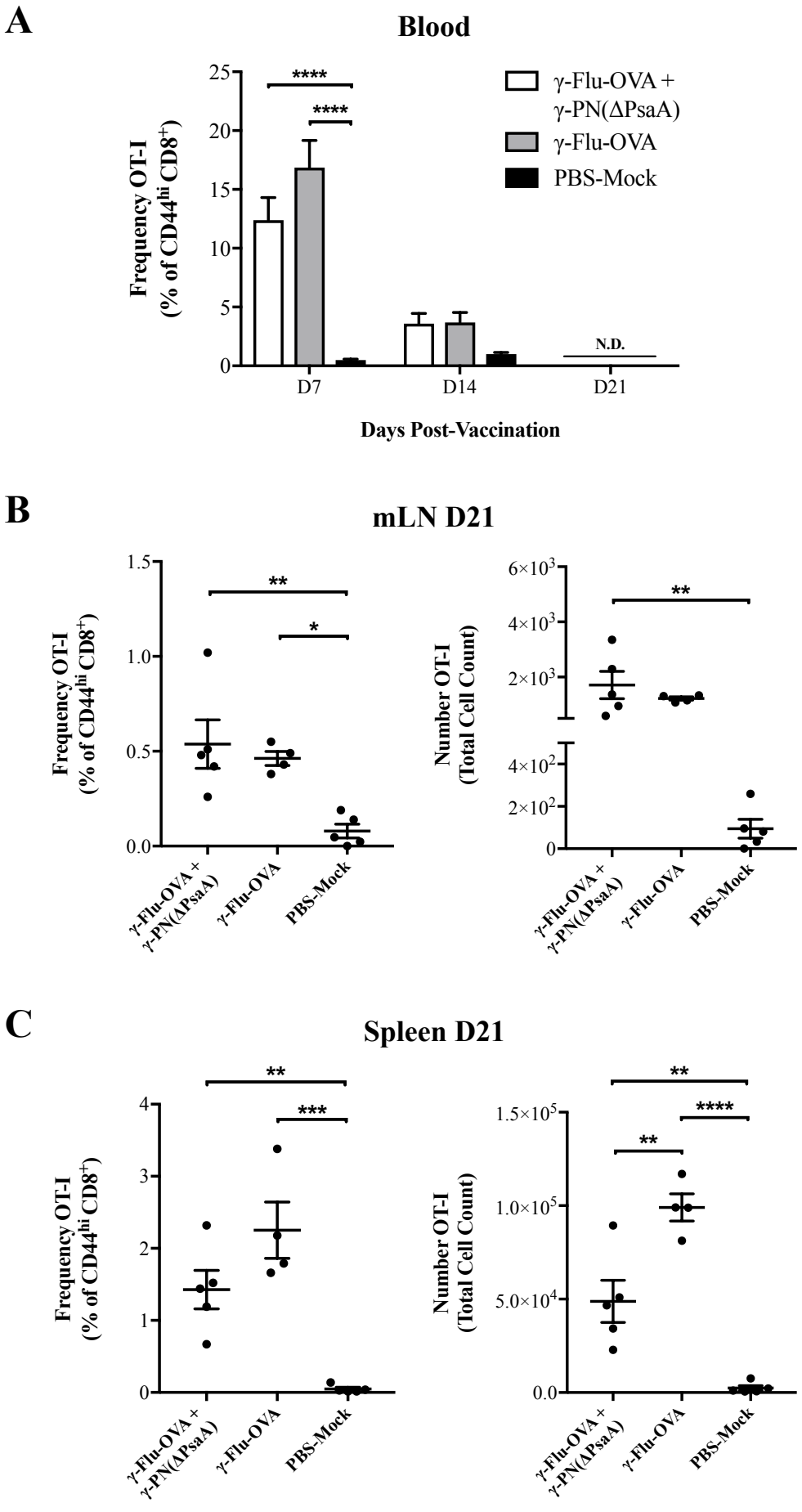
A
Blood
Frequency OT-I (% of CD44hi CD8+)
γ-Flu-OVA + γ-PN(ΔPsaA)
γ-Flu-OVA
PBS-Mock
****
****
N.D.
D7
D14
D21
Days Post-Vaccination
B
mLN D21
Frequency OT-I (% of CD44hi CD8+)
Number OT-I (Total Cell Count)
**
*
**
γ-Flu-OVA + γ-PN(ΔPsaA)
γ-Flu-OVA
PBS-Mock
C
Spleen D21
Frequency OT-I (% of CD44hi CD8+)
Number OT-I (Total Cell Count)
**
***
**
****
γ-Flu-OVA + γ-PN(ΔPsaA)
γ-Flu-OVA
PBS-Mock

Figure 4.8. Magnitude of IAV-specific T-cell populations in peripheral blood and secondary lymphoid organs. OT-I cells were transferred IV to wild-type C57BL/6 mice. 24 h later, mice were vaccinated IN with γ-Flu-OVA alone or co-vaccinated with γ-Flu-OVA + γ-PN(ΔPsaA). (A) Blood was harvested by submandibular bleed on days 7, 14, and 21 post-vaccination, and cells analysed for the frequency of activated OT-I cells ($CD44^{hi}CD8^{+}CD45.1^{+}$) by flow cytometry. Data are presented as mean frequency ± SEM (n = 5), and analysed using Two-way ANOVA (****, $P < 0.0001$). N.D. not detected. (B) Mediastinal lymph node (mLN), and (C) spleen harvested from C57BL/6 mice on day 21 post-vaccination, and analysed for activated OT-I cells by flow cytometry. Data presented as frequency and total cell counts ± SEM (n = 5) for each organ. Data analysed by One-way ANOVA (*, $P < 0.05$, **, $P < 0.01$, ***, $P < 0.001$, ****, $P < 0.0001$).

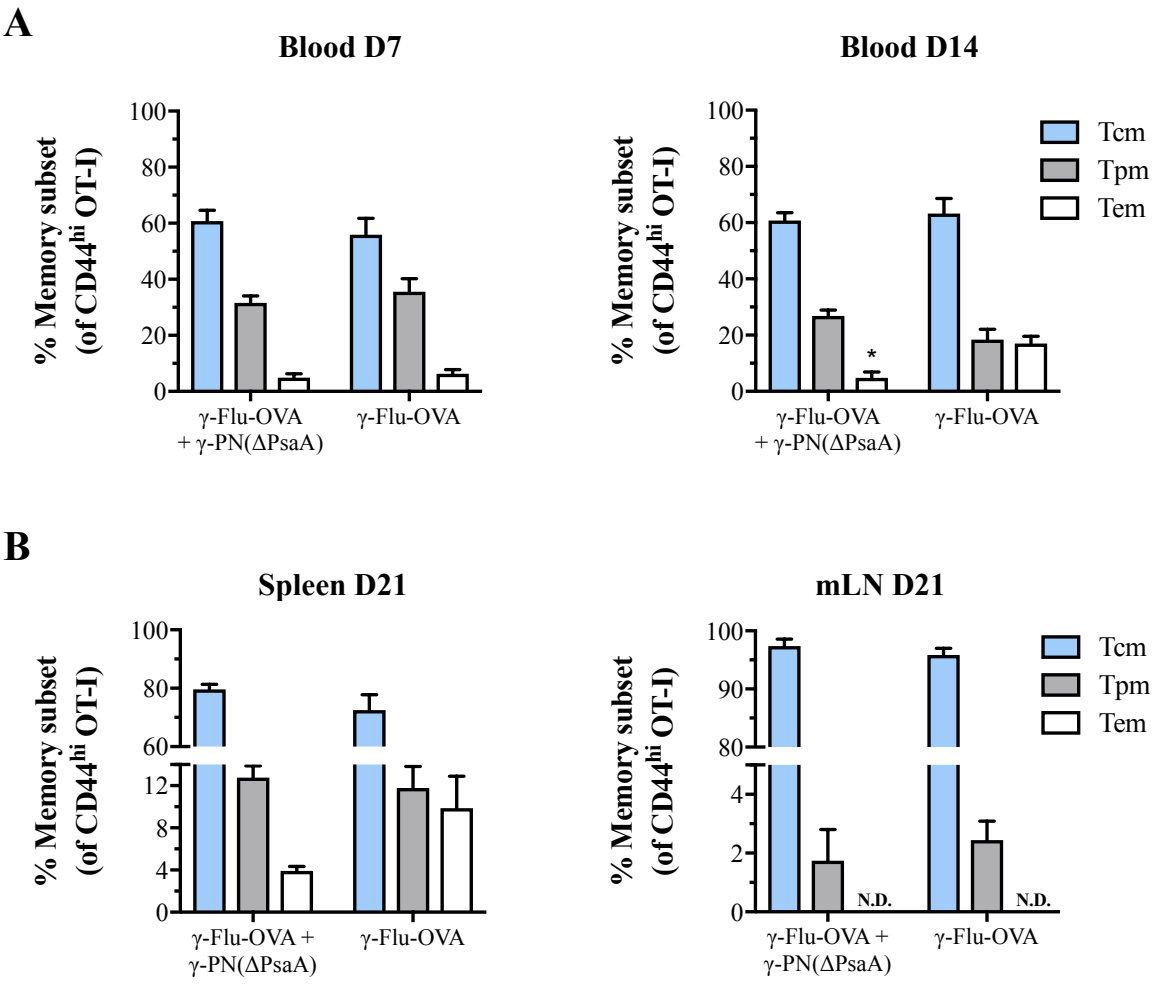

Figure 4.9. Proportions of circulating IAV-specific CD8$^+$ memory cells following co-administration of γ-Flu-OVA and γ-PN(ΔPsaA). OT-I cells were transferred IV to wild-type C57BL/6 mice. 24 h later, mice were vaccinated IN with γ-Flu-OVA alone or co-vaccinated with γ-Flu-OVA + γ-PN(ΔPsaA). Blood was harvested by submandibular bleed on days 7 and 14 post-vaccination, and cells were analysed for proportions of circulating memory OT-I cell subsets (Tcm, central memory, Tpm, peripheral memory, Tem, effector memory) by flow cytometry. (B) Spleen and mediastinal lymph node (mLN) harvested from C57BL/6 mice on day 21 post-vaccination, and similarly analysed by flow cytometry. Data presented as mean frequency ± SEM (n = 5), analysed by Two-way ANOVA (*, $P < 0.05$, when comparing the same cell subset between vaccine groups). N.D. not detected.

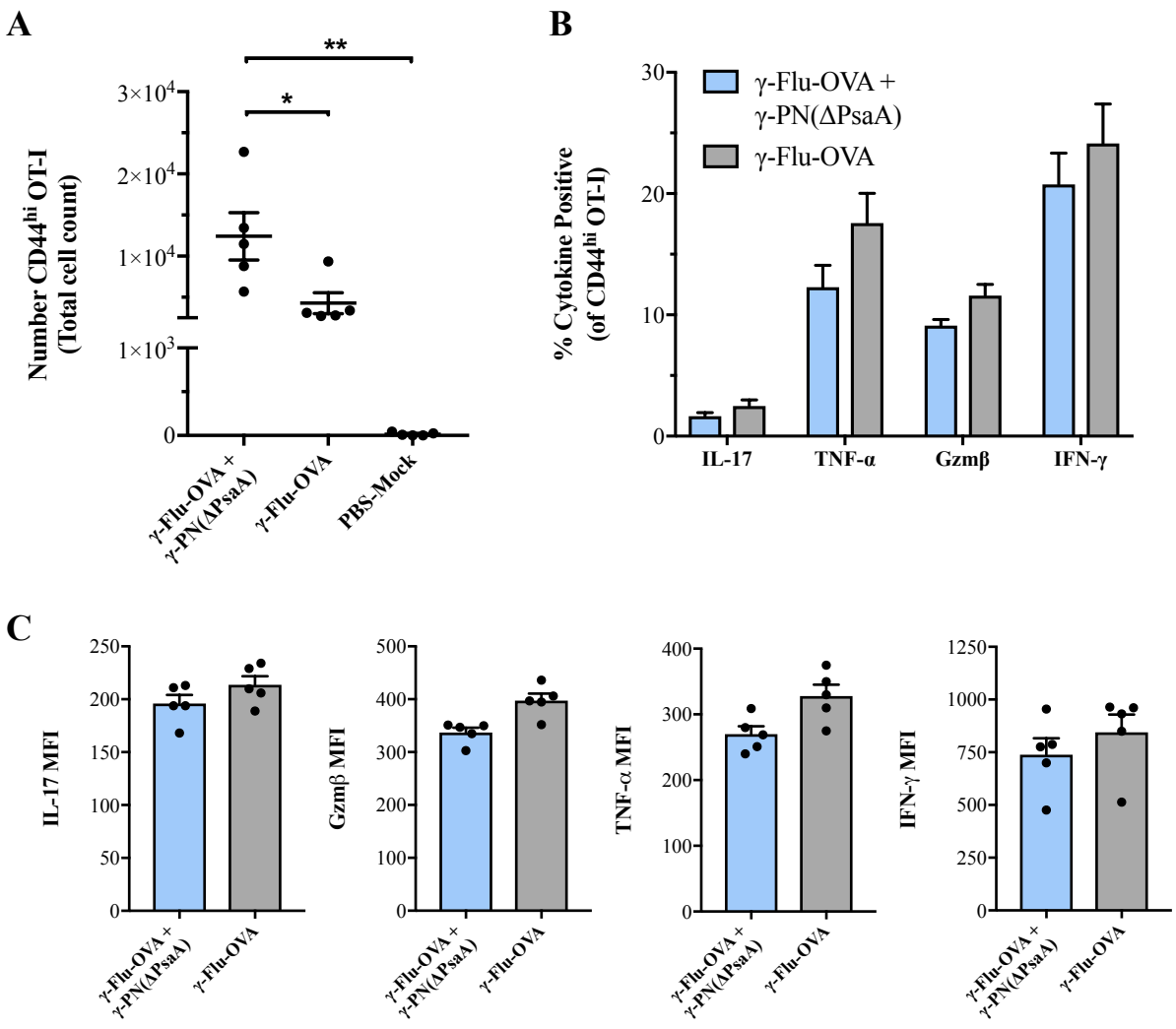

Figure 4.10. Magnitude of IAV-specific CD8$^+$ T-cell response in the lung is enhanced by co-vaccination with γ-Flu-OVA and γ-PN(ΔPsaA). OT-I cells transferred IV to wild-type C57BL/6 mice. 24 h later, mice vaccinated IN with γ-Flu-OVA alone or co-vaccinated with γ-Flu-OVA + γ-PN(ΔPsaA). On day 21 post-vaccination, lungs were harvested for analysis of OT-I cells by flow cytometry. (A) Total number of activated OT-I cells (CD44^{hi}CD8$^+$CD45.1$^+$) in the lungs of vaccinated and control mice, presented as mean ± SEM (n = 5), analysed by One-Way ANOVA (*, $P < 0.05$, **, $P < 0.01$). (B) Single cell lung suspensions stimulated *ex vivo* for 4 h with SIINFEKL peptide prior to intracellular cytokine staining and flow cytometry analysis. Data presented as mean frequency ± SEM (n = 5) of cytokine positive OT-I cells. (C) MFI quantified for each cytokine, presented as mean ± SEM.

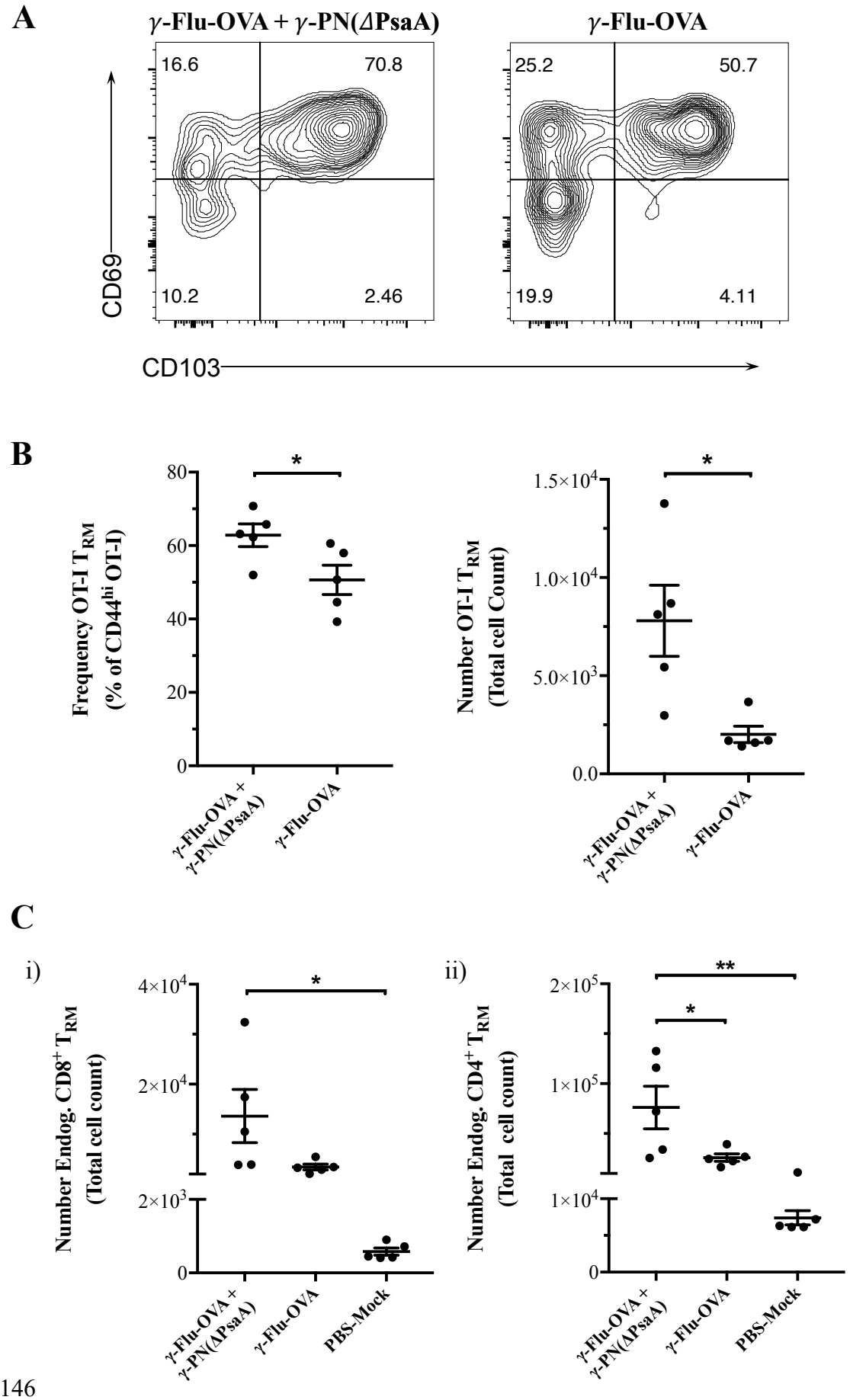
A
γ-Flu-OVA + γ-PN(ΔPsaA)
γ-Flu-OVA
16.6
70.8
10.2
2.46
25.2
50.7
19.9
4.11
CD69
CD103
B
Frequency OT-I T_RM (% of CD44^hi OT-I)
Number OT-I T_RM (Total cell Count)
γ-Flu-OVA + γ-PN(ΔPsaA)
γ-Flu-OVA
C
i)
Number Endog. CD8+ T_RM (Total cell count)
ii)
Number Endog. CD4+ T_RM (Total cell count)
γ-Flu-OVA + γ-PN(ΔPsaA)
γ-Flu-OVA
PBS-Mock

Figure 4.11. Enhanced populations of IAV-specific (OT-I) and endogenous Tissue Resident Memory Cells (T_{RM}) in the lungs of co-vaccinated mice. OT-I cells were transferred IV to wild-type C57BL/6 mice. 24 h later, mice were vaccinated IN with γ-Flu-OVA alone or co-vaccinated with γ-Flu-OVA + γ-PN(ΔPsaA). Control mice were PBS-Mock vaccinated. 21 days post-vaccination, lungs were harvested for analysis of activated OT-I cells ($CD44^{hi}CD45.1^{+}$) and endogenous T-cells ($CD44^{hi}CD45.1^{-}$) expressing a T_{RM} phenotype ($CD69^{+}CD103^{+}$) by flow cytometry. (A) Representative plots of T_{RM} gating on OT-I cells from the lung of single and co-vaccinated mice. Cells were pre-gated on live/dead. (B) OT-I T_{RM} cells detected in the lungs of vaccinated mice, presented as frequency and total cell count (mean ± SEM, n = 5), analysed by two-tailed unpaired *t*-test (*, $P < 0.05$). (C) Endogenous (i) $CD8^{+}$ T_{RM} cells ($CD69^{+}CD103^{+}$), and (ii) $CD4^{+}$ T_{RM} cells ($CD11a^{hi}CD69^{+}$), presented as total cell count (mean ± SEM, n = 5), analysed by One-Way ANOVA (*, $P < 0.05$, **, $P < 0.01$).

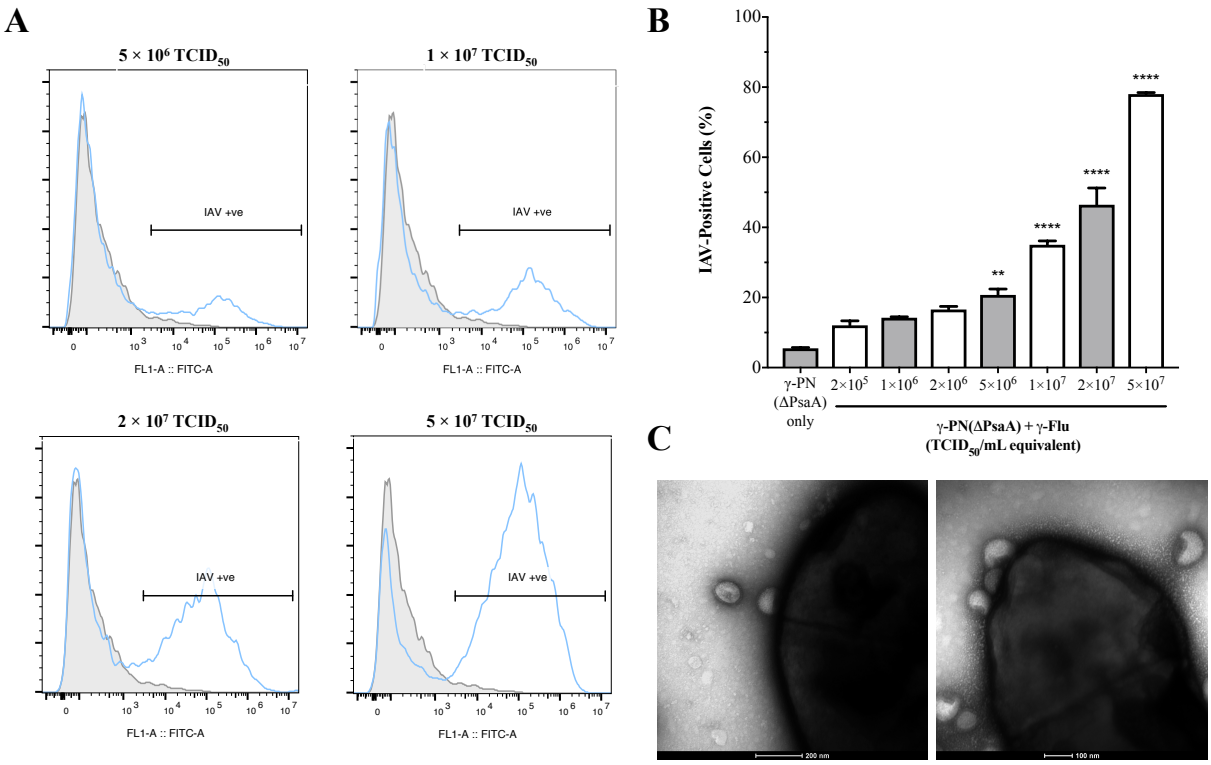

Figure 4.12. Direct association of γ-Flu and γ-PN(ΔPsaA) whole inactivated vaccines. γ-PN(ΔPsaA) whole inactivated pneumococcal vaccine was mixed with increasing amounts of γ-Flu ($TCID_{50}$/mL equivalent, as indicated), and incubated statically for 30 min at 37°C. Unbound virions were removed by pelleting and extensive washing of pneumococci. Pneumococci were then stained with an IAV-specific FITC-conjugated antibody, and single cells analysed by flow cytometry. (A) Representative plots of FITC fluorescence (indicating IAV) for γ-PN(ΔPsaA) alone (grey), or γ-PN(ΔPsaA) incubated with increasing concentrations of γ-Flu (blue line). (B) Percentage of IAV-positive pneumococci was quantified for each γ-Flu concentration tested, and presented as mean ± SEM (n = 3). Data analysed by One-way ANOVA compared to γ-PN(ΔPsaA) only (**, $P < 0.01$, ***, $P < 0.001$, **** $P < 0.0001$). (C) γ-Flu-OVA and γ-PN(ΔPsaA) vaccines were mixed on ice, then centrifuged and washed as above. Samples were negatively stained and imaged by transmission electron microscopy. Representative images, scale bar = 200 nm and 100 nm.

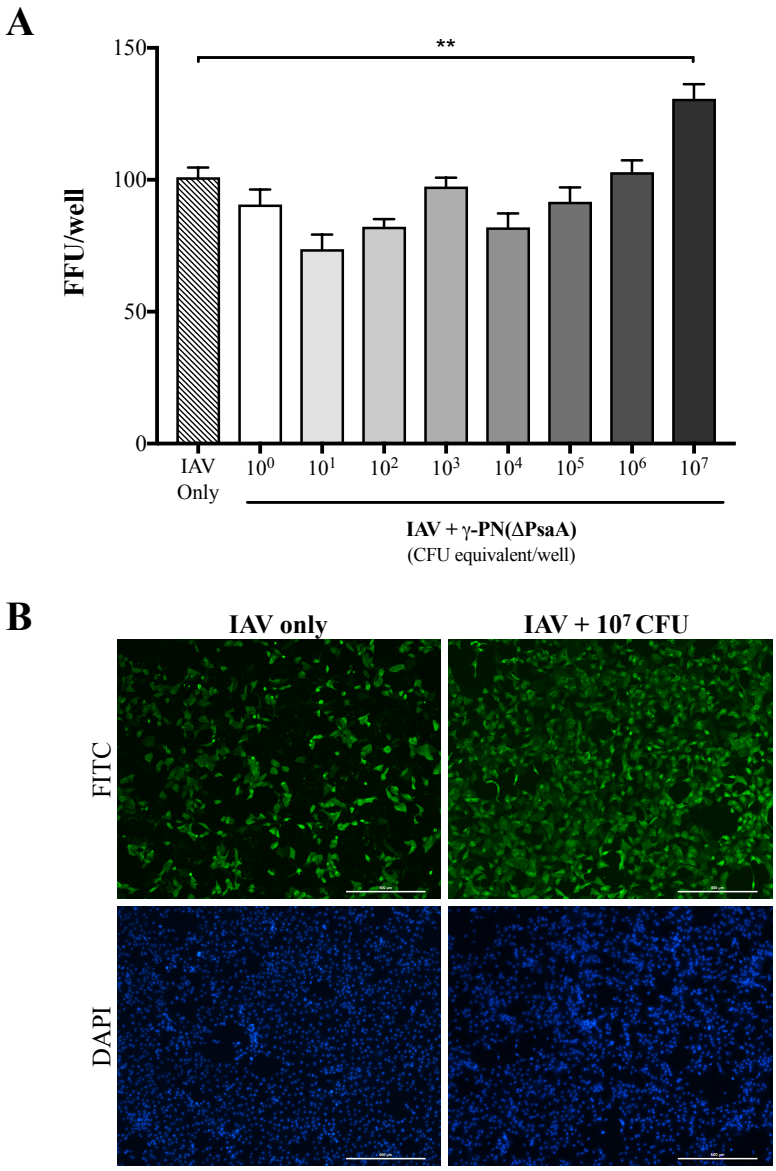

Figure 4.13. Presence of γ-PN(ΔPsaA) enhances IAV infection of MDCK cells. (A) Increasing concentrations of γ-PN(ΔPsaA) were incubated with live A/PR8, and mixtures added to MDCK cells at 100 focus forming units/well for 2 h to allow viral adhesion. Cells were then washed to remove free virions and pneumococci, and incubated for a further 22 h. Immunofluorescent staining was used to detect viral infection. (A) FFU were quantified in each well, data presented as mean ± SEM (n = 8) and analysed by One-Way ANOVA (**, $P < 0.01$). (B) Representative images of monolayers after incubation with A/PR8 virus alone or in combination with 10^7 CFU equivalent γ-PN(ΔPsaA). Virus was added to monolayers at MOI 0.1 in both cases. FITC channel (green) indicates IAV infection, and DAPI channel (blue) indicates cell nuclei. Scale bar = 500 μm.

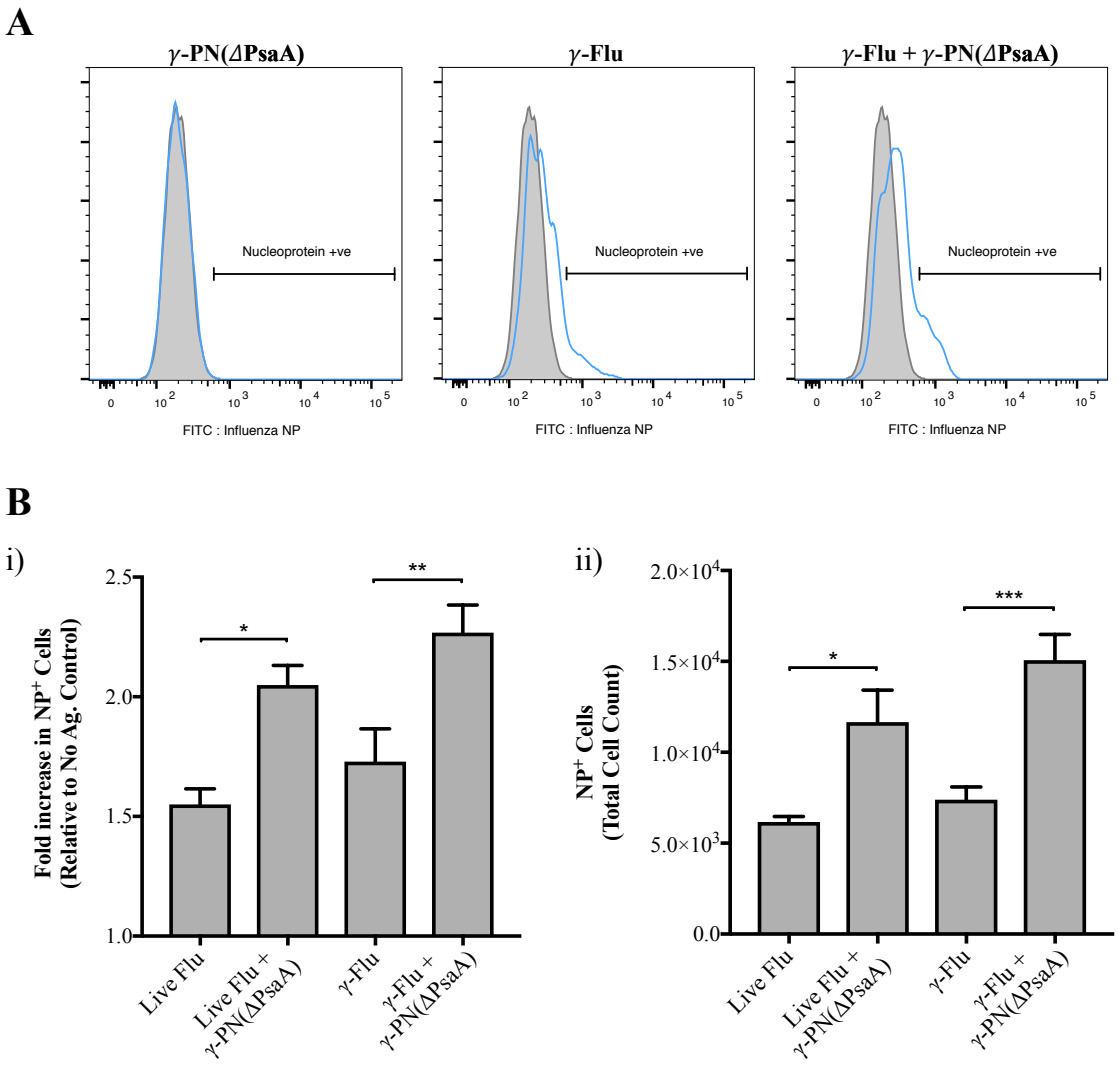

Figure 4.14. Enhanced uptake of γ-Flu virions by macrophages *in vitro* when mixed with γ-PN(ΔPsaA). (A) Differentiated THP-1 macrophage-like cells were incubated with γ-Flu, γ-PN(ΔPsaA), or a combination of the two for 3 h. Cells were then extensively washed to remove unbound antigen, and processed for analysis by flow cytometry. Representative histograms of FITC fluorescence (indicating intracellular IAV nucleoprotein, NP) after incubation with media only (grey) or inactivated vaccines (blue line). (B) THP-1 macrophage-like cells were incubated with live or irradiated IAV with and without γ-PN(ΔPsaA). Data presented as i) fold increase in NP positive cells relative to the media only control, and ii) total number of NP positive cells (± SEM, n = 4). Data is representative of two independent experiments. Data analysed by One-Way ANOVA (*, $P < 0.05$, **, $P < 0.01$, ***, $P < 0.001$).

CHAPTER 5

Final Discussion

Conventional views of pathogen dynamics rarely deviate from the consideration of single pathogens acting independently of one another. However, in more recent times, interactions between pathogens are increasingly recognised as critical contributors to both health and disease progression [533-538]. These interactions are particularly prevalent at sites that harbour complex populations of commensal and occasionally pathogenic microbes, such as the gut and the respiratory tract. In the respiratory tract, viral infections are known to predispose a host to secondary bacterial infection and invasive disease [539-541]. The synergy between respiratory pathogens IAV and *S. pneumoniae* is a well-known example of this, with primary IAV infection increasing both incidence and severity of invasive pneumococcal disease. The risk of secondary bacterial pneumonia is particularly prevalent during IAV pandemic periods, and often accounts for a large portion of IAV-related fatalities [542-544]. Considering that current strategies to avoid both sequential and simultaneous infection with IAV and *S. pneumoniae* remain unsuccessful, the increasing threat of an avian influenza pandemic makes the need for alternative preventative measures considerably more urgent. Furthermore, existing inactivated IAV vaccines will not offer any protection against suddenly emerging pandemic strains due to lack of cross-protection. The live attenuated influenza vaccine (LAIV) currently licensed in certain regions can induce this cross-protection, however LAIV is associated with a high risk of viral recombination [405], and is not recommended for use in certain groups including the immune-compromised [404]. These shortcomings limit its suitability for use during a future pandemic.

A promising candidate for an alternative 'pandemic vaccine' has been developed by our lab and refined in the current study. Our approach involves the inactivation of whole IAV using gamma-irradiation, to generate an inactivated vaccine preparation (termed γ-Flu). Non-adjuvanted intranasal vaccination with our preparation confers significant protection against homotypic and heterosubtypic IAV challenges, including highly pathogenic avian H5N1 [361, 362]. Data presented here demonstrate that irradiation doses as high as 50 kGy have minimal impact on vaccine performance, and thus are suitable for γ-Flu inactivation. Highly pathogenic agents such as avian H5N1 are required to be inactivated with 50 kGy prior to transport or laboratory use. Hence, the maintenance of γ-Flu immunogenicity after 50 kGy-treatment observed here could facilitate the inclusion of

potentially pandemic-causing IAV strains in future vaccine formulations. Furthermore, the utilisation of 50 kGy means a SAL of 10^{-6} for our IAV preparation is exceeded. This heightens the safety profile of our vaccine to enable future clinical development using highly pathogenic and/or pandemic IAV. Unlike the LAIV, our 50 kGy-inactivated formulation also carries minimal to no risk of viral recombination, further increasing its suitability for use during pandemic periods. Hence, our irradiated vaccine is likely to be safe for administration to all groups including the elderly and immune-compromised.

Use of gamma-irradiation for vaccine purposes has also been applied to the generation of a broad-spectrum pneumococcal vaccine by our lab. This formulation is comprised of irradiated whole un-encapsulated pneumococci (termed γ-PN), and non-adjuvanted intranasal vaccination with this preparation has been shown to protect against homologous and heterologous pneumococcal challenges [235]. Our lab has also previously investigated the co-administration of our γ-Flu and γ-PN vaccines, as a novel approach to confer broad-spectrum protection against the synergy of live IAV and *S. pneumoniae*. Prior publication demonstrated that co-administration of these two vaccines effectively protects against IAV and pneumococcal infections individually, as well as against lethal co-infection [403]. The mixing of whole viral and bacterial inactivated vaccines has not been investigated outside of our group to our knowledge, and the success of this approach thus far has the potential to reshape the combination vaccine field. In addition to protecting against individual and co-infection challenge models, co-administration of γ-Flu with γ-PN was shown to considerably enhance pneumococcal-specific responses [403]. Specifically, γ-PN-induced antibody responses and IL-17 production were dramatically increased, in co-vaccinated mice compared to those receiving γ-PN alone. This enhancement in immune responses was also associated with reduced pneumococcal nasopharyngeal carriage.

Remarkably, the current study illustrates that co-administering γ-Flu with the further attenuated pneumococcal vaccine (γ-PN(ΔPsaA)) similarly enhances IAV-specific immune responses, and actually heightens protection against IAV challenge. My data therefore illustrates bi-directional adjuvant activity for our co-administered vaccines. This dual enhancement of pathogen-specific responses paired with the conferral of broad-

spectrum protection against non-vaccine IAV strains and pneumococcal serotypes make our formulation an ideal pandemic vaccine candidate.

It is important to note that 50 kGy-treated γ-Flu preparations appeared to be slightly less effective at preventing weight loss after IAV challenge when compared to preparations treated with a substantially lower dose of 25 kGy (**Fig. 2.4**). This was only observed when using intentionally reduced vaccine doses, and the survival rate for all vaccinated mice in these titration experiments was 100% for both 25 kGy and 50 kGy-treated preparations. Data also suggests IAV-specific cytotoxic T-cell responses were slightly affected by the high irradiation dose used. Whilst the difference between efficacy of CTLs induced by 25 kGy- and 50 kGy-treated γ-Flu was not significantly different, the trend for 50 kGy-treated γ-Flu to induce less potent CTLs was apparent (**Fig. 2.5**). This slight impact on vaccine efficacy could potentially be overcome by increasing vaccine dose, or administering γ-Flu with an adjuvant. Fortuitously, my data shows that γ-PN(ΔPsaA) functions as a mucosal adjuvant for enhancement of IAV-specific responses. When co-administered with our inactivated pneumococcal vaccine, 50 kGy-treated γ-Flu conferred 100% protection against a heterosubtypic challenge (**Fig. 4.3**), indicating induction of robust cytotoxic T-cell responses in co-vaccinated mice. In contrast, γ-Flu administered alone provided only 60% protection against the intentionally harsh heterosubtypic challenge. Weight loss following both drifted pdmH1N1 and heterosubtypic H3N2 challenge was also minimised in co-vaccinated mice compared to those receiving γ-Flu alone. Thus, any deleterious effects of high irradiation dose on γ-Flu efficacy appeared to be entirely negated by co-administration with γ-PN(ΔPsaA). The use of irradiated pneumococci as a mucosal adjuvant simultaneously provides serotype-independent protection against pneumococcal infection, as shown by Babb *et al.* [403].

Interestingly, an experimental bacterial 'ghost' vaccine has been reported to have an adjuvant activity to co-administered viral antigens [409]. Controlled lysis was utilised to generate non-living bacterial 'ghosts', which were devoid of all cytoplasmic contents whilst bacterial morphology, envelope and surface structures were effectively maintained. Co-administration of bacterial ghosts with HIV proteins resulted in elevated HIV-specific humoral responses. Foreign antigens have also been loaded inside the

cytoplasmic lumen of these bacterial ghosts, and expressed on the surface or in the periplasmic space [410, 411]. Bacterial ghosts were shown to induce potent protective responses at mucosal surfaces against these 'ghost-delivered' foreign antigens, and bias the immune response toward the T_H1 type [412, 413], which is typically indicative of $CD8^+$ T-cell activation [414]. In contrast to HIV proteins administered alone, our γ-Flu vaccine alone induces highly effective neutralising antibody responses. Thus, no enhancement of humoral immunity was observed after co-administration of γ-Flu with whole irradiated pneumococci, as serum from both γ-Flu-vaccinated and co-vaccinated mice could neutralise 100% of A/PR8 infection *in vitro*. Importantly, enhanced populations of IAV-specific $CD8^+$ T-cells were detected in the lungs of co-vaccinated mice compared to animals receiving γ-Flu alone (**Fig. 4.10A**). This suggests a similar bias towards T_H1 and activation of $CD8^+$ T-cell responses following co-vaccination with γ-PN(ΔPsaA).

Furthermore, γ-PN(ΔPsaA) was shown to be a strong inducer of TLR2 signalling *in vitro* when compared to the previous version of our pneumococcal vaccine (**Fig. 3.10B**). Heightened TLR2 signalling has actually been linked to enhancement of IAV-specific responses in other studies. Chua *et al.* demonstrated that co-administration of a split IAV vaccine with a TLR2 agonist-based lipopeptide adjuvant (R_4Pam_2Cys) prior to challenge improved viral clearance from the lungs of mice. Enhanced nucleoprotein-specific $CD8^+$ T-cell responses were also observed in co-vaccinated mice compared to those receiving split IAV alone [545]. Heightened TLR2 signalling may be a specific mechanism by which co-administration with γ-PN(ΔPsaA) enhances the IAV-specific T-cell responses observed here. Follow-up studies could utilise TLR2-deficient mice to assess whether this particular receptor plays a role.

My data also suggests that the enhancement of IAV-specific immunity by γ-PN(ΔPsaA) may be related to augmented uptake of γ-Flu virions. In fact, enhanced IAV uptake by both epithelial (**Fig. 4.13**) and macrophage (**Fig. 4.14**) cell lines were observed *in vitro* when γ-PN(ΔPsaA) was mixed with IAV prior to inoculation. This enhanced IAV uptake appears to be mediated by a direct interaction between the whole IAV and pneumococcal vaccines when mixed in suspension (**Fig. 4.12**). To our knowledge, we are the first to

report this direct interaction between inactivated IAV and *S. pneumoniae.* A collaborator has recently observed a similar interaction between live IAV and *S. pneumoniae* (unpublished data), and thus my data demonstrates these pathogens retain their ability to directly bind even after inactivation by gamma-irradiation. This phenomena allows us to hijack existing pathogen-pathogen interactions to dramatically increase vaccine uptake and immune stimulation. Whilst the mechanism of IAV-pneumococcal interaction is yet to be elucidated, the downstream effects on vaccine-induced immune responses are of immense interest. For example, the enhanced uptake of γ-Flu by macrophages is expected to augment immune signalling. Due to the direct nature of the pathogen-pathogen interaction, recognition and phagocytosis of the entire IAV-pneumococci complex by phagocytic cells is highly likely. This would result in considerably augmented TLR signalling due to the presence of both viral and bacterial PAMPs within these cells. For example, our irradiated pneumococci present PAMPs on the cell surface for TLR2 and TLR4 stimulation, as well as containing intracellular components for stimulation of TLR9, e.g. via bacterial CpG-DNA [415, 209]. Internal components of γ-Flu similarly stimulate TLRs, e.g. TLR7 via viral ssRNA [350]. When compared to uptake of γ-Flu alone, simultaneous internalisation of γ-Flu + γ-PN(ΔPsaA) would induce a substantially altered cytokine milieu. In fact, IAV-infected human monocyte-derived macrophages (MDMs) have been shown to upregulate production of a wide variety of inflammatory mediators after subsequent exposure to *S. pneumoniae.* In particular, production of pro-inflammatory chemokine IP-10 was found to be synergistically enhanced in co-infected MDMs compared to those exposed to either of the single pathogens [546]. From a vaccination perspective, this inflammatory environment would be beneficial in facilitating trafficking of sizeable lymphocyte populations to the lung. Indeed, enhanced populations of IAV-specific $CD8^+$ T-cells were detected in the lung following co-vaccination (**Fig. 4.10A**), with heightened proportions of IAV-specific T_{RM} cells (**Fig. 4.11**).

In addition to trafficking, presence of γ-PN(ΔPsaA)-induced inflammatory cytokines could also aid the conversion of recruited lymphocytes to memory phenotypes, and promote maintenance of memory T-cell pools in the lung tissue itself. For example, both TGF-β and TNF have been implicated in T-cell conversion to a T_{RM} phenotype [509, 500,

510, 511], and both cytokines are induced following intranasal *S. pneumoniae* infection and pneumococcal carriage respectively [513, 512]. Influx of additional macrophages to the site of vaccination would further promote this cytokine-driven immune activation. However, as neither the γ-Flu or γ-PN(ΔPsaA) vaccine components can replicate or proliferate respectively, this inflammatory cytokine milieu is expected to subside following clearance of the inactivated pathogens. Hence, this cytokine response would persist for a short time period only. In the context of a live infection with IAV and *S. pneumoniae*, increased uptake by phagocytes and the resulting inflammatory state is likely to be substantially more prolonged due to productive infection. This would cause excess immunopathology and tissue damage. In fact, the IP-10-CXCR3 axis has been associated with acute immune lung injury and exacerbated pathology during acute respiratory distress syndrome [547, 548]. *In vivo* study of IAV and pneumococcal super-infection also indicated that upregulation of IP-10 and other pro-inflammatory cytokines had a crucial role in the susceptibility of mice to lung neutrophilia, severe immunopathology, and mortality [549]. Investigation of the magnitude and longevity of the inflammatory cytokine milieu induced in the lung after co-vaccination, and after co-infection with live IAV and *S. pneumoniae* should be thoroughly investigated, as should the contribution of direct IAV-pneumococcal interactions to the induction of these inflammatory states.

As mentioned beforehand, direct interaction between IAV and *S. pneumoniae* has not been reported previously by any other group. However, interaction between IAV and other streptococci has been observed. Okamoto *et al.* reported a direct interaction between IAV and Group A *Streptococcus* (GAS, *Streptococcus pyogenes*), and demonstrated substantially less binding between IAV and a non-encapsulated mutant compared to wild-type GAS, indicating that the streptococcal CPS is a pre-requisite for viral interaction [550]. Another group demonstrated a similar requirement for pneumococcal CPS for viral-bacterial interaction, with a sialic acid moiety in the capsule of swine pathogen *Streptococcus suis* directly mediating binding to swine influenza viruses (SIV) [551]. Follow-up study highlighted that the HA of both H1N1 and H3N2 SIV subtypes, and human IAV isolate A/WSN/1933 (H1N1) were able to bind to the sialic acid present in the CPS of *S. suis* [552]. Hosaka *et al.* also demonstrated a CPS

sialic-acid dependent interaction with IAV for Group B Streptococcus (GBS, *Streptococcus agalactiae*) [553]. The virus-binding capability of GBS was specifically shown to be dependent on side chain length of the terminal sialic acid, and pre-treatment with bacterial neuraminidase resulted in loss of virus binding. Interestingly, both chained and single GBS cells were found to aggregate when incubated with high doses of virus [553]. Strikingly, the CPS-dependent interaction of other streptococci with influenza viruses is in direct contrast to data presented here. In fact, my data shows that direct binding between IAV and *S. pneumoniae* occurs in the absence of any pneumococcal CPS, as our γ-PN(ΔPsaA) is completely unencapsulated. Thus, the presence of CPS sialic acid moieties are unlikely to contribute to the observed viral-bacterial interaction.

Interestingly, respiratory syncytial virus (RSV) has also been shown to directly bind *S. pneumoniae* in a capsule-independent manner [554]. Hament *et al.* observed RSV-pneumococcal interactions for multiple pneumococcal serotypes, indicating a capsule-independent mechanism. RSV also bound in higher amounts to an un-encapsulated mutant than to wild-type pneumococci, confirming pneumococcal CPS was not a prerequisite for RSV binding, and actually interfered with viral-pneumococcal complex formation. Binding of RSV to *S. pneumoniae,* and to non-typeable *Haemophilus influenzae* has also been demonstrated by Avadhanula *et al.* [555]. The binding in both instances was dose-dependent, which is similar to data presented here for binding of IAV to *S. pneumoniae* (**Fig. 4.12A** and **Fig. 4.12B**). Interaction of RSV with both *S. pneumoniae* and *H. influenzae* was found to be dependent on RSV surface glycoprotein G [555]. This protein has also been associated with RSV binding to *Neisseria meningitidis* [556]. RSV G protein functions in viral attachment to host cells, and binds glycosaminoglycans such as heparan sulphate on the cell surface to initiate infection [557, 558]. However, the precise mechanism by which G protein mediates binding to the aforementioned bacteria is currently unknown. The mechanism(s) behind the pneumococcal-IAV interactions observed here are also yet to be elucidated, and are of immense interest to our group. The direct interactions are likely to contribute substantially to the lethal synergism observed when these two respiratory pathogens simultaneously infect a host. Thorough investigation will be conducted into the surface

proteins and/or components of the pneumococcal cell wall permitting the observed binding to IAV, and to other respiratory viruses of interest.

Pathogen-pathogen interactions occurring at other body sites, such as the gut, may also be of interest for future studies. In fact, enteric viruses such as Norovirus and Poliovirus have recently been shown to directly bind to multiple species of bacteria that comprise the host gut microbiota [537, 559-563]. An intact gut microbiota was also found to be critical for rotavirus infection in mice, suggesting a similar binding-based mechanism to mediate host cell infection [564]. These interactions may similarly cause differential immune uptake and processing of enteric pathogens, potentially contributing to prolonged inflammation and heightened disease severity.

Overall, this study has highlighted the immense value of co-administering whole inactivated IAV and *S. pneumoniae* for vaccine purposes. I believe the observed interactions and the resulting enhancement of IAV-specific immunity are due to the unique nature of our whole-inactivated vaccine components. It is hypothesised that the same effects would not be observed if we had been using split vaccines or purified protein components only. This study has also refined both of the γ-Flu and γ-PN(ΔPsaA) vaccines individually in terms of safety and immunogenicity, with the intent of enabling clinical advancement of this very promising pandemic co-vaccination approach. Future study will continue the investigation of cytokine/chemokine profiles and lymphocyte trafficking to the lung following co-vaccination, as well as dissecting the complex interplay between phagocytes and T lymphocytes following exposure to both viral and bacterial vaccine components. An increased understanding of pathogen-pathogen interactions in the context of mucosal vaccination and live infection could also reveal novel therapeutic options to alleviate the pathology associated with respiratory co-infection, and could be instrumental in reducing mortality during future IAV pandemics.

REFERENCES

1. Medina, R.A. and Garcia-Sastre, A., 2011. Influenza A viruses: new research developments. Nat Rev Microbiol, **9**: 590-603.
2. World Health Organization. *Influenza*. Biologicals 2017 13 June 2017 25 August 2017]; Available from: http://www.who.int/biologicals/vaccines/influenza/en/.
3. Taubenberger, J.K. and Morens, D.M., 2008. The pathology of influenza virus infections. Annu Rev Pathol, **3**: 499-522.
4. Glezen, W.P., 1996. Emerging infections: pandemic influenza. Epidemiol Rev, **18**: 64-76.
5. Lamb, R.A., Krug, R.M., *Orthomyxoviridae: the viruses and their replication.*, in *Fields Virology* P.H. DM Knipe, DE Griffin, Editor. 2001, Lippincott Williams & Wilkins. p. 1487 - 1531.
6. Liu, X.L., Zhao, Z.D., and Liu, W.J., 2013. Insights into the Roles of Cyclophilin A During Influenza Virus Infection. Viruses-Basel, **5**: 182-191.
7. Palese, P. and Shah, M.L., *Orthomyxoviridae: the viruses and their replication.*, in *Fields Virology*, H.P. Knipe DM, Editor. 2007, Lippincott, Williams & Wilkins: Philadelphia. p. 1647–1690.
8. Osterhaus, A.D., Rimmelzwaan, G.F., Martina, B.E., Bestebroer, T.M., and Fouchier, R.A., 2000. Influenza B virus in seals. Science, **288**: 1051-1053.
9. Youzbashi, E., Marschall, M., Chaloupka, I., and Meier-Ewert, H., 1996. [Distribution of influenza C virus infection in dogs and pigs in Bavaria]. Tierarztl Prax, **24**: 337-342.
10. Jiang, W.M., Wang, S.C., Peng, C., Yu, J.M., Zhuang, Q.Y., Hou, G.Y., Liu, S., Li, J.P., and Chen, J.M., 2014. Identification of a potential novel type of influenza virus in Bovine in China. Virus Genes, **49**: 493-496.
11. Ducatez, M.F., Pelletier, C., and Meyer, G., 2015. Influenza D virus in cattle, France, 2011-2014. Emerg Infect Dis, **21**: 368-371.
12. Chiapponi, C., Faccini, S., De Mattia, A., Baioni, L., Barbieri, I., Rosignoli, C., Nigrelli, A., and Foni, E., 2016. Detection of Influenza D Virus among Swine and Cattle, Italy. Emerging Infectious Diseases, **22**: 352-354.
13. Ferguson, L., Eckard, L., Epperson, W.B., Long, L.P., Smith, D., Huston, C., Genova, S., Webby, R., and Wan, X.F., 2015. Influenza D virus infection in Mississippi beef cattle. Virology, **486**: 28-34.
14. Ferguson, L., Olivier, A.K., Genova, S., Epperson, W.B., Smith, D.R., Schneider, L., Barton, K., McCuan, K., Webby, R.J., and Wan, X.F., 2016. Pathogenesis of Influenza D Virus in Cattle. J Virol, **90**: 5636-5642.
15. White, S.K., Ma, W.J., McDaniel, C.J., Gray, G.C., and Lednicky, J.A., 2016. Serologic evidence of exposure to influenza D virus among persons with occupational contact with cattle. Journal of Clinical Virology, **81**: 31-33.
16. Gamblin, S.J. and Skehel, J.J., 2010. Influenza hemagglutinin and neuraminidase membrane glycoproteins. J Biol Chem, **285**: 28403-28409.
17. Obenauer, J.C., Denson, J., Mehta, P.K., Su, X., Mukatira, S., Finkelstein, D.B., Xu, X., Wang, J., Ma, J., Fan, Y., Rakestraw, K.M., Webster, R.G., Hoffmann, E., Krauss, S., Zheng, J., Zhang, Z., and Naeve, C.W., 2006. Large-scale sequence analysis of avian influenza isolates. Science, **311**: 1576-1580.
18. World Health Organization, 1980. A revision of the system of nomenclature for influenza viruses: a WHO Memorandum. Bulletin of the World Health Organization, **58**: 585-591.

19. Muramoto, Y., Noda, T., Kawakami, E., Akkina, R., and Kawaoka, Y., 2013. Identification of novel influenza A virus proteins translated from PA mRNA. J Virol, **87**: 2455-2462.
20. Shi, Y., Wu, Y., Zhang, W., Qi, J.X., and Gao, G.F., 2014. Enabling the 'host jump': structural determinants of receptor-binding specificity in influenza A viruses. Nature Reviews Microbiology, **12**: 822-831.
21. Shaw, M.L., Stone, K.L., Colangelo, C.M., Gulcicek, E.E., and Palese, P., 2008. Cellular proteins in influenza virus particles. PLoS Pathog, **4**: e1000085.
22. Jagger, B.W., Wise, H.M., Kash, J.C., Walters, K.A., Wills, N.M., Xiao, Y.L., Dunfee, R.L., Schwartzman, L.M., Ozinsky, A., Bell, G.L., Dalton, R.M., Lo, A., Efstathiou, S., Atkins, J.F., Firth, A.E., Taubenberger, J.K., and Digard, P., 2012. An overlapping protein-coding region in influenza A virus segment 3 modulates the host response. Science, **337**: 199-204.
23. Wise, H.M., Foeglein, A., Sun, J., Dalton, R.M., Patel, S., Howard, W., Anderson, E.C., Barclay, W.S., and Digard, P., 2009. A complicated message: Identification of a novel PB1-related protein translated from influenza A virus segment 2 mRNA. J Virol, **83**: 8021-8031.
24. Zheng, W. and Tao, Y.J., 2013. Structure and assembly of the influenza A virus ribonucleoprotein complex. FEBS Lett, **587**: 1206-1214.
25. Bender, B.S. and Small, P.A., Jr., 1992. Influenza: pathogenesis and host defense. Semin Respir Infect, **7**: 38-45.
26. Rodgers, B.C. and Mims, C.A., 1982. Influenza virus replication in human alveolar macrophages. J Med Virol, **9**: 177-184.
27. Weinheimer, V.K., Becher, A., Tonnies, M., Holland, G., Knepper, J., Bauer, T.T., Schneider, P., Neudecker, J., Ruckert, J.C., Szymanski, K., Temmesfeld-Wollbrueck, B., Gruber, A.D., Bannert, N., Suttorp, N., Hippenstiel, S., Wolff, T., and Hocke, A.C., 2012. Influenza A viruses target type II pneumocytes in the human lung. J Infect Dis, **206**: 1685-1694.
28. Iwasaki, A. and Pillai, P.S., 2014. Innate immunity to influenza virus infection. Nature Reviews Immunology, **14**: 315-328.
29. Jakab, G.J., 1981. Mechanisms of virus-induced bacterial superinfections of the lung. Clin Chest Med, **2**: 59-66.
30. Lakadamyali, M., Rust, M.J., and Zhuang, X.W., 2004. Endocytosis of influenza viruses. Microbes and Infection, **6**: 929-936.
31. de Vries, E., Tscherne, D.M., Wienholts, M.J., Cobos-Jimenez, V., Scholte, F., Garcia-Sastre, A., Rottier, P.J.M., and de Haan, C.A.M., 2011. Dissection of the Influenza A Virus Endocytic Routes Reveals Macropinocytosis as an Alternative Entry Pathway. Plos Pathogens, **7**.
32. Fujioka, Y., Tsuda, M., Hattori, T., Sasaki, J., Sasaki, T., Miyazaki, T., and Ohba, Y., 2011. The Ras-PI3K Signaling Pathway Is Involved in Clathrin-Independent Endocytosis and the Internalization of Influenza Viruses. PLoS One, **6**.
33. Kato, H., Sato, S., Yoneyama, M., Yamamoto, M., Uematsu, S., Matsui, K., Tsujimura, T., Takeda, K., Fujita, T., Takeuchi, O., and Akira, S., 2005. Cell type-specific involvement of RIG-I in antiviral response. Immunity, **23**: 19-28.
34. Hornung, V., Ellegast, J., Kim, S., Brzozka, K., Jung, A., Kato, H., Poeck, H., Akira, S., Conzelmann, K.K., Schlee, M., Endres, S., and Hartmann, G., 2006. 5 '-triphosphate RNA is the ligand for RIG-I. Science, **314**: 994-997.

35. Pichlmair, A., Schulz, O., Tan, C.P., Naslund, T.I., Liljestrom, P., Weber, F., and Sousa, C.R.E., 2006. RIG-I-mediated antiviral responses to single-stranded RNA bearing 5 '-phosphates. Science, **314**: 997-1001.
36. Baum, A., Sachidanandam, R., and Garcia-Sastre, A., 2010. Preference of RIG-I for short viral RNA molecules in infected cells revealed by next-generation sequencing. Proceedings of the National Academy of Sciences of the United States of America, **107**: 16303-16308.
37. Rehwinkel, J., Tan, C.P., Goubau, D., Schulz, O., Pichlmair, A., Bier, K., Robb, N., Vreede, F., Barclay, W., Fodor, E., and Sousa, C.R.E., 2010. RIG-I Detects Viral Genomic RNA during Negative-Strand RNA Virus Infection. Cell, **140**: 397-U143.
38. Jiang, F.G., Ramanathan, A., Miller, M.T., Tang, G.Q., Gale, M., Patel, S.S., and Marcotrigiano, J., 2011. Structural basis of RNA recognition and activation by innate immune receptor RIG-I. Nature, **479**: 423-U184.
39. Kowalinski, E., Lunardi, T., McCarthy, A.A., Louber, J., Brunel, J., Grigorov, B., Gerlier, D., and Cusack, S., 2011. Structural Basis for the Activation of Innate Immune Pattern-Recognition Receptor RIG-I by Viral RNA. Cell, **147**: 423-435.
40. Luo, D.H., Ding, S.C., Vela, A., Kohlway, A., Lindenbach, B.D., and Pyle, A.M., 2011. Structural Insights into RNA Recognition by RIG-I. Cell, **147**: 409-422.
41. Pang, I.K. and Iwasaki, A., 2011. Inflammasomes as mediators of immunity against influenza virus. Trends in Immunology, **32**: 34-41.
42. Martinon, F., Mayor, A., and Tschopp, J., 2009. The Inflammasomes: Guardians of the Body. Annual Review of Immunology, **27**: 229-265.
43. Thomas, P.G., Dash, P., Aldridge, J.R., Ellebedy, A.H., Reynolds, C., Funk, A.J., Martin, W.J., Lamkanfi, M., Webby, R.J., Boyd, K.L., Doherty, P.C., and Kanneganti, T.D., 2009. The Intracellular Sensor NLRP3 Mediates Key Innate and Healing Responses to Influenza A Virus via the Regulation of Caspase-1. Immunity, **30**: 566-575.
44. Ichinohe, T., Pang, I.K., and Iwasaki, A., 2010. Influenza virus activates inflammasomes via its intracellular M2 ion channel. Nature Immunology, **11**: 404-U461.
45. Zhu, P.Y., Liang, L.B., Shao, X.Y., Luo, W.Y., Jiang, S.T., Zhao, Q.Q., Sun, N., Zhao, Y.H., Li, J.P., Wang, J.G., Zhou, Y., Zhang, J., Wang, G.W., Jiang, L., Chen, H.L., and Li, C.J., 2017. Host Cellular Protein TRAPPC6A Delta Interacts with Influenza A Virus M2 Protein and Regulates Viral Propagation by Modulating M2 Trafficking. Journal of Virology, **91**.
46. McAuley, J.L., Tate, M.D., MacKenzie-Kludas, C.J., Pinar, A., Zeng, W.G., Stutz, A., Latz, E., Brown, L.E., and Mansell, A., 2013. Activation of the NLRP3 Inflammasome by IAV Virulence Protein PB1-F2 Contributes to Severe Pathophysiology and Disease. Plos Pathogens, **9**.
47. Medzhitov, R., 2001. Toll-like receptors and innate immunity. Nature Reviews Immunology, **1**: 135-145.
48. Akira, S., Uematsu, S., and Takeuchi, O., 2006. Pathogen recognition and innate immunity. Cell, **124**: 783-801.
49. Schulz, O., Diebold, S.S., Chen, M., Naslund, T.I., Nolte, M.A., Alexopoulou, L., Azuma, Y.T., Flavell, R.A., Liljestrom, P., and Sousa, C.R.E., 2005. Toll-like receptor 3 promotes cross-priming to virus-infected cells. Nature, **433**: 887-892.

50. Diebold, S.S., Kaisho, T., Hemmi, H., Akira, S., and Sousa, C.R.E., 2004. Innate antiviral responses by means of TLR7-mediated recognition of single-stranded RNA. Science, **303**: 1529-1531.
51. Lund, J.M., Alexopoulou, L., Sato, A., Karow, M., Adams, N.C., Gale, N.W., Iwasaki, A., and Flavell, R.A., 2004. Recognition of single-stranded RNA viruses by Toll-like receptor 7. Proceedings of the National Academy of Sciences of the United States of America, **101**: 5598-5603.
52. Brass, A.L., Huang, I.C., Benita, Y., John, S.P., Krishnan, M.N., Feeley, E.M., Ryan, B.J., Weyer, J.L., van der Weyden, L., Fikrig, E., Adams, D.J., Xavier, R.J., Farzan, M., and Elledge, S.J., 2009. The IFITM Proteins Mediate Cellular Resistance to Influenza A H1N1 Virus, West Nile Virus, and Dengue Virus. Cell, **139**: 1243-1254.
53. Bailey, C.C., Huang, I.C., Kam, C., and Farzan, M., 2012. Ifitm3 Limits the Severity of Acute Influenza in Mice. Plos Pathogens, **8**.
54. Everitt, A.R., Clare, S., Pertel, T., John, S.P., Wash, R.S., Smith, S.E., Chin, C.R., Feeley, E.M., Sims, J.S., Adams, D.J., Wise, H.M., Kane, L., Goulding, D., Digard, P., Anttila, V., Baillie, J.K., Walsh, T.S., Hume, D.A., Palotie, A., Xue, Y.L., Colonna, V., Tyler-Smith, C., Dunning, J., Gordon, S.B., Smyth, R.L., Openshaw, P.J., Dougan, G., Brass, A.L., Kellam, P., Investigators, G., and Investigators, M., 2012. IFITM3 restricts the morbidity and mortality associated with influenza. Nature, **484**: 519-U146.
55. Schulz, O., Pichlmair, A., Rehwinkel, J., Rogers, N.C., Scheuner, D., Kato, H., Takeuchi, O., Akira, S., Kaufman, R.J., and Reis e Sousa, C., 2010. Protein kinase R contributes to immunity against specific viruses by regulating interferon mRNA integrity. Cell Host Microbe, **7**: 354-361.
56. Kim, H.M., Lee, Y.W., Lee, K.J., Kim, H.S., Cho, S.W., Van Rooijen, N., Guan, Y., and Seo, S.H., 2008. Alveolar macrophages are indispensable for controlling influenza viruses in lungs of pigs. Journal of Virology, **82**: 4265-4274.
57. Cooper, M.A., Fehniger, T.A., Turner, S.C., Chen, K.S., Ghaheri, B.A., Ghayur, T., Carson, W.E., and Caligiuri, M.A., 2001. Human natural killer cells: a unique innate immunoregulatory role for the CD56(bright) subset. Blood, **97**: 3146-3151.
58. Jost, S. and Altfeld, M., 2013. Control of Human Viral Infections by Natural Killer Cells. Annual Review of Immunology, Vol 31, **31**: 163-194.
59. Schultz-Cherry, S., 2015. Role of NK Cells in Influenza Infection. Influenza Pathogenesis and Control - Vol Ii, **386**: 109-120.
60. McGill, J., Heusel, J.W., and Legge, K.L., 2009. Innate immune control and regulation of influenza virus infections. J Leukoc Biol, **86**: 803-812.
61. Gazit, R., Gruda, R., Elboim, M., Arnon, T.I., Katz, G., Achdout, H., Hanna, J., Qimron, U., Landau, G., Greenbaum, E., Zakay-Rones, Z., Porgador, A., and Mandelboim, O., 2006. Lethal influenza infection in the absence of the natural killer cell receptor gene Ncr1. Nature Immunology, **7**: 517-523.
62. Hashimoto, Y., Moki, T., Takizawa, T., Shiratsuchi, A., and Nakanishi, Y., 2007. Evidence for phagocytosis of influenza virus-infected, apoptotic cells by neutrophils and macrophages in mice. J Immunol, **178**: 2448-2457.
63. Kessel, C.H.G. and Lambrecht, B.N., 2008. Division of labor between dendritic cell subsets of the lung. Mucosal Immunology, **1**: 442-450.

64. Brincks, E.L., Katewa, A., Kucaba, T.A., Griffith, T.S., and Legge, K.L., 2008. CD8 T cells utilize TRAIL to control influenza virus infection. J Immunol, **181**: 4918-4925.
65. Kreijtz, J.H., Fouchier, R.A., and Rimmelzwaan, G.F., 2011. Immune responses to influenza virus infection. Virus Res, **162**: 19-30.
66. McMichael, A.J., Gotch, F.M., Noble, G.R., and Beare, P.A., 1983. Cytotoxic T-cell immunity to influenza. N Engl J Med, **309**: 13-17.
67. Gotch, F., Mcmichael, A., Smith, G., and Moss, B., 1987. Identification of Viral Molecules Recognized by Influenza-Specific Human Cytotoxic Lymphocytes-T. Journal of Experimental Medicine, **165**: 408-416.
68. Jameson, J., Cruz, J., and Ennis, F.A., 1998. Human cytotoxic T-lymphocyte repertoire to influenza A viruses. Journal of Virology, **72**: 8682-8689.
69. Boon, A.C.M., de Mutsert, G., Graus, Y.M.F., Fouchier, R.A.M., Sintnicolaas, K., Osterhaus, A.D.M.E., and Rimmelzwaan, G.F., 2002. The magnitude and specificity of influenza A virus-specific cytotoxic T-lymphocyte responses in humans is related to HLA-A and -B phenotype. Journal of Virology, **76**: 582-590.
70. Wang, M., Lamberth, K., Harndahl, M., Roder, G., Stryhn, A., Larsen, M.V., Nielsen, M., Lundegaard, C., Tang, S.T., Dziegiel, M.H., Rosenkvist, J., Pedersen, A.E., Buus, S., Claesson, M.H., and Lund, O., 2007. CTL epitopes for influenza A including the H5N1 bird flu; genome-, pathogen-, and HLA-wide screening. Vaccine, **25**: 2823-2831.
71. Soghoian, D.Z. and Streeck, H., 2010. Cytolytic CD4(+) T cells in viral immunity. Expert Rev Vaccines, **9**: 1453-1463.
72. Lamb, J.R., Woody, J.N., Hartzman, R.J., and Eckels, D.D., 1982. In vitro influenza virus-specific antibody production in man: antigen-specific and HLA-restricted induction of helper activity mediated by cloned human T lymphocytes. J Immunol, **129**: 1465-1470.
73. Wright, P.F., Neumann, G., and Kawaoka, Y., *Orthomyxoviruses*. Fields Virology ed. P.M.H. D.M. Knipe, D.E. Griffin, R.A. Lamb, M.A. Martin. Vol. 5th Edition. 2007: Lippincott Williams and Wilkins.
74. Acosta-Rodriguez, E.V., Napolitani, G., Lanzavecchia, A., and Sallusto, F., 2007. Interleukins 1 beta and 6 but not transforming growth factor-beta are essential for the differentiation of interleukin 17-producing human T helper cells. Nature Immunology, **8**: 942-949.
75. Ben-Sasson, S.Z., Hu-Li, J., Quiel, J., Cauchetaux, S., Ratner, M., Shapira, I., Dinarello, C.A., and Paul, W.E., 2009. IL-1 acts directly on CD4 T cells to enhance their antigen-driven expansion and differentiation. Proceedings of the National Academy of Sciences of the United States of America, **106**: 7119-7124.
76. Tamura, S. and Kurata, T., 2004. Defense mechanisms against influenza virus infection in the respiratory tract mucosa. Jpn J Infect Dis, **57**: 236-247.
77. McMurry, J.A., Johansson, B.E., and De Groot, A.S., 2008. A call to cellular & humoral arms: enlisting cognate T cell help to develop broad-spectrum vaccines against influenza A. Hum Vaccin, **4**: 148-157.
78. Ekiert, D.C., Bhabha, G., Elsliger, M.A., Friesen, R.H., Jongeneelen, M., Throsby, M., Goudsmit, J., and Wilson, I.A., 2009. Antibody recognition of a highly conserved influenza virus epitope. Science, **324**: 246-251.
79. Sui, J., Hwang, W.C., Perez, S., Wei, G., Aird, D., Chen, L.M., Santelli, E., Stec, B., Cadwell, G., Ali, M., Wan, H., Murakami, A., Yammanuru, A., Han, T., Cox,

N.J., Bankston, L.A., Donis, R.O., Liddington, R.C., and Marasco, W.A., 2009. Structural and functional bases for broad-spectrum neutralization of avian and human influenza A viruses. Nature Structural & Molecular Biology, **16**: 265-273.
80. Mandelboim, O., Lieberman, N., Lev, M., Paul, L., Arnon, T.I., Bushkin, Y., Davis, D.M., Strominger, J.L., Yewdell, J.W., and Porgador, A., 2001. Recognition of haemagglutinins on virus-infected cells by NKp46 activates lysis by human NK cells. Nature, **409**: 1055-1060.
81. Mozdzanowska, K., Maiese, K., Furchner, M., and Gerhard, W., 1999. Treatment of influenza virus-infected SCID mice with nonneutralizing antibodies specific for the transmembrane proteins matrix 2 and neuraminidase reduces the pulmonary virus titer but fails to clear the infection. Virology, **254**: 138-146.
82. Australian Technical Advisory Group on Immunisation (ATAGI), 2017, ATAGI advice for immunisation providers regarding the administration of seasonal influenza vaccines in 2017 (ATAGI 62nd Meeting). Australian Government.
83. Australian Technical Advisory Group on Immunisation (ATAGI), *Part 4 Vaccine Preventable Diseases - Influenza*, in *The Australian Immunisation Handbook*. 2017, Australian Government Department of Health,: Canberra.
84. Protein Sciences Corporation, 2017, FluBlock: Full Prescribing Information (Influenza Vaccine BLA STN 125285). U.S. Food and Drug Administration (FDA),. p. 16.
85. Pebody, R., McMenamin, J., and Nohynek, H., 2017. Live attenuated influenza vaccine (LAIV): recent effectiveness results from the USA and implications for LAIV programmes elsewhere. Arch Dis Child.
86. Zhou, B., Meliopoulos, V.A., Wang, W., Lin, X., Stucker, K.M., Halpin, R.A., Stockwell, T.B., Schultz-Cherry, S., and Wentworth, D.E., 2016. Reversion of Cold-Adapted Live Attenuated Influenza Vaccine into a Pathogenic Virus. J Virol, **90**: 8454-8463.
87. Maassab, H.F., 1967. Adaptation and growth characteristics of influenza virus at 25 degrees c. Nature, **213**: 612-614.
88. Jin, H., Lu, B., Zhou, H., Ma, C.H., Zhao, J., Yang, C.F., Kemble, G., and Greenberg, H., 2003. Multiple amino acid residues confer temperature sensitivity to human influenza virus vaccine strains (FluMist) derived from cold-adapted A/Ann Arbor/6/60. Virology, **306**: 18-24.
89. Chan, W., Zhou, H., Kemble, G., and Jin, H., 2008. The cold adapted and temperature sensitive influenza A/Ann Arbor/6/60 virus, the master donor virus for live attenuated influenza vaccines, has multiple defects in replication at the restrictive temperature. Virology, **380**: 304-311.
90. Zhou, B., Li, Y., Speer, S.D., Subba, A., Lin, X., and Wentworth, D.E., 2012. Engineering temperature sensitive live attenuated influenza vaccines from emerging viruses. Vaccine, **30**: 3691-3702.
91. Mina, M.J., McCullers, J.A., and Klugman, K.P., 2014. Live attenuated influenza vaccine enhances colonization of Streptococcus pneumoniae and Staphylococcus aureus in mice. MBio, **5**.
92. Ambrose, C.S., Luke, C., and Coelingh, K., 2008. Current status of live attenuated influenza vaccine in the United States for seasonal and pandemic influenza. Influenza and Other Respiratory Viruses, **2**: 193-202.

93. Sun, K., Ye, J.Q., Perez, D.R., and Metzger, D.W., 2011. Seasonal FluMist Vaccination Induces Cross-Reactive T Cell Immunity against H1N1 (2009) Influenza and Secondary Bacterial Infections. J Immunol, **186**: 987-993.
94. Cheng, X., Zengel, J.R., Suguitan, A.L., Xu, Q., Wang, W.J., Lin, J., and Jin, H., 2013. Evaluation of the Humoral and Cellular Immune Responses Elicited by the Live Attenuated and Inactivated Influenza Vaccines and Their Roles in Heterologous Protection in Ferrets. Journal of Infectious Diseases, **208**: 594-602.
95. Caspard, H., Mallory, R.M., Yu, J., and Ambrose, C.S., 2017. Live-Attenuated Influenza Vaccine Effectiveness in Children From 2009 to 2015-2016: A Systematic Review and Meta-Analysis. Open Forum Infect Dis, **4**: ofx111.
96. Grohskopf, L.A., Sokolow, L.Z., Broder, K.R., Walter, E.B., Bresee, J.S., Fry, A.M., and Jernigan, D.B., 2017. Prevention and Control of Seasonal Influenza with Vaccines: Recommendations of the Advisory Committee on Immunization Practices - United States, 2017-18 Influenza Season. MMWR Recomm Rep, **66**: 1-20.
97. Hayden, F.G., 1999. Update on influenza and rhinovirus infections. Adv Exp Med Biol, **458**: 55-67.
98. Monto, A.S., Robinson, D.P., Herlocher, M.L., Hinson, J.M., Jr., Elliott, M.J., and Crisp, A., 1999. Zanamivir in the prevention of influenza among healthy adults: a randomized controlled trial. JAMA, **282**: 31-35.
99. Hayden, F.G., 2006. Antiviral resistance in influenza viruses--implications for management and pandemic response. N Engl J Med, **354**: 785-788.
100. Hayden, F.G., 2006. Antivirals for influenza: historical perspectives and lessons learned. Antiviral Res, **71**: 372-378.
101. Hayden, F.G. and Pavia, A.T., 2006. Antiviral management of seasonal and pandemic influenza. J Infect Dis, **194 Suppl 2**: S119-126.
102. Couch, R.B., 2000. Prevention and treatment of influenza. N Engl J Med, **343**: 1778-1787.
103. Fleishman, S.J., Whitehead, T.A., Ekiert, D.C., Dreyfus, C., Corn, J.E., Strauch, E.M., Wilson, I.A., and Baker, D., 2011. Computational design of proteins targeting the conserved stem region of influenza hemagglutinin. Science, **332**: 816-821.
104. Belshe, R.B., 2007. The burden of Inluenza and strategies for prevention. Managed Care, **16**: 2-6.
105. Geeraedts, F. and Huckriede, A., 2011. Influenza Vaccines: What Do We Want and How Can We Get It? Crossroads between Innate and Adaptive Immunity Iii, **780**: 161-174.
106. Australian Technical Advisory Group on Immunisation (ATAGI), *The Australian immunisation handbook. 10th ed (January 2014 update)*. 2014, Canberra: Australian Government Department of Health.
107. Castilla, J., Martinez-Baz, I., Martinez-Artola, V., Reina, G., Pozo, F., Garcia Cenoz, M., Guevara, M., Moran, J., Irisarri, F., Arriazu, M., Albeniz, E., Ezpeleta, C., Barricarte, A., Primary Health Care Sentinel, N., and Network for Influenza Surveillance in Hospitals of, N., 2013. Decline in influenza vaccine effectiveness with time after vaccination, Navarre, Spain, season 2011/12. Euro Surveill, **18**.
108. Pebody, R., Andrews, N., McMenamin, J., Durnall, H., Ellis, J., Thompson, C.I., Robertson, C., Cottrell, S., Smyth, B., Zambon, M., Moore, C., Fleming, D.M., and Watson, J.M., 2013. Vaccine effectiveness of 2011/12 trivalent seasonal

influenza vaccine in preventing laboratory-confirmed influenza in primary care in the United Kingdom: evidence of waning intra-seasonal protection. Euro Surveill, **18**.

109. Andrews, N., McMenamin, J., Durnall, H., Ellis, J., Lackenby, A., Robertson, C., von Wissmann, B., Cottrell, S., Smyth, B., Moore, C., Gunson, R., Zambon, M., Fleming, D., and Pebody, R., 2014. Effectiveness of trivalent seasonal influenza vaccine in preventing laboratory-confirmed influenza in primary care in the United Kingdom: 2012/13 end of season results. Euro Surveill, **19**: 5-13.
110. Sullivan, S.G., Komadina, N., Grant, K., Jelley, L., Papadakis, G., and Kelly, H., 2014. Influenza vaccine effectiveness during the 2012 influenza season in Victoria, Australia: influences of waning immunity and vaccine match. J Med Virol, **86**: 1017-1025.
111. Gherasim, A., Pozo, F., de Mateo, S., Gamarra, I.A., Garcia-Cenoz, M., Vega, T., Martinez, E., Gimenez, J., Castrillejo, D., Larrauri, A., cyc, E.V.A.t., and the, V.W.G., 2016. Waning protection of influenza vaccine against mild laboratory confirmed influenza A(H3N2) and B in Spain, season 2014-15. Vaccine, **34**: 2371-2377.
112. Chen, R. and Holmes, E.C., 2006. Avian influenza virus exhibits rapid evolutionary dynamics. Mol Biol Evol, **23**: 2336-2341.
113. Nobusawa, E. and Sato, K., 2006. Comparison of the mutation rates of human influenza A and B viruses. J Virol, **80**: 3675-3678.
114. Rimmelzwaan, G.F., Berkhoff, E.G., Nieuwkoop, N.J., Fouchier, R.A., and Osterhaus, A.D., 2004. Functional compensation of a detrimental amino acid substitution in a cytotoxic-T-lymphocyte epitope of influenza a viruses by comutations. J Virol, **78**: 8946-8949.
115. Rimmelzwaan, G.F., Berkhoff, E.G., Nieuwkoop, N.J., Smith, D.J., Fouchier, R.A., and Osterhaus, A.D., 2005. Full restoration of viral fitness by multiple compensatory co-mutations in the nucleoprotein of influenza A virus cytotoxic T-lymphocyte escape mutants. J Gen Virol, **86**: 1801-1805.
116. Scholtissek, C., Rohde, W., Von Hoyningen, V., and Rott, R., 1978. On the origin of the human influenza virus subtypes H2N2 and H3N2. Virology, **87**: 13-20.
117. Fouchier, R.A.M., Munster, V., Wallensten, A., Bestebroer, T.M., Herfst, S., Smith, D., Rimmelzwaan, G.F., Olsen, B., and Osterhaus, A.D.M.E., 2005. Characterization of a novel influenza a virus hemagglutinin subtype (H16) obtained from black-headed gulls. Journal of Virology, **79**: 2814-2822.
118. Yoon, S.W., Webby, R.J., and Webster, R.G., *Evolution and Ecology of Influenza A Viruses*, in *Influenza Pathogenesis and Control - Volume I*, O.M. Compans R., Editor. 2014, Springer, Cham. p. 359-375.
119. Wu, Y., Wu, Y., Tefsen, B., Shi, Y., and Gao, G.F., 2014. Bat-derived influenza-like viruses H17N10 and H18N11. Trends Microbiol, **22**: 183-191.
120. Sun, X.M., Shi, Y., Lu, X.S., He, J.H., Gao, F., Yan, J.H., Qi, J.X., and Gao, G.F., 2013. Bat-Derived Influenza Hemagglutinin H17 Does Not Bind Canonical Avian or Human Receptors and Most Likely Uses a Unique Entry Mechanism. Cell Reports, **3**: 769-778.
121. Tong, S., Zhu, X., Li, Y., Shi, M., Zhang, J., Bourgeois, M., Yang, H., Chen, X., Recuenco, S., Gomez, J., Chen, L.M., Johnson, A., Tao, Y., Dreyfus, C., Yu, W., McBride, R., Carney, P.J., Gilbert, A.T., Chang, J., Guo, Z., Davis, C.T., Paulson, J.C., Stevens, J., Rupprecht, C.E., Holmes, E.C., Wilson, I.A., and Donis, R.O.,

2013. New world bats harbor diverse influenza A viruses. PLoS Pathog, **9**: e1003657.
122. Zhu, X.Y., Yu, W.L., McBride, R., Li, Y., Chen, L.M., Donis, R.O., Tong, S.X., Paulson, J.C., and Wilson, I.A., 2013. Hemagglutinin homologue from H17N10 bat influenza virus exhibits divergent receptor-binding and pH-dependent fusion activities. Proceedings of the National Academy of Sciences of the United States of America, **110**: 1458-1463.
123. Garcia-Sastre, A., 2012. The neuraminidase of bat influenza viruses is not a neuraminidase. Proc Natl Acad Sci U S A, **109**: 18635-18636.
124. Zhu, X., Yang, H., Guo, Z., Yu, W., Carney, P.J., Li, Y., Chen, L.M., Paulson, J.C., Donis, R.O., Tong, S., Stevens, J., and Wilson, I.A., 2012. Crystal structures of two subtype N10 neuraminidase-like proteins from bat influenza A viruses reveal a diverged putative active site. Proc Natl Acad Sci U S A, **109**: 18903-18908.
125. Taubenberger, J.K. and Morens, D.M., 2006. 1918 influenza: the mother of all pandemics. Emerging Infectious Diseases, **12**: 15-22.
126. Taubenberger, J.K., Reid, A.H., and Fanning, T.G., 2000. The 1918 influenza virus: A killer comes into view. Virology, **274**: 241-245.
127. Reid, A.H., Fanning, T.G., Hultin, J.V., and Taubenberger, J.K., 1999. Origin and evolution of the 1918 "Spanish" influenza virus hemagglutinin gene. Proceedings of the National Academy of Sciences of the United States of America, **96**: 1651-1656.
128. Simonsen, L., Clarke, M.J., Schonberger, L.B., Arden, N.H., Cox, N.J., and Fukuda, K., 1998. Pandemic versus epidemic influenza mortality: A pattern of changing age distribution. Journal of Infectious Diseases, **178**: 53-60.
129. Kilbourne, E.D., 2006. Influenza pandemics of the 20th century. Emerging Infectious Diseases, **12**: 9-14.
130. Oxford, J.S., 2000. Influenza A pandemics of the 20th century with special reference to 1918: virology, pathology and epidemiology. Reviews in Medical Virology, **10**: 119-133.
131. Schulman, J.L. and Kilbourne, E.D., 1969. Independent Variation in Nature of Hemagglutinin and Neuraminidase Antigens of Influenza Virus - Distinctiveness of Hemagglutinin Antigen of Hong Kong/68 Virus. Proceedings of the National Academy of Sciences of the United States of America, **63**: 326-+.
132. Monto, A.S. and Kendal, A.P., 1973. Effect of neuraminidase antibody on Hong Kong influenza. Lancet, **1**: 623-625.
133. Viboud, C., Grais, R.F., Lafont, B.A.P., Miller, M.A., Simonsen, L., and M, M.I.S., 2005. Multinational impact of the 1968 Hong Kong influenza pandemic: Evidence for a smoldering pandemic. Journal of Infectious Diseases, **192**: 233-248.
134. Eickhoff, T.C. and Meiklejohn, G., 1969. Protection against Hong Kong influneza by adjuvant vaccine containing A2-Ann Arbor-67. Bull World Health Organ, **41**: 562-563.
135. Osterholm, M.T. and Kelley, N.S., 2012. Mammalian-transmissible H5N1 influenza: facts and perspective. MBio, **3**: e00045-00012.
136. World Health Organisation, 2017, Influenza at the human-animal interface: Summary and assessment, 28 September to 30 October 2017, in *Monthly Risk Assessment Summary*. World Health Organisation.

137. Beigel, J.H., Farrar, J., Han, A.M., Hayden, F.G., Hyer, R., de Jong, M.D., Lochindarat, S., Nguyen, T.K., Nguyen, T.H., Tran, T.H., Nicoll, A., Touch, S., Yuen, K.Y., and Writing Committee of the World Health Organization Consultation on Human Influenza, A.H., 2005. Avian influenza A (H5N1) infection in humans. N Engl J Med, **353**: 1374-1385.
138. Peiris, J.S.M., Hui, K.P.Y., and Yen, H.L., 2010. Host response to influenza virus: protection versus immunopathology. Current Opinion in Immunology, **22**: 475-481.
139. van Riel, D., Leijten, L.M.E., van der Eerden, M., Hoogsteden, H.C., Boven, L.A., Lambrecht, B.N., Osterhaus, A.D.M.E., and Kuiken, T., 2011. Highly Pathogenic Avian Influenza Virus H5N1 Infects Alveolar Macrophages without Virus Production or Excessive TNF-Alpha Induction. Plos Pathogens, **7**.
140. Cheung, C.Y., Poon, L.L., Lau, A.S., Luk, W., Lau, Y.L., Shortridge, K.F., Gordon, S., Guan, Y., and Peiris, J.S., 2002. Induction of proinflammatory cytokines in human macrophages by influenza A (H5N1) viruses: a mechanism for the unusual severity of human disease? Lancet, **360**: 1831-1837.
141. Connor, R.J., Kawaoka, Y., Webster, R.G., and Paulson, J.C., 1994. Receptor Specificity in Human, Avian, and Equine H2 and H3 Influenza-Virus Isolates. Virology, **205**: 17-23.
142. Suzuki, Y., 2005. Sialobiology of influenza molecular mechanism of host range variation of influenza viruses. Biological & Pharmaceutical Bulletin, **28**: 399-408.
143. Tumpey, T.M., Maines, T.R., Van Hoeven, N., Glaser, L., Solorzano, A., Pappas, C., Cox, N.J., Swayne, D.E., Palese, P., Katz, J.M., and Garcia-Sastre, A., 2007. A two-amino acid change in the hemagglutinin of the 1918 influenza virus abolishes transmission. Science, **315**: 655-659.
144. Chen, L.M., Blixt, O., Stevens, J., Lipatov, A.S., Davis, C.T., Collins, B.E., Cox, N.J., Paulson, J.C., and Donis, R.O., 2012. In vitro evolution of H5N1 avian influenza virus toward human-type receptor specificity. Virology, **422**: 105-113.
145. Herfst, S., Schrauwen, E.J., Linster, M., Chutinimitkul, S., de Wit, E., Munster, V.J., Sorrell, E.M., Bestebroer, T.M., Burke, D.F., Smith, D.J., Rimmelzwaan, G.F., Osterhaus, A.D., and Fouchier, R.A., 2012. Airborne transmission of influenza A/H5N1 virus between ferrets. Science, **336**: 1534-1541.
146. Imai, M., Watanabe, T., Hatta, M., Das, S.C., Ozawa, M., Shinya, K., Zhong, G., Hanson, A., Katsura, H., Watanabe, S., Li, C., Kawakami, E., Yamada, S., Kiso, M., Suzuki, Y., Maher, E.A., Neumann, G., and Kawaoka, Y., 2012. Experimental adaptation of an influenza H5 HA confers respiratory droplet transmission to a reassortant H5 HA/H1N1 virus in ferrets. Nature, **486**: 420-428.
147. Linster, M., van Boheemen, S., de Graaf, M., Schrauwen, E.J.A., Lexmond, P., Manz, B., Bestebroer, T.M., Baumann, J., van Riel, D., Rimmelzwaan, G.F., Osterhaus, A., Matrosovich, M., Fouchier, R.A.M., and Herfst, S., 2014. Identification, characterization, and natural selection of mutations driving airborne transmission of A/H5N1 virus. Cell, **157**: 329-339.
148. Centres for Disease Control and Prevention (CDC), 2015, Highly Pathogenic Asian-Origin Avian Influenza A (H5N1) Virus, in *Avian Influenza*. CDC.
149. Olsen, S.J., Ungchusak, K., Sovann, L., Uyeki, T.M., Dowell, S.F., Cox, N.J., Aldis, W., and Chunsuttiwat, S., 2005. Family clustering of avian influenza A (H5N1). Emerg Infect Dis, **11**: 1799-1801.

150. Ungchusak, K., Auewarakul, P., Dowell, S.F., Kitphati, R., Auwanit, W., Puthavathana, P., Uiprasertkul, M., Boonnak, K., Pittayawonganon, C., Cox, N.J., Zaki, S.R., Thawatsupha, P., Chittaganpitch, M., Khontong, R., Simmerman, J.M., and Chunsutthiwat, S., 2005. Probable person-to-person transmission of avian influenza A (H5N1). N Engl J Med, **352**: 333-340.
151. Sedyaningsih, E.R., Isfandari, S., Setiawaty, V., Rifati, L., Harun, S., Purba, W., Imari, S., Giriputra, S., Blair, P.J., Putnam, S.D., Uyeki, T.M., and Soendoro, T., 2007. Epidemiology of cases of H5N1 virus infection in Indonesia, July 2005-June 2006. J Infect Dis, **196**: 522-527.
152. Oner, A.F., Bay, A., Arslan, S., Akdeniz, H., Sahin, H.A., Cesur, Y., Epcacan, S., Yilmaz, N., Deger, I., Kizilyildiz, B., Karsen, H., and Ceyhan, M., 2006. Avian influenza A (H5N1) infection in eastern Turkey in 2006. N Engl J Med, **355**: 2179-2185.
153. World Health Organisation, 2017, Analysis of recent scientific information on avian influenza A(H7N9) virus.
154. Zhu, H., Wang, D., Kelvin, D.J., Li, L., Zheng, Z., Yoon, S.W., Wong, S.S., Farooqui, A., Wang, J., Banner, D., Chen, R., Zheng, R., Zhou, J., Zhang, Y., Hong, W., Dong, W., Cai, Q., Roehrl, M.H., Huang, S.S., Kelvin, A.A., Yao, T., Zhou, B., Chen, X., Leung, G.M., Poon, L.L., Webster, R.G., Webby, R.J., Peiris, J.S., Guan, Y., and Shu, Y., 2013. Infectivity, transmission, and pathology of human-isolated H7N9 influenza virus in ferrets and pigs. Science, **341**: 183-186.
155. Imai, M., Watanabe, T., Kiso, M., Nakajima, N., Yamayoshi, S., Iwatsuki-Horimoto, K., Hatta, M., Yamada, S., Ito, M., Sakai-Tagawa, Y., Shirakura, M., Takashita, E., Fujisaki, S., McBride, R., Thompson, A.J., Takahashi, K., Maemura, T., Mitake, H., Chiba, S., Zhong, G.X., Fan, S.F., Oishi, K., Yasuhara, A., Takada, K., Nakao, T., Fukuyama, S., Yamashita, M., Lopes, T.J.S., Neumann, G., Odagiri, T., Watanabe, S., Shu, Y.L., Paulson, J.C., Hasegawa, H., and Kawaoka, Y., 2017. A Highly Pathogenic Avian H7N9 Influenza Virus Isolated from A Human Is Lethal in Some Ferrets Infected via Respiratory Droplets. Cell Host & Microbe, **22**: 615-+.
156. O'Brien, K.L., Wolfson, L.J., Watt, J.P., Henkle, E., Deloria-Knoll, M., McCall, N., Lee, E., Mulholland, K., Levine, O.S., Cherian, T., and Dis, H.P.G.B., 2009. Burden of disease caused by Streptococcus pneumoniae in children younger than 5 years: global estimates. Lancet, **374**: 893-902.
157. Adams, W.G., Deaver, K.A., Cochi, S.L., Plikaytis, B.D., Zell, E.R., Broome, C.V., and Wenger, J.D., 1993. Decline of childhood Haemophilus influenzae type b (Hib) disease in the Hib vaccine era. JAMA, **269**: 221-226.
158. National Center for Immunization and Respiratory Diseases (Division of Bacterial Diseases), 2015, Clinical Features, in *Streptococcus pneumoniae*. Centres for Disease Control and Prevention.
159. Baraff, L.J., Lee, S.I., and Schriger, D.L., 1993. Outcomes of bacterial meningitis in children: a meta-analysis. Pediatr Infect Dis J, **12**: 389-394.
160. Knuf, M., Habermehl, P., Cimino, C., Petersen, G., and Schmitt, H.J., 2006. Immunogenicity, reactogenicity and safety of a 7-valent pneumococcal conjugate vaccine (PCV7) concurrently administered with a DTPa-HBV-IPV/Hib combination vaccine in healthy infants. Vaccine, **24**: 4727-4736.

161. Geno, K.A., Gilbert, G.L., Song, J.Y., Skovsted, I.C., Klugman, K.P., Jones, C., Konradsen, H.B., and Nahm, M.H., 2015. Pneumococcal Capsules and Their Types: Past, Present, and Future. Clin Microbiol Rev, **28**: 871-899.
162. Makarewicz, O., Lucas, M., Brandt, C., Herrmann, L., Albersmeier, A., Ruckert, C., Blom, J., Goesmann, A., van der Linden, M., Kalinowski, J., and Pletz, M.W., 2017. Whole Genome Sequencing of 39 Invasive Streptococcus pneumoniae Sequence Type 199 Isolates Revealed Switches from Serotype 19A to 15B. PLoS One, **12**: e0169370.
163. Faden, H., Duffy, L., Wasielewski, R., Wolf, J., Krystofik, D., and Tung, Y., 1997. Relationship between nasopharyngeal colonization and the development of otitis media in children. Journal of Infectious Diseases, **175**: 1440-1445.
164. Gray, B.M., Converse, G.M., and Dillon, H.C., 1980. Epidemiologic Studies of Streptococcus-Pneumoniae in Infants - Acquisition, Carriage, and Infection during the 1st 24 Months of Life. Journal of Infectious Diseases, **142**: 923-933.
165. Vives, M., Garcia, M.E., Saenz, P., Mora, M.A., Mata, L., Sabharwal, H., and Svanborg, C., 1997. Nasopharyngeal colonization in Costa Rican children during the first year of life. Pediatr Infect Dis J, **16**: 852-858.
166. Coles, C.L., Kanungo, R., Rahmathullah, L., Thulasiraj, R.D., Katz, J., Santosham, M., and Tielsch, J.M., 2001. Pneumococcal nasopharyngeal colonization in young South Indian infants. Pediatr Infect Dis J, **20**: 289-295.
167. Hendley, J.O., Sande, M.A., Stewart, P.M., and Gwaltney, J.M., Jr., 1975. Spread of Streptococcus pneumoniae in families. I. Carriage rates and distribution of types. J Infect Dis, **132**: 55-61.
168. Bridy-Pappas, A.E., Margolis, M.B., Center, K.J., and Isaacman, D.J., 2005. Streptococcus pneumoniae: description of the pathogen, disease epidemiology, treatment, and prevention. Pharmacotherapy, **25**: 1193-1212.
169. Hussain, M., Melegaro, A., Pebody, R.G., George, R., Edmunds, W.J., Talukdar, R., Martin, S.A., Efstratiou, A., and Miller, E., 2005. A longitudinal household study of Streptococcus pneumoniae nasopharyngeal carriage in a UK setting. Epidemiol Infect, **133**: 891-898.
170. Bogaert, D., de Groot, R., and Hermans, P.W.M., 2004. Streptococcus pneumoniae colonisation: the key to pneumococcal disease. Lancet Infectious Diseases, **4**: 144-154.
171. Henriques-Normark, B. and Tuomanen, E.I., 2013. The Pneumococcus: Epidemiology, Microbiology, and Pathogenesis. Cold Spring Harbor Perspectives in Medicine, **3**.
172. Brueggemann, A.B., Peto, T.E.A., Crook, D.W., Butler, J.C., Kristinsson, K.G., and Spratt, B.G., 2004. Temporal and geographic stability of the serogroup-specific invasive disease potential of Streptococcus pneumoniae in children. Journal of Infectious Diseases, **190**: 1203-1211.
173. Sandgren, A., Sjostrom, K., Olsson-Liljequist, B.O., Christensson, B., Samuelsson, A., Kronvall, G., and Normark, B.H., 2004. Effect of clonal and serotype-specific properties on the invasive capacity of Streptococcus pneumoniae. Journal of Infectious Diseases, **189**: 785-796.
174. Sandgren, A., Sjostrom, K., Olsson-Liljequist, B., Christensson, B., Samuelsson, A., Kronvall, G., and Henriques Normark, B., 2004. Effect of clonal and serotype-specific properties on the invasive capacity of Streptococcus pneumoniae. J Infect Dis, **189**: 785-796.

175. McCullers, J.A., 2006. Insights into the interaction between influenza virus and pneumococcus. Clin Microbiol Rev, **19**: 571-582.
176. World Health Organisation, 2016, Pneumonia [Fact Sheet]. WHO.
177. Pletz, M.W. and Welte, T., 2014. Pneumococcal and influenza vaccination. Community-Acquired Pneumonia: 266-284.
178. National Center for Immunization and Respiratory Diseases (Division of Bacterial Diseases). *For Clinicians: Clinical Features*. Pneumococcal Disease 2017 05/01/2018]; Available from: https://www.cdc.gov/pneumococcal/clinicians/clinical-features.html.
179. Lucas, M.J., Brouwer, M.C., and van de Beek, D., 2016. Neurological sequelae of bacterial meningitis. J Infect, **73**: 18-27.
180. National Center for Immunization and Respiratory Diseases (Division of Bacterial Diseases), 2017, Symptoms and Complications, in *Pneumococcal Disease*. Centres for Disease Control and Prevention.
181. Rosenow, C., Ryan, P., Weiser, J.N., Johnson, S., Fontan, P., Ortqvist, A., and Masure, H.R., 1997. Contribution of novel choline-binding proteins to adherence, colonization and immunogenicity of Streptococcus pneumoniae. Mol Microbiol, **25**: 819-829.
182. Cundell, D.R., Gerard, N.P., Gerard, C., Idanpaan-Heikkila, I., and Tuomanen, E.I., 1995. Streptococcus pneumoniae anchor to activated human cells by the receptor for platelet-activating factor. Nature, **377**: 435-438.
183. Bergmann, S., Rohde, M., Chhatwal, G.S., and Hammerschmidt, S., 2001. alpha-Enolase of Streptococcus pneumoniae is a plasmin(ogen)-binding protein displayed on the bacterial cell surface. Mol Microbiol, **40**: 1273-1287.
184. Holmes, A.R., McNab, R., Millsap, K.W., Rohde, M., Hammerschmidt, S., Mawdsley, J.L., and Jenkinson, H.F., 2001. The pavA gene of Streptococcus pneumoniae encodes a fibronectin-binding protein that is essential for virulence. Mol Microbiol, **41**: 1395-1408.
185. Jedrzejas, M.J., Mello, L.V., de Groot, B.L., and Li, S., 2002. Mechanism of hyaluronan degradation by Streptococcus pneumoniae hyaluronate lyase. Structures of complexes with the substrate. J Biol Chem, **277**: 28287-28297.
186. Tong, H.H., Blue, L.E., James, M.A., and DeMaria, T.F., 2000. Evaluation of the virulence of a Streptococcus pneumoniae neuraminidase-deficient mutant in nasopharyngeal colonization and development of otitis media in the chinchilla model. Infection and Immunity, **68**: 921-924.
187. Yother, J. and White, J.M., 1994. Novel surface attachment mechanism of the Streptococcus pneumoniae protein PspA. J Bacteriol, **176**: 2976-2985.
188. Zhang, J.R., Mostov, K.E., Lamm, M.E., Nanno, M., Shimida, S., Ohwaki, M., and Tuomanen, E., 2000. The polymeric immunoglobulin receptor translocates pneumococci across human nasopharyngeal epithelial cells. Cell, **102**: 827-837.
189. Abeyta, M., Hardy, G.G., and Yother, J., 2003. Genetic alteration of capsule type but not PspA type affects accessibility of surface-bound complement and surface antigens of Streptococcus pneumoniae. Infection and Immunity, **71**: 218-225.
190. Paterson, G.K. and Mitchell, T.J., 2006. Innate immunity and the pneumococcus. Microbiology, **152**: 285-293.
191. Wartha, F., Beiter, K., Albiger, B., Fernebro, J., Zychlinsky, A., Normark, S., and Henriques-Normark, B., 2007. Capsule and D-alanylated lipoteichoic acids

protect Streptococcus pneumoniae against neutrophil extracellular traps. Cell Microbiol, **9**: 1162-1171.
192. Ren, B., Szalai, A.J., Thomas, O., Hollingshead, S.K., and Briles, D.E., 2003. Both family 1 and family 2 PspA proteins can inhibit complement deposition and confer virulence to a capsular serotype 3 strain of Streptococcus pneumoniae. Infection and Immunity, **71**: 75-85.
193. Angel, C.S., Ruzek, M., and Hostetter, M.K., 1994. Degradation of C3 by Streptococcus pneumoniae. J Infect Dis, **170**: 600-608.
194. Lu, L., Ma, Z., Jokiranta, T.S., Whitney, A.R., DeLeo, F.R., and Zhang, J.R., 2008. Species-specific interaction of Streptococcus pneumoniae with human complement factor H. J Immunol, **181**: 7138-7146.
195. Dieudonne-Vatran, A., Krentz, S., Blom, A.M., Meri, S., Henriques-Normark, B., Riesbeck, K., and Albiger, B., 2009. Clinical isolates of Streptococcus pneumoniae bind the complement inhibitor C4b-binding protein in a PspC allele-dependent fashion. J Immunol, **182**: 7865-7877.
196. Canvin, J.R., Marvin, A.P., Sivakumaran, M., Paton, J.C., Boulnois, G.J., Andrew, P.W., and Mitchell, T.J., 1995. The role of pneumolysin and autolysin in the pathology of pneumonia and septicemia in mice infected with a type 2 pneumococcus. J Infect Dis, **172**: 119-123.
197. Mitchell, A.M. and Mitchell, T.J., 2010. Streptococcus pneumoniae: virulence factors and variation. Clin Microbiol Infect, **16**: 411-418.
198. Steinfort, C., Wilson, R., Mitchell, T., Feldman, C., Rutman, A., Todd, H., Sykes, D., Walker, J., Saunders, K., Andrew, P.W., and et al., 1989. Effect of Streptococcus pneumoniae on human respiratory epithelium in vitro. Infection and Immunity, **57**: 2006-2013.
199. Paton, J.C. and Ferrante, A., 1983. Inhibition of human polymorphonuclear leukocyte respiratory burst, bactericidal activity, and migration by pneumolysin. Infection and Immunity, **41**: 1212-1216.
200. Ferrante, A., Rowan-Kelly, B., and Paton, J.C., 1984. Inhibition of in vitro human lymphocyte response by the pneumococcal toxin pneumolysin. Infection and Immunity, **46**: 585-589.
201. Yuste, J., Botto, M., Paton, J.C., Holden, D.W., and Brown, J.S., 2005. Additive inhibition of complement deposition by pneumolysin and PspA facilitates Streptococcus pneumoniae septicemia. J Immunol, **175**: 1813-1819.
202. Takeuchi, O. and Akira, S., 2010. Pattern recognition receptors and inflammation. Cell, **140**: 805-820.
203. Schwandner, R., Dziarski, R., Wesche, H., Rothe, M., and Kirschning, C.J., 1999. Peptidoglycan- and lipoteichoic acid-induced cell activation is mediated by toll-like receptor 2. Journal of Biological Chemistry, **274**: 17406-17409.
204. Michelsen, K.S., Aicher, A., Mohaupt, M., Hartung, T., Dimmeler, S., Kirschning, C.J., and Schumann, R.R., 2001. The role of toll-like receptors (TLRs) in bacteria-induced maturation of murine dendritic cells (DCs) - Peptidoglycan and lipoteichoic acid are inducers of DC maturation and require TLR2. Journal of Biological Chemistry, **276**: 25680-25686.
205. Malley, R., Henneke, P., Morse, S.C., Cieslewicz, M.J., Lipsitch, M., Thompson, C.M., Kurt-Jones, E., Paton, J.C., Wessels, M.R., and Golenbock, D.T., 2003. Recognition of pneumolysin by toll-like receptor 4 confers resistance to

pneumococcal infection. Proceedings of the National Academy of Sciences of the United States of America, **100**: 1966-1971.
206. Akira, S., Takeda, K., and Kaisho, T., 2001. Toll-like receptors: critical proteins linking innate and acquired immunity. Nature Immunology, **2**: 675-680.
207. Khan, A.Q., Chen, Q.Y., Wu, Z.Q., Paton, J.C., and Snapper, C.M., 2005. Both innate immunity and type 1 humoral immunity to Streptococcus pneumoniae are mediated by MyD88 but differ in their relative levels of dependence on Toll-like receptor 2. Infection and Immunity, **73**: 298-307.
208. Lee, K.S., Scanga, C.A., Bachelder, E.M., Chen, Q.Y., and Snapper, C.M., 2007. TLR2 synergizes with both TLR4 and TLR9 for induction of the MyD88-dependent splenic cytokine and chemokine response to Streptococcus pneumoniae. Cellular Immunology, **245**: 103-110.
209. Koppe, U., Suttorp, N., and Opitz, B., 2012. Recognition of Streptococcus pneumoniae by the innate immune system. Cellular Microbiology, **14**: 460-466.
210. Letiembre, M., Echchannaoui, H., Bachmann, P., Ferracin, F., Nieto, C., Espinosa, M., and Landmann, R., 2005. Toll-like receptor 2 deficiency delays pneumococcal phagocytosis and impairs oxidative killing by granulocytes. Infection and Immunity, **73**: 8397-8401.
211. Albiger, B., Dahlberg, S., Sandgren, A., Wartha, F., Beiter, K., Katsuragi, H., Akira, S., Normark, S., and Henriques-Normark, B., 2007. Toll-like receptor 9 acts at an early stage in host defence against pneumococcal infection. Cellular Microbiology, **9**: 633-644.
212. Davis, K.M., Nakamura, S., and Weiser, J.N., 2011. Nod2 sensing of lysozyme-digested peptidoglycan promotes macrophage recruitment and clearance of S. pneumoniae colonization in mice. Journal of Clinical Investigation, **121**: 3666-3676.
213. McNeela, E.A., Burke, A., Neill, D.R., Baxter, C., Fernandes, V.E., Ferreira, D., Smeaton, S., El-Rachkidy, R., McLoughlin, R.M., Mori, A., Moran, B., Fitzgerald, K.A., Tschopp, J., Petrilli, V., Andrew, P.W., Kadioglu, A., and Lavelle, E.C., 2010. Pneumolysin activates the NLRP3 inflammasome and promotes proinflammatory cytokines independently of TLR4. PLoS Pathog, **6**: e1001191.
214. Szalai, A.J., Agrawal, A., Greenhough, T.J., and Volanakis, J.E., 1997. C-reactive protein: structural biology, gene expression, and host defense function. Immunol Res, **16**: 127-136.
215. Mold, C., Rodic-Polic, B., and Du Clos, T.W., 2002. Protection from Streptococcus pneumoniae infection by C-reactive protein and natural antibody requires complement but not Fc gamma receptors. J Immunol, **168**: 6375-6381.
216. Carroll, M.C., 2004. The complement system in regulation of adaptive immunity. Nature Immunology, **5**: 981-986.
217. Opitz, B., van Laak, V., Eitel, J., and Suttorp, N., 2010. Innate immune recognition in infectious and noninfectious diseases of the lung. Am J Respir Crit Care Med, **181**: 1294-1309.
218. Roche, A.M., King, S.J., and Weiser, J.N., 2007. Live attenuated Streptococcus pneumoniae strains induce serotype-independent mucosal and systemic protection in mice. Infection and Immunity, **75**: 2469-2475.
219. Richards, L., Ferreira, D.M., Miyaji, E.N., Andrew, P.W., and Kadioglu, A., 2010. The immunising effect of pneumococcal nasopharyngeal colonisation; protection

against future colonisation and fatal invasive disease. Immunobiology, **215**: 251-263.
220. Cohen, J.M., Khandavilli, S., Camberlein, E., Hyams, C., Baxendale, H.E., and Brown, J.S., 2011. Protective Contributions against Invasive Streptococcus pneumoniae Pneumonia of Antibody and Th17-Cell Responses to Nasopharyngeal Colonisation. PLoS One, **6**.
221. Cohen, J.M., Chimalapati, S., de Vogel, C., van Belkum, A., Baxendale, H.E., and Brown, J.S., 2012. Contributions of capsule, lipoproteins and duration of colonisation towards the protective immunity of prior Streptococcus pneumoniae nasopharyngeal colonisation. Vaccine, **30**: 4453-4459.
222. Ferreira, D.M., Neill, D.R., Bangert, M., Gritzfeld, J.F., Green, N., Wright, A.K., Pennington, S.H., Bricio-Moreno, L., Moreno, A.T., Miyaji, E.N., Wright, A.D., Collins, A.M., Goldblatt, D., Kadioglu, A., and Gordon, S.B., 2013. Controlled human infection and rechallenge with Streptococcus pneumoniae reveals the protective efficacy of carriage in healthy adults. Am J Respir Crit Care Med, **187**: 855-864.
223. Wright, A.K., Bangert, M., Gritzfeld, J.F., Ferreira, D.M., Jambo, K.C., Wright, A.D., Collins, A.M., and Gordon, S.B., 2013. Experimental human pneumococcal carriage augments IL-17A-dependent T-cell defence of the lung. PLoS Pathog, **9**: e1003274.
224. Wilson, R., Cohen, J.M., Jose, R.J., de Vogel, C., Baxendale, H., and Brown, J.S., 2015. Protection against Streptococcus pneumoniae lung infection after nasopharyngeal colonization requires both humoral and cellular immune responses. Mucosal Immunology, **8**: 627-639.
225. Overweg, K., Kerr, A., Sluijter, M., Jackson, M.H., Mitchell, T.J., de Jong, A.P.J.M., de Groot, R., and Hermans, P.W.M., 2000. The putative proteinase maturation protein A of Streptococcus pneumoniae is a conserved surface protein with potential to elicit protective immune responses. Infection and Immunity, **68**: 4180-4188.
226. Roche, A.M. and Weiser, J.N., 2010. Identification of the targets of cross-reactive antibodies induced by Streptococcus pneumoniae colonization. Infection and Immunity, **78**: 2231-2239.
227. Rapola, S., Jantti, V., Haikala, R., Syrjanen, R., Carlone, G.M., Sampson, J.S., Briles, D.E., Paton, J.C., Takala, A.K., Kilpi, T.M., and Kayhty, H., 2000. Natural development of antibodies to pneumococcal surface protein A, pneumococcal surface adhesin A, and pneumolysin in relation to pneumococcal carriage and acute otitis media. J Infect Dis, **182**: 1146-1152.
228. Malley, R., 2010. Antibody and cell-mediated immunity to Streptococcus pneumoniae: implications for vaccine development. J Mol Med (Berl), **88**: 135-142.
229. Khan, M.N. and Pichichero, M.E., 2013. CD4 T cell memory and antibody responses directed against the pneumococcal histidine triad proteins PhtD and PhtE following nasopharyngeal colonization and immunization and their role in protection against pneumococcal colonization in mice. Infection and Immunity, **81**: 3781-3792.
230. Dworkin, M.S., Ward, J.W., Hanson, D.L., Jones, J.L., Kaplan, J.E., Adult, and Adolescent Spectrum of, H.I.V.D.P., 2001. Pneumococcal disease among human

immunodeficiency virus-infected persons: incidence, risk factors, and impact of vaccination. Clin Infect Dis, **32**: 794-800.
231. Zhang, L., Li, Z., Wan, Z., Kilby, A., Kilby, J.M., and Jiang, W., 2015. Humoral immune responses to Streptococcus pneumoniae in the setting of HIV-1 infection. Vaccine, **33**: 4430-4436.
232. McCool, T.L. and Weiser, J.N., 2004. Limited role of antibody in clearance of Streptococcus pneumoniae in a murine model of colonization. Infection and Immunity, **72**: 5807-5813.
233. Malley, R., Trzcinski, K., Srivastava, A., Thompson, C.M., Anderson, P.W., and Lipsitch, M., 2005. CD4+ T cells mediate antibody-independent acquired immunity to pneumococcal colonization. Proc Natl Acad Sci U S A, **102**: 4848-4853.
234. Trzcinski, K., Thompson, C., Malley, R., and Lipsitch, M., 2005. Antibodies to conserved pneumococcal antigens correlate with, but are not required for, protection against pneumococcal colonization induced by prior exposure in a mouse model. Infection and Immunity, **73**: 7043-7046.
235. Babb, R., Chen, A., Hirst, T.R., Kara, E.E., McColl, S.R., Ogunniyi, A.D., Paton, J.C., and Alsharifi, M., 2016. Intranasal vaccination with gamma-irradiated Streptococcus pneumoniae whole-cell vaccine provides serotype-independent protection mediated by B-cells and innate IL-17 responses. Clin Sci (Lond), **130**: 697-710.
236. Malley, R., Srivastava, A., Lipsitch, M., Thompson, C.M., Watkins, C., Tzianabos, A., and Anderson, P.W., 2006. Antibody-independent, interleukin-17A-mediated, cross-serotype immunity to pneumococci in mice immunized intranasally with the cell wall polysaccharide. Infection and Immunity, **74**: 2187-2195.
237. Lu, Y.J., Gross, J., Bogaert, D., Finn, A., Bagrade, L., Zhang, Q., Kolls, J.K., Srivastava, A., Lundgren, A., Forte, S., Thompson, C.M., Harney, K.F., Anderson, P.W., Lipsitch, M., and Malley, R., 2008. Interleukin-17A mediates acquired immunity to pneumococcal colonization. PLoS Pathog, **4**: e1000159.
238. Zhang, Z., Clarke, T.B., and Weiser, J.N., 2009. Cellular effectors mediating Th17-dependent clearance of pneumococcal colonization in mice. Journal of Clinical Investigation, **119**: 1899-1909.
239. Aujla, S.J., Chan, Y.R., Zheng, M.Q., Fei, M.J., Askew, D.J., Pociask, D.A., Reinhart, T.A., McAllister, F., Edeal, J., Gaus, K., Husain, S., Kreindler, J.L., Dubin, P.J., Pilewski, J.M., Myerburg, M.M., Mason, C.A., Iwakura, Y., and Kolls, J.K., 2008. IL-22 mediates mucosal host defense against Gram-negative bacterial pneumonia. Nat Med, **14**: 275-281.
240. Chen, K., McAleer, J.P., Lin, Y., Paterson, D.L., Zheng, M.Q., Alcorn, J.F., Weaver, C.T., and Kolls, J.K., 2011. Th17 Cells Mediate Clade-Specific, Serotype-Independent Mucosal Immunity. Immunity, **35**: 997-1009.
241. Lehmann, D., Willis, J., Moore, H.C., Giele, C., Murphy, D., Keil, A.D., Harrison, C., Bayley, K., Watson, M., and Richmond, P., 2010. The changing epidemiology of invasive pneumococcal disease in aboriginal and non-aboriginal western Australians from 1997 through 2007 and emergence of nonvaccine serotypes. Clin Infect Dis, **50**: 1477-1486.
242. Moberley, S., Krause, V., Cook, H., Mulholland, K., Carapetis, J., Torzillo, P., and Andrews, R., 2010. Failure to vaccinate or failure of vaccine? Effectiveness

of the 23-valent pneumococcal polysaccharide vaccine program in Indigenous adults in the Northern Territory of Australia. Vaccine, **28**: 2296-2301.

243. Pilishvili, T., Lexau, C., Farley, M.M., Hadler, J., Harrison, L.H., Bennett, N.M., Reingold, A., Thomas, A., Schaffner, W., Craig, A.S., Smith, P.J., Beall, B.W., Whitney, C.G., Moore, M.R., and Active Bacterial Core Surveillance/Emerging Infections Program, N., 2010. Sustained reductions in invasive pneumococcal disease in the era of conjugate vaccine. J Infect Dis, **201**: 32-41.
244. De Wals, P., Lefebvre, B., Deceuninck, G., and Longtin, J., 2018. Incidence of invasive pneumococcal disease before and during an era of use of three different pneumococcal conjugate vaccines in Quebec. Vaccine, **36**: 421-426.
245. Pollard, A.J., Perrett, K.P., and Beverley, P.C., 2009. Maintaining protection against invasive bacteria with protein-polysaccharide conjugate vaccines. Nature Reviews Immunology, **9**: 213-220.
246. Advisory Committee on Immunization Practices (ACIP), 2010, Licensure of a 13-Valent Pneumococcal Conjugate Vaccine (PCV13) and Recommendations for Use Among Children, in *Morbitity and Mortality Weekly Report*. Centres for Disease Control and Prevention (CDC): U.S. Government Printing Office (GPO), Washington, DC. p. 20402-29371.
247. Brueggemann, A.B., Pai, R., Crook, D.W., and Beall, B., 2007. Vaccine escape recombinants emerge after pneumococcal vaccination in the United States. PLoS Pathog, **3**: e168.
248. Hicks, L.A., Harrison, L.H., Flannery, B., Hadler, J.L., Schaffner, W., Craig, A.S., Jackson, D., Thomas, A., Beall, B., Lynfield, R., Reingold, A., Farley, M.M., and Whitney, C.G., 2007. Incidence of pneumococcal disease due to non-pneumococcal conjugate vaccine (PCV7) serotypes in the United States during the era of widespread PCV7 vaccination, 1998-2004. J Infect Dis, **196**: 1346-1354.
249. Kaplan, S.L., Barson, W.J., Lin, P.L., Romero, J.R., Bradley, J.S., Tan, T.Q., Hoffman, J.A., Givner, L.B., and Mason, E.O., Jr., 2013. Early trends for invasive pneumococcal infections in children after the introduction of the 13-valent pneumococcal conjugate vaccine. Pediatr Infect Dis J, **32**: 203-207.
250. Liyanapathirana, V., Nelson, E.A., Ang, I., Subramanian, R., Ma, H., and Ip, M., 2015. Emergence of serogroup 15 Streptococcus pneumoniae of diverse genetic backgrounds following the introduction of pneumococcal conjugate vaccines in Hong Kong. Diagn Microbiol Infect Dis, **81**: 66-70.
251. Weinberger, R., von Kries, R., van der Linden, M., Rieck, T., Siedler, A., and Falkenhorst, G., 2018. Invasive pneumococcal disease in children under 16years of age: Incomplete rebound in incidence after the maximum effect of PCV13 in 2012/13 in Germany. Vaccine, **36**: 572-577.
252. Izurieta, P., Bahety, P., Adegbola, R., Clarke, C., and Hoet, B., 2017. Public health impact of pneumococcal conjugate vaccine infant immunization programs: assessment of invasive pneumococcal disease burden and serotype distribution. Expert Rev Vaccines.
253. Alari, A., Chaussade, H., Domenech De Celles, M., Le Fouler, L., Varon, E., Opatowski, L., Guillemot, D., and Watier, L., 2016. Impact of pneumococcal conjugate vaccines on pneumococcal meningitis cases in France between 2001 and 2014: a time series analysis. BMC Med, **14**: 211.
254. Chapoutot, A.G., Dessein, R., Guilluy, O., Lagree, M., Wallet, F., Varon, E., Martinot, A., and Dubos, F., 2016. Impact of the 13-valent pneumococcal

conjugate vaccine on the incidence of pneumococcal meningitis in children. Epidemiol Infect, **144**: 607-611.
255. Brouwer, M.C. and van de Beek, D., 2018. Epidemiology of community-acquired bacterial meningitis. Curr Opin Infect Dis, **31**: 78-84.
256. Olarte, L., Barson, W.J., Barson, R.M., Lin, P.L., Romero, J.R., Tan, T.Q., Givner, L.B., Bradley, J.S., Hoffman, J.A., Hulten, K.G., Mason, E.O., and Kaplan, S.L., 2015. Impact of the 13-Valent Pneumococcal Conjugate Vaccine on Pneumococcal Meningitis in US Children. Clin Infect Dis, **61**: 767-775.
257. Farrell, D.J., Klugman, K.P., and Pichichero, M., 2007. Increased antimicrobial resistance among nonvaccine serotypes of Streptococcus pneumoniae in the pediatric population after the introduction of 7-valent pneumococcal vaccine in the United States. Pediatric Infectious Disease Journal, **26**: 123-128.
258. Paul W Roche, V.K., Heather Cook, Jenny Barralet David Coleman, Amy Sweeny, James Fielding, Carolien Giele, Robin Gilmour, Ros Holland, Riemke Kampen (Enhanced Invasive Pneumococcal Disease Surveillance Working Group), 2008. INVASIVE PNEUMOCOCCAL DISEASE IN AUSTRALIA, 2006. Commun Dis Intell, **32**: 18-30.
259. Imohl, M., Reinert, R.R., and van der Linden, M., 2010. Temporal Variations among Invasive Pneumococcal Disease Serotypes in Children and Adults in Germany (1992-2008). Int J Microbiol, **2010**: 874189.
260. Croucher, N.J., Finkelstein, J.A., Pelton, S.I., Mitchell, P.K., Lee, G.M., Parkhill, J., Bentley, S.D., Hanage, W.P., and Lipsitch, M., 2013. Population genomics of post-vaccine changes in pneumococcal epidemiology. Nat Genet, **45**: 656-663.
261. Pai, R., Moore, M.R., Pilishvili, T., Gertz, R.E., Whitney, C.G., Beall, B., and Surveillance, A.B.C., 2005. Postvaccine genetic structure of Streptococcus pneumoniae serotype 19A from children in the United States. Journal of Infectious Diseases, **192**: 1988-1995.
262. Pelton, S.I., Huot, H., Finkelstein, A.A., Bishop, C.J., Hsu, K.K., Kellenberg, J., Huang, S.S., Goldstein, R., and Hanage, W.P., 2007. Emergence of 19A as virulent and multidrug resistant pneumococcus in Massachusetts following universal immunization of infants with pneumococcal conjugate vaccine. Pediatric Infectious Disease Journal, **26**: 468-472.
263. Techasaensiri, C., Messina, A.F., Katz, K., Ahmad, N., Huang, R., and McCracken, G.H., Jr., 2010. Epidemiology and evolution of invasive pneumococcal disease caused by multidrug resistant serotypes of 19A in the 8 years after implementation of pneumococcal conjugate vaccine immunization in Dallas, Texas. Pediatr Infect Dis J, **29**: 294-300.
264. Smith, M.W., Schmidt, J.E., Rehg, J.E., Orihuela, C.J., and McCullers, J.A., 2007. Induction of pro- and anti-inflammatory molecules in a mouse model of pneumococcal pneumonia after influenza. Comparative Medicine, **57**: 82-89.
265. Sun, K. and Metzger, D.W., 2008. Inhibition of pulmonary antibacterial defense by interferon-gamma during recovery from influenza infection. Nat Med, **14**: 558-564.
266. Chien, Y.W., Klugman, K.P., and Morens, D.M., 2009. Bacterial pathogens and death during the 1918 influenza pandemic. N Engl J Med, **361**: 2582-2583.
267. Nelson, G.E., Gershman, K.A., Swerdlow, D.L., Beall, B.W., and Moore, M.R., 2012. Invasive Pneumococcal Disease and Pandemic (H1N1) 2009, Denver, Colorado, USA. Emerging Infectious Diseases, **18**: 208-216.

268. Short, K.R., Habets, M.N., Hermans, P.W.M., and Diavatopoulos, D.A., 2012. Interactions between Streptococcus pneumoniae and influenza virus: a mutually beneficial relationship? Future Microbiology, **7**: 609-624.
269. Fineberg, H.V., 2014. Pandemic preparedness and response--lessons from the H1N1 influenza of 2009. N Engl J Med, **370**: 1335-1342.
270. Kash, J.C., Walters, K.A., Davis, A.S., Sandouk, A., Schwartzman, L.M., Jagger, B.W., Chertow, D.S., Li, Q., Kuestner, R.E., Ozinsky, A., and Taubenberger, J.K., 2011. Lethal synergism of 2009 pandemic H1N1 influenza virus and Streptococcus pneumoniae coinfection is associated with loss of murine lung repair responses. MBio, **2**.
271. Diavatopoulos, D.A., Short, K.R., Price, J.T., Wilksch, J.J., Brown, L.E., Briles, D.E., Strugnell, R.A., and Wijburg, O.L., 2010. Influenza A virus facilitates Streptococcus pneumoniae transmission and disease. Faseb Journal, **24**: 1789-1798.
272. McCullers, J.A., McAuley, J.L., Browall, S., Iverson, A.R., Boyd, K.L., and Normark, B.H., 2010. Influenza Enhances Susceptibility to Natural Acquisition of and Disease due to Streptococcus pneumoniae in Ferrets. Journal of Infectious Diseases, **202**: 1287-1295.
273. Nakamura, S., Davis, K.M., and Weiser, J.N., 2011. Synergistic stimulation of type I interferons during influenza virus coinfection promotes Streptococcus pneumoniae colonization in mice. Journal of Clinical Investigation, **121**: 3657-3665.
274. Tong, H.H., Weiser, J.N., James, M.A., and DeMaria, T.F., 2001. Effect of influenza A virus infection on nasopharyngeal colonization and otitis media induced by transparent or opaque phenotype variants of Streptococcus pneumoniae in the chinchilla model. Infection and Immunity, **69**: 602-606.
275. McCullers, J.A. and Bartmess, K.C., 2003. Role of neuraminidase in lethal synergism between influenza virus and Streptococcus pneumoniae. J Infect Dis, **187**: 1000-1009.
276. Horner, G.J. and Gray, F.D., Jr., 1973. Effect of uncomplicated, presumptive influenza on the diffusing capacity of the lung. Am Rev Respir Dis, **108**: 866-869.
277. Short, K.R., Reading, P.C., Brown, L.E., Pedersen, J., Gilbertson, B., Job, E.R., Edenborough, K.M., Habets, M.N., Zomer, A., Hermans, P.W., Diavatopoulos, D.A., and Wijburg, O.L., 2013. Influenza-induced inflammation drives pneumococcal otitis media. Infection and Immunity, **81**: 645-652.
278. Shahangian, A., Chow, E.K., Tian, X.L., Kang, J.R., Ghaffari, A., Liu, S.Y., Belperio, J.A., Cheng, G.H., and Deng, J.C., 2009. Type I IFNs mediate development of postinfluenza bacterial pneumonia in mice. Journal of Clinical Investigation, **119**: 1910-1920.
279. Li, W., Moltedo, B., and Moran, T.M., 2012. Type I interferon induction during influenza virus infection increases susceptibility to secondary Streptococcus pneumoniae infection by negative regulation of gammadelta T cells. J Virol, **86**: 12304-12312.
280. van der Poll, T., Marchant, A., Keogh, C.V., Goldman, M., and Lowry, S.F., 1996. Interleukin-10 impairs host defense in murine pneumococcal pneumonia. J Infect Dis, **174**: 994-1000.

281. McCullers, J.A. and Rehg, J.E., 2002. Lethal synergism between influenza virus and Streptococcus pneumoniae: characterization of a mouse model and the role of platelet-activating factor receptor. J Infect Dis, **186**: 341-350.
282. Ballinger, M.N. and Standiford, T.J., 2010. Postinfluenza bacterial pneumonia: host defenses gone awry. J Interferon Cytokine Res, **30**: 643-652.
283. Small, C.L., Shaler, C.R., McCormick, S., Jeyanathan, M., Damjanovic, D., Brown, E.G., Arck, P., Jordana, M., Kaushic, C., Ashkar, A.A., and Xing, Z., 2010. Influenza infection leads to increased susceptibility to subsequent bacterial superinfection by impairing NK cell responses in the lung. J Immunol, **184**: 2048-2056.
284. van der Sluijs, K.F., van Elden, L.J., Nijhuis, M., Schuurman, R., Pater, J.M., Florquin, S., Goldman, M., Jansen, H.M., Lutter, R., and van der Poll, T., 2004. IL-10 is an important mediator of the enhanced susceptibility to pneumococcal pneumonia after influenza infection. J Immunol, **172**: 7603-7609.
285. Wu, Y., Tu, W., Lam, K.T., Chow, K.H., Ho, P.L., Guan, Y., Peiris, J.S., and Lau, Y.L., 2015. Lethal coinfection of influenza virus and Streptococcus pneumoniae lowers antibody response to influenza virus in lung and reduces numbers of germinal center B cells, T follicular helper cells, and plasma cells in mediastinal lymph Node. J Virol, **89**: 2013-2023.
286. Tong, H.H., Long, J.P., Shannon, P.A., and DeMaria, T.F., 2003. Expression of cytokine and chemokine genes by human middle ear epithelial cells induced by influenza A virus and Streptococcus pneumoniae opacity variants. Infection and Immunity, **71**: 4289-4296.
287. Tong, H.H., Long, J.P., Li, D., and DeMaria, T.F., 2004. Alteration of gene expression in human middle ear epithelial cells induced by influenza A virus and its implication for the pathogenesis of otitis media. Microb Pathog, **37**: 193-204.
288. Mina, M.J., Klugman, K.P., Rosch, J.W., and McCullers, J.A., 2015. Live Attenuated Influenza Virus Increases Pneumococcal Translocation and Persistence Within the Middle Ear. Journal of Infectious Diseases, **212**: 195-201.
289. Valour, F., Cotte, L., Voirin, N., Godinot, M., Ader, F., Ferry, T., Vanhems, P., and Chidiac, C., 2014. Vaccination coverage against hepatitis A and B viruses, Streptococcus pneumoniae, seasonal flu, and A(H1N1)2009 pandemic influenza in HIV-infected patients. Vaccine, **32**: 4558-4564.
290. Hmamouchi, I., Winthrop, K., Launay, O., and Dougados, M., 2015. Low rate of influenza and pneumococcal vaccine coverage in rheumatoid arthritis: data from the international COMORA cohort. Vaccine, **33**: 1446-1452.
291. Giese, C., Mereckiene, J., Danis, K., O'Donnell, J., O'Flanagan, D., and Cotter, S., 2016. Low vaccination coverage for seasonal influenza and pneumococcal disease among adults at-risk and health care workers in Ireland, 2013: The key role of GPs in recommending vaccination. Vaccine, **34**: 3657-3662.
292. Gilchrist, S.A., Nanni, A., and Levine, O., 2012. Benefits and effectiveness of administering pneumococcal polysaccharide vaccine with seasonal influenza vaccine: an approach for policymakers. Am J Public Health, **102**: 596-605.
293. Ozgur, S.K., Beyazova, U., Kemaloglu, Y.K., Maral, I., Sahin, F., Camurdan, A.D., Kizil, Y., Dinc, E., and Tuzun, H., 2006. Effectiveness of inactivated influenza vaccine for prevention of otitis media in children. Pediatr Infect Dis J, **25**: 401-404.

294. Grilli, G., Fuiano, L., Biasio, L.R., Pregliasco, F., Plebani, A., Leibovitz, M., Ugazio, A.G., Vacca, F., and Profeta, M.L., 1997. Simultaneous influenza and pneumococcal vaccination in elderly individuals. Eur J Epidemiol, **13**: 287-291.
295. Nichol, K.L., 1999. The additive benefits of influenza and pneumococcal vaccinations during influenza seasons among elderly persons with chronic lung disease. Vaccine, **17 Suppl 1**: S91-93.
296. Chan, T.C., Hung, I.F., Luk, J.K., Shea, Y.F., Chan, F.H., Woo, P.C., and Chu, L.W., 2012. Prevention of mortality and pneumonia among nursing home older adults by dual pneumococcal and seasonal influenza vaccination during a pandemic caused by novel pandemic influenza A (H1N1). J Am Med Dir Assoc, **13**: 698-703.
297. Chang, Y.C., Chou, Y.J., Liu, J.Y., Yeh, T.F., and Huang, N., 2012. Additive benefits of pneumococcal and influenza vaccines among elderly persons aged 75 years or older in Taiwan--a representative population-based comparative study. J Infect, **65**: 231-238.
298. Dominguez, A., Castilla, J., Godoy, P., Delgado-Rodriguez, M., Saez, M., Soldevila, N., Astray, J., Mayoral, J.M., Martin, V., Quintana, J.M., Gonzalez-Candelas, F., Galan, J.C., Tamames, S., Castro, A., Baricot, M., Garin, O., Pumarola, T., Cases, C., and Controls in Pandemic Influenza Working, G., 2013. Effectiveness of vaccination with 23-valent pneumococcal polysaccharide vaccine in preventing hospitalization with laboratory confirmed influenza during the 2009-2010 and 2010-2011 seasons. Hum Vaccin Immunother, **9**: 865-873.
299. Zhang, Y.Y., Tang, X.F., Du, C.H., Wang, B.B., Bi, Z.W., and Dong, B.R., 2016. Comparison of dual influenza and pneumococcal polysaccharide vaccination with influenza vaccination alone for preventing pneumonia and reducing mortality among the elderly: A meta-analysis. Hum Vaccin Immunother, **12**: 3056-3064.
300. Sumitani, M., Tochino, Y., Kamimori, T., Fujiwara, H., and Fujikawa, T., 2008. Additive inoculation of influenza vaccine and 23-valent pneumococcal polysaccharide vaccine to prevent lower respiratory tract infections in chronic respiratory disease patients. Intern Med, **47**: 1189-1197.
301. Frenck, R.W., Jr., Gurtman, A., Rubino, J., Smith, W., van Cleeff, M., Jayawardene, D., Giardina, P.C., Emini, E.A., Gruber, W.C., Scott, D.A., and Schmole-Thoma, B., 2012. Randomized, controlled trial of a 13-valent pneumococcal conjugate vaccine administered concomitantly with an influenza vaccine in healthy adults. Clin Vaccine Immunol, **19**: 1296-1303.
302. Schwarz, T.F., Flamaing, J., Rumke, H.C., Penzes, J., Juergens, C., Wenz, A., Jayawardene, D., Giardina, P., Emini, E.A., Gruber, W.C., and Schmoele-Thoma, B., 2011. A randomized, double-blind trial to evaluate immunogenicity and safety of 13-valent pneumococcal conjugate vaccine given concomitantly with trivalent influenza vaccine in adults aged ≥65 years. Vaccine, **29**: 5195-5202.
303. Ofori-Anyinam, O., Leroux-Roels, G., Drame, M., Aerssens, A., Maes, C., Amanullah, A., Schuind, A., Li, P., Jain, V.K., and Innis, B.L., 2017. Immunogenicity and safety of an inactivated quadrivalent influenza vaccine co-administered with a 23-valent pneumococcal polysaccharide vaccine versus separate administration, in adults ≥50years of age: Results from a phase III, randomized, non-inferiority trial. Vaccine, **35**: 6321-6328.
304. Elliott, L.H., McCormick, J.B., and Johnson, K.M., 1982. Inactivation of Lassa, Marburg, and Ebola viruses by gamma irradiation. J Clin Microbiol, **16**: 704-708.

305. Lahtz, C., Bates, S.E., Jiang, Y., Li, A.X., Wu, X., Hahn, M.A., and Pfeifer, G.P., 2012. Gamma irradiation does not induce detectable changes in DNA methylation directly following exposure of human cells. PLoS One, **7**: e44858.
306. Jordan, R.T. and Kempe, L.L., 1956. Inactivation of some animal viruses with gamma radiation from cobalt-60. Proc Soc Exp Biol Med, **91**: 212-215.
307. Kaplan, C., 1960. The antigenicity of gamma-irradiated vaccinia virus. J Hyg (Lond), **58**: 391-398.
308. Polley, J.R., 1961. Preparation of non-infective soluble antigens with gamma radiation. Can J Microbiol, **7**: 135-139.
309. World Health Organization, 2004, Annex 4: Guidelines on viral inactivation and removal procedures intended to assure the viral safety of human blood plasma products. , in *WHO Technical Report*.
310. Department of Agriculture Fisheries and Forestry Biosecurity, 2014, 'Gamma Irradiation as a Treatment to Address Pathogens of Animal Biosecurity Concern - Final Policy Review'. Canberra, CC BY 3.0.
311. Lomax, M.E., Folkes, L.K., and O'Neill, P., 2013. Biological consequences of radiation-induced DNA damage: relevance to radiotherapy. Clin Oncol (R Coll Radiol), **25**: 578-585.
312. Hume, A.J., Ames, J., Rennick, L.J., Duprex, W.P., Marzi, A., Tonkiss, J., and Muhlberger, E., 2016. Inactivation of RNA Viruses by Gamma Irradiation: A Study on Mitigating Factors. Viruses, **8**.
313. Cheung, D.T., Perelman, N., Tong, D., and Nimni, M.E., 1990. The effect of gamma-irradiation on collagen molecules, isolated alpha-chains, and crosslinked native fibers. J Biomed Mater Res, **24**: 581-589.
314. Feldberg, R.S. and Carew, J.A., 1981. Water radiolysis products and nucleotide damage in gamma-irradiated DNA. Int J Radiat Biol Relat Stud Phys Chem Med, **40**: 11-17.
315. Teebor, G.W., Boorstein, R.J., and Cadet, J., 1988. The repairability of oxidative free radical mediated damage to DNA: a review. Int J Radiat Biol, **54**: 131-150.
316. Lee, S., Lee, S., and Bin Song, K., 2003. Effect of gamma-irradiation on the physicochemical properties of porcine and bovine blood plasma proteins. Food Chemistry, **82**: 521-526.
317. Chiu, S.M., Friedman, L.R., Sokany, N.M., Xue, L.Y., and Oleinick, N.L., 1986. Nuclear matrix proteins are crosslinked to transcriptionally active gene sequences by ionizing radiation. Radiat Res, **107**: 24-38.
318. von Woedtke, T. and Kramer, A., 2008. The limits of sterility assurance. GMS Krankenhhyg Interdiszip, **3**: Doc19.
319. International Atomic Energy Agency, 1990. Sterility assurance level. Guidelines for Industrial Radiation Sterilisation of Disposable Medical Products (Cobalt-60 Gamma-Irradiation), Vol IAEA-TECDOC-539: 39.
320. Alsharifi, M. and Mullbacher, A., 2010. The gamma-irradiated influenza vaccine and the prospect of producing safe vaccines in general. Immunol Cell Biol, **88**: 103-104.
321. Hasanain, F., Guenther, K., Mullett, W.M., and Craven, E., 2014. Gamma sterilization of pharmaceuticals--a review of the irradiation of excipients, active pharmaceutical ingredients, and final drug product formulations. PDA J Pharm Sci Technol, **68**: 113-137.

322. Whitby, J.L. and Gelda, A.K., 1979. Use of incremental doses of cobalt 60 radiation as a means to determine radiation sterilization dose. J Parenter Drug Assoc, **33**: 144-155.
323. Gazso, L. and Gyulai, G. Radiation technology against bioterrorism. in RTO SCI Symposium: systems, concepts and integration (SCI) methods and technologies for defence against terrorism. 2004. London, United Kingdom: Radiation Technology Organisation.
324. Spotts Whitney, E.A., Beatty, M.E., Taylor, T.H., Jr., Weyant, R., Sobel, J., Arduino, M.J., and Ashford, D.A., 2003. Inactivation of Bacillus anthracis spores. Emerg Infect Dis, **9**: 623-627.
325. Chowdhury, M.S.U., Rowley, D.B., Anellis, A., and Levinson, H.S., 1976. Influence of Postirradiation Incubation-Temperature on Recovery of Radiation-Injured Clostridium-Botulinum 62a-Spores. Applied and Environmental Microbiology, **32**: 172-178.
326. Abshire, R.L., Bain, B., and Williams, T., 1980. Resistance and Recovery Studies on Ultraviolet-Irradiated Spores of Bacillus-Pumilus. Applied and Environmental Microbiology, **39**: 695-701.
327. Heidelbaugh, N.D. and Giron, D.J., 1969. Effect of Processing on Recovery of Polio Virus from Inoculated Foods. Journal of Food Science, **34**: 239-241.
328. Bidawid, S., Farber, J.M., and Sattar, S.A., 2000. Inactivation of hepatitis A virus (HAV) in fruits and vegetables by gamma irradiation. International Journal of Food Microbiology, **57**: 91-97.
329. Farkas, J., 1998. Irradiation as a method for decontaminating food - A review. International Journal of Food Microbiology, **44**: 189-204.
330. The U.S. Food and Drug Administration (FDA) *Food Irradiation: What you need to know*. 2014.
331. Farkas, J. and Farkas, C.M., 2011. History and Future of Food Irradiation. Trends Food Science & Technology, **22**: 121-126.
332. Doue, B., 2001. Radiation doses and dose distribution during industrial sterilization by gamma rays and acclerated electron beams (Part I). Medical Device Technol.: 32-35.
333. Erickson, G.A., Landgraf, J.G., Wessman, S.J., Koski, T.A., and Moss, L.M., 1989. Detection and elimination of adventitious agents in continuous cell lines. Dev Biol Stand, **70**: 59-66.
334. House, C., House, J.A., and Yedloutschnig, R.J., 1990. Inactivation of viral agents in bovine serum by gamma irradiation. Can J Microbiol, **36**: 737-740.
335. Kitchen, A.D., Mann, G.F., Harrison, J.F., and Zuckerman, A.J., 1989. Effect of gamma irradiation on the human immunodeficiency virus and human coagulation proteins. Vox Sang, **56**: 223-229.
336. Grieb, T., Forng, R.Y., Brown, R., Owolabi, T., Maddox, E., McBain, A., Drohan, W.N., Mann, D.M., and Burgess, W.H., 2002. Effective use of gamma irradiation for pathogen inactivation of monoclonal antibody preparations. Biologicals, **30**: 207-216.
337. Leveton, L.B., Sox, H.C., Jr., and Stoto, M.A., 1996. HIV and the blood supply: an analysis of crisis decision making. Executive summary. The Institute of Medicine, National Academy of Sciences Committee to Study HIV Transmission Through Blood and Blood Products. Transfusion, **36**: 919-927.

338. Schlegel, A., Immelmann, A., and Kempf, C., 2001. Virus inactivation of plasma-derived proteins by pasteurization in the presence of guanidine hydrochloride. Transfusion, **41**: 382-389.
339. Klamroth, R., Groner, A., and Simon, T.L., 2014. Pathogen inactivation and removal methods for plasma-derived clotting factor concentrates. Transfusion, **54**: 1406-1417.
340. Miekka, S.I., Forng, R.Y., Rohwer, R.G., MacAuley, C., Stafford, R.E., Flack, S.L., MacPhee, M., Kent, R.S., and Drohan, W.N., 2003. Inactivation of viral and prion pathogens by gamma-irradiation under conditions that maintain the integrity of human albumin. Vox Sang, **84**: 36-44.
341. Sanders, B., Koldijk, M., and Schuitemaker, H., *Inactivated Viral Vaccines*, in *Vaccine Analysis: Strategies, Principles, and Control*, B.K. Nunnally, Turula, V.E., and Sitrin, R.D., Editors. 2015, Springer: Berlin.
342. Roberts, J.J. and Warwick, G.P., 1963. The Reaction of Beta-Propiolactone with Guanosine, Deoxyguanylic Acid and Rna. Biochem Pharmacol, **12**: 1441-1442.
343. Colburn, N.H., Richardson, R.G., and Boutwell, R.K., 1965. Studies of the reaction of beta-propiolactone with deoxyguanosine and related compounds. Biochem Pharmacol, **14**: 1113-1118.
344. Mate, U., Solomon, J.J., and Segal, A., 1977. In vitro binding of beta-propiolactone to calf thymus DNA and mouse liver DNA to form 1-(2-carboxyethyl) adenine. Chem Biol Interact, **18**: 327-336.
345. Hemminki, K., 1981. Reactions of beta-propiolactone, beta-butyrolactone and gamma-butyrolactone with nucleic acids. Chem Biol Interact, **34**: 323-331.
346. Segal, A., Solomon, J.J., Mignano, J., and Dino, J., 1981. The isolation and characterization of 3-(2-carboxyethyl)cytosine following in vitro reaction of beta-propiolactone with calf thymus DNA. Chem Biol Interact, **35**: 349-361.
347. Perrin, P. and Morgeaux, S., 1995. Inactivation of DNA by beta-propiolactone. Biologicals, **23**: 207-211.
348. Bonnafous, P., Nicolai, M.C., Taveau, J.C., Chevalier, M., Barriere, F., Medina, J., Le Bihan, O., Adam, O., Ronzon, F., and Lambert, O., 2014. Treatment of influenza virus with beta-propiolactone alters viral membrane fusion. Biochim Biophys Acta, **1838**: 355-363.
349. Furuya, Y., Regner, M., Lobigs, M., Koskinen, A., Mullbacher, A., and Alsharifi, M., 2010. Effect of inactivation method on the cross-protective immunity induced by whole 'killed' influenza A viruses and commercial vaccine preparations. J Gen Virol, **91**: 1450-1460.
350. Furuya, Y., Chan, J., Wan, E.C., Koskinen, A., Diener, K.R., Hayball, J.D., Regner, M., Mullbacher, A., and Alsharifi, M., 2011. Gamma-irradiated influenza virus uniquely induces IFN-I mediated lymphocyte activation independent of the TLR7/MyD88 pathway. PLoS One, **6**: e25765.
351. Cardoso, A.I., Beauverger, P., Gerlier, D., Wild, T.F., and Rabourdin-Combe, C., 1995. Formaldehyde inactivation of measles virus abolishes CD46-dependent presentation of nucleoprotein to murine class I-restricted CTLs but not to class II-restricted helper T cells. Virology, **212**: 255-258.
352. Bachmann, M.F., Kundig, T.M., Kalberer, C.P., Hengartner, H., and Zinkernagel, R.M., 1993. Formalin inactivation of vesicular stomatitis virus impairs T-cell- but not T-help-independent B-cell responses. J Virol, **67**: 3917-3922.

353. Magnani, D.M., Harms, J.S., Durward, M.A., and Splitter, G.A., 2009. Nondividing but Metabolically Active Gamma-Irradiated Brucella melitensis Is Protective against Virulent B. melitensis Challenge in Mice. Infection and Immunity, **77**: 5181-5189.
354. Fisher, J. and Lighter, J., 2013, Tuberculosis Vaccine And Method Of Using Same, United States Patent and Trademark Office, Editor. MICO BIO, INC. : United States.
355. Nishihara, H., Lawrence, C.A., Taplin, G.V., and Carpenter, C.M., 1963. Immunogenicity of Gamma-Irradiated Mycobacterium Tuberculosis H37rv (Giv) in Mice. Am Rev Respir Dis, **88**: 827-832.
356. Roy, S., Sharma, S., Sharma, M., Aggarwal, R., and Bose, M., 2004. Induction of nitric oxide release from the human alveolar epithelial cell line A549: an in vitro correlate of innate immune response to Mycobacterium tuberculosis. Immunology, **112**: 471-480.
357. Fang, F.C., 2012. Antimicrobial actions of nitric oxide. Nitric Oxide-Biology and Chemistry, **27**: S10-S10.
358. Pereira, R.M.S., Calegari-Silva, T.C., Hernandez, M.O., Saliba, A.M., Redner, P., Pessolani, M.C.V., Sarno, E.N., Sampaio, E.P., and Lopes, U.G., 2005. Mycobacterium leprae induces NF-kappa B-dependent transcription repression in human Schwann cells. Biochemical and Biophysical Research Communications, **335**: 20-26.
359. Ammar, A., El-Bialy, A., Yousef, S., EL Nemer, M., 2014. Evaluation of irradiated vaccine prepared from Salmonella typhimurium isolated from buffalo calves. International Journal of Research in Pure and Applied Microbiology, **4**: 10-14.
360. Dabral, N., Martha Moreno, L., Sriranganathan, N., and Vemulapalli, R., 2014. Oral immunization of mice with gamma-irradiated Brucella neotomae induces protection against intraperitoneal and intranasal challenge with virulent B. abortus 2308. PLoS One, **9**: e107180.
361. Alsharifi, M., Furuya, Y., Bowden, T.R., Lobigs, M., Koskinen, A., Regner, M., Trinidad, L., Boyle, D.B., and Mullbacher, A., 2009. Intranasal flu vaccine protective against seasonal and H5N1 avian influenza infections. PLoS One, **4**: e5336.
362. Furuya, Y., Chan, J., Regner, M., Lobigs, M., Koskinen, A., Kok, T., Manavis, J., Li, P., Mullbacher, A., and Alsharifi, M., 2010. Cytotoxic T cells are the predominant players providing cross-protective immunity induced by {gamma}-irradiated influenza A viruses. J Virol, **84**: 4212-4221.
363. Budimir, N., de Haan, A., Meijerhof, T., Gostick, E., Price, D.A., Huckriede, A., and Wilschut, J., 2013. Heterosubtypic cross-protection induced by whole inactivated influenza virus vaccine in mice: influence of the route of vaccine administration. Influenza Other Respir Viruses, **7**: 1202-1209.
364. Paton, J.C., Lock, R.A., Lee, C.J., Li, J.P., Berry, A.M., Mitchell, T.J., Andrew, P.W., Hansman, D., and Boulnois, G.J., 1991. Purification and Immunogenicity of Genetically Obtained Pneumolysin Toxoids and Their Conjugation to Streptococcus-Pneumoniae Type-19f Polysaccharide. Infection and Immunity, **59**: 2297-2304.
365. Alexander, J.E., Lock, R.A., Peeters, C.C.A.M., Poolman, J.T., Andrew, P.W., Mitchell, T.J., Hansman, D., and Paton, J.C., 1994. Immunization of Mice with

Pneumolysin Toxoid Confers a Significant Degree of Protection against at Least 9 Serotypes of Streptococcus pneumoniae. Infection and Immunity, **62**: 5683-5688.

366. Ogunniyi, A.D., Folland, R.L., Briles, D.E., Hollingshead, S.K., and Paton, J.C., 2000. Immunization of mice with combinations of pneumococcal virulence proteins elicits enhanced protection against challenge with Streptococcus pneumoniae. Infection and Immunity, **68**: 3028-3033.
367. Ogunniyi, A.D., Grabowicz, M., Briles, D.E., Cook, J., and Paton, J.C., 2007. Development of a vaccine against invasive pneumococcal disease based on combinations of virulence proteins of Streptococcus pneumoniae. Infection and Immunity, **75**: 350-357.
368. Chen, A., Mann, B., Gao, G.L., Heath, R., King, J., Maissoneuve, J., Alderson, M., Tate, A., Hollingshead, S.K., Tweten, R.K., Briles, D.E., Tuomanen, E.I., and Paton, J.C., 2015. Multivalent Pneumococcal Protein Vaccines Comprising Pneumolysoid with Epitopes/Fragments of CbpA and/or PspA Elicit Strong and Broad Protection. Clinical and Vaccine Immunology, **22**: 1079-1089.
369. Malley, R., Lipsitch, M., Stack, A., Saladino, R., Fleisher, G., Pelton, S., Thompson, C., Briles, D., and Anderson, P., 2001. Intranasal immunization with killed unencapsulated whole cells prevents colonization and invasive disease by capsulated pneumococci. Infection and Immunity, **69**: 4870-4873.
370. Deforest, A., Long, S.S., Lischner, H.W., Girone, J.A., Clark, J.L., Srinivasan, R., Maguire, T.G., Diamond, S.A., Schiller, R.P., Rothstein, E.P., and et al., 1988. Simultaneous administration of measles-mumps-rubella vaccine with booster doses of diphtheria-tetanus-pertussis and poliovirus vaccines. Pediatrics, **81**: 237-246.
371. Dashefsky, B., Wald, E., Guerra, N., and Byers, C., 1990. Safety, Tolerability, and Immunogenicity of Concurrent Administration of Haemophilus-Influenzae Type-B Conjugate Vaccine (Meningococcal Protein Conjugate) with Either Measles-Mumps-Rubella Vaccine or Diphtheria-Tetanus-Pertussis and Oral Poliovirus Vaccines in 14-Month-Old to 23-Month-Old Infants. Pediatrics, **85**: 682-689.
372. Giammanco, G., Livolti, S., Mauro, L., Bilancia, G.G., Salemi, I., Barone, P., and Musumeci, S., 1991. Immune-Response to Simultaneous Administration of a Recombinant-DNA Hepatitis-B Vaccine and Multiple Compulsory Vaccines in Infancy. Vaccine, **9**: 747-750.
373. King, G.E. and Hadler, S.C., 1994. Simultaneous Administration of Childhood Vaccines - an Important Public-Health Policy That Is Safe and Efficacious. Pediatric Infectious Disease Journal, **13**: 394-407.
374. National Center for Immunization and Respiratory Diseases, 2011. General recommendations on immunization --- recommendations of the Advisory Committee on Immunization Practices (ACIP). MMWR Recomm Rep, **60**: 1-64.
375. Grohskopf, L.A., Sokolow, L.Z., Olsen, S.J., Bresee, J.S., Broder, K.R., and Karron, R.A., 2015. Prevention and Control of Influenza with Vaccines: Recommendations of the Advisory Committee on Immunization Practices, United States, 2015-16 Influenza Season. MMWR Morb Mortal Wkly Rep, **64**: 818-825.

376. Yvonnet, B., Coursaget, P., Deubel, V., Diop-Mar, I., Digoutte, J.P., and Chiron, J.P., 1986. Simultaneous administration of hepatitis B and yellow fever vaccines. J Med Virol, **19**: 307-311.
377. Stefano, I., Sato, H.K., Pannuti, C.S., Omoto, T.M., Mann, G., Freire, M.S., Yamamura, A.M.Y., Vasconcelos, P.F.C., Oselka, G.W., Weckx, L.W., Salgado, M.F., Noale, L.F.O., and Souza, V.A.U.F., 1999. Recent immunization against measles does not interfere with the sero-response to yellow fever vaccine. Vaccine, **17**: 1042-1046.
378. Edwards, K. and Decker, M., *Pertussis Vaccine*, in *Vaccines*, S. Plotkin, Orenstein, W., and Offitt, P., Editors. 2008, Saunders PA: USA. p. 471-528.
379. Skibinski, D.A., Baudner, B.C., Singh, M., and O'Hagan, D.T., 2011. Combination vaccines. J Glob Infect Dis, **3**: 63-72.
380. Zepp, F., Schmitt, H.J., Cleerbout, J., Verstraeten, T., Schuerman, L., and Jacquet, J.M., 2009. Review of 8 years of experience with Infanrix hexa (TM) (DTPa-HBV-IPV/Hib hexavalent vaccine). Expert Review of Vaccines, **8**: 663-678.
381. White, C., Halperin, S.A., and Scheifele, D.W., 2009. Pediatric combined formulation DTaP-IPV/Hib vaccine. Expert Rev Vaccines, **8**: 831-840.
382. Eskola, J., Ward, J., Dagan, R., Goldblatt, D., Zepp, F., and Siegrist, C.A., 1999. Combined vaccination of Haemophilus influenzae type b conjugate and diphtheria-tetanus-pertussis containing acellular pertussis. Lancet, **354**: 2063-2068.
383. Greenberg, D.P., Wong, V.K., Partridge, S., Chang, S.J., Jing, J.N., Howe, B.J., and Ward, J.I., 2000. Immunogenicity of a Haemophilus influenzae type b-tetanus toroid conjugate vaccine when mixed with a diphtheria-tetanus-acellular pertussis-hepatitis B combination vaccine. Pediatric Infectious Disease Journal, **19**: 1135-1140.
384. Slack, M.H., Schapira, D., Thwaites, R.J., Burrage, M., Southern, J., Andrews, N., Borrow, R., Goldblatt, D., and Miller, E., 2001. Immune response of premature infants to meningococcal serogroup C and combined diphtheria-tetanus toxoids-acellular pertussis-Haemophilus influenzae type b conjugate vaccines. J Infect Dis, **184**: 1617-1620.
385. Sturgess, A.W., Rush, K., Charbonneau, R.J., Lee, J.I., West, D.J., Sitrin, R.D., and Hennessy, J.P., Jr., 1999. Haemophilus influenzae type b conjugate vaccine stability: catalytic depolymerization of PRP in the presence of aluminum hydroxide. Vaccine, **17**: 1169-1178.
386. Schutze, M.P., Deriaud, E., Przewlocki, G., and Leclerc, C., 1989. Carrier-Induced Epitopic Suppression Is Initiated through Clonal Dominance. J Immunol, **142**: 2635-2640.
387. Burrage, M., Robinson, A., Borrow, R., Andrews, N., Southern, J., Findlow, J., Martin, S., Thornton, C., Goldblatt, D., Corbel, M., Sesardic, D., Cartwright, K., Richmond, P., and Miller, E., 2002. Effect of vaccination with carrier protein on response to meningococcal C conjugate vaccines and value of different immunoassays as predictors of protection. Infection and Immunity, **70**: 4946-4954.
388. Mawas, F., Newman, G., Burns, S., and Corbel, M.J., 2005. Suppression and modulation of cellular and humoral immune responses to Haemophilus influenzae type B (Hib) conjugate vaccine in hib-diphtheria-tetanus toxoids-acellular pertussis combination vaccines: a study in a rat model. J Infect Dis, **191**: 58-64.

389. Mawas, F., Dickinson, R., Douglas-Bardsley, A., Xing, D.K.L., Sesardic, D., and Corbel, M.J., 2006. Immune interaction between components of acellular pertussis-diphtheria-tetanus (DTaP) vaccine and Haemophilus influenzae b (Hib) conjugate vaccine in a rat model. Vaccine, **24**: 3505-3512.
390. Sanofi Pasteur, 2007, Vivaxim® Data Sheet Sanofi Pasteur. p. 1-10.
391. Van Hoecke, C., Lebacq, E., Beran, J., Prymula, R., and Collard, F., 1998. Concomitant vaccination against hepatitis A and typhoid fever. J Travel Med, **5**: 116-120.
392. Beran, J., Beutels, M., Levie, K., Van Damme, P., Dieussaert, I., Gillet, M., Van Hoecke, C., and Tornieporth, N., 2000. A single dose, combined vaccine against typhoid fever and hepatitis A: consistency, immunogenicity and reactogenicity. J Travel Med, **7**: 246-252.
393. van den Dobbelsteen, G.P., van Dijken, H.H., Pillai, S., and van Alphen, L., 2007. Immunogenicity of a combination vaccine containing pneumococcal conjugates and meningococcal PorA OMVs. Vaccine, **25**: 2491-2496.
394. van der Ley, P., Steeghs, L., Hamstra, H.J., ten Hove, J., Zomer, B., and van Alphen, L., 2001. Modification of lipid A biosynthesis in Neisseria meningitidis lpxL mutants: influence on lipopolysaccharide structure, toxicity, and adjuvant activity. Infection and Immunity, **69**: 5981-5990.
395. Aaberge, I.S., Oster, P., Helland, O.S., Kristoffersen, A.C., Ypma, E., Hoiby, E.A., Feiring, B., and Nokleby, H., 2005. Combined administration of meningococcal serogroup B outer membrane vesicle vaccine and conjugated serogroup C vaccine indicated for prevention of meningococcal disease is safe and immunogenic. Clin Diagn Lab Immunol, **12**: 599-605.
396. Blazevic, V., Lappalainen, S., Nurminen, K., Huhti, L., and Vesikari, T., 2011. Norovirus VLPs and rotavirus VP6 protein as combined vaccine for childhood gastroenteritis. Vaccine, **29**: 8126-8133.
397. Tamminen, K., Lappalainen, S., Huhti, L., Vesikari, T., and Blazevic, V., 2013. Trivalent combination vaccine induces broad heterologous immune responses to norovirus and rotavirus in mice. PLoS One, **8**: e70409.
398. Blazevic, V., Malm, M., Arinobu, D., Lappalainen, S., and Vesikari, T., 2016. Rotavirus capsid VP6 protein acts as an adjuvant in vivo for norovirus virus-like particles in a combination vaccine. Human Vaccines & Immunotherapeutics, **12**: 740-748.
399. Babb, R., Chan, J., Khairat, J.E., Furuya, Y., and Alsharifi, M., 2014. Gamma-Irradiated Influenza A Virus Provides Adjuvant Activity to a Co-Administered Poorly Immunogenic SFV Vaccine in Mice. Front Immunol, **5**: 267.
400. Estes, D.M., Tuo, W., Brown, W.C., and Goin, J., 1998. Effects of type I/type II interferons and transforming growth factor-beta on B-cell differentiation and proliferation. Definition of costimulation and cytokine requirements for immunoglobulin synthesis and expression. Immunology, **95**: 604-611.
401. Jego, G., Palucka, A.K., Blanck, J.P., Chalouni, C., Pascual, V., and Banchereau, J., 2003. Plasmacytoid dendritic cells induce plasma cell differentiation through type I interferon and interleukin 6. Immunity, **19**: 225-234.
402. Alsharifi, M., Lobigs, M., Regner, M., Lee, E., Koskinen, A., and Mullbacher, A., 2005. Type I interferons trigger systemic, partial lymphocyte activation in response to viral infection. J Immunol, **175**: 4635-4640.

403. Babb, R., Chen, A., Ogunniyi, A.D., Hirst, T.R., Kara, E.E., McColl, S.R., Alsharifi, M., and Paton, J.C., 2017. Enhanced protective responses to a serotype-independent pneumococcal vaccine when combined with an inactivated influenza vaccine. Clin Sci (Lond), **131**: 169-180.
404. Moore, D.L., 2018. Vaccine recommendations for children and youth for the 2017/2018 influenza season. Paediatr Child Health, **23**: e10-e13.
405. Hai, R., Garcia-Sastre, A., Swayne, D.E., and Palese, P., 2011. A reassortment-incompetent live attenuated influenza virus vaccine for protection against pandemic virus strains. J Virol, **85**: 6832-6843.
406. Hajam, I.A., Dar, P.A., Won, G., and Lee, J.H., 2017. Bacterial ghosts as adjuvants: mechanisms and potential. Veterinary Research, **48**.
407. Schnare, M., Barton, G.M., Holt, A.C., Takeda, K., Akira, S., and Medzhitov, R., 2001. Toll-like receptors control activation of adaptive immune responses. Nature Immunology, **2**: 947-950.
408. Akira, S. and Hemmi, H., 2003. Recognition of pathogen-associated molecular patterns by TLR family. Immunol Lett, **85**: 85-95.
409. Szostak, M.P., Hensel, A., Eko, F.O., Klein, R., Auer, T., Mader, H., Haslberger, A., Bunka, S., Wanner, G., and Lubitz, W., 1996. Bacterial ghosts: non-living candidate vaccines. J Biotechnol, **44**: 161-170.
410. Huter, V., Szostak, M.P., Gampfer, J., Prethaler, S., Wanner, G., Gabor, F., and Lubitz, W., 1999. Bacterial ghosts as drug carrier and targeting vehicles. Journal of Controlled Release, **61**: 51-63.
411. Mayr, U.B., Walcher, P., Azimpour, C., Riedmann, E., Haller, C., and Lubitz, W., 2005. Bacterial ghosts as antigen delivery vehicles. Advanced Drug Delivery Reviews, **57**: 1381-1391.
412. Eko, F.O., Szostak, M.P., Wanner, G., and Lubitz, W., 1994. Production of Vibrio-Cholerae Ghosts (Vcg) by Expression of a Cloned Phage Lysis Gene - Potential for Vaccine Development. Vaccine, **12**: 1231-1237.
413. Riedmann, E.M., Kyd, J.M., Smith, A.M., Gomez-Gallego, S., Jalava, K., Cripps, A.W., and Lubitz, W., 2003. Construction of recombinant S-layer proteins (rSbsA) and their expression in bacterial ghosts - a delivery system for the nontypeable Haemophilus influenzae antigen Omp26. Fems Immunology and Medical Microbiology, **37**: 185-192.
414. Huang, H., Hao, S.G., Li, F., Ye, Z.M., Yang, J.B., and Xiang, J., 2007. CD4(+) Th1 cells promote CD8(+) Tc1 cell survival, memory response, tumor localization and therapy by targeted delivery of interleukin 2 via acquired pMHC I complexes. Immunology, **120**: 148-159.
415. Hacker, G., Redecke, V., and Hacker, H., 2002. Activation of the immune system by bacterial CpG-DNA. Immunology, **105**: 245-251.
416. Wang, W.B., Peng, H.R., Tao, Q.Y., Zhao, X.T., Tang, H.L., Tang, Z.W., Wang, Y., Wang, Y., Zhao, P., and Qi, Z.T., 2014. Serologic assay for avian-origin influenza A (H7N9) virus in adults of Shanghai, Guangzhou and Yunnan, China. Journal of Clinical Virology, **60**: 305-308.
417. Wang, X., Fang, S.S., Lu, X., Xu, C.L., Cowling, B.J., Tang, X.J., Peng, B., Wu, W.H., He, J.F., Tang, Y.J., Xie, X., Mei, S.J., Kong, D.F., Zhang, R.L., Ma, H.W., and Cheng, J.Q., 2014. Seroprevalence to Avian Influenza A(H7N9) Virus Among Poultry Workers and the General Population in Southern China: A Longitudinal Study. Clinical Infectious Diseases, **59**: E76-E83.

418. Yang, S.G., Chen, Y., Cui, D.W., Yao, H.P., Lou, J.Z., Huo, Z.X., Xie, G.L., Yu, F., Zheng, S.F., Yang, Y.D., Zhu, Y.X., Lu, X.Q., Liu, X.L., Lau, S.Y., Chan, J.F.W., To, K.K.W., Yuen, K.Y., Chen, H.L., and Li, L.J., 2014. Avian-Origin Influenza A(H7N9) Infection in Influenza A(H7N9)-Affected Areas of China: A Serological Study. Journal of Infectious Diseases, **209**: 265-269.
419. Feng, K., Divers, E., Ma, Y., and Li, J., 2011. Inactivation of a human norovirus surrogate, human norovirus virus-like particles, and vesicular stomatitis virus by gamma irradiation. Appl Environ Microbiol, **77**: 3507-3517.
420. Ormerod, M.G., 1965. Free-Radical Formation in Irradiated Deoxyribonucleic Acid. Int J Radiat Biol Relat Stud Phys Chem Med, **9**: 291-300.
421. Sullivan, R., Scarpino, P.V., Fassolitis, A.C., Larkin, E.P., and Peeler, J.T., 1973. Gamma radiation inactivation of coxsackievirus B-2. Appl Microbiol, **26**: 14-17.
422. Cottey, R., Rowe, C.A., and Bender, B.S., 2001, Influenza Virus, in *Current Protocols in Immunology*, J.E. Coligan, Editor.
423. Sheffield, F.W., Smith, W., and Belyavin, G., 1954. Purification of influenza virus by red-cell adsorption and elution. Br J Exp Pathol, **35**: 214-222.
424. World Health Organisation, 2005, WHO Expert Committee on Biological Standardization, in *WHO Technical Reports Series, Report No. 54*. World Health Organisation: Geneva, Switzerland.
425. Chan, J., Babb, R., David, S.C., McColl, S.R., and Alsharifi, M., 2016. Vaccine-Induced Antibody Responses Prevent the Induction of Interferon Type I Responses Upon a Homotypic Live Virus Challenge. Scand J Immunol, **83**: 165-173.
426. Ginoza, W. and Norman, A., 1957. Radiosensitive molecular weight of tobacco mosaic virus nucleic acid. Nature, **179**: 520-521.
427. Sanner, T. and Pihl, A., 1969. Significance and mechanism of the indirect effect in bacterial cells. The relative protective effect of added compounds in Escherichia coli B, irradiated in liquid and in frozen suspension. Radiat Res, **37**: 216-227.
428. Kempner, E.S. and Haigler, H.T., 1982. The influence of low temperature on the radiation sensitivity of enzymes. J Biol Chem, **257**: 13297-13299.
429. Hiemstra, H., Tersmette, M., Vos, A.H., Over, J., van Berkel, M.P., and de Bree, H., 1991. Inactivation of human immunodeficiency virus by gamma radiation and its effect on plasma and coagulation factors. Transfusion, **31**: 32-39.
430. Hamer, A.J., Stockley, I., and Elson, R.A., 1999. Changes in allograft bone irradiated at different temperatures. Journal of Bone and Joint Surgery-British Volume, **81B**: 342-344.
431. Kempner, E.S., 2001. Effects of high-energy electrons and gamma rays directly on protein molecules. J Pharm Sci, **90**: 1637-1646.
432. Mullbacher, A., Ada, G.L., and Hla, R.T., 1988. Gamma-irradiated influenza A virus can prime for a cross-reactive and cross-protective immune response against influenza A viruses. Immunol Cell Biol, **66 (Pt 2)**: 153-157.
433. Beauregard, G. and Potier, M., 1985. Temperature dependence of the radiation inactivation of proteins. Anal Biochem, **150**: 117-120.
434. Kempner, E.S. and Miller, J.H., 1994. Effect of environmental conditions on radiation target size analyses. Anal Biochem, **216**: 451-455.
435. Grieb, T.A., Forng, R.Y., Stafford, R.E., Lin, J., Almeida, J., Bogdansky, S., Ronholdt, C., Drohan, W.N., and Burgess, W.H., 2005. Effective use of optimized,

high-dose (50 kGy) gamma irradiation for pathogen inactivation of human bone allografts. Biomaterials, **26**: 2033-2042.
436. International Atomic Energy Agency, 1973, Manual on radiation sterilization of medical and biological materials, in *International Atomic Energy Agency: Technical reports series*. p. 327.
437. Isaacson, R., 2009, Sterilization - Validation qualification requirements, in *Maufacture of Sterile Medicines - Advanced Workshop*. World Health Organisation (WHO).
438. 11137-2:, I., 2013, Sterilization of health care products — Radiation — Part 2: Establishing the sterilization dose. The International Organization for Standardization,.
439. Jenkins E, P.M., Bakken R, et al. *A Multisystem Approach for the Evaluation of Inactivation Efficiency for Venezuelan Equine Encephalitis Virus (VEEV) Vaccine Candidates*. in *12th Annual Conference on Vaccine Research*. 2009. Baltimore, MD.
440. Martin, S.S., Bakken, R.R., Lind, C.M., Garcia, P., Jenkins, E., Glass, P.J., Parker, M.D., Hart, M.K., and Fine, D.L., 2010. Comparison of the immunological responses and efficacy of gamma-irradiated V3526 vaccine formulations against subcutaneous and aerosol challenge with Venezuelan equine encephalitis virus subtype IAB. Vaccine, **28**: 1031-1040.
441. Li, Z.X., Lin, H., Cao, L.M., and Jamil, K., 2007. The influence of gamma irradiation on the allergenicity of shrimp (Penaeus vannamei). Journal of Food Engineering, **79**: 945-949.
442. National Center for Immunization and Respiratory Diseases. *Streptococcus pneumoniae - Clinical Features*. Streptococcus pneumoniae September 6, 2017.
443. Henriques-Normark, B. and Tuomanen, E.I., 2013. The pneumococcus: epidemiology, microbiology, and pathogenesis. Cold Spring Harb Perspect Med, **3**: a010215.
444. Hicks, L.A., Harrison, L.H., Flannery, B., Hadler, J.L., Schaffner, W., Craig, A.S., Jackson, D., Thomas, A., Beall, B., Lynfield, R., Reingold, A., Farley, M.M., and Whitney, C.G., 2007. Incidence of pneumococcal disease due to non-pneumococcal conjugate vaccine (PCV7) serotypes in the united states during the era of widespread PCV7 vaccination, 1998-2004. Journal of Infectious Diseases, **196**: 1346-1354.
445. Sa-Leao, R., Nunes, S., Brito-Avo, A., Frazao, N., Simoes, A.S., Crisostomo, M.I., Paulo, A.C.S., Saldanha, J., Santos-Sanches, I., and de Lencastre, H., 2009. Changes in pneumococcal serotypes and antibiotypes carried by vaccinated and unvaccinated day-care centre attendees in Portugal, a country with widespread use of the seven-valent pneumococcal conjugate vaccine. Clinical Microbiology and Infection, **15**: 1002-1007.
446. Beall, B.W., Gertz, R.E., Hulkower, R.L., Whitney, C.G., Moore, M.R., and Brueggemann, A.B., 2011. Shifting genetic structure of invasive serotype 19A pneumococci in the United States. J Infect Dis, **203**: 1360-1368.
447. Park, I.H., Geno, K.A., Sherwood, L.K., Nahm, M.H., and Beall, B., 2014. Population-based analysis of invasive nontypeable pneumococci reveals that most have defective capsule synthesis genes. PLoS One, **9**.
448. Keller, L.E., Robinson, D.A., and McDaniel, L.S., 2016. Nonencapsulated Streptococcus pneumoniae: Emergence and Pathogenesis. MBio, **7**: e01792.

449. Wilson, R., Cohen, J.M., Reglinski, M., Jose, R.J., Chan, W.Y., Marshall, H., de Vogel, C., Gordon, S., Goldblatt, D., Petersen, F.C., Baxendale, H., and Brown, J.S., 2017. Naturally Acquired Human Immunity to Pneumococcus Is Dependent on Antibody to Protein Antigens. PLoS Pathog, **13**: e1006137.
450. Gupta, R., Shah, P., and Swiatlo, E., 2009. Differential gene expression in Streptococcus pneumoniae in response to various iron sources. Microb Pathog, **47**: 101-109.
451. Bayle, L., Chimalapati, S., Schoehn, G., Brown, J., Vernet, T., and Durmort, C., 2011. Zinc uptake by Streptococcus pneumoniae depends on both AdcA and AdcAII and is essential for normal bacterial morphology and virulence. Mol Microbiol, **82**: 904-916.
452. Shafeeq, S., Kloosterman, T.G., and Kuipers, O.P., 2011. Transcriptional response of Streptococcus pneumoniae to Zn2+) limitation and the repressor/activator function of AdcR. Metallomics, **3**: 609-618.
453. Wakeman, C.A. and Skaar, E.P., 2012. Metalloregulation of Gram-positive pathogen physiology. Curr Opin Microbiol, **15**: 169-174.
454. Jomaa, M., Terry, S., Hale, C., Jones, C., Dougan, G., and Brown, J., 2006. Immunization with the iron uptake ABC transporter proteins PiaA and PiuA prevents respiratory infection with Streptococcus pneumoniae. Vaccine, **24**: 5133-5139.
455. Rajam, G., Anderton, J.M., Carlone, G.M., Sampson, J.S., and Ades, E.W., 2008. Pneumococcal surface adhesin A (PsaA): a review. Crit Rev Microbiol, **34**: 163-173.
456. Rosch, J.W., Gao, G., Ridout, G., Wang, Y.D., and Tuomanen, E.I., 2009. Role of the manganese efflux system mntE for signalling and pathogenesis in Streptococcus pneumoniae. Mol Microbiol, **72**: 12-25.
457. Honsa, E.S., Johnson, M.D., and Rosch, J.W., 2013. The roles of transition metals in the physiology and pathogenesis of Streptococcus pneumoniae. Front Cell Infect Microbiol, **3**: 92.
458. Berry, A.M. and Paton, J.C., 1996. Sequence heterogeneity of PsaA, a 37-kilodalton putative adhesin essential for virulence of Streptococcus pneumoniae. Infection and Immunity, **64**: 5255-5262.
459. Marra, A., Lawson, S., Asundi, J.S., Brigham, D., and Hromockyj, A.E., 2002. In vivo characterization of the psa genes from Streptococcus pneumoniae in multiple models of infection. Microbiology, **148**: 1483-1491.
460. Johnston, J.W., Briles, D.E., Myers, L.E., and Hollingshead, S.K., 2006. Mn2+-dependent regulation of multiple genes in Streptococcus pneumoniae through PsaR and the resultant impact on virulence. Infection and Immunity, **74**: 1171-1180.
461. Kadioglu, A., Weiser, J.N., Paton, J.C., and Andrew, P.W., 2008. The role of Streptococcus pneumoniae virulence factors in host respiratory colonization and disease. Nat Rev Microbiol, **6**: 288-301.
462. Tseng, H.J., McEwan, A.G., Paton, J.C., and Jennings, M.P., 2002. Virulence of Streptococcus pneumoniae: PsaA mutants are hypersensitive to oxidative stress. Infection and Immunity, **70**: 1635-1639.
463. Dintilhac, A., Alloing, G., Granadel, C., and Claverys, J.P., 1997. Competence and virulence of Streptococcus pneumoniae: Adc and PsaA mutants exhibit a

requirement for Zn and Mn resulting from inactivation of putative ABC metal permeases. Mol Microbiol, **25**: 727-739.
464. McAllister, L.J., Tseng, H.J., Ogunniyi, A.D., Jennings, M.P., McEwan, A.G., and Paton, J.C., 2004. Molecular analysis of the psa permease complex of Streptococcus pneumoniae. Mol Microbiol, **53**: 889-901.
465. Ogunniyi, A.D., Mahdi, L.K., Jennings, M.P., McEwan, A.G., McDevitt, C.A., Van der Hoek, M.B., Bagley, C.J., Hoffmann, P., Gould, K.A., and Paton, J.C., 2010. Central role of manganese in regulation of stress responses, physiology, and metabolism in Streptococcus pneumoniae. J Bacteriol, **192**: 4489-4497.
466. Glover, D.T., Hollingshead, S.K., and Briles, D.E., 2008. Streptococcus pneumoniae surface protein PcpA elicits protection against lung infection and fatal sepsis. Infection and Immunity, **76**: 2767-2776.
467. Manzoor, I., Shafeeq, S., and Kuipers, O.P., 2015. Ni2+-Dependent and PsaR-Mediated Regulation of the Virulence Genes pcpA, psaBCA, and prtA in Streptococcus pneumoniae. PLoS One, **10**: e0142839.
468. Harvey, R.M., Ogunniyi, A.D., Chen, A.Y., and Paton, J.C., 2011. Pneumolysin with low hemolytic activity confers an early growth advantage to Streptococcus pneumoniae in the blood. Infection and Immunity, **79**: 4122-4130.
469. Fischer, E.R., Hansen, B.T., Nair, V., Hoyt, F.H., and Dorward, D.W., 2012. Scanning electron microscopy. Curr Protoc Microbiol, **Chapter 2**: Unit 2B 2.
470. Thermo-Scientific, 2002, Instructions: pierce(TM) BCA protein assay kit; product #23225. Pierce Biotechnology, Rockford.
471. Chen, A., Mann, B., Gao, G., Heath, R., King, J., Maissoneuve, J., Alderson, M., Tate, A., Hollingshead, S.K., Tweten, R.K., Briles, D.E., Tuomanen, E.I., and Paton, J.C., 2015. Multivalent Pneumococcal Protein Vaccines Comprising Pneumolysoid with Epitopes/Fragments of CbpA and/or PspA Elicit Strong and Broad Protection. Clin Vaccine Immunol, **22**: 1079-1089.
472. Martin, J.E., Lisher, J.P., Winkler, M.E., and Giedroc, D.P., 2017. Perturbation of manganese metabolism disrupts cell division in Streptococcus pneumoniae. Mol Microbiol, **104**: 334-348.
473. Berry, A.M., Ogunniyi, A.D., Miller, D.C., and Paton, J.C., 1999. Comparative virulence of Streptococcus pneumoniae strains with insertion-duplication, point, and deletion mutations in the pneumolysin gene. Infection and Immunity, **67**: 981-985.
474. Jakubovics, N.S. and Jenkinson, H.F., 2001. Out of the iron age: new insights into the critical role of manganese homeostasis in bacteria. Microbiology-Sgm, **147**: 1709-1718.
475. Grifantini, R., Toukoki, C., Colaprico, A., and Gryllos, I., 2011. Peroxide stimulon and role of PerR in group A Streptococcus. J Bacteriol, **193**: 6539-6551.
476. Scheuhammer, A.M. and Cherian, M.G., 1985. Binding of manganese in human and rat plasma. Biochim Biophys Acta, **840**: 163-169.
477. Krachler, M., Rossipal, E., and Micetic-Turk, D., 1999. Concentrations of trace elements in sera of newborns, young infants, and adults. Biol Trace Elem Res, **68**: 121-135.
478. Martin, J.E. and Giedroc, D.P., 2016. Functional Determinants of Metal Ion Transport and Selectivity in Paralogous Cation Diffusion Facilitator Transporters CzcD and MntE in Streptococcus pneumoniae. J Bacteriol, **198**: 1066-1076.

479. Daly, M.J., Gaidamakova, E.K., Matrosova, V.Y., Vasilenko, A., Zhai, M., Venkateswaran, A., Hess, M., Omelchenko, M.V., Kostandarithes, H.M., Makarova, K.S., Wackett, L.P., Fredrickson, J.K., and Ghosal, D., 2004. Accumulation of Mn(II) in Deinococcus radiodurans facilitates gamma-radiation resistance. Science, **306**: 1025-1028.
480. Daly, M.J., Gaidamakova, E.K., Matrosova, V.Y., Kiang, J.G., Fukumoto, R., Lee, D.Y., Wehr, N.B., Viteri, G.A., Berlett, B.S., and Levine, R.L., 2010. Small-molecule antioxidant proteome-shields in Deinococcus radiodurans. PLoS One, **5**: e12570.
481. Barnese, K., Gralla, E.B., Valentine, J.S., and Cabelli, D.E., 2012. Biologically relevant mechanism for catalytic superoxide removal by simple manganese compounds. Proc Natl Acad Sci U S A, **109**: 6892-6897.
482. Culotta, V.C. and Daly, M.J., 2013. Manganese complexes: diverse metabolic routes to oxidative stress resistance in prokaryotes and yeast. Antioxid Redox Signal, **19**: 933-944.
483. Sharma, A., Gaidamakova, E.K., Matrosova, V.Y., Bennett, B., Daly, M.J., and Hoffman, B.M., 2013. Responses of Mn2+ speciation in Deinococcus radiodurans and Escherichia coli to gamma-radiation by advanced paramagnetic resonance methods. Proc Natl Acad Sci U S A, **110**: 5945-5950.
484. Kloosterman, T.G., Witwicki, R.M., van der Kooi-Pol, M.M., Bijlsma, J.J., and Kuipers, O.P., 2008. Opposite effects of Mn2+ and Zn2+ on PsaR-mediated expression of the virulence genes pcpA, prtA, and psaBCA of Streptococcus pneumoniae. J Bacteriol, **190**: 5382-5393.
485. Hendriksen, W.T., Bootsma, H.J., van Diepen, A., Estevao, S., Kuipers, O.P., de Groot, R., and Hermans, P.W., 2009. Strain-specific impact of PsaR of Streptococcus pneumoniae on global gene expression and virulence. Microbiology, **155**: 1569-1579.
486. Anderson, R.J., Guru, S., Weeratna, R., Makinen, S., Falconer, D.J., Sheppard, N.C., Lang, S., Chang, B., Goenaga, A.L., Green, B.A., Merson, J.R., Gracheck, S.J., and Eyles, J.E., 2016. In vivo screen of genetically conserved Streptococcus pneumoniae proteins for protective immunogenicity. Vaccine, **34**: 6292-6300.
487. Hayday, A.C., 2000. [gamma][delta] cells: a right time and a right place for a conserved third way of protection. Annual Review of Immunology, Vol 31, **18**: 975-1026.
488. Kabelitz, D., Glatzel, A., and Wesch, D., 2000. Antigen recognition by human gammadelta T lymphocytes. Int Arch Allergy Immunol, **122**: 1-7.
489. Cho, J.S., Pietras, E.M., Garcia, N.C., Ramos, R.I., Farzam, D.M., Monroe, H.R., Magorien, J.E., Blauvelt, A., Kolls, J.K., Cheung, A.L., Cheng, G., Modlin, R.L., and Miller, L.S., 2010. IL-17 is essential for host defense against cutaneous Staphylococcus aureus infection in mice. Journal of Clinical Investigation, **120**: 1762-1773.
490. Deetz, C.O., Hebbeler, A.M., Propp, N.A., Cairo, C., Tikhonov, I., and Pauza, C.D., 2006. Gamma interferon secretion by human Vgamma2Vdelta2 T cells after stimulation with antibody against the T-cell receptor plus the Toll-Like receptor 2 agonist Pam3Cys. Infection and Immunity, **74**: 4505-4511.
491. Beetz, S., Wesch, D., Marischen, L., Welte, S., Oberg, H.H., and Kabelitz, D., 2008. Innate immune functions of human gammadelta T cells. Immunobiology, **213**: 173-182.

492. Pietschmann, K., Beetz, S., Welte, S., Martens, I., Gruen, J., Oberg, H.H., Wesch, D., and Kabelitz, D., 2009. Toll-like receptor expression and function in subsets of human gammadelta T lymphocytes. Scand J Immunol, **70**: 245-255.
493. Wesch, D., Peters, C., Oberg, H.H., Pietschmann, K., and Kabelitz, D., 2011. Modulation of gammadelta T cell responses by TLR ligands. Cell Mol Life Sci, **68**: 2357-2370.
494. Blyth, C.C., Webb, S.A., Kok, J., Dwyer, D.E., van Hal, S.J., Foo, H., Ginn, A.N., Kesson, A.M., Seppelt, I., Iredell, J.R., Investigators, A.I., and Investigators, C.M., 2013. The impact of bacterial and viral co-infection in severe influenza. Influenza Other Respir Viruses, **7**: 168-176.
495. Bosch, A.A., Biesbroek, G., Trzcinski, K., Sanders, E.A., and Bogaert, D., 2013. Viral and bacterial interactions in the upper respiratory tract. PLoS Pathog, **9**: e1003057.
496. Chertow, D.S. and Memoli, M.J., 2013. Bacterial coinfection in influenza: a grand rounds review. JAMA, **309**: 275-282.
497. Morens, D.M., Taubenberger, J.K., and Fauci, A.S., 2008. Predominant role of bacterial pneumonia as a cause of death in pandemic influenza: implications for pandemic influenza preparedness. J Infect Dis, **198**: 962-970.
498. Centers for Disease Control and Prevention (CDC), 2009. Bacterial coinfections in lung tissue specimens from fatal cases of 2009 pandemic influenza A (H1N1) - United States, May-August 2009. MMWR Morb Mortal Wkly Rep, **58**: 1071-1074.
499. National Center for Immunization and Respiratory Diseases (NCIRD). *Live Attenuated Influenza Vaccine [LAIV] (The Nasal Spray Flu Vaccine)*. 2018; Available from: https://www.cdc.gov/flu/about/qa/nasalspray.htm.
500. Mackay, L.K., Rahimpour, A., Ma, J.Z., Collins, N., Stock, A.T., Hafon, M.L., Vega-Ramos, J., Lauzurica, P., Mueller, S.N., Stefanovic, T., Tscharke, D.C., Heath, W.R., Inouye, M., Carbone, F.R., and Gebhardt, T., 2013. The developmental pathway for CD103(+)CD8+ tissue-resident memory T cells of skin. Nature Immunology, **14**: 1294-1301.
501. Mueller, S.N., Gebhardt, T., Carbone, F.R., and Heath, W.R., 2013. Memory T cell subsets, migration patterns, and tissue residence. Annual Review of Immunology, Vol 31, **31**: 137-161.
502. Schenkel, J.M. and Masopust, D., 2014. Tissue-resident memory T cells. Immunity, **41**: 886-897.
503. Carbone, F.R., 2015. Tissue-Resident Memory T Cells and Fixed Immune Surveillance in Nonlymphoid Organs. J Immunol, **195**: 17-22.
504. Cibrian, D. and Sanchez-Madrid, F., 2017. CD69: from activation marker to metabolic gatekeeper. European Journal of Immunology, **47**: 946-953.
505. Krammer, F. and Palese, P., 2015. Advances in the development of influenza virus vaccines. Nat Rev Drug Discov, **14**: 167-182.
506. Desheva, Y.A., Leontieva, G.F., Kramskaya, T.A., Smolonogina, T.A., Grabovskaya, K.B., Kiseleva, I.V., Rudenko, L.G., and Suvorov, A.N., 2016. Evaluation in Mouse Model of Combined Virus-bacterial Vaccine Based on Attenuated Influenza A(H7N3) Virus and the Group B Streptococcus Recombinant Polypeptides. Open Microbiol J, **10**: 168-175.
507. McMaster, S.R., Gabbard, J.D., Koutsonanos, D.G., Compans, R.W., Tripp, R.A., Tompkins, S.M., and Kohlmeier, J.E., 2015. Memory T cells generated by prior

exposure to influenza cross react with the novel H7N9 influenza virus and confer protective heterosubtypic immunity. PLoS One, **10**: e0115725.
508. Chang, J.T., Wherry, E.J., and Goldrath, A.W., 2014. Molecular regulation of effector and memory T cell differentiation. Nature Immunology, **15**: 1104-1115.
509. Casey, K.A., Fraser, K.A., Schenkel, J.M., Moran, A., Abt, M.C., Beura, L.K., Lucas, P.J., Artis, D., Wherry, E.J., Hogquist, K., Vezys, V., and Masopust, D., 2012. Antigen-independent differentiation and maintenance of effector-like resident memory T cells in tissues. J Immunol, **188**: 4866-4875.
510. Skon, C.N., Lee, J.Y., Anderson, K.G., Masopust, D., Hogquist, K.A., and Jameson, S.C., 2013. Transcriptional downregulation of S1pr1 is required for the establishment of resident memory CD8+ T cells. Nature Immunology, **14**: 1285-1293.
511. Mueller, S.N. and Mackay, L.K., 2016. Tissue-resident memory T cells: local specialists in immune defence. Nature Reviews Immunology, **16**: 79-89.
512. Williams, A.E., Jose, R.J., Brown, J.S., and Chambers, R.C., 2015. Enhanced inflammation in aged mice following infection with Streptococcus pneumoniae is associated with decreased IL-10 and augmented chemokine production. Am J Physiol Lung Cell Mol Physiol, **308**: L539-549.
513. Neill, D.R., Coward, W.R., Gritzfeld, J.F., Richards, L., Garcia-Garcia, F.J., Dotor, J., Gordon, S.B., and Kadioglu, A., 2014. Density and duration of pneumococcal carriage is maintained by transforming growth factor beta1 and T regulatory cells. Am J Respir Crit Care Med, **189**: 1250-1259.
514. Nakanishi, Y., Lu, B., Gerard, C., and Iwasaki, A., 2009. CD8(+) T lymphocyte mobilization to virus-infected tissue requires CD4(+) T-cell help. Nature, **462**: 510-513.
515. Laidlaw, B.J., Zhang, N., Marshall, H.D., Staron, M.M., Guan, T., Hu, Y., Cauley, L.S., Craft, J., and Kaech, S.M., 2014. CD4+ T cell help guides formation of CD103+ lung-resident memory CD8+ T cells during influenza viral infection. Immunity, **41**: 633-645.
516. Glennie, N.D., Yeramilli, V.A., Beiting, D.P., Volk, S.W., Weaver, C.T., and Scott, P., 2015. Skin-resident memory CD4+ T cells enhance protection against Leishmania major infection. Journal of Experimental Medicine, **212**: 1405-1414.
517. Slutter, B., Van Braeckel-Budimir, N., Abboud, G., Varga, S.M., Salek-Ardakani, S., and Harty, J.T., 2017. Dynamics of influenza-induced lung-resident memory T cells underlie waning heterosubtypic immunity. Sci Immunol, **2**.
518. Kohlmeier, J.E. and Woodland, D.L., 2009. Immunity to respiratory viruses. Annual Review of Immunology, Vol 31, **27**: 61-82.
519. Schenkel, J.M., Fraser, K.A., Vezys, V., and Masopust, D., 2013. Sensing and alarm function of resident memory CD8(+) T cells. Nature Immunology, **14**: 509-513.
520. Ariotti, S., Hogenbirk, M.A., Dijkgraaf, F.E., Visser, L.L., Hoekstra, M.E., Song, J.Y., Jacobs, H., Haanen, J.B., and Schumacher, T.N., 2014. T cell memory. Skin-resident memory CD8(+) T cells trigger a state of tissue-wide pathogen alert. Science, **346**: 101-105.
521. Schenkel, J.M., Fraser, K.A., Beura, L.K., Pauken, K.E., Vezys, V., and Masopust, D., 2014. T cell memory. Resident memory CD8 T cells trigger protective innate and adaptive immune responses. Science, **346**: 98-101.

522. Woodland, D.L. and Kohlmeier, J.E., 2009. Migration, maintenance and recall of memory T cells in peripheral tissues. Nature Reviews Immunology, **9**: 153-161.
523. Walther, E., Xu, Z., Richter, M., Kirchmair, J., Grienke, U., Rollinger, J.M., Krumbholz, A., Saluz, H.P., Pfister, W., Sauerbrei, A., and Schmidtke, M., 2016. Dual Acting Neuraminidase Inhibitors Open New Opportunities to Disrupt the Lethal Synergism between Streptococcus pneumoniae and Influenza Virus. Front Microbiol, **7**: 357.
524. Sedmak, J.J. and Grossberg, S.E., 1973. Interferon bioassay: reduction in yield of myxovirus neuraminidases. J Gen Virol, **21**: 1-7.
525. Rimmelzwaan, G.F., Baars, M., Claas, E.C., and Osterhaus, A.D., 1998. Comparison of RNA hybridization, hemagglutination assay, titration of infectious virus and immunofluorescence as methods for monitoring influenza virus replication in vitro. J Virol Methods, **74**: 57-66.
526. Mohler, L., Flockerzi, D., Sann, H., and Reichl, U., 2005. Mathematical model of influenza A virus production in large-scale microcarrier culture. Biotechnol Bioeng, **90**: 46-58.
527. Pozzi, L.A., Maciaszek, J.W., and Rock, K.L., 2005. Both dendritic cells and macrophages can stimulate naive CD8 T cells in vivo to proliferate, develop effector function, and differentiate into memory cells. J Immunol, **175**: 2071-2081.
528. Sung, J.H., Zhang, H., Moseman, E.A., Alvarez, D., Iannacone, M., Henrickson, S.E., de la Torre, J.C., Groom, J.R., Luster, A.D., and von Andrian, U.H., 2012. Chemokine guidance of central memory T cells is critical for antiviral recall responses in lymph nodes. Cell, **150**: 1249-1263.
529. Chatziandreou, N., Farsakoglu, Y., Palomino-Segura, M., D'Antuono, R., Pizzagalli, D.U., Sallusto, F., Lukacs-Kornek, V., Uguccioni, M., Corti, D., Turley, S.J., Lanzavecchia, A., Carroll, M.C., and Gonzalez, S.F., 2017. Macrophage Death following Influenza Vaccination Initiates the Inflammatory Response that Promotes Dendritic Cell Function in the Draining Lymph Node. Cell Reports, **18**: 2427-2440.
530. Alymova, I.V., Portner, A., Takimoto, T., Boyd, K.L., Babu, Y.S., and McCullers, J.A., 2005. The novel parainfluenza virus hemagglutinin-neuraminidase inhibitor BCX 2798 prevents lethal synergism between a paramyxovirus and Streptococcus pneumoniae. Antimicrob Agents Chemother, **49**: 398-405.
531. Stark, J.M., Stark, M.A., Colasurdo, G.N., and LeVine, A.M., 2006. Decreased bacterial clearance from the lungs of mice following primary respiratory syncytial virus infection. J Med Virol, **78**: 829-838.
532. Kukavica-Ibrulj, I., Hamelin, M.E., Prince, G.A., Gagnon, C., Bergeron, Y., Bergeron, M.G., and Boivin, G., 2009. Infection with human metapneumovirus predisposes mice to severe pneumococcal pneumonia. J Virol, **83**: 1341-1349.
533. Xiang, J., Wunschmann, S., Diekema, D.J., Klinzman, D., Patrick, K.D., George, S.L., and Stapleton, J.T., 2001. Effect of coinfection with GB virus C on survival among patients with HIV infection. N Engl J Med, **345**: 707-714.
534. Madhi, S.A., Klugman, K.P., and Vaccine Trialist, G., 2004. A role for Streptococcus pneumoniae in virus-associated pneumonia. Nat Med, **10**: 811-813.
535. Barton, E.S., White, D.W., Cathelyn, J.S., Brett-McClellan, K.A., Engle, M., Diamond, M.S., Miller, V.L., and Virgin, H.W.t., 2007. Herpesvirus latency confers symbiotic protection from bacterial infection. Nature, **447**: 326-329.

536. Kane, M., Case, L.K., Kopaskie, K., Kozlova, A., MacDearmid, C., Chervonsky, A.V., and Golovkina, T.V., 2011. Successful transmission of a retrovirus depends on the commensal microbiota. Science, **334**: 245-249.
537. Kuss, S.K., Best, G.T., Etheredge, C.A., Pruijssers, A.J., Frierson, J.M., Hooper, L.V., Dermody, T.S., and Pfeiffer, J.K., 2011. Intestinal microbiota promote enteric virus replication and systemic pathogenesis. Science, **334**: 249-252.
538. Johnson, P.T. and Hoverman, J.T., 2012. Parasite diversity and coinfection determine pathogen infection success and host fitness. Proc Natl Acad Sci U S A, **109**: 9006-9011.
539. Thorburn, K., Harigopal, S., Reddy, V., Taylor, N., and van Saene, H.K., 2006. High incidence of pulmonary bacterial co-infection in children with severe respiratory syncytial virus (RSV) bronchiolitis. Thorax, **61**: 611-615.
540. Finelli, L., Fiore, A., Dhara, R., Brammer, L., Shay, D.K., Kamimoto, L., Fry, A., Hageman, J., Gorwitz, R., Bresee, J., and Uyeki, T., 2008. Influenza-associated pediatric mortality in the United States: increase of Staphylococcus aureus coinfection. Pediatrics, **122**: 805-811.
541. Richard, N., Komurian-Pradel, F., Javouhey, E., Perret, M., Rajoharison, A., Bagnaud, A., Billaud, G., Vernet, G., Lina, B., Floret, D., and Paranhos-Baccala, G., 2008. The impact of dual viral infection in infants admitted to a pediatric intensive care unit associated with severe bronchiolitis. Pediatr Infect Dis J, **27**: 213-217.
542. Brundage, J.F. and Shanks, G.D., 2008. Deaths from bacterial pneumonia during 1918-19 influenza pandemic. Emerg Infect Dis, **14**: 1193-1199.
543. Metersky, M.L., Masterton, R.G., Lode, H., File, T.M., Jr., and Babinchak, T., 2012. Epidemiology, microbiology, and treatment considerations for bacterial pneumonia complicating influenza. International Journal of Infectious Diseases, **16**: e321-331.
544. Morris, D.E., Cleary, D.W., and Clarke, S.C., 2017. Secondary Bacterial Infections Associated with Influenza Pandemics. Front Microbiol, **8**: 1041.
545. Chua, B.Y., Wong, C.Y., Mifsud, E.J., Edenborough, K.M., Sekiya, T., Tan, A.C., Mercuri, F., Rockman, S., Chen, W., Turner, S.J., Doherty, P.C., Kelso, A., Brown, L.E., and Jackson, D.C., 2015. Inactivated Influenza Vaccine That Provides Rapid, Innate-Immune-System-Mediated Protection and Subsequent Long-Term Adaptive Immunity. MBio, **6**: e01024-01015.
546. Hoffmann, J., Machado, D., Terrier, O., Pouzol, S., Messaoudi, M., Basualdo, W., Espinola, E.E., Guillen, R.M., Rosa-Calatrava, M., Picot, V., Benet, T., Endtz, H., Russomando, G., and Paranhos-Baccala, G., 2016. Viral and bacterial co-infection in severe pneumonia triggers innate immune responses and specifically enhances IP-10: a translational study. Sci Rep, **6**: 38532.
547. Jiang, Y., Xu, J., Zhou, C., Wu, Z., Zhong, S., Liu, J., Luo, W., Chen, T., Qin, Q., and Deng, P., 2005. Characterization of cytokine/chemokine profiles of severe acute respiratory syndrome. Am J Respir Crit Care Med, **171**: 850-857.
548. Ichikawa, A., Kuba, K., Morita, M., Chida, S., Tezuka, H., Hara, H., Sasaki, T., Ohteki, T., Ranieri, V.M., dos Santos, C.C., Kawaoka, Y., Akira, S., Luster, A.D., Lu, B., Penninger, J.M., Uhlig, S., Slutsky, A.S., and Imai, Y., 2013. CXCL10-CXCR3 enhances the development of neutrophil-mediated fulminant lung injury of viral and nonviral origin. Am J Respir Crit Care Med, **187**: 65-77.

549. Damjanovic, D., Lai, R., Jeyanathan, M., Hogaboam, C.M., and Xing, Z., 2013. Marked improvement of severe lung immunopathology by influenza-associated pneumococcal superinfection requires the control of both bacterial replication and host immune responses. American Journal of Pathology, **183**: 868-880.
550. Okamoto, S., Kawabata, S., Terao, Y., Fujitaka, H., Okuno, Y., and Hamada, S., 2004. The Streptococcus pyogenes capsule is required for adhesion of bacteria to virus-infected alveolar epithelial cells and lethal bacterial-viral superinfection. Infection and Immunity, **72**: 6068-6075.
551. Wang, Y., Gagnon, C.A., Savard, C., Music, N., Srednik, M., Segura, M., Lachance, C., Bellehumeur, C., and Gottschalk, M., 2013. Capsular sialic acid of Streptococcus suis serotype 2 binds to swine influenza virus and enhances bacterial interactions with virus-infected tracheal epithelial cells. Infection and Immunity, **81**: 4498-4508.
552. Wu, N.H., Meng, F., Seitz, M., Valentin-Weigand, P., and Herrler, G., 2015. Sialic acid-dependent interactions between influenza viruses and Streptococcus suis affect the infection of porcine tracheal cells. J Gen Virol, **96**: 2557-2568.
553. Hosaka, Y., Ikeura, A., Harada, Y., Kuroda, K., Hamayasu, H., Suzuki, T., Yamada, K., Kawase, Y., and Suzuki, Y., 2000. Binding of influenza type A viruses to group B Streptococcus and haemagglutination by virus-bound bacteria. J Electron Microsc (Tokyo), **49**: 765-773.
554. Hament, J.M., Aerts, P.C., Fleer, A., van Dijk, H., Harmsen, T., Kimpen, J.L., and Wolfs, T.F., 2005. Direct binding of respiratory syncytial virus to pneumococci: a phenomenon that enhances both pneumococcal adherence to human epithelial cells and pneumococcal invasiveness in a murine model. Pediatric Research, **58**: 1198-1203.
555. Avadhanula, V., Wang, Y., Portner, A., and Adderson, E., 2007. Nontypeable Haemophilus influenzae and Streptococcus pneumoniae bind respiratory syncytial virus glycoprotein. Journal of Medical Microbiology, **56**: 1133-1137.
556. Raza, M.W., Blackwell, C.C., Ogilvie, M.M., Saadi, A.T., Stewart, J., Elton, R.A., and Weir, D.M., 1994. Evidence for the role of glycoprotein G of respiratory syncytial virus in binding of Neisseria meningitidis to HEp-2 cells. FEMS Immunol Med Microbiol, **10**: 25-30.
557. Barretto, N., Hallak, L.K., and Peeples, M.E., 2003. Neuraminidase treatment of respiratory syncytial virus-infected cells or virions, but not target cells, enhances cell-cell fusion and infection. Virology, **313**: 33-43.
558. Pickens, J.A. and Tripp, R.A., 2018. Verdinexor Targeting of CRM1 is a Promising Therapeutic Approach against RSV and Influenza Viruses. Viruses, **10**.
559. Jones, M.K., Watanabe, M., Zhu, S., Graves, C.L., Keyes, L.R., Grau, K.R., Gonzalez-Hernandez, M.B., Iovine, N.M., Wobus, C.E., Vinje, J., Tibbetts, S.A., Wallet, S.M., and Karst, S.M., 2014. Enteric bacteria promote human and mouse norovirus infection of B cells. Science, **346**: 755-759.
560. Robinson, C.M., Jesudhasan, P.R., and Pfeiffer, J.K., 2014. Bacterial lipopolysaccharide binding enhances virion stability and promotes environmental fitness of an enteric virus. Cell Host Microbe, **15**: 36-46.
561. Li, D., Breiman, A., le Pendu, J., and Uyttendaele, M., 2015. Binding to histo-blood group antigen-expressing bacteria protects human norovirus from acute heat stress. Front Microbiol, **6**: 659.

562. Almand, E.A., Moore, M.D., Outlaw, J., and Jaykus, L.A., 2017. Human norovirus binding to select bacteria representative of the human gut microbiota. PLoS One, **12**: e0173124.
563. Erickson, A.K., Jesudhasan, P.R., Mayer, M.J., Narbad, A., Winter, S.E., and Pfeiffer, J.K., 2018. Bacteria Facilitate Enteric Virus Co-infection of Mammalian Cells and Promote Genetic Recombination. Cell Host Microbe, **23**: 77-88 e75.
564. Uchiyama, R., Chassaing, B., Zhang, B., and Gewirtz, A.T., 2014. Antibiotic treatment suppresses rotavirus infection and enhances specific humoral immunity. J Infect Dis, **210**: 171-182.

Appendix

- Gating Strategies for Flow Cytometry
- Statement of Authorship Form (Chapter 2)
- Published Manuscript:

  David, S.C., Lau, J., Singleton, E.V., Babb, R., Davies, J., Hirst, T.R., McColl, S.R., Paton, J.C., Alsharifi, M., 2017. The effect of gamma-irradiation conditions on the immunogenicity of whole-inactivated Influenza A virus vaccine. *Vaccine,* **35**: 1071-1079.

Flow Cytometry Gating Strategies

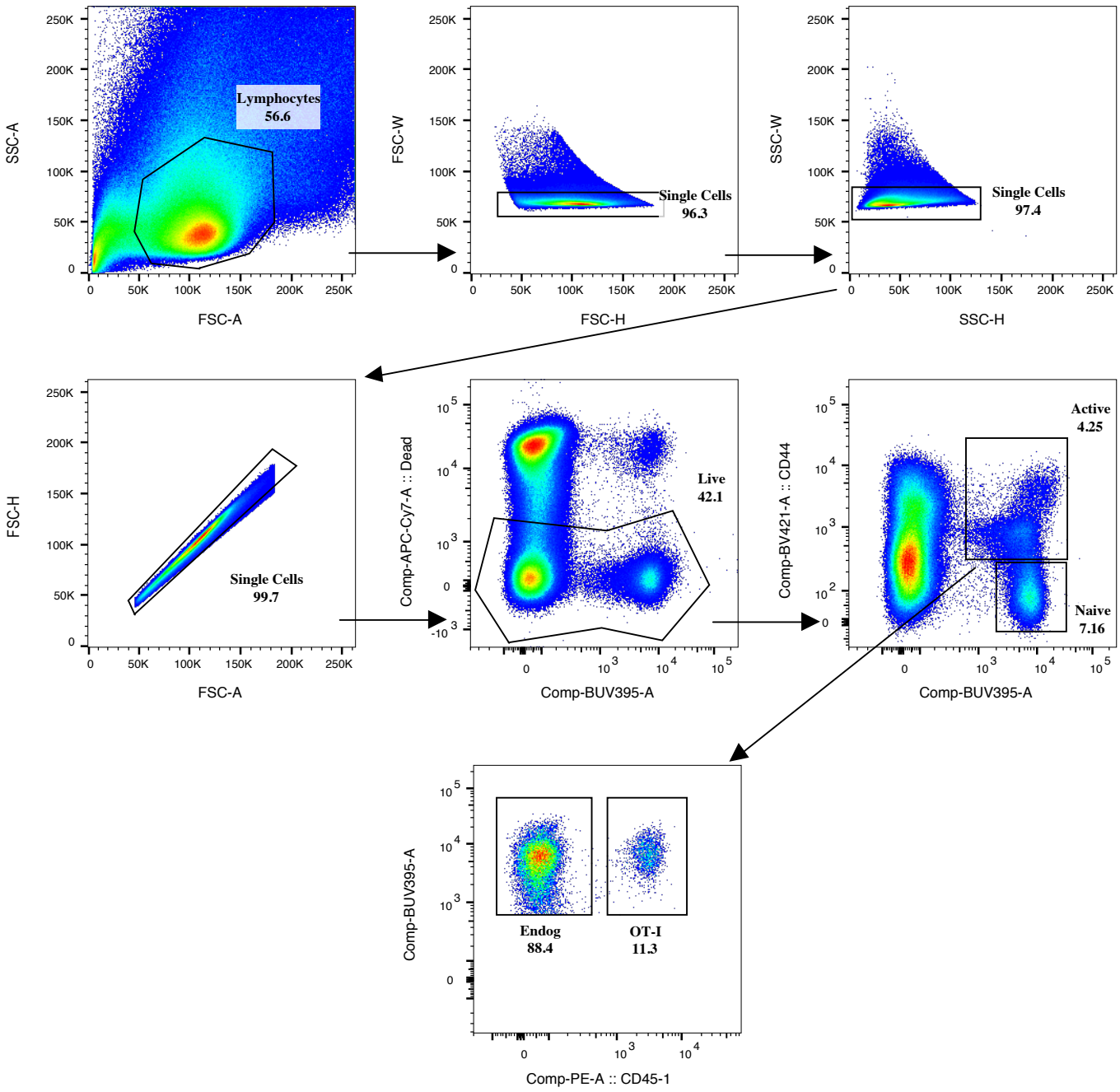

Appendix 1. Gating Strategy for detection of transferred OT-I cells. Transferred OT-I cells from CD45.1 mice were identified by first gating on size and singularity, followed by exclusion of dead cells. Live cells were then gated on CD8 (BUV395) and CD44 (BV421) to identify activated $CD8^+$ T-cells. Expression of CD45.1 on these activated cells then allowed discrimination of endogenous $CD8^+$ T-cells and transferred OT-I cells.

Cells pre-gated on Lymphocytes → Single Cells → Live/Dead

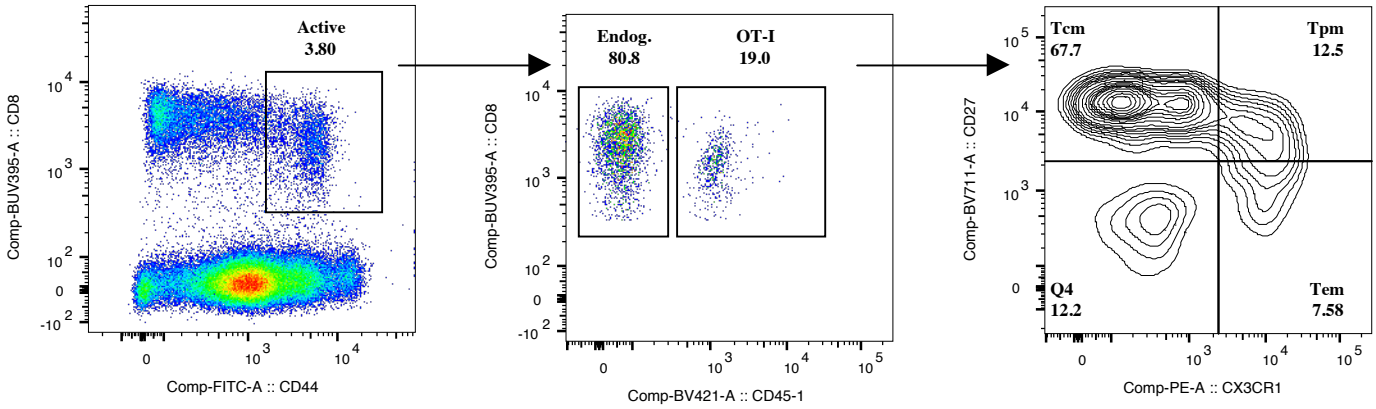

Appendix 2. Gating strategy for detection of circulating memory cell subsets T_{CM} (central memory), T_{PM} (peripheral memory), and T_{EM} (effector memory). Cells were gated based on size and singularity, followed by exclusion of dead cells, as per Appendix 1. Live cells were then gated on CD8 and CD44 to identify activated $CD8^+$ T-cells. CD45.1 expression allowed identification of endogenous $CD8^+$ T-cells and transferred OT-I cells. Each population was then gated based on CD27 and CX3CR1 to identify circulating memory cell subsets T_{CM} ($CD27^+CX3CR1^-$), T_{PM} ($CD27^+CX3CR1^+$), and T_{EM} ($CD27^-CX3CR1^+$).

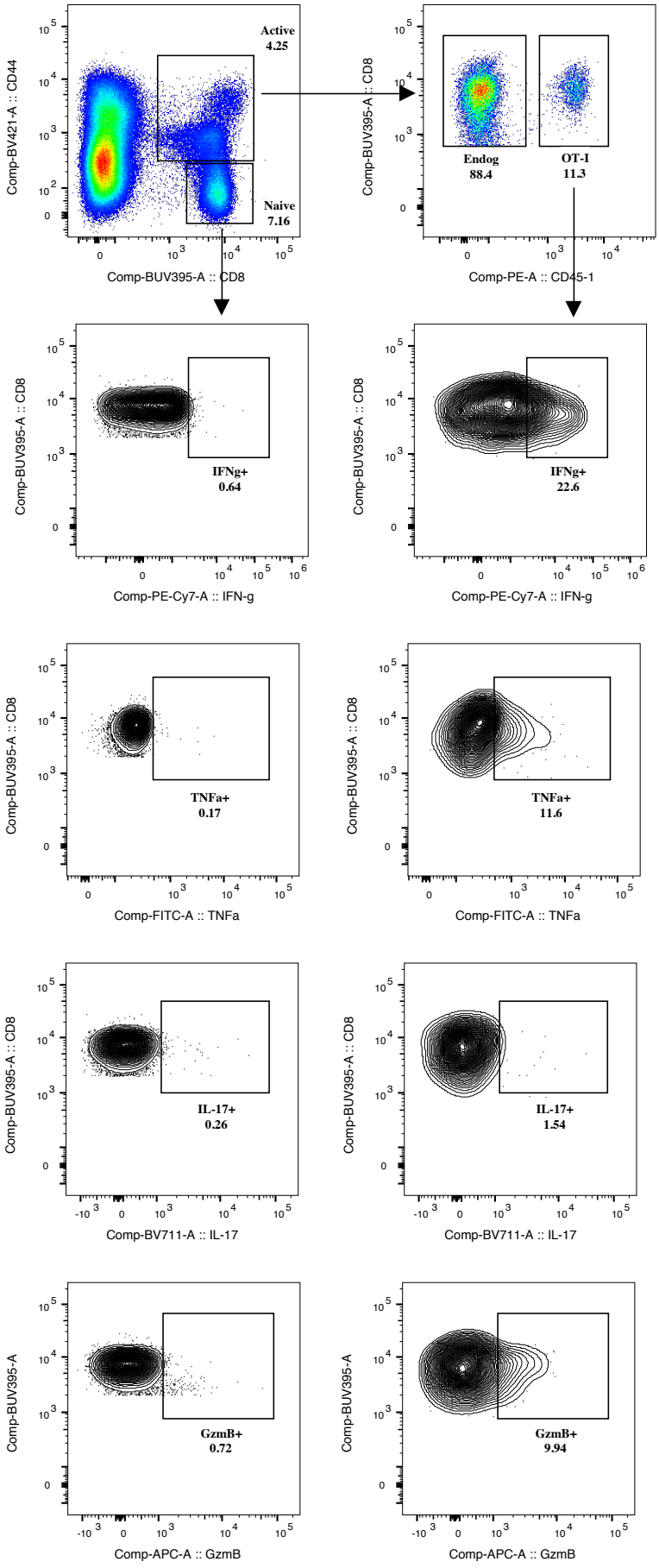
Active
4.25
Naive
7.16
Comp-BV421-A :: CD44
Comp-BUV395-A :: CD8
Endog
88.4
OT-I
11.3
Comp-BUV395-A :: CD8
Comp-PE-A :: CD45-1
IFNg+
0.64
IFNg+
22.6
Comp-BUV395-A :: CD8
Comp-PE-Cy7-A :: IFN-g
TNFa+
0.17
TNFa+
11.6
Comp-BUV395-A :: CD8
Comp-FITC-A :: TNFa
IL-17+
0.26
IL-17+
1.54
Comp-BUV395-A :: CD8
Comp-BV711-A :: IL-17
GzmB+
0.72
GzmB+
9.94
Comp-BUV395-A
Comp-APC-A :: GzmB

Appendix 3. Gating strategy for detection of cytokine-positive T-cells. Cells were gated first on size and singularity, followed by exclusion of dead cells, as per Appendix 1. Activated $CD8^+$ T-cells were gated for based on CD8 and CD44 co-expression. Naïve $CD8^+$ T-cells were identified by the absence of CD44. This naïve population was used to set positive gates for expression of the cytokines Gzmβ, TNF-α, IL-17, and IFN-γ. Activated $CD8^+$ T-cells were divided into endogenous $CD8^+$ T-cells and transferred OT-I populations using CD45.1 expression. The cytokine gates set using the naïve population were subsequently applied to activated $CD8^+$ T-cell subsets to identify cytokine-expressing cells.

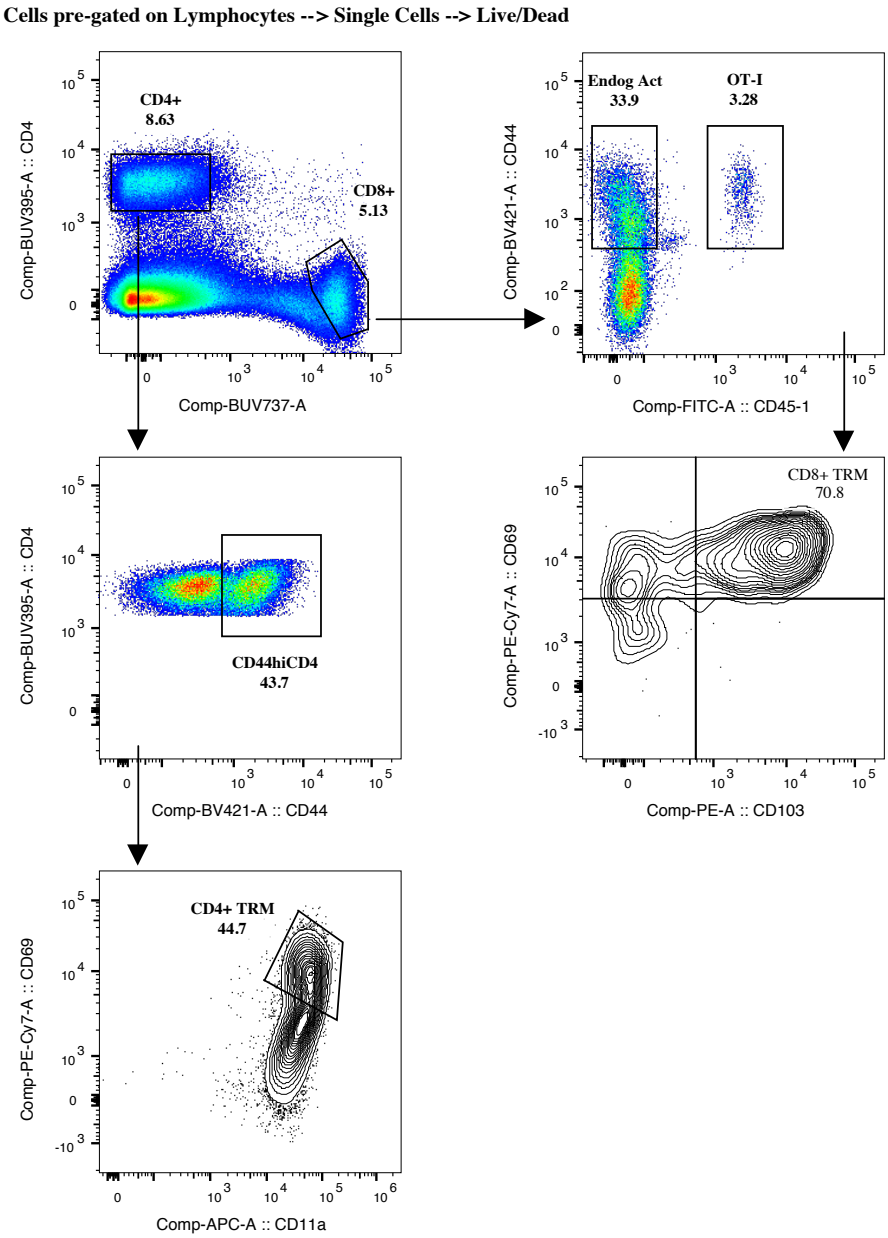

Appendix 4. Gating Strategy to identify Tissue Resident Memory (T_{RM}) cells. Cells were first gated based on size and singularity, followed by exclusion of dead cells, as per Appendix 1. CD8 (BUV737) and CD4 (BUV395) expression were then used to identify $CD4^+$ and $CD8^+$ T-cell populations. CD44 expression was used to identify activated T-cells in each subset, and the $CD8^+$ T-cell subset was additionally divided into endogenous $CD8^+$ T-cells and transferred OT-I cells based on CD45.1. $CD4^+$ T_{RM} cells were then identified using CD69 and CD11a co-expression. $CD8^+$ T_{RM} (both endogenous and transferred OT-I) were identified based on CD69 and CD103 co-expression.

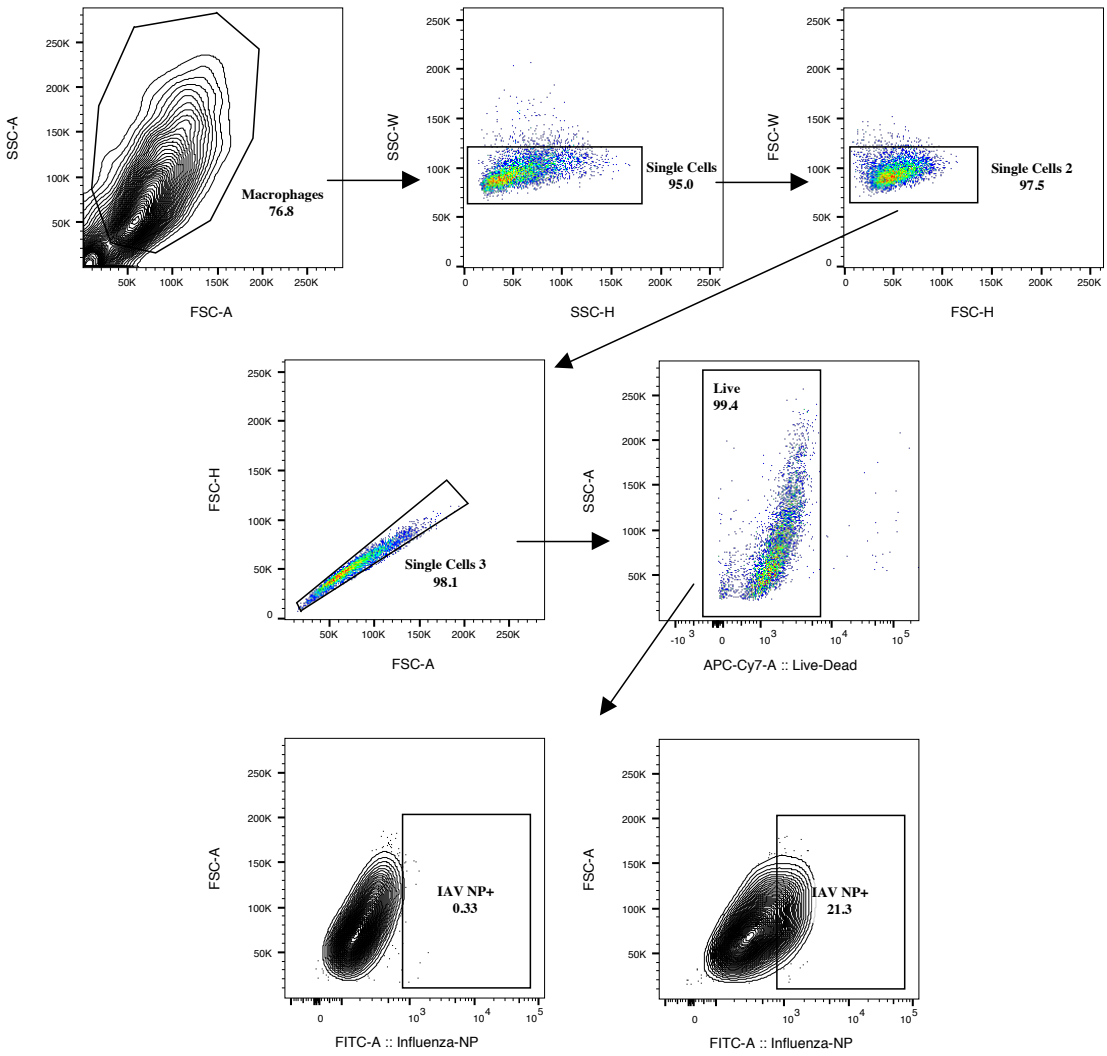

Appendix 5. Gating strategy for detection of IAV-positive macrophages. Cells were first gated based on size and singularity, followed by exclusion of dead cells. Live cells from samples not exposed to IAV (left) were then used to set the positive gate for IAV nucleoprotein (NP). This gate was then applied to samples exposed to live or irradiated IAV (right).

Statement of Authorship

Title of Paper	The effect of gamma-irradiation conditions on the immunogenicity of whole-inactivated Influenza A virus vaccine
Publication Status	☒ Published ☐ Accepted for Publication ☐ Submitted for Publication ☐ Unpublished and Unsubmitted w ork w ritten in manuscript style
Publication Details	David, S.C., Lau, J., Singleton, E.V., Babb, R., Davies, J., et al., 2017. The effect of gamma-irradiation conditions on the immunogenicity of whole-inactivated Influenza A virus vaccine. Vaccine, 35(7): p. 1071-1079.

Principal Author

Name of Principal Author (Candidate)	Shannon C. David
Contribution to the Paper	Designed and performed experiments, performed analysis on all data, and wrote the manuscript.
Overall percentage (%)	85%
Certification:	This paper reports on original research I conducted during the period of my Higher Degree by Research candidature and is not subject to any obligations or contractual agreements with a third party that would constrain its inclusion in this thesis. I am the primary author of this paper.
Signature	Date 23/01/2018

Co-Author Contributions

By signing the Statement of Authorship, each author certifies that:

i. the candidate's stated contribution to the publication is accurate (as detailed above);

ii. permission is granted for the candidate in include the publication in the thesis; and

iii. the sum of all co-author contributions is equal to 100% less the candidate's stated contribution.

Name of Co-Author	Josyane Lau
Contribution to the Paper	Performed experiments and prepared reagents.
Signature	Date 06 June 2018.

Name of Co-Author	Eve Victoria Singleton
Contribution to the Paper	Performed experiments, prepared reagents, aided in data analysis, and edited the manuscript.
Signature	Date 24/01/2018

Name of Co-Author	Rachelle Babb		
Contribution to the Paper	Performed experiments and prepared reagents.		
Signature		Date	22/05/18

Name of Co-Author	Justin Davies		
Contribution to the Paper	Prepared reagents, performed statistical analysis, and edited the manuscript.		
Signature		Date	24/05/2018

Name of Co-Author	Timothy R. Hirst		
Contribution to the Paper	Supervised development of work, aided in data interpretation and manuscript editing.		
Signature		Date	10/5/18

Name of Co-Author	Shaun R. McColl		
Contribution to the Paper	Supervised development of work, aided in data interpretation and manuscript editing.		
Signature		Date	16/5/18

Name of Co-Author	James C. Paton		
Contribution to the Paper	Supervised development of work, aided in data interpretation and manuscript editing.		
Signature		Date	30/1/18

Name of Co-Author	Mohammed Alsharifi		
Contribution to the Paper	Conceived and designed the study, supervised development of work, aided in data interpretation and manuscript editing, and was corresponding author.		
Signature		Date	23/01/2018

Vaccine 35 (2017) 1071–1079

Contents lists available at ScienceDirect

Vaccine

journal homepage: www.elsevier.com/locate/vaccine

The effect of gamma-irradiation conditions on the immunogenicity of whole-inactivated Influenza A virus vaccine

Shannon C. David [a], Josyane Lau [a], Eve V. Singleton [a], Rachelle Babb [a], Justin Davies [b], Timothy R. Hirst [a,c], Shaun R. McColl [a], James C. Paton [a], Mohammed Alsharifi [a,c,*]

[a] Research Centre for Infectious Diseases, and Department of Molecular and Cellular Biology, School of Biological Sciences, University of Adelaide, Adelaide, SA 5005, Australia
[b] Australian Nuclear Science and Technology Organisation, Lucas Heights, NSW 2234, Australia
[c] Gamma Vaccines Pty Ltd, Mountbatten Park, Yarralumla, ACT 2600, Australia

ARTICLE INFO

Article history:
Received 27 September 2016
Received in revised form 25 November 2016
Accepted 16 December 2016
Available online 18 January 2017

Keywords:
Influenza A virus
Gamma-irradiation
Immunogenicity
Protective immunity

ABSTRACT

Gamma-irradiation, particularly an irradiation dose of 50 kGy, has been utilised widely to sterilise highly pathogenic agents such as Ebola, Marburg Virus, and Avian Influenza H5N1. We have reported previously that intranasal vaccination with a gamma-irradiated Influenza A virus vaccine (γ-Flu) results in cross-protective immunity. Considering the possible inclusion of highly pathogenic Influenza strains in future clinical development of γ-Flu, an irradiation dose of 50 kGy may be used to enhance vaccine safety beyond the internationally accepted Sterility Assurance Level (SAL). Thus, we investigated the effect of irradiation conditions, including high irradiation doses, on the immunogenicity of γ-Flu. Our data confirm that irradiation at low temperatures (using dry-ice) is associated with reduced damage to viral structure compared with irradiation at room temperature. In addition, a single intranasal vaccination with γ-Flu irradiated on dry-ice with either 25 or 50 kGy induced seroconversion and provided complete protection against lethal Influenza A challenge. Considering that low temperature is expected to reduce the protein damage associated with exposure to high irradiation doses, we titrated the vaccine dose to verify the efficacy of 50 kGy γ-Flu. Our data demonstrate that exposure to 50 kGy on dry-ice is associated with limited effect on vaccine immunogenicity, apparent only when using very low vaccine doses. Overall, our data highlight the immunogenicity of influenza virus irradiated at 50 kGy for induction of high titre antibody and cytotoxic T-cell responses. This suggests these conditions are suitable for development of γ-Flu vaccines based on highly pathogenic Influenza A viruses.

1. Introduction

Emergence of Highly Pathogenic Avian Influenza (HPAI) strains, H5N1, H5N6, H7N9, and H9N2, represent major health concerns due to the risk of worldwide pandemics [1]. Since 2003, the World Health Organisation (WHO) reported over 800 cases of human infection with avian H5N1, with an average mortality rate of 53% [2]. Most infections with H5N1 occur via infected poultry, though rare clusters of human-human transmission have been reported between family groups in Thailand [3,4], Indonesia [5], Turkey [6], and Vietnam [4]. HPAI may gain mutations to facilitate aerosol transmission between humans, as notably, a mere 5 mutations in a laboratory H5N1 strain allowed efficient aerosol transmission between ferrets [7–9]. Existing inactivated Influenza vaccines induce strain-specific antibody responses, hence protective efficacy against emerging seasonal and pandemic strains is limited [12,13]. We reported the possible use of gamma-irradiated Influenza A virus (γ-Flu) as a vaccine candidate capable of inducing cross-protection against seasonal and pandemic virus strains [10,11,16].

To ensure sterility of irradiated influenza materials, the concept of Sterility Assurance Level (SAL) has been adopted and a value of 10^{-3} or 10^{-6} (one in a thousand or million chance of having live micro-organisms after treatment) has been arbitrarily determined and widely accepted [19]. The Australian Department of Agriculture recently considered an irradiation dose of 50 kGy as mandatory for sterilisation of highly pathogenic agents [14,15]. Considering the risk of avian Influenza pandemics, inclusion of HPAI strains may be warranted in future γ-Flu preparations; hence vaccine irradiation dose may be increased to meet the safety requirement. However, increasing irradiation dose may affect vac-

* Corresponding author at: Research Centre for Infectious Diseases, and Department of Molecular and Cellular Biology, School of Biological Sciences, University of Adelaide, Adelaide, SA 5005, Australia.
E-mail address: mohammed.alsharifi@adelaide.edu.au (M. Alsharifi).

http://dx.doi.org/10.1016/j.vaccine.2016.12.044
0264-410X/

cine efficacy. In addition, while damaging effect of γ-irradiation is dose-dependent [17,18]; the extent of structural damage is influenced by irradiation temperature [20,21,36–38]. Importantly, protein antigenicity is better maintained when virus samples are irradiated on dry-ice (DI) [23]. In the current study, we investigated the effect of irradiation dose and temperature on the immunogenicity of γ-Flu.

2. Materials and methods

2.1. Ethics statement

This study was conducted in strict accordance with Australian Code of Practice for Care and Use of Animals for Scientific Purposes (7th edition [2004], 8th edition [2013]) and South Australian Animal Welfare Act 1985. Experimental protocol approved by Animal Ethics Committee at The University of Adelaide (S-2013/014 & S-2016/036).

2.2. Cells & viruses

Influenza A virus [A/Puerto Rico/8/34 (H1N1) (A/PR8)] was grown in allantoic cavity of 10-day-old embryonated chicken eggs. Eggs injected with 10^3 $TCID_{50}$ A/PR8, incubated for 48 h at 37 °C, and chilled at 4 °C overnight. Allantoic fluid harvested, pooled and stored at −80 °C. Virus stock titrated in Madin-Darby Canine Kidney (MDCK) cells using $TCID_{50}$ assay [24] and estimated as 1.5×10^6 $TCID_{50}$/mL. Virus stock concentrated using chick erythrocytes (cRBCs) as previously described [25]. Concentrated A/PR8 stock titre estimated as 2×10^8 $TCID_{50}$/mL. For Haemagglutination Assay, live or irradiated stocks were serially diluted in PBS using 96-well round-bottom plate and 0.8% cRBCs in PBS added. Plates were incubated at 4 °C and haemagglutination patterns analysed 24 h later.

2.3. Vaccine preparations

A/PR8 stocks inactivated by exposure to γ-radiation from ^{60}Co irradiation facility at Australian Nuclear Science and Technology Organisation (ANSTO), either on dry-ice or at room temperature. Sterility confirmed by passages as recommended by WHO [26]. Lack of detectable HA activity, as measured by Haemagglutination assay, in allantoic fluid from 3 passages indicated complete loss of virus infectivity.

2.4. Transmission Electron Microscopy (TEM)

Irradiated A/PR8 (γ-A/PR8) samples loaded into 3 mm formvar-amorphous carbon-coated copper grids and left for 2 min. Excess solution removed by blotting. Samples stained with 2% Uranyl Acetate for 2 min, then blotted and left to dry at RT for 10 min before visualisation with FEI Tecnai G2 Spirit Transmission Electron Microscope (Adelaide Microscopy, University of Adelaide).

2.5. SDS-PAGE

Irradiated and control samples heat-treated at 85 °C for 20 min. Viral proteins separated by electrophoresis on Pre-Cast NuPAGE Novex 4–12% Bis-Tris gel (Thermo Fisher Scientific), then stained with Coomassie Brilliant Blue. Novex Sharp Pre-Stained Protein Standards (Thermo Fisher Scientific) used for MW comparison.

2.6. Mice & treatment

Six-week-old female wild-type BALB/c mice (H-2^d) supplied by Laboratory Animal Services, University of Adelaide. Mice were anaesthetized intraperitoneally (IP) with 10 μL/gram body weight ketamine anaesthetic (1% xylazine, 10% ketamine in sterile H_20), and vaccinated intranasally (IN) with one or two doses 14 days apart of γ-A/PR8. Control animals treated with PBS. 21 days post-vaccination, animals were anaesthetised, challenged IN with A/PR8 (1.6×10^2 $TCID_{50}$/mouse), and monitored for 3 weeks for clinical symptoms and weight loss. Animals were culled if they lost 20% of starting body weight.

2.7. Measurement of influenza-specific antibody responses

Blood samples collected from all mice via submandibular bleeding 20 days post-vaccination and serum levels of A/PR8-specific IgG were determined by ELISA as described previously [27]. Absorbance measured at 450/620 nm using Biotrack II plate reader, end point titres expressed as reciprocal of the last dilution where OD value ⩾ cut-off value. Cut-off value was determined as mean +(3 × S.D.) of OD values of samples from control mice.

2.8. In vitro neutralisation assay

96-well tissue-culture plates seeded with 6×10^4 MDCK cells/well. A/PR8 activated by treatment with 2 μg/mL TPCK-trypsin (Sigma-Aldrich) for 30 min at 37 °C. Heat-inactivated sera were serially diluted, mixed with A/PR8 (diluted in allantoic fluid + 4 μg/mL TPCK-trypsin) in 1:1 ratio, and incubated for 1 h at 37 °C. Mixture added to MDCK monolayers at MOI of 0.1 and incubated for 2 h at 37 °C. Then, inoculum was removed, monolayers washed with PBS and returned to incubator for 22 h in serum-free media. Monolayers washed, fixed and permeabilised with acetone/methanol (1:1 ratio) at 4 °C and incubated with polyclonal murine anti-A/PR8 sera (generated as previously described [28]) for 1 h at 4 °C. Alexa-Fluor® 488 goat anti-mouse IgG (H + L) (Life Technologies) added for 1 h at 4 °C. Nuclei stained with DAPI (1 μg/mL) for 30 min at room temperature (RT). Images acquired using a Nikon TiE inverted fluorescence microscope and analysed using NIS elements software (Tokyo, Japan).

2.9. Cytotoxic T-cell assay

Mice primed by intravenous injection of live or γ-A/PR8. 6 days later, target splenocytes from naïve mice labelled with 5,6-carboxyfluorescein diacetate succinimidyl ester (CFSE) (0.125 mM) or CellTrace™ Far-Red DDAO-SE (2 μM, Thermo Fisher Molecular-Probes). CFSE population pulsed with Influenza A nucleoprotein peptide (GL Biochem (Shanghai) Ltd, sequence: TYQRTRALV). Target cells mixed at 1:1 ratio (CFSE/CellTrace Red) and adoptively transferred into primed mice using intravenous injection (10^7 cells/mouse). 24 h later, mice sacrificed, spleens harvested, processed to single-cell suspensions, and analysed using FACS (LSRII, BD Biosciences). Data analysed using FlowJo (Treestar Incorporated). Specific lysis as follows: lysis [%] = [1 − (%primed pulsed targets/%primed non-pulsed targets)/(%unprimed pulsed targets/%unprimed non-pulsed targets)] × 100.

2.10. Statistical analysis

Quantitative results expressed as mean ± SEM. Unpaired Student's *t*-test used for comparison of data from two separate groups, and One-way ANOVA used for comparison of data from 3 or more groups. Statistical analysis performed using GraphPad Prism 6, ver-

sion 6.0d (GraphPad Software, La Jolla, CA, USA). *P* values < 0.05 (95% confidence) considered statistically significant.

3. Results

3.1. The effect of irradiation conditions on HA titres and virion morphology

A/PR8 virus samples were exposed to 25 or 50 kGy of γ-radiation, either at room temperature (RT) or on dry-ice (DI). Haemagglutination assay used to determine the effect of irradiation conditions on HAU titres. Fig. 1A shows RT irradiation resulted in 90% and 99% loss of HAU titres for 25 and 50 kGy respectively. In contrast, only 50% loss in HAU was detected after irradiation on DI, regardless of irradiation dose. Considering that HAU titre is dependent on binding of HA to cRBCs, loss in HAU titres after irradiation at RT may be associated with structural damage. Therefore, TEM was used to visualise overall structure of irradiated viruses (Fig. 1B). Samples irradiated on DI show a more intact virus structure compared to preparations irradiated at RT. It should be noted that DI samples were resolved at 220,000× magnification, whilst clear resolution for RT samples could only be visualised at lesser magnification of 135,000×. Additionally, we detected dark aggregates in RT images, indicating potential formation of protein aggregates or split viral particles. We used SDS-PAGE to compare integrity of viral proteins in irradiated samples and non-irradiated controls. All major viral proteins were visible in control non-irradiated samples (Fig. 1C). The three influenza polymerase proteins resolved as two bands, with PB1 and PB2 migrating together to form a less defined band. Bands consistent with molecular weights for NP and M1 were visible for all samples. Importantly, uncleaved (HA0) and cleaved (HA1, HA2) forms of HA were present in control samples and DI irradiated samples. In contrast, HA0 and HA1 bands appeared faint in RT irradiated samples, consistent with reduced HAU titres. Furthermore, lanes related to RT samples showed an increase in smearing of proteins as opposed to formation of discrete bands, indicative of increased protein damage. Considering the significant reduction in HA titre and the observed effect on virion structure and protein integrity (Fig. 1), RT samples were considered inappropriate vaccine preparations and excluded from further testing.

3.2. Estimating D_{10} value and SAL

Sterility of 25 and 50 kGy-irradiated materials was confirmed using 3 passages in 10-day-old embryonated eggs. Additionally, to test whether these doses met the internationally accepted SAL, aliquots of cRBC-concentrated live virus were subjected to different irradiation doses and tested for reduction in virus titre using $TCID_{50}$ assay. We detected a log-linear relationship between the increased irradiation dose and the associated reduction in virus titre (Fig. 2). Based on this linear inactivation curve ($R^2 = 0.9511$), we estimated a D_{10} value of 2.04 kGy. To calculate SAL, we considered the linear inactivation curve, the D_{10} value, the initial titre of 2×10^8 $TCID_{50}$/mL, and the need for 11 or 14 $\log_{10}$ titre reductions to achieve SAL of 10^{-3} or 10^{-6}, respectively. Therefore, SAL for our

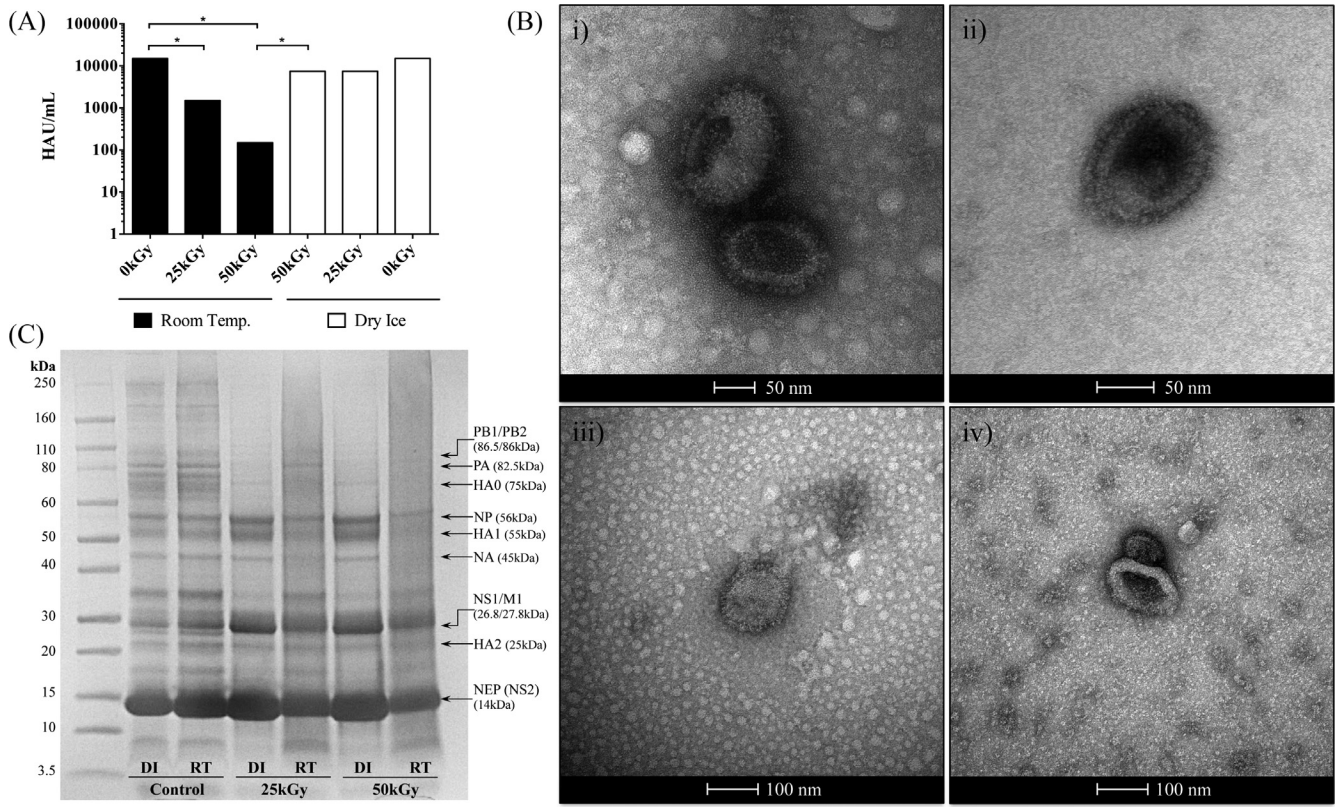

Fig. 1. The effect of irradiation dose and temperature on the structure of Influenza A virus. (A) A/PR8 samples exposed to 25 or 50 kGy of γ-irradiation either on dry-ice (DI) or at room temperature (RT). 0 kGy samples were used as controls and virus titre was estimated using haemagglutination assay and expressed as HAU/mL. Each column indicates mean value of quadruplicates ± SEM, and data analysed by One-way ANOVA (*$P < 0.05$). (B) Transmission Electron Microscopy (TEM) used to visualise morphology changes following irradiation on dry-ice using 25 kGy (i) or 50 kGy (ii), or RT using 25 kGy (iii) or 50 kGy (iv). Virus preparations negatively stained with 2% uranyl acetate and visualised using FEI Tecnai G2 Spirit Transmission Electron Microscope. (C) SDS-PAGE of heat-lysed Influenza preparations, both irradiated samples and non-irradiated controls. Influenza proteins labelled according to their known MW from UniProtKB database (*Influenza A virus (strain A/Puerto Rico/8/1934 H1N1)*), and according to those identified by Shaw et al. [47].

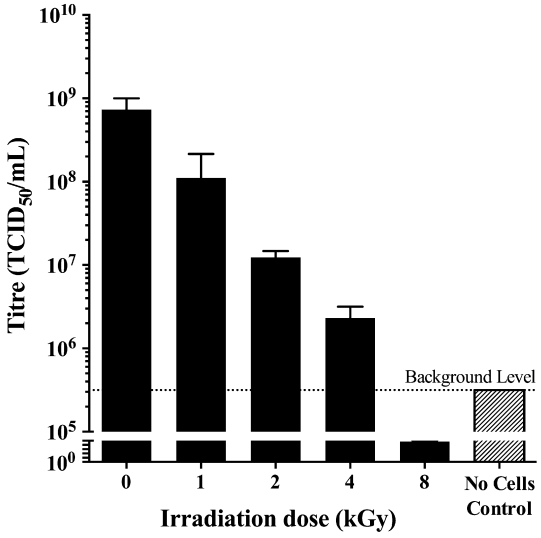

Fig. 2. Inactivation curve of A/PR8 following exposure to different doses of γ-rays. Samples of A/PR8 virus were exposed to increasing doses of γ-irradiation, and virus infectivity was determined by $TCID_{50}$ assay. Background level was measured by the binding of cRBCs to A/PR8 after incubation for 5 days in the absence of MDCK cells.

vaccine could be calculated using the formula "SAL = D_{10} value × 11" or "SAL = D_{10} value × 14", giving 22.4 kGy or 28.6 kGy for SAL value of 10^{-3} or 10^{-6}, respectively. This indicates that materials exposed to 25 or 50 kGy meet the internationally accepted SAL for γ-irradiated pathogens. In fact, 50 kGy represents a much higher dose than required to achieve sterility, representing about 24 $\log_{10}$ reductions in virus titre. Importantly, we confirmed complete inactivation of our preparations in accordance with WHO recommended method of two passages in 10-day-old embryonated eggs [26], and performed 3 passages with no detectable HA in allantoic fluid.

3.3. The effect of irradiation dose on induction of protective immunity

To study the effect of irradiation dose on vaccine efficacy, mice were vaccinated with 25 or 50 kGy γ-A/PR8 irradiated on dry-ice. Serum samples were taken on day 20 post-vaccination and analysed for Flu-specific IgG titres using ELISA. Fig. 3A shows both preparations induced elevated A/PR8-specific IgG titres in serum following mucosal vaccination compared to controls and titres for 25 and 50 kGy γ-A/PR8 vaccinated groups were comparable. Additionally, vaccinated and control animals were challenged IN with lethal A/PR8 21 days post-vaccination, and monitored for clinical symptoms and weight loss. Fig. 3B shows γ-A/PR8 irradiated with either 25 or 50 kGy induced 100% protection against lethal IN challenge and vaccinated mice did not show any weight loss compare to controls. Our data indicate that both preparations (25 and 50 kGy) are highly immunogenic and show comparable protective efficacies when using 32 μL/mouse of undiluted vaccine preparation (6.4×10^6 $TCID_{50}$ equivalent/mouse).

3.4. The effect of vaccine dose on vaccine efficacy

Our data and published studies [21,29–34] clearly indicate that structural damage could be controlled using freezing irradiation conditions. Nonetheless, increased exposure to γ-rays may be associated with reduced vaccine efficacy, albeit to a limited extend. To test this, mice were vaccinated with a single intranasal dose of γ-A/PR8, using either one-half or one-eighth of the dose used in Fig. 3. Protective efficacy was monitored following challenge with live A/PR8. Fig. 4A shows that vaccination with reduced doses of 25 or 50 kGy γ-A/PR8 resulted in 100% survival. However, we observed some weight loss (∼10%) in animals vaccinated with one-eighth dose of 50 kGy γ-A/PR8 prior to full recovery. No weight loss was observed for the other vaccinated groups. We also analysed antibody responses; whilst all reduced doses induced seroconversion following intranasal vaccination, we detected a 50% reduction in IgG titres in serum samples from mice vaccinated with 50 kGy γ-A/PR8 compared to samples from mice vaccinated with 25 kGy γ-A/PR8. However, this reduction did not reach statistical significance (Fig. 4B). This indicates that while 50 kGy γ-A/PR8 appears to be immunogenic and confers high protective efficacy, exposure to 50 kGy may be associated with some damage to viral proteins. As such, this may have affected antibody responses and the ability of γ-A/PR8 to induce protection without weight loss, when using a reduced antigen dose.

To further investigate the effect of high radiation dose on γ-A/PR8, we employed a two-dose vaccination strategy using a very low vaccine dose of 5×10^4 $TCID_{50}$ equivalent/mouse, approximately one-hundredth of the dose used in Fig. 3. A single vaccination with this reduced vaccine dose was not sufficient to induce protective immunity against lethal challenge, regardless of irradiation dose (Fig. 5A). Consequently, mice were vaccinated with two doses of 5×10^4 $TCID_{50}$ equivalent, two weeks apart, followed by a lethal A/PR8 challenge 3 weeks later. When considering the two-dose strategy, vaccination with 25 kGy γ-A/PR8 resulted in significant protection (50% survival) following homotypic challenge. In contrast, two-dose vaccination with 50 kGy γ-A/PR8 was not associated with any protection. Interestingly, analysing antibody titres in serum harvested 24 h pre-2nd vaccination and 24 h pre-challenge showed both 25 and 50 kGy γ-A/PR8 induced comparable Flu-specific IgG titres (Fig. 5B). Additionally, *in vivo* CTL assay was performed to determine whether the observed difference in protection was due to T-cell mediated mechanisms rather than antibody responses. As shown in Fig. 5C, 50 kGy γ-A/PR8 induced slightly less potent CTL responses against nucleoprotein peptide (NPP) pulsed target cells compared to both 25 kGy γ-A/PR8 and live virus control, however this trend was not statistically significant.

3.5. Neutralising antibody responses induced by γ-A/PR8

Antibody levels detected using ELISA in immune sera from mice vaccinated with 25 and 50 kGy γ-A/PR8 did not differ significantly, despite observed differences in protective efficacies (Fig. 5). Therefore, we investigated whether high radiation dose affected the quality of humoral responses rather than quantity. Serum samples from mice vaccinated with 6.4×10^6 $TCID_{50}$ and 2 doses of 5×10^4 $TCID_{50}$ γ-A/PR8 were tested using an in vitro neutralisation assay to quantify neutralising antibody responses. MDCK cells were infected with sera-treated A/PR8 at MOI of 0.1. PBS-treated A/PR8 was used as a virus-only control. Fluorescent staining of infected monolayers showed incubation of A/PR8 with sera from control mice (mock-sera) did not affect the ability of A/PR8 to infect MDCK cells, as infectivity for both mock-sera treated virus and the virus-only control were comparable. Importantly, A/PR8 treatment with immune sera from mice vaccinated with 6.4×10^6 $TCID_{50}$ of 25 and 50 kGy γ-A/PR8 showed complete abrogation of virus infectivity (100% neutralisation), indicating that both vaccines induced strong neutralizing antibody responses (Fig. 6A). Different serum dilutions (1:20, 1:40 and 1:80) were also tested, and no difference in virus neutralisation was detected. Conversely, when testing serum samples from mice vaccinated with 5×10^4 $TCID_{50}$ γ-A/PR8, we detected differences in virus neutralisation between immune sera from mice vaccinated with 25 versus 50 kGy γ-A/PR8. Importantly, serum samples from both 25 and 50 kGy γ-A/PR8 vaccinated groups induced significant virus neu-

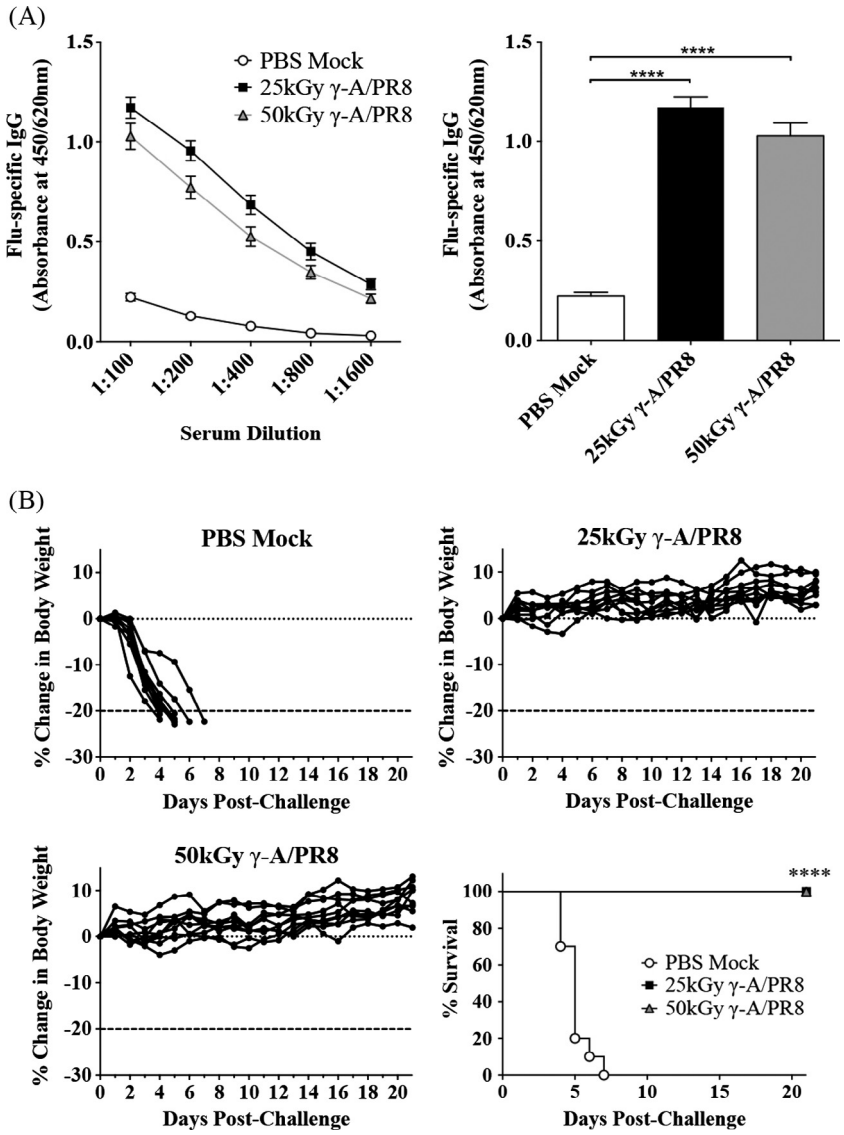

Fig. 3. Intranasal vaccination with 25 kGy and 50 kGy γ-A/PR8 induces homotypic protection against lethal challenge. Mice vaccinated IN with 6.4×10^6 $TCID_{50}$ equivalent/mouse of γ-A/PR8 vaccine irradiated with 25 or 50 kGy on dry-ice. (A) Serum samples harvested on day 20 post-vaccination were analysed for Flu-specific IgG by direct ELISA using serial serum dilutions, and 1:100 dilution of immune sera was selected for statistical analysis. (B) Weight loss of vaccinated mice following IN challenge on day 21with lethal dose of A/PR8, and percentage survival. Data compiled from two independent experiments (n = 10). Data analysed by (A) One-Way ANOVA and (B) Fisher's Exact test ($^{****}P < 0.0001$).

tralisation when compared to control samples. However, neutralisation ability between samples from vaccinated groups was different, as sera from the 25 kGy γ-A/PR8 vaccinated group appeared to be ~ 2.3-fold more effective at neutralizing A/PR8 (determined by difference between means of normalized FITC fluorescence) when compared to sera from 50 kGy γ-A/PR8 vaccinated mice (Fig. 6B).

4. Discussion

Rapid emergence of HPAI strains highlights the urgent need to develop safe vaccines capable of providing protection against circulating as well as emerging pandemic Influenza A viruses. We reported previously that vaccination with γ-Flu confers protection against lethal homotypic and heterosubtypic Influenza A virus challenges, including HPAI H5N1 [10,35]. Considering the risk of a worldwide pandemic, inclusion of HPAI virus strains may be desirable in future clinical developments of γ-Flu. To comply with safety regulations regarding irradiation of pathogenic agents, 50 kGy may be considered. Therefore, we estimated the irradiation dose required to achieve a SAL of 10^{-3} or 10^{-6}, and investigated the effect of high irradiation dose and temperature conditions on γ-Flu efficacy.

It has been reported previously that freezing target materials at ultra-low temperatures during irradiation reduces free radical formation and consequently minimizing the indirect damage to proteins [21,33]. For example, γ-irradiation of frozen plasma samples has been effective in sterilizing HIV virus with minimal impact on functionality of coagulation factors [40]. Furthermore, irradiation of freeze-dried materials was associated with maintained protein biological activity even after exposure to 45 kGy [39]. Our data indicate that we could maintain surface protein functionality and viral morphology by irradiating frozen materials in contrast to irradiation at RT. Interestingly, Feng et al. [22] used SDS-PAGE to demonstrate the decrease in the abundance of Murine Norovirus-1 capsid protein VP1 as irradiation dose increased. We

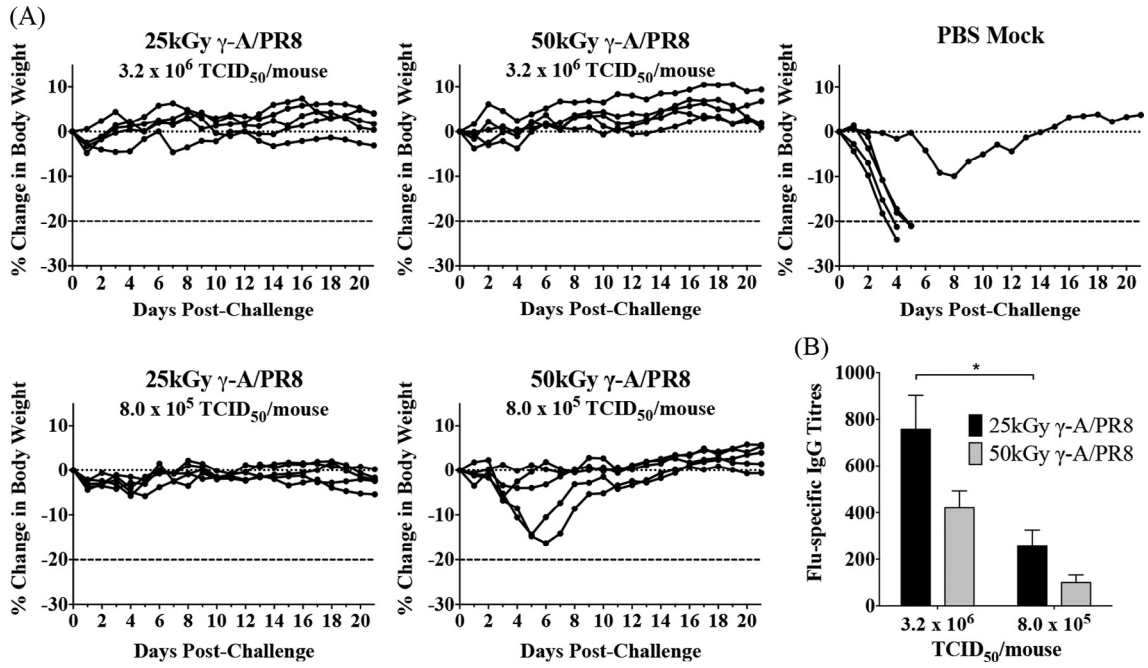

Fig. 4. The efficacy of γ-A/PR8 vaccine. Mice vaccinated IN with 3.2×10^6 or 8.0×10^5 $TCID_{50}$ equivalent/mouse of γ-A/PR8 vaccine irradiated on dry-ice. (A) Weight loss of vaccinated mice following IN challenge with lethal dose of A/PR8. (B) Serum samples harvested on day 20 post-vaccination were analysed for Flu-specific IgG by direct ELISA. Absorbance readings at 450/620 nm of naïve sera used to calculate relative IgG titres. Data presented as mean ± SEM, and analysed by One-Way ANOVA (∗, $P < 0.05$).

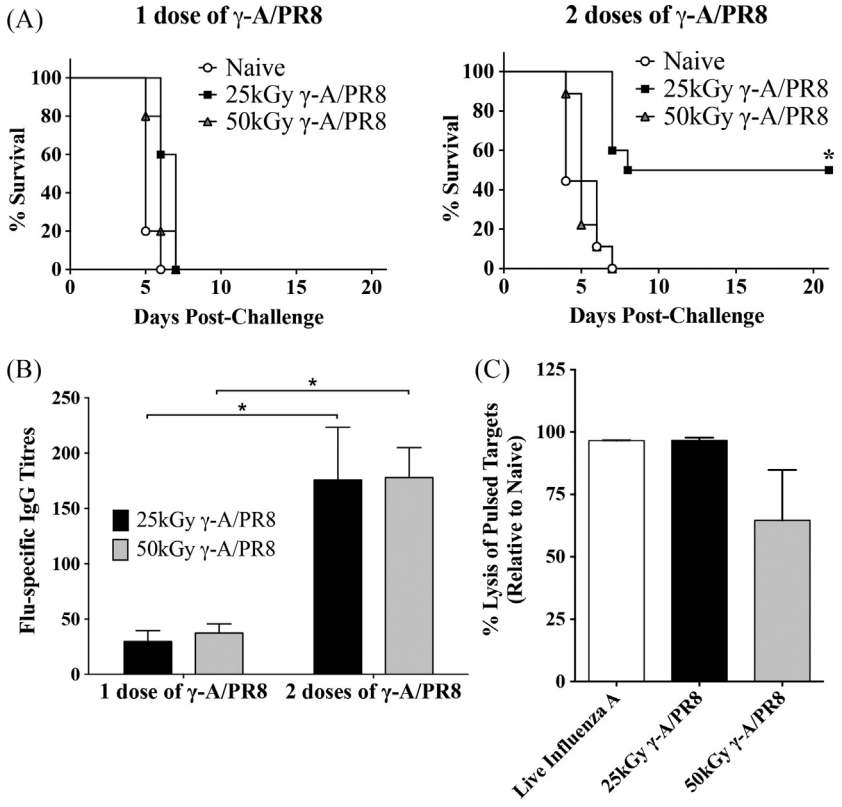

Fig. 5. Enhanced protective efficacy of 25 kGy γ-A/PR8 compared to 50 kGy when using low vaccine dose. (A) Mice vaccinated IN with either a single dose of γ-A/PR8 irradiated on dry-ice (5×10^4 $TCID_{50}$ equivalent/mouse), or two doses administered two weeks apart. 3 weeks post-vaccination, mice were challenged IN with lethal dose of A/PR8, and monitored for survival. Data presented as survival rate (n = 10), and analysed by Fisher's exact test ($^*P < 0.05$). (B) Serum samples harvested via submandibular bleed 24 h pre-challenge from all mice, and tested for Flu-specific IgG using direct ELISA. Absorbance readings at 450/620 nm of naïve sera used to calculate relative IgG titres. Data presented as mean ± SEM, significance determined by One-Way ANOVA ($^*P < 0.05$). (C) CTL-mediated killing of NPP pulsed target splenocytes 24 h after adoptive transfer into mice primed with live influenza, 25 kGy or 50 kGy γ-A/PR8 (dry-ice irradiated). Percentage killing determined in relation to unprimed controls, data presented as mean ± SEM and analysed by One-Way ANOVA.

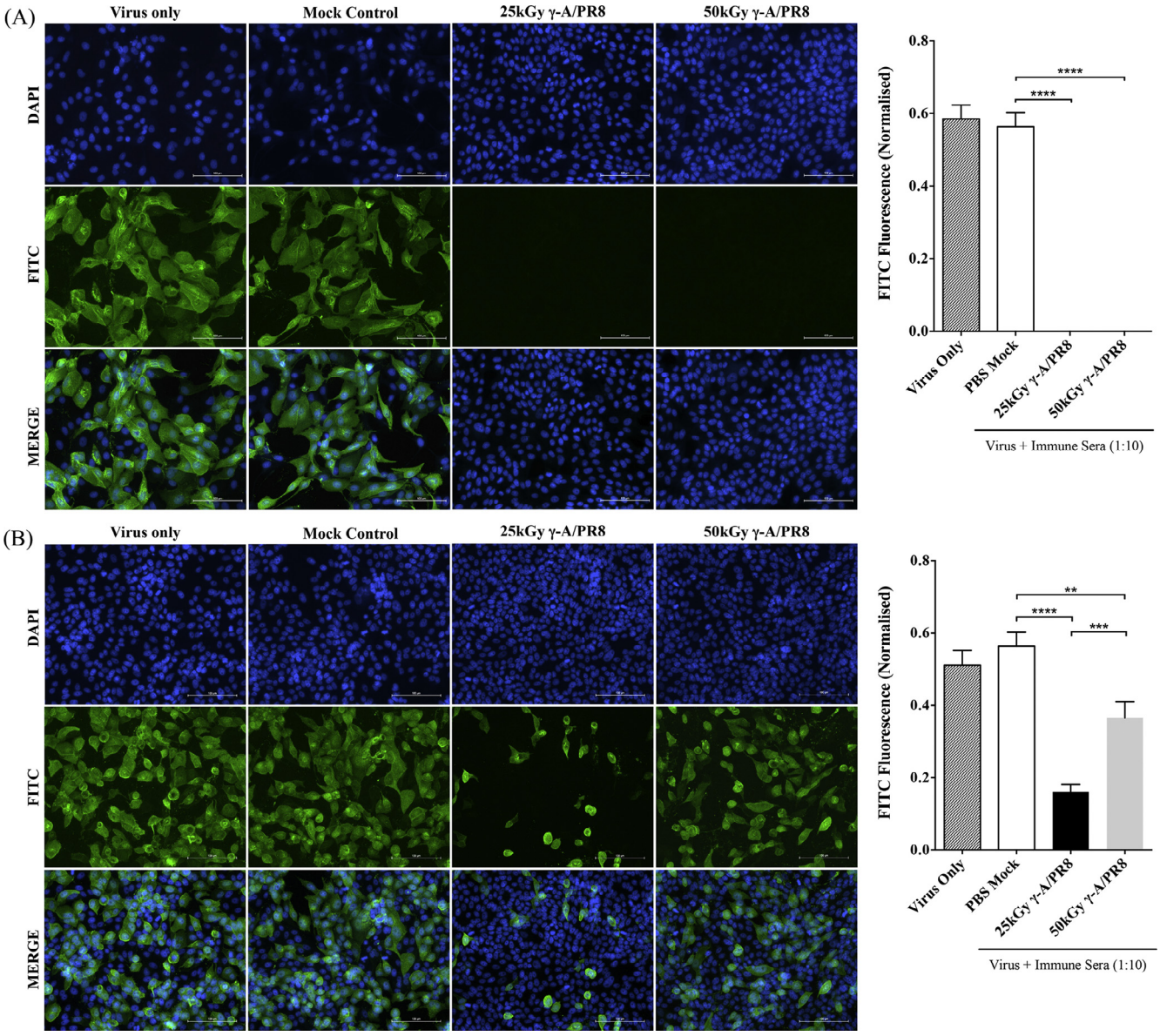

Fig. 6. In vitro A/PR8 neutralisation by immune sera from vaccinated mice. Mice vaccinated IN with (A) 6.4×10^6 $TCID_{50}$, or (B) two doses of 5×10^4 $TCID_{50}$ equivalent γ-A/PR8 irradiated on dry-ice. Serum samples harvested via submandibular bleed on day 20 post-vaccination, and neutralisation efficacy of naïve (PBS mock-vaccinated) and γ-A/PR8-vaccinated immune sera at 1:10 dilution determined by *in vitro* neutralisation assay. After incubation with sera-treated virus, A/PR8 positive MDCK cells visualised using Nikon TiE inverted fluorescence microscope, with DAPI channel detecting cell nuclei, and FITC channel detecting A/PR8. Scale bar = 100 μm. FITC fluorescence quantified using NIS elements software, and normalised using corresponding quantified DAPI fluorescence. Data presented as mean ± SEM (n = 8), and significance determined by One-Way ANOVA ($^{**}P < 0.01$, $^{***}P < 0.001$, $^{****}P < 0.0001$).

showed a similar trend for γ-A/PR8 samples irradiated at RT as we detected increased protein smearing with higher irradiation dose, as opposed to formation of many discrete bands (Fig. 1C). In contrast, materials irradiated on dry-ice showed discrete protein bands, particularly key proteins NA, HA1, and NP (45, 55, and 56 kDa respectively) that were maintained even following exposure to 50 kGy. In addition, RT samples failed to induce flu-specific serum antibody responses and sufficient homotypic protection (data not shown). Thus, we concluded that irradiation at RT is not suitable for vaccine development.

To ensure our dry-ice preparations satisfied requirements for internationally accepted standards [15,41–43], we established the killing curve of A/PR8 using vaccine samples irradiated at different doses. Our data show a clear log-linear relationship between increased irradiation doses and the associated reduced virus titre. This mathematical relationship was used to calculate a D_{10} value of 2.04 kGy and a SAL value of 22.4–28.6 kGy. Therefore, 25 kGy sufficiently complies with guidelines of the International Atomic Energy Agency (IAEA) and International Standards Organisation (ISO). It is important to note that guidelines related to SAL should be accompanied by approved sterility tests, which we performed based on WHO recommendations. While SAL for our preparation is achieved using 25 kGy, 50 kGy may still be desirable to inactivate HPAI. Interestingly, 50 kGy is reported as the lowest dose capable of inactivating Venezuelan equine encephalitis virus (VEEV) [44], and an exposure to 50 kGy on dry-ice was reported to reduce γ-VEEV antigenicity and epitope integrity [45]. In contrast, our data show vaccination with 25 or 50 kGy dry-ice γ-A/PR8 resulted in significantly elevated A/PR8-specific IgG titres and 100% protection against lethal challenge.

Despite high efficacy of 50 kGy γ-A/PR8, we further investigated whether exposure to high irradiation dose affected vaccine

immunogenicity, and whether increased vaccination dose could overcome such effects. To address these possibilities, we used reduced γ-A/PR8 vaccine doses. Remarkably, these doses conferred 100% protection against lethal challenge. We did notice that animals vaccinated with 8×10^5 $TCID_{50}$ equivalent/mouse (one-eighth dose) of 50 kGy γ-A/PR8 lost some weight prior to full recovery, in contrast to animals vaccinated with the same dose of 25 kGy γ-A/PR8. This minor difference in vaccine efficacy was confirmed using a severely reduced vaccine dose (5×10^4 $TCID_{50}$ equivalent/mouse) administered using a two-dose strategy. While 25 and 50 kGy γ-A/PR8 induced comparable levels of A/PR8-specific IgG, we detected a significant difference in A/PR8 neutralisation by immune sera associated the difference in vaccine protective efficacy using this low-dose setting. Interestingly, a study investigating γ-irradiation of allergens showed irradiation with 15 kGy abolished binding of IgE from allergic individuals to allergen proteins [46]. High irradiation potentially damaged allergen epitopes, consequently affecting antibody binding. Similarly, antibodies induced by 50 kGy-treated virus samples may recognise slightly damaged epitopes rather than native epitopes, hence live virus epitopes are less well recognised and consequently virus neutralisation is reduced. Importantly, our data indicate that using higher vaccination doses could overcome the reduced efficacy of 50 kGy γ-A/PR8, as equal and highly effective virus neutralisation for 25 and 50 kGy γ-A/PR8 was observed when using high vaccine dose. Additionally, both 25 and 50 kGy γ-A/PR8 preparations induced CTL responses against internal Influenza peptides that resembled CTL activity induced by live virus.

5. Conclusion

Overall, our data show no detectable difference in performance between 25 and 50 kGy γ-A/PR8 when using standard doses. Reduction in 50 kGy γ-A/PR8 efficacy is only apparent when using intentionally low vaccination dose, which is not relevant to a clinical setting nor for future γ-Flu development. This study has demonstrated the suitability of using freezing conditions for γ-irradiation of viruses to produce inactivated vaccines that elicit strong protective immunity. This supports the use of 50 kGy for developing future γ-Flu vaccines that include HPAI virus strains.

Author contributions

MA, SCD & TRH conceived and designed the study. SCD, JL, EVS, RB & JD performed experiments and prepared reagents. SCD, EVS & JD performed statistical analyses. MA, SCD, JD, TRH, JCP & SRM wrote the manuscript.

Conflict of interest

The authors have no conflicting financial interests, except MA is head of the vaccine research group at the University of Adelaide and the Chief Scientific Officer of Gamma Vaccines Pty Ltd. TRH is the Executive Chairman of Gamma Vaccines Pty Ltd. This does not alter adherence to policies on sharing data and materials.

Acknowledgements

The authors thank Adelaide University Microscopy (Adelaide, Australia), with special mention to Lynette Waterhouse for operation of FEI Tecnai G2 Spirit TEM. Dr. Michael Beard and lab members generously provided reagents and assistance for immunofluorescence imaging. We thank Jasmine J. Wilson, Todd Norton and Dr. Nicholas Eyre for help with figure editing. We also acknowledge the following funding sources supporting this research: an Australian Institute of Nuclear Science and Engineering (AINSE) Research Award (ALNGRA15517; to M.A.); an Australian Postgraduate Award (to S.D.); and a National Health and Medical Research Council Senior Principal Research Fellowship (awarded to J.C.P.).

References

[1] Osterholm MT, Kelley NS. Mammalian-transmissible H5N1 influenza: facts and perspective. MBio 2012;3. e00045-12.
[2] World Health Organisation. Influenza at the human-animal interface: Summary and assessment, 21 January to 25 February 2016. Monthly Risk Assessment Summary: World Health Organisation; 2016.
[3] Ungchusak K, Auewarakul P, Dowell SF, Kitphati R, Auwanit W, Puthavathana P, et al. Probable person-to-person transmission of avian Influenza A (H5N1). N Engl J Med 2005;352:333–40.
[4] Olsen SJ, Ungchusak K, Sovann L, Uyeki TM, Dowell SF, Cox NJ, et al. Family clustering of avian Influenza A (H5N1). Emerg Infect Dis 2005;11:1799–801.
[5] Sedyaningsih ER, Isfandari S, Setiawaty V, Rifati L, Harun S, Purba W, et al. Epidemiology of cases of H5N1 virus infection in Indonesia, July 2005-June 2006. J Infect Dis 2007;196:522–7.
[6] Oner AF, Bay A, Arslan S, Akdeniz H, Sahin HA, Cesur Y, et al. Avian Influenza A (H5N1) infection in eastern Turkey in 2006. N Engl J Med 2006;355:2179–85.
[7] Herfst S, Schrauwen EJ, Linster M, Chutinimitkul S, de Wit E, Munster VJ, et al. Airborne transmission of Influenza A/H5N1 virus between ferrets. Science 2012;336:1534–41.
[8] Imai M, Watanabe T, Hatta M, Das SC, Ozawa M, Shinya K, et al. Experimental adaptation of an influenza H5 HA confers respiratory droplet transmission to a reassortant H5 HA/H1N1 virus in ferrets. Nature 2012;486:420–8.
[9] Centres for Disease Control and Prevention (CDC). Highly Pathogenic Asian-Origin Avian Influenza A (H5N1) Virus. Avian Influenza: CDC; 2015.
[10] Alsharifi M, Furuya Y, Bowden TR, Lobigs M, Koskinen A, Regner M, et al. Intranasal flu vaccine protective against seasonal and H5N1 avian influenza infections. PLoS One 2009;4:e5336.
[11] Furuya Y, Regner M, Lobigs M, Koskinen A, Mullbacher A, Alsharifi M. Effect of inactivation method on the cross-protective immunity induced by whole 'killed Influenza A viruses and commercial vaccine preparations. J Gen Virol 2010;91:1450–60.
[12] Tamura S, Kurata T. Defense mechanisms against influenza virus infection in the respiratory tract mucosa. Jpn J Infect Dis 2004;57:236–47.
[13] Alsharifi M, Mullbacher A. The gamma-irradiated influenza vaccine and the prospect of producing safe vaccines in general. Immunol Cell Biol 2010;88:103–4.
[14] Farkas J, Farkas CM. History and future of food irradiation. Trends Food Sci Technol 2011;22:121–6.
[15] Department of Agriculture Fisheries and Forestry Biosecurity. Gamma Irradiation as a treatment to address pathogens of animal biosecurity concern - final policy review. Canberra: Department of Agriculture [CC BY 3.02014].
[16] Furuya Y, Chan J, Wan EC, Koskinen A, Diener KR, Hayball JD, et al. Gamma-irradiated influenza virus uniquely induces IFN-I mediated lymphocyte activation independent of the TLR7/MyD88 pathway. PLoS One 2011;6:e25765.
[17] Ginoza W. The effects of ionizing radiation on nucleic acids of bacteriophages and bacterial cells. Annu Rev Microbiol 1967;21:325–68.
[18] Rohwer RG. Scrapie infectious agent is virus-like in size and susceptibility to inactivation. Nature 1984;308:658–62.
[19] International Atomic Energy Agency. Guidelines for industrial radiation sterilization of disposable medical products (cobalt-60 gamma irradiation). The technical reports series. Vienna: International Atomic Energy Agency; 1990. p. 39.
[20] Sullivan R, Scarpino PV, Fassolitis AC, Larkin EP, Peeler JT. Gamma radiation inactivation of coxsackievirus B-2. Appl Microbiol 1973;26:14–7.
[21] Ormerod MG. Free-radical formation in irradiated deoxyribonucleic acid. Int J Radiat Biol Relat Stud Phys Chem Med 1965;9:291–300.
[22] Feng K, Divers E, Ma Y, Li J. Inactivation of a human norovirus surrogate, human norovirus virus-like particles, and vesicular stomatitis virus by gamma irradiation. Appl Environ Microbiol 2011;77:3507–17.
[23] Jordan RT, Kempe LL. Inactivation of some animal viruses with gamma radiation from cobalt-60. Proc Soc Exp Biol Med Soc Exp Biol Med 1956;91:212–5.
[24] Cottey R, Rowe CA, Bender BS. Influenza virus. In: Coligan JE, editor. Current protocols in immunology. John Wiley and Sons, Inc.; 2001. http://dx.doi.org/10.1002/0471142735.im1911s42. Chapter 19:Unit 19.11.
[25] Sheffield FW, Smith W, Belyavin G. Purification of influenza virus by red-cell adsorption and elution. Br J Exp Pathol 1954;35:214–22.
[26] World Health Organisation. WHO Expert Committee on Biological Standardization. WHO technical reports series, report no. 54. Geneva (Switzerland): World Health Organisation; 2005.
[27] Babb R, Chan J, Khairat JE, Furuya Y, Alsharifi M. Gamma-irradiated Influenza A virus provides adjuvant activity to a co-administered poorly immunogenic SFV vaccine in mice. Front Immunol 2014;5:267.

[28] Chan J, Babb R, David SC, McColl SR, Alsharifi M. Vaccine-induced antibody responses prevent the induction of interferon type I responses upon a homotypic live virus challenge. Scand J Immunol 2016;83:165–73.
[29] Hiemstra H, Tersmette M, Vos AH, Over J, van Berkel MP, de Bree H. Inactivation of human immunodeficiency virus by gamma radiation and its effect on plasma and coagulation factors. Transfusion 1991;31:32–9.
[30] Kempner ES. Effects of high-energy electrons and gamma rays directly on protein molecules. J Pharm Sci 2001;90:1637–46.
[31] Sanner T, Pihl A. Significance and mechanism of the indirect effect in bacterial cells. The relative protective effect of added compounds in *Escherichia coli* B, irradiated in liquid and in frozen suspension. Radiat Res 1969;37:216–27.
[32] Hamer AJ, Stockley I, Elson RA. Changes in allograft bone irradiated at different temperatures. J Bone Joint Surg Br 1999;81B:342–4.
[33] Kempner ES, Haigler HT. The influence of low temperature on the radiation sensitivity of enzymes. J Biol Chem 1982;257:13297–9.
[34] Ginoza W, Norman A. Radiosensitive molecular weight of tobacco mosaic virus nucleic acid. Nature 1957;179:520–1.
[35] Mullbacher A, Ada GL, Hla RT. Gamma-irradiated Influenza A virus can prime for a cross-reactive and cross-protective immune response against Influenza A viruses. Immunol Cell Biol 1988;66(Pt 2):153–7.
[36] Grieb TA, Forng RY, Stafford RE, Lin J, Almeida J, Bogdansky S, et al. Effective use of optimized, high-dose (50 kGy) gamma irradiation for pathogen inactivation of human bone allografts. Biomaterials 2005;26:2033–42.
[37] Kempner ES, Miller JH. Effect of environmental conditions on radiation target size analyses. Anal Biochem 1994;216:451–5.
[38] Beauregard G, Potier M. Temperature dependence of the radiation inactivation of proteins. Anal Biochem 1985;150:117–20.
[39] Grieb T, Forng RY, Brown R, Owolabi T, Maddox E, McBain A, et al. Effective use of gamma irradiation for pathogen inactivation of monoclonal antibody preparations. Biol: J Int Assoc Biol Standardization 2002;30:207–16.
[40] Kitchen AD, Mann GF, Harrison JF, Zuckerman AJ. Effect of gamma irradiation on the human immunodeficiency virus and human coagulation proteins. Vox Sang 1989;56:223–9.
[41] International Atomic Energy Agency. Manual on radiation sterilization of medical and biological materials. International Atomic Energy Agency: Technical reports series1973. p. 327.
[42] Isaacson R. Sterilization - validation qualification requirements. Manufacture of sterile medicines - advanced workshop. World Health Organisation (WHO); 2009.
[43] ANSI/AAMI/ISO. ANSI/AAMI/ISO 11137-2: 2013. Sterilization of health care products—radiation. AAMI; 2013.
[44] Jenkins EPM, Bakken R, et al. A multisystem approach for the evaluation of inactivation efficiency for Venezuelan equine encephalitis virus (VEEV) vaccine candidates. In: 12th Annual conference on vaccine research. Baltimore, MD; 2009.
[45] Martin SS, Bakken RR, Lind CM, Garcia P, Jenkins E, Glass PJ, et al. Comparison of the immunological responses and efficacy of gamma-irradiated V3526 vaccine formulations against subcutaneous and aerosol challenge with Venezuelan equine encephalitis virus subtype IAB. Vaccine 2010;28:1031–40.
[46] Li ZX, Lin H, Cao LM, Jamil K. The influence of gamma irradiation on the allergenicity of shrimp (Penaeus vannamei). J Food Eng 2007;79:945–9.
[47] Shaw ML, Stone KL, Colangelo CM, Gulcicek EE, Palese P. Cellular proteins in influenza virus particles. PLoS Pathog 2008;4:e1000085.